Jin-Ming Lin
Chao Lu
Hui Chen *Editors*

Ultra-Weak Chemiluminescence

Ultra-Weak Chemiluminescence

Jin-Ming Lin · Chao Lu · Hui Chen
Editors

Ultra-Weak Chemiluminescence

Springer

Editors
Jin-Ming Lin
Department of Chemistry
Tsinghua University
Beijing, China

Hui Chen
College of Material Science
and Technology
Beijing Forestry University
Beijing, China

Chao Lu
State Key Laboratory of Chemical
Resource Engineering
Beijing University of Chemical Technology
Beijing, China

Preface

Chemiluminescence involves chemical reactions which produce electronically excited states in sufficient quantity, and sufficiently quickly, to allow the occurring of the emission of light. It is concerned primarily with the emission of visible or near-visible radiation. Thus, chemiluminescence can be visible and bright, visible and dim, or invisible and ultra-weak. They can occur in gases, in liquids, and at the interface between solids and either a gas or liquid phase. Now many hundreds of organic and inorganic chemical reactions have been discovered which produce visible light. However, little works have been done on the ultra-weak chemiluminescence from inorganic chemical reactions.

We began to do research in developing new chemiluminescence systems and making apparatus for chemiluminescence detection since 1990s. During the past 30 years, our research group has made a great progress in principles and application of chemiluminescence, especially on the promotion of industrialization of chemiluminescence immunoassay technology. Chemiluminescence is a highly sensitive and most useful analytical technique, and is of great important in many fields, because of its low background interference and simple instrumentation. From the year's cooperation with enterprises, we find the education of basic knowledge of chemiluminescence is essential for the promotion of this technology. More than ten years ago, we have published two books in about chemiluminescence in Chinese language, such as Chemiluminescence-Basic Principles (Beijing Chemical Press, 2004) and Applications and Chemiluminescence Immunoassay (Beijing Chemical Press, 2008). Now, we are very pleased to do the further introduction of ultra-weak chemiluminescence combining the series research results of our group. We hope it will be helpful to the world's research and application of chemiluminescence.

This book is about the ultra-weak chemiluminescence. The emission of light caused by a chemical reaction is invisible to the naked eye but detectable by a sensitive photomultiplier tube. Recently, the ultra-weak chemiluminescence has had an impact on chemistry, on cell biology, and on biochemical and environmental analysis. Many of our cells are capable of producing an ultra-weak chemiluminescence spontaneously. The emission of a weak chemiluminescence from cells in the plant and animal kingdom during mitosis in ultraviolet region now has been observed.

Red ultra-weak chemiluminescence has even been detected in human breath. The reactions responsible for this invisible ultra-weak chemiluminescence are oxidation involving oxygen, oxygen metabolites, and radicals.

The inorganic elements which can participate in ultra-weak chemiluminescent reactions range from the alkali metals and heavy metals such as mercury and lead, to non-metals such as O, S, N, P, As, and the halogens. Compounds such as sulfate or sulfite, carbonate or bicarbonate, nitrite, and periodate would produce ultra-weak chemiluminescence when they coexisted with hydrogen peroxide in solutions. Research of these chemiluminescence mechanisms did great help for the explanation of most luminescent phenomena in nature and the understanding of the interaction of compounds containing carbon, nitrogen, sulfur, oxygen, halogen, and other elements, such as CO_2, CO_3^{2-}, HCO_3^-, NO_2^-, NO_2, NO_3^-, SO_2, SO_3^{2-}, IO_4^-, H_2O_2, and O_2. Compounds of silicon, the next element to carbon in group IV of the periodic table, also can produce chemiluminescence. Ultra-weak chemiluminescence is also responsible for light emission in many flames including those of N_2O, H_2S, CS_2, CO, and CN in air or oxygen. The ultra-weak red flash from the addition of H_2O_2 to sodium hypochlorite (NaClO), observed firstly by Mulliken in 1928, now has been known to be caused by singlet oxygen.

This book describes the study method of ultra-weak chemiluminescence providing many new technologies and new principles. Ultra-weak chemiluminescence in aqueous phase system is generated mainly by redox reactions with proper chemiluminescent reagents. To the inorganic ultra-weak chemiluminescence, the low intensity of these luminescence phenomena is because of a low overall quantum yield, or because of a low rate of reaction and/or the concentration of the chemiluminescent components is too low to generate a visible, functional light emission. The ultra-weak chemiluminescence can be induced or enhanced by addition of a variety of compounds. These compounds may themselves be chemiluminescent, or they may act on the pathway required to generate the endogenous ultra-weak chemiluminescence. For example, polycyclic aromatic hydrocarbon can enhance the ultra-weak chemiluminescence from the reaction of sodium hydrosulfite ($NaHSO_3$) with H_2O_2 by forming a new emitter from the radical reduction reaction. The enhancers fall into three broad categories: provision of chemiluminescent substrate, provision of oxidant, such as a hydroperoxide, and the energy transfer acceptors.

In recent years, great progress in ultra-weak chemiluminescence field has occurred, thanks to the development of new chemical probes, enhancers, and advanced instrumentation for light measurement and imaging. Specially, with the fast development of nanotechnology, many new nanomaterials have been applied in the ultra-weak chemiluminescence system to enhance the chemiluminescence intensity for further application. The cadmium series quantum dots, metal nanoalloys, carbon nanodots, and rare-earth-doped nanoparticles have been used to enhance the ultra-weak chemiluminescence from the decomposition of peroxymonocarbonate, peroxomonosulfite, and peroxynitrous acid, respectively. The enhanced chemiluminescence can be realized through a redox reaction by forming electron- and hole-injected nanoparticles. Metal surface plasmons also can enhance ultra-weak chemiluminescence by the chemically induced electronic excited states coupling to

surface plasmons. The surface plasmons-assisted metal catalysis process has been observed in the copper/nickel nanocomposite-enhanced ultra-weak chemiluminescence arising from peroxymonocarbonate. Energy transfer through electrons and radical annihilation is also involved in many well-known ultra-weak chemiluminescence reactions. The color of the emission is dependent on the fluorescent acceptor. The non-radiative energy transfer occurs only over very short distances of <0.1 nm, whereas others occur over distances as long as 10 nm. The result is a change in quantum yield, color, and sometimes rate of reaction.

The aim of this book is to provide a wide, but balanced, perspective on chemical reactions which produce ultra-weak chemiluminescence. The content includes fifteen chapters: what is so special about an ultra-weak chemiluminescence (Chap. 1), where they can be found (Chaps. 2–5), the kinds of active oxygen species in ultra-weak chemiluminescence (Chaps. 6 and 7), and ultra-weak chemiluminescence enhanced by functional materials (Chaps. 8–11). We attempted to highlight the unique aspects of ultra-weak chemiluminescence in analysis and to pinpoint where real discoveries have arisen from its use in chemistry, biology, medicine, environment, and forensic science.

The book is aimed at researchers and undergraduates in chemistry, physics, and biology. It describes particularly my own enthusiasm for studying ultra-weak chemiluminescence. We have deliberately repeated a few points in more than one chapter, so that each chapter may be read independently. It is our wish to encourage more people to discover more about this most exciting useful technique.

I would like to express my thanks to collaborators and colleagues too numerous to mention and also to many of my postgraduates.

December 2021

Jin-Ming Lin
Professor of Chemistry
Tsinghua University
Beijing, China

Contents

Chapter 1
Introduction of Ultra-Weak Chemiluminescence

Xiangnan Dou, Syed Niaz Ali Shah, and Jin-Ming Lin

Abstract This chapter gives an overview of the basic principle of chemiluminescence and ultra-weak chemiluminescence. The development of various ultra-weak CL systems will be introduced. The ultra-weak chemiluminescence based on reactive oxygen species will be focused in this chapter. Ultra-weak chemiluminescence hinders its application in analytical chemistry due to its low luminous efficiency. The roles of nanoparticles in enhancing these ultra-weak CL systems will also be reviewed.

Keywords Chemiluminescence · Ultra-weak chemiluminescence · Principle · Application

1.1 Introduction

Chemiluminescence (CL) is light emitted from a chemical reaction. The requirements for chemiluminescence are (1) The chemical reaction must provide enough excitation energy to enable the electron to transition from the ground state to the excited state, and (2) The energy from the chemical reaction can be accepted by at least one substance and generate an excited state; (3) the electronically excited products have chemiluminescence quantum yield to release photon or transfer its energy to other luminophores [1]. CL is typically observed during redox reaction processes. The chemiluminescence quantum yield, Φ_{CL}, is determined by the efficiency of generating the excited state product and the efficiency of an emitted photon of the excited state product. Φ_{CL} does not usually surpass 0.1–0.001% in most circumstances. Only a few CL systems, such as the unique substituted oxiamide or dioxetane intermediate, may achieve a yield of 30% [2]. High quantum yields ranging from 1 to 100% of luminescence emerges during oxidation of the luciferin, mediated by the enzyme luciferase in living cells. Luciferin and luciferase are substrates and enzymes that interact to produce visible light. It is the enzyme with a unique microenvironment and

X. Dou · S. N. A. Shah · J.-M. Lin (✉)
Department of Chemistry, Tsinghua University, Beijing 100084, China
e-mail: jmlin@mail.tsinghua.edu.cn

reactive properties that are frequently used as a reaction medium in bioluminescence. The quantum yields of the excited state species and emission in bioluminescent emission based on an enzymatic reaction are quite high. This means that some ultra-weak CL systems could be produced as CL reaction media, the quantum yield of CL may be improved.

The CL technique has the advantage of having mild response conditions and being simple to manage. CL provides several distinct advantages as an analytical method:

(1) Unlike fluorescence and UV–visible analysis, CL does not require an external light source, making it simple to integrate with other equipment like chromatography and capillary electrophoresis.

(2) The sensitivity of CL analysis is very high. CL excitation energy derives from chemical reactions (mostly redox reactions). As a result, CL analysis lowers the signal's effect on the source stability by eliminating Rayleigh and Raman scattering. A low level of noise and a high signal-to-noise ratio is achieved by the CL method, which has a detection limit as low as attomole (10^{-18}) or even zeptomole (10^{-21}).

(3) CL analysis may be used to detect substances involved in CL processes, including CL substrates, catalysts, inhibitors, and sensitizers.

During the last 40 years, many analysts have become interested in CL analysis because of its great sensitivity and ease of instrumentation. In contrast to the fluorescence approach, the exciting light source for CL is not required. As a result, the CL has found widespread application in clinical chemistry, biochemistry, and environmental chemistry, etc. The most evident manifestation of the rapid development is the large number of articles devoted solely to CL [3–10]. Because of its extraordinarily high sensitivity and other advantages, analytical methods comprising CL have recently attracted a lot of interest in a variety of sectors. Luminol, lucigenin, and oxalate esters are common CL systems [10, 11]. The CL method's exceptional sensitivity, however, presented a selectivity problem. Although various new CL systems are being developed for the identification of analytes [12–15], most CL systems could not be employed to directly determine the analytes. These limited CL systems only meet the needs of researchers for practical application. It's worth noting that the scarcity of functional CL systems is a key roadblock to CL's mainstream adoption. The quest for a new CL system is critical for expanding the scope of CL methods. Taking note of the fact that many redox reactions generate relatively faint light, the efforts on finding new CL systems is the main focus. The introduction of sensitizers or catalysts has already been shown to dramatically improve the CL properties of such weak CL systems [16, 17].

Many analysts worked hard to increase the CL intensity as well as the selectivity. Many new CL systems, both homogeneous and heterogeneous, have been created because of their work.

1.2 Principle of Chemiluminescence

CL can be produced by a chemical reaction that releases between 41 and 72 kcal per mole energy on its way to the product [18, 19]. There are three primary phases in the CL response. The first is the production of an intermediate that can react to provide enough energy to emit a visible light photon. The development of an electrically excited state is the next step. The CL reactions are distinguished from the rest of the chemical reactions by this step. The excited state's emission of light is the final stage [19]. The molecule's vibrational and rotational shifts are frequently accompanied by the electronic transition. Transitions from π bonding to π^* anti-bonding orbital $(\pi - \pi^*)$ or from a non-bonding to an anti-bonding orbital $(n - \pi^*)$ are the most common in organic compounds. CL denotes the return of an electron to its ground state accompanied by the emission of a photon. Excited molecules can also lose energy through a variety of mechanisms including chemical processes, collisional deactivation, internal conversion, and inter-system crossing. As a result, when these radiationless processes compete with CL, they are considered undesirable from an analytical perspective. The chemical interaction between the molecules A and B, as well as the energy transfer during the reaction, is depicted in Fig. 1.1.

In the first step, the reaction of A and B forms an excited state compound (C^*) which has a quantum yield Φ_{EX}.

$$A + B \xrightarrow{\text{Energy transfer}} C* \tag{1.1}$$

We can see from Fig. 1.1 that the excited molecule (C^*) can emit CL in two different ways.

(1) In the first case, C^* is a luminescence emitter that may be viewed through the luminescence emission.
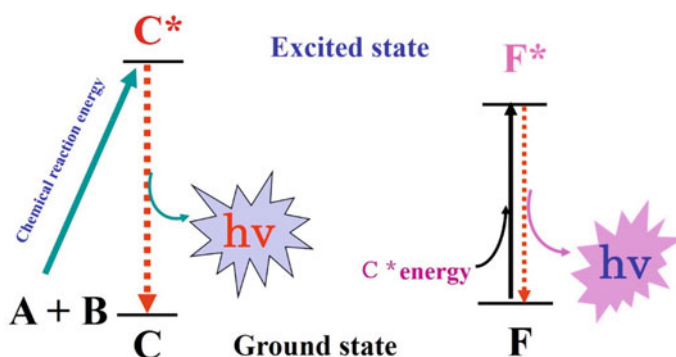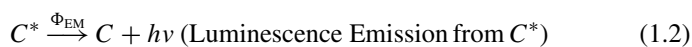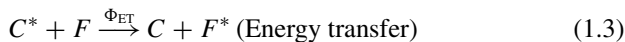
$$C^* \xrightarrow{\Phi_{EM}} C + hv \text{ (Luminescence Emission from } C^*) \tag{1.2}$$

Fig. 1.1 The basic principle of chemiluminescence

(2)   When the excited molecule C^* transferred its energy to the fluorescent molecule (F), the emission was increased by a more sensitive fluorescence. As a result, F is referred to as a CL enhancer, and the process is referred to as an enhancement CL reaction.

$$C^* + F \xrightarrow{\Phi_{ET}} C + F^* \text{ (Energy transfer)} \qquad (1.3)$$

$$F^* \xrightarrow{\Phi_F} F + hv \text{ (Fluorescence Emission from } F^*) \qquad (1.4)$$

As soon as the CL reaction was initiated in the first instance. The quantum yield (CL) is the fraction of molecules that produce a photon when they return to their ground state. It is calculated as the product of two ratios:

$$\Phi_{CL} = \Phi_{EX} \cdot \Phi_{EM} \qquad (1.5)$$

Traditional CL systems often have very poor quantum yields, either because of heat release or because of quenching from the surrounding environment. To avoid this difficulty, it is recommended that a fluorescent chemical with a reasonably high quantum yield be added to the reaction mixture to facilitate the transfer of energy to the fluorescent species [18]. As its name implies, this type of CL system emits its ultimate emission from an excited state created by direct oxidation of the excitation step. It is referred to as the direct CL system. The indirect CL system, on the other hand, is a CL system in which the final emission occurs indirectly because of energy transfer from the first created excited state, as opposed to the direct CL system [19]. Recently, nanomaterials (NMs) have been widely used to increase the CL intensity of classical systems, which is a significant advancement.

Inorganic reactions in CL systems produce weak CL emissions because of the low quantum yield of the inorganic reactions. For analytical applications, then, it is important to increase the CL intensity level. Compounds such as NMs, transition elements, and/or reaction techniques such as catalytic and energy transfer processes have been proposed to improve the CL signals of these compounds [20]. Currently, there is a considerable deal of interest in CL signal enhancement [21]. The research orientation in CL is partially devoted to the development of novel CL systems and partly to the application of these systems to real samples, with the former being the primary focus. This type of research can be primarily focused on discovering new CL reagents, such as substrates, sensitizers, and catalysts [22].

In general, the CL reaction is a redox reaction [23], which involves the participation of a variety of reactive oxygen species (ROS) [24, 25]. Hydroxyl radical ($^{\bullet}OH$), superoxide radical ($^{\bullet}O_2^-$), and substrate radicals, as well as singlet oxygen ($^1O_2$), are all examples of ROS [24–26]. Increased ROS generation is a frequently used technique for increasing the CL intensity of a system [27]. The peroxide-induced CL systems have garnered considerable attention and are widely used in a variety of fields. Hydrogen peroxide (H_2O_2), peroxymonocarbonate, peroxysulfite, and peroxynitrite are all examples of peroxides [28]. H_2O_2 has a critical role

in the CL responses [23]. The breakdown of H_2O_2 in a CL reaction generates reactive oxygen species (ROS) [13, 29]. Many CL emissions from a system are possible because of the system's multiple CL paths. Multiple CL pathways can occur concurrently in the same system. The quenching of CL signals occurs when a CL pathway is blocked. CL emission may have increased because of the closure of a less efficient CL pathway [24]. To detect and track these radicals in a CL system, electron paramagnetic resonance (EPR) and free radical scavengers are utilized.

1.3 Development of Ultra-Weak CL Systems

CL provides several advantages for analytical chemistry applications, including high sensitivity, a broad linear range, simple and inexpensive apparatus, and minimal background noise. However, many CL systems use certain conventional reagents, including luminol, lucigenin, acridinium, AMPPD, and $Ru(bpy)_3^{2+}$, the majority of which are organic molecules. We have attempted to build various new CL systems based on inorganic reactions throughout the last two decades, notwithstanding the difficulty of directly detecting light emissions using CL approaches due to the poor quantum yield. The book focuses on the construction of ultra-weak CL systems using peroxymonocarbonate, peroxynitrous/peroxynitrite, peroxysulfite, periodate, or hydrogen peroxide as starting materials. Additionally, it will address ultra-weak CL that has been boosted or amplified by nanoparticles, quantum dots, or layered double hydroxide (LDH), as well as aggregation-induced emission (AIE).

1.3.1 Hydrogen Peroxide-Based Chemiluminescence

1.3.1.1 Fenton/Fenton like System

The Fenton reaction, which produces hydroxyl radicals, is commonly utilized in the practice of scientific research as a source of radicals. It is the Fenton reaction that produces the light radiation that may be measured by a contemporary luminometer. The metal (M)-catalyzed breakdown of H_2O_2 results in the formation of the $^{\bullet}OH$ radical [30].

$$H_2O_2 + M^n \rightarrow M^{n+1} + {}^{\bullet}OH + {}^{-}OH \tag{1.6}$$
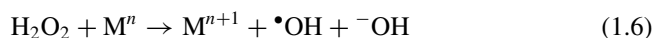
Initially, the Fenton reaction resulted in the creation of reactive oxygen species (ROS), which then resulted in the emission of CL. When the Fenton reagent is introduced, a flash of light can be seen. The singlet oxygen ($^1O_2$) is the emissive species that emits luminescence. The following is an example of the ROS production response resulting from the Fenton reaction [31]. Lin et al. used CDs for the enhancement of the Fenton system [32, 33].

$$^{\bullet}OH + H_2O_2 \rightarrow HO_2^{\bullet} + H_2O \tag{1.7}$$

$$^{\bullet}OH + {}^{\bullet}OH \rightarrow O_2(^1\Delta_g) + O_2 + H_2O \tag{1.8}$$

$$2HO_2^{\bullet} \rightarrow O_2(^1\Delta_g) + H_2O_2 + O_2 \tag{1.9}$$
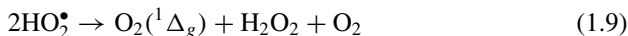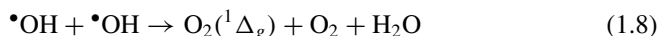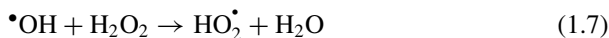
1.3.1.2 Peroxynitrite (ONOO⁻) CL System

Peroxynitrite (ONOO⁻) is a substantial nitric oxide derivative that has a wide range of uses in several fields. Even though peroxynitrite has a half-life of 10–20 ms, it is sufficiently stable to permeate biological membranes, diffuse one to two cell diameters, and interact with many essential biomolecules [34].

The coupling of NO$^{\bullet}$ and $^{\bullet}O_2^-$ radicals in biological systems is most likely the source of ONOO⁻ (Eq. 1.10) [35]. Furthermore, ONOO⁻ can be produced by mixing acidified H_2O_2 with nitrite in real-time. Nitrite reacts with hydrogen peroxide in an acidic medium to form ONOOH (Eq. 1.11), which is unstable and can be decomposed into ONOO⁻. Weak chemiluminescence was observed during the decomposition of ONOO⁻.

$$^{\bullet}O_2^- + NO^{\bullet} \rightarrow ONOO^- \tag{1.10}$$

$$H_2O_2 + HNO_2 \rightarrow ONOOH + H_2O \tag{1.11}$$

$$^-OH + ONOOH \rightarrow ONOO^- + H_2O \tag{1.12}$$
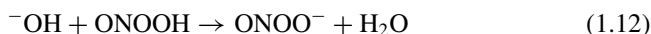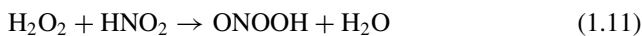
Several studies described how fluorescent compounds and NMs such as CdTe QDs, Mg–Al carbonate LDHs, CDs, and Au NPs improve the CL from ONOO⁻ [36–38]. Carbonate has been shown to react with ONOO⁻ to form the adduct $ONOOCO_2^-$, which decomposes fast into $^{\bullet}NO_2$ and the carbonate radical ($CO_3^{\bullet-}$), according to the literature. It is the conversion of the $CO_3^{\bullet-}$ radical into CO_2 in its excited form that causes the CL emission. CDs were shown to significantly increase the CL from the peroxynitrous acid (ONOOH) and CO_3^{2-} CL system described by Lin et al. [39] (Fig. 1.2).

1.3.1.3 Peroxysulfite (HSO₄⁻) CL System

Early in the twentieth century, the H_2O_2–HSO_3^- CL phenomena were identified by Stauff [40]. A peroxysulfite compound (HSO_4^- or $HOOSO_2^-$) is generated during the interaction of HSO_3^- with hydrogen peroxide. This compound is unstable and can be converted into the radicals $^{\bullet}SO_3^-$ and $^{\bullet}OH$ in the presence of H_2O_2. There
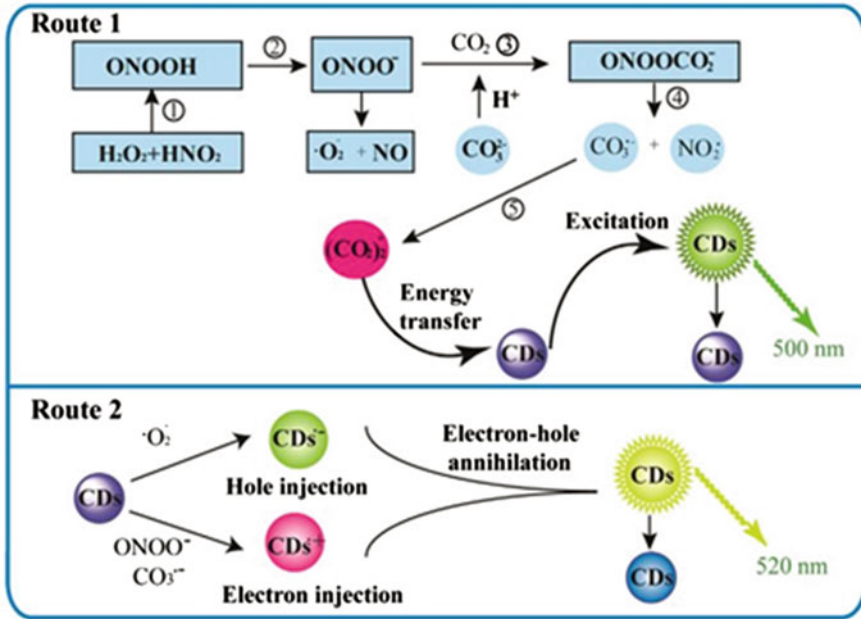
Fig. 1.2 Schematic of the CL process in the carbon nanodots–NaNO₂–H₂O₂–Na₂CO₃ system using a schematic diagram [39]

are many CL emitting molecules, such as SO_2^* and $^1O_2$ that have been produced through radical reactions [41, 42].

$$H_2O_2 + HSO_3^- \rightarrow HOOSO_2^- + H_2O \qquad (1.13)$$

$$HOOSO_2^- \rightarrow {}^\bullet OH + {}^\bullet SO_3^- \qquad (1.14)$$

$$2HO_2^\bullet \rightarrow {}^1O_2 + H_2O_2 \qquad (1.15)$$

$$HSO_3^- + {}^\bullet OH \rightarrow {}^\bullet SO_3^- + H_2O \qquad (1.16)$$

$$2{}^\bullet SO_3^- \rightarrow S_2O_6^{2-} \qquad (1.17)$$

$$S_2O_6^{2-} \rightarrow SO_2^* + SO_4^{2-} \qquad (1.18)$$

$$SO_2^* \rightarrow SO_2 + h\nu \qquad (1.19)$$
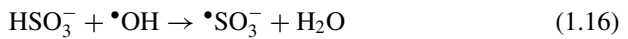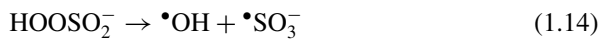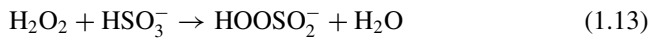
Xue et al. investigated the influence of CDs on the H_2O_2–HSO_3^- CL system and discovered that they had an enhanced effect [43]. In the H_2O_2–$NaHSO_3$ system, the CDs aided in the production of the emitter species SO_2^* and $^1O_2$ by facilitating the creation of these species (Fig. 1.3a). The CL of the H_2O_2–$NaHSO_3$ system was also improved using plasmonic luminous core–shell nanocomposites. According to [44], the combination of chemically produced excited states with surface plasmons results in an amplifying effect (Fig. 1.3b).

As a result of its high oxidation potential and proclivity to react through oxygen transfer, peroxysulfite (HSO_4^-) is one of the most promising oxidants for organic molecules in use today. Comparative to other common reagents such as peroxodisulphate and peroxomonophosphoric acid, it has also been shown to be a powerful oxidizing agent. Chaps. 5 and 6 will discuss the CL of HSO_4^- in further detail.

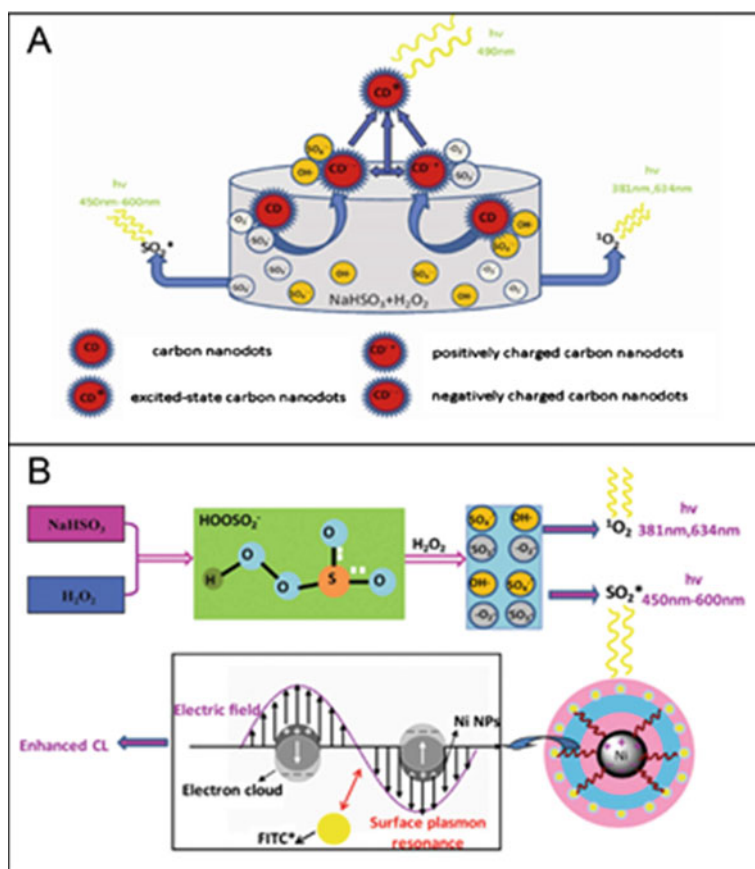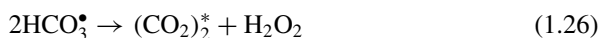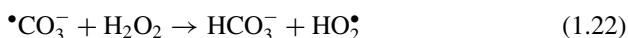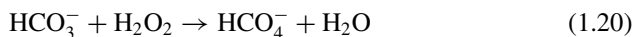**Fig. 1.3 a** The mechanism of the CL reaction in the H_2O_2–$NaHSO_3$ CDs system [43]; **b** the enhancement of CL intensity from the H_2O_2–$NaHSO_3$ system by plasmonic luminous nanocomposites [44]

1.3.1.4 Peroxymonocarbonate CL System

Peroxymonocarbonate (HCO_4^-) has been reported as a product of the interaction of hydrogen peroxide with bicarbonate since the 1980s. The breakdown of HCO_4^- resulted in the formation of CL. Carbonate radical was created as a result of it. The CL emitters includes singlet oxygen ($^1O_2$), singlet oxygen molecular pair [$(O_2)_2^*$], and excited double $(CO_2)_2^*$.

$$HCO_3^- + H_2O_2 \rightarrow HCO_4^- + H_2O \tag{1.20}$$

$$HCO_4^- \rightarrow {}^\bullet OH + {}^\bullet CO_3^- \tag{1.21}$$

$${}^\bullet CO_3^- + H_2O_2 \rightarrow HCO_3^- + HO_2^\bullet \tag{1.22}$$

$$HO_2^\bullet \rightarrow {}^\bullet O_2^- + H^+ \tag{1.23}$$

$$2HO_2^\bullet \rightarrow H_2O_2 + {}^1O_2 \tag{1.24}$$

$$4{}^\bullet O_2^- + 4H_2O \rightarrow (O_2)_2^* + 4{}^- OH + 2H_2O_2 \tag{1.25}$$

$$2HCO_3^\bullet \rightarrow (CO_2)_2^* + H_2O_2 \tag{1.26}$$

Many articles are focused on improving the peroxymonocarbonate system's ultra-weak CL. Cu/Ni metal NPs were used to increase the ultra-weak CL utilizing surface plasmons [45]. Protein-stabilized zinc/copper nanoclusters have been shown to greatly increase the CL of peroxymonocarbonate [46]. The catalysis of Zn/Cu@BSA nanoclusters and the metal surface plasmon-linked emission of excited $(CO_2)_2^*$ resulted in the enhanced CL.

1.3.1.5 Periodate CL System

The periodate produces soft oxidation products and has been used for the micro-analysis of different compounds [18, 47]. The periodate reacts with H_2O_2 in acidic, neutral, and basic mediums to produce $^1O_2$ as an emissive species [48]. Various researchers used different enhancers to amplify the CL intensity of this system [49]. Lin et al. [50] used sodium dodecylbenzene sulfonate (SDBS) modified layered double hydroxides to enhance the CL intensity of the IO_4^-–H_2O_2 system (Fig. 1.4a). Our group used nitrogen-doped CDs for the enhancement of this system [51, 52]. Shah et al. [53] reviewed the details on the improvement and application of the periodate-peroxide CL system recently.
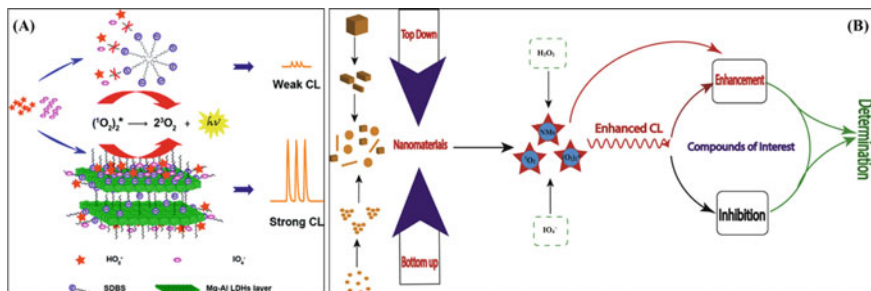
Fig. 1.4 a The mechanism of CL enhancement by sodium dodecylbenzene sulfonate (SDBS)-modified LDHs [50]. **b** Detailed about the improvement and application of the periodate-peroxide CL system [53]

1.3.2 The Role of NPs in the CL System

Because of their possible application in CL, nanomaterials (NMs) with good optical and electrical characteristics have gotten a lot of attention. Many studies have attempted to employ nanoparticles (NPs) to boost CL in various ultra-weak CL systems, including H_2O_2–$NaHCO_3$, H_2O_2–$NaIO_4$, H_2O_2–$NaNO_2$, H_2O_2–$NaClO$, H_2O_2–$NaHSO_3$, and others [52, 54, 55]. NPs can directly participate in redox reactions or operate as catalysts or energy acceptors in CL processes, to boost CL intensity. The role of NPs in the CL system is summarized below.

1.3.2.1 Direct CL

Excitons being a bound state of the introduced electrons and holes in the conduction and valence bands of the nanomaterials, respectively, is usually generated during a CL reaction involving nanomaterials. The relaxation of excitons resulted in the NPs-based CL. The CL system of CdTe QDs–calcein–$K_3Fe(CN)_6$ was developed by Zhang et al. [56], in which CdTe QDs directly participating in the reaction by oxidized to excited CdTe QDs by $K_3Fe(CN)_6$. The excited CdTe QDs are capable of transferring their energy to the calcein acceptor through a process known as energy transfer.

$$K_3Fe(CN)_6 + CdTeQDs \rightarrow K_4Fe(CN)_6 + CdTeQDs^* \qquad (1.27)$$

$$CdTeQDs^* + Calcein \rightarrow CdTeQDs + Calcein^* \qquad (1.28)$$

$$Calcein^* \rightarrow Calcein + h\nu \qquad (1.29)$$
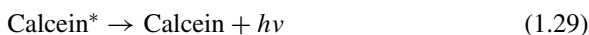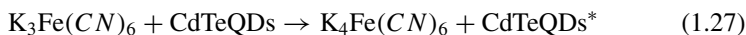
Lin et al. discovered carbon dots could react with acidic $KMnO_4$ and cerium (IV) to emit CL [57]. Such oxidants could cause holes to form in the CDs. The injection of holes into carbon dots by an oxidant increases the number of holes in the CDs and speeds up electron–hole annihilation, resulting in energy release in the form of CL emission.

Li et al. [58] discovered that CdTe/CdS/ZnS QDs exhibit novel CL performance with KIO_4. The direct oxidation of CdTe/CdS/ZnS QDs by dissolved O_2 produced a superoxide radical ($^\bullet O_2^-$), $QD(e_{1se}^-)$ and $QD(h_{1sh}^+)$ excitons were generated by injecting electrons and holes from $^\bullet O_2^-$ and $^\bullet OH$ radicals, respectively, resulting in QDs* in the excited state.

$$QD + O_2 \rightarrow {}^\bullet O_2^- + QD^{+\bullet} \tag{1.30}$$

$$2{}^\bullet O_2^- + 2H_2O \rightarrow {}^1O_2 + 2^-OH + H_2O_2 \tag{1.31}$$

$${}^\bullet O_2^- + H_2O_2 \rightarrow {}^-OH + {}^\bullet OH + O_2 \tag{1.32}$$

$$QD + {}^\bullet O_2^- \rightarrow O_2 + QD(e_{1se}^-) \tag{1.33}$$

$$QD + {}^\bullet OH \rightarrow {}^-OH + QD(h_{1sh}^+) \tag{1.34}$$

$$QD(e_{1se}^-) + QD(h_{1sh}^+) \rightarrow QD^* \tag{1.35}$$

$$QD^* \rightarrow QD + h\nu \tag{1.36}$$
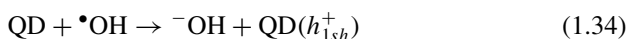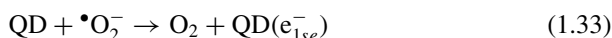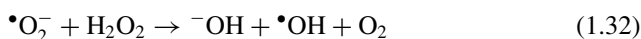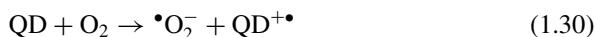
1.3.2.2 CL Catalyst

Many research groups have investigated the catalytic effect of NMs. The NMs-based catalytic CL system was developed as an analytical chemical sensor. The catalytic effect or enhancement of CL processes by NMs is attributed to the formation of reactive oxygen radicals such as $^\bullet OH$ radical, and $^\bullet O_2^-$ radical, which are initiated by catalysts or enhancers. The NMs, particularly those containing transition metals, exhibit a significant catalytic outcome on H_2O_2-based CL systems, such as luminol–H_2O_2 and lucigenin–H_2O_2.

Furthermore, CL responses varied depending on the morphology and composition of catalytic NMs. Take, for example, the work of Li et al. [59], who investigated the CL response of triangular Au NPs in the luminol–H_2O_2 system and contrasted it with the reaction of spherical Au NPs. According to the researchers, when compared to spherical Au NPs, triangular Au NPs exhibited much higher catalytic activity due to a higher surface-to-volume ratio and a greater number of active surface sites. These

triangular Au NPs exhibited improved activity in the formation of reactive oxygen radicals and electron transferability on their surfaces. It has also been demonstrated that the CL system of luminol–H_2O_2 catalyzed by triangular Au NPs has excellent analytical application for the detection of aminothiols.

Because of the redox feature of the distinct electron and hole states of QDs, they can act as a catalyst in CL systems. With QDs, the injection of holes from a strong oxidizer or electrons from a reducer can alter the valence and conduction bands of the QDs. During the injection procedure, ROS such as $^\bullet OH$, $^\bullet O_2{}^-$ radicals will be created. By radical reactions, these radical species can oxidize CL reagents, resulting in increased CL, or generating CL emitters. L-cysteine capped Mn-doped ZnS QDs have previously been shown to improve CL of the H_2O_2-NaClO system [60]. The increased CL of NaClO–H_2O_2 is due to the sensitizer's catalysis in creating reactive intermediates as well as the electron-transfer mechanism [53].

The CL's efficiencies were affected by the types of reactants and catalysts used. Chen et al. [61] demonstrated improved CL of the H_2O_2–$NaHCO_3$ system with the addition of CdTe QDs. The excited CdTe QDs were produced by combining the hole and electron injected QDs, which cause the enhancement of CL. They investigated the size effect of various catalyst types on the CL of the H_2O_2–$NaHCO_3$ system. CdTe QDs were compared to CdSe and CdS QDs with emission wavelengths of 549 and 607 nm, respectively. They discovered that CdTe QDs with a larger size than CdSe and CdS quantum dots at the same concentration could significantly increase CL intensity.

1.4 Conclusion

The purpose of this chapter is to introduce the basic principles of chemiluminescence and the development of ultra-weak CL systems, focusing on the CL from the decomposition of peroxynitrite ($ONOO^-$), peroxymonocarbonate ($HCO_4{}^-$), peroxysulfite ($HSO_4{}^-$), and periodate ($IO_4{}^-$), as well as the application of NPs to develop new reactive oxygen (ROS) CL systems and enhance the weak CL systems. More information on the CL of these inorganic compounds can be found in Chaps. 2, 3, 4, 5, 6, 7, 8, 9, 10 and 11 of this book.

References

1. Musfeldt JL (1998) Luminescence of solids edited by D. R. Vij. Plenum Press: New York. J Am Chem Soc 121:4310–4310. https://doi.org/10.1021/ja985728i
2. Cadenas E (1982) Chemical and biological generation of excited states. Herausgegeben von W. Adam und G. Cilento. Academic Press, New York. Angew Chem 96:452. https://doi.org/10.1002/ange.19840960631
3. Cormier M (2013) Chemiluminescence and bioluminescence. Springer Science and Business Media

4. Andreotti PE (1988) Chemiluminescence: principles and applications in biology and medicine. In: Campbell AK (ed) Ellis Horwood, Chichester, UK. https://doi.org/10.1002/jps.2600780920
5. Blum LJ (1997) Bio- and chemi-luminescent sensors
6. Chen H, Gao Q, Li J, Lin J-M (2016) Graphene materials-based chemiluminescence for sensing. J Photochem Photobiol C: Photochem Rev 27:54–71. https://doi.org/10.1016/j.jphotochemrev.2016.04.003
7. Shah SNA, Lin J-M (2017) Recent advances in chemiluminescence based on carbonaceous dots. Adv Colloid Interface Sci 241:24–36. https://doi.org/10.1016/j.cis.2017.01.003
8. Yang M, Huang J, Fan J, Du J, Pu K, Peng X (2020) Chemiluminescence for bioimaging and therapeutics: recent advances and challenges. Chem Soc Rev 49:6800–6815. https://doi.org/10.1039/D0CS00348D
9. Al Mughairy B, Al-Lawati HAJ (2020) Recent analytical advancements in microfluidics using chemiluminescence detection systems for food analysis. TrAC, Trends Anal Chem 124:115802. https://doi.org/10.1016/j.trac.2019.115802
10. Birks JW (1989) Chemiluminescence and photochemical reaction detection in chromatography. VCH Publishers, New York
11. Rongen HAH, Hoetelmans RMW, Bult A, Van Bennekom WP (1994) Chemiluminescence and immunoassays. J Pharm Biomed Anal 12:433–462. https://doi.org/10.1016/0731-7085(94)80027-8
12. Yu W, Zhao L (2021) Chemiluminescence detection of reactive oxygen species generation and potential environmental applications. TrAC, Trends Anal Chem 136:116197. https://doi.org/10.1016/j.trac.2021.116197
13. Dou X, Zhang Q, Shah SNA, Khan M, Uchiyama K, Lin J-M (2019) MoS2-quantum dot triggered reactive oxygen species generation and depletion: responsible for enhanced chemiluminescence. Chem Sci 10:497–500. https://doi.org/10.1039/C8SC03511C
14. Aslan K, Geddes CD (2009) Metal-enhanced chemiluminescence: advanced chemiluminescence concepts for the 21st century. Chem Soc Rev 38:2556–2564. https://doi.org/10.1039/b807498b
15. Chen J, Qiu H, Zhao S (2020) Fabrication of chemiluminescence resonance energy transfer platform based on nanomaterial and its application in optical sensing, biological imaging and photodynamic therapy. TrAC, Trends Anal Chem 122:115747. https://doi.org/10.1016/j.trac.2019.115747
16. Ishimaru N, Lin J-M, Yamada M (1998) Luminol-free chlorine chemiluminescence in an oil-in-water microemulsion medium. Anal Commun 35:67–69. https://doi.org/10.1039/A708423D
17. Tsukada S, Miki H, Lin J-M, Suzuki T, Yamada M (1998) Chemiluminescence from fluorescent organic compounds induced by cobalt(II) catalyzed decomposition of peroxomonosulfate. Anal Chim Acta 371:163–170. https://doi.org/10.1016/S0003-2670(98)00356-0
18. Evmiridis NP, Vlessidis AG, Thanasoulias NC (2007) Chemical analysis through CL-Detection Assisted By Periodate Oxidation. Bioinorg Chem Appl 2007:092595. https://doi.org/10.1155/2007/92595
19. Schuster GB (1979) Chemiluminescence of organic peroxides. Conversion of ground-state reactants to excited-state products by the chemically initiated electron-exchange luminescence mechanism. Acc Chem Res 12:366–373. https://doi.org/10.1021/ar50142a003
20. Chen H, Lin L, Li H, Lin J-M (2014) Quantum dots-enhanced chemiluminescence: mechanism and application. Coord Chem Rev 263:86–100. https://doi.org/10.1016/j.ccr.2013.07.013
21. Gnaim S, Scomparin A, Eldar-Boock A, Bauer CR, Satchi-Fainaro R, Shabat D (2019) Light emission enhancement by supramolecular complexation of chemiluminescence probes designed for bioimaging. Chem Sci 10:2945–2955. https://doi.org/10.1039/c8sc05174g
22. Song H, Su Y, Zhang L, Lv Y (2019) Quantum dots-based chemiluminescence probes: an overview. Luminescence 34:530–543. https://doi.org/10.1002/bio.3633
23. Dou X, Zheng Y, Uchiyama K, Lin J-M (2016) Fluorescent carbon nanoparticles: Mimicking hydrogen peroxide properties in a chemiluminescence system. Chem Commun 52:14137–14140. https://doi.org/10.1039/c6cc07285b

24. Ma AJ, Chang YT, Lin WY (2013) A kinetic treatment of stopped-flow time courses for multiple chemiluminescence of the KIO_4-luminol-Mn^{2+} system. Luminescence 28:355–362. https://doi.org/10.1002/bio.2389

25. Huang TY, Lin WY (2011) A stopped-flow study of the dual chemiluminescence for the luminol-KIO_4-Mn^{2+} system in strong alkaline solutions. Luminescence 26:118–124. https://doi.org/10.1002/bio.1193

26. Chen X, Tian X, Shin I, Yoon J (2011) Fluorescent and luminescent probes for detection of reactive oxygen and nitrogen species. Chem Soc Rev 40:4783–4804. https://doi.org/10.1039/c1cs15037e

27. Chen YC, Lin WY (2010) Enhancement of chemiluminescence of the KIO4–luminol system by gallic acid, acetaldehyde and Mn^{2+}: application for the determination of catecholamines. Luminescence 25:43–49. https://doi.org/10.1002/bio.1141

28. Lin Z, Chen H, Lin J-M (2013) Peroxide induced ultra-weak chemiluminescence and its application in analytical chemistry. Analyst 138:5182–5193. https://doi.org/10.1039/c3an00910f

29. Zhang M, Yao Q, Guan W, Lu C, Lin J-M (2014) Layered double hydroxide-supported carbon dots as an efficient heterogeneous Fenton-like catalyst for generation of hydroxyl radicals. J Phys Chem C 118:10441–10447. https://doi.org/10.1021/jp5012268

30. Lu C, Song G, Lin J-M (2006) Reactive oxygen species and their chemiluminescence-detection methods. TrAC, Trends Anal Chem 25:985–995. https://doi.org/10.1016/j.trac.2006.07.007

31. Aristova N, Ivanova I, Trofimova S, Knyazev D, Piskarev I (2011) Influence of luminol on the chemiluminescence intensity in Fenton's reaction. High Energ Chem 45:505–509. https://doi.org/10.1134/S0018143911060038

32. Shah SNA, Lin L, Zheng Y, Zhang D, Lin J-M (2017) Redox cycling of iron by carbon dot enhanced chemiluminescence: mechanism of electron–hole induction in carbon dot. Phys Chem Chem Phys 19:21604–21611. https://doi.org/10.1039/C7CP03724D

33. Shah SNA, Dou X, Khan M, Uchiyama K, Lin J-M (2019) N-doped carbon dots/H2O2 chemiluminescence system for selective detection of Fe2+ ion in environmental samples. Talanta 196:370–375. https://doi.org/10.1016/j.talanta.2018.12.091

34. Pacher P, Beckman JS, Liaudet L (2007) Nitric oxide and peroxynitrite in health and disease. Physiol Rev 87:315–424. https://doi.org/10.1152/physrev.00029.2006

35. Radi R, Cosgrove TP, Beckman J, Freeman B (1993) Peroxynitrite-induced luminol chemiluminescence. Biochem J 290:51–57. https://doi.org/10.1042/bj2900051

36. Dong S, Guan W, Lu C (2013) Quantum dots in organo-modified layered double hydroxide framework-improved peroxynitrous acid chemiluminescence for nitrite sensing. Sens Actuators, B Chem 188:597–602. https://doi.org/10.1016/j.snb.2013.07.060

37. Adegoke O, Nyokong T (2013) Probing the sensitive and selective luminescent detection of peroxynitrite using thiol-capped CdTe and CdTe@ ZnS quantum dots. J Lumin 134:448–455. https://doi.org/10.1016/j.jlumin.2012.08.002

38. Zhang H, Zhang L, Lu C, Zhao L, Zheng Z (2012) CdTe nanocrystals-enhanced chemiluminescence from peroxynitrous acid–carbonate and its application to the direct determination of nitrite. Spectrochim Acta Part A Mol Biomol Spectrosc 85:217–222. https://doi.org/10.1016/j.saa.2011.09.063

39. Lin Z, Dou X, Li H, Ma Y, Lin J-M (2015) Nitrite sensing based on the carbon dots-enhanced chemiluminescence from peroxynitrous acid and carbonate. Talanta 132:457–462. https://doi.org/10.1016/j.talanta.2014.09.046

40. Stauff J (1967) Jaeschke W (1975) A chemiluminescence technique for measuring atmospheric trace concentrations of sulfur dioxide. Atmos Environ 9:1038–1039. https://doi.org/10.1016/0004-6981(75)90028-1

41. Zheng Y, Dou X, Li H, Lin J-M (2016) Bisulfite induced chemiluminescence of gC3N4 nanosheets and enhanced by metal ions. Nanoscale 8:4933–4937. https://doi.org/10.1039/C5NR08943C

42. Shah SNA, Zheng Y, Li H, Lin J-M (2016) Chemiluminescence character of ZnS quantum dots with bisulphite-hydrogen peroxide system in acidic medium. J Phys Chem C 120:9308–9316. https://doi.org/10.1021/acs.jpcc.6b01925

43. Xue W, Lin Z, Chen H, Lu C, Lin J-M (2011) Enhancement of ultraweak chemiluminescence from reaction of hydrogen peroxide and bisulfite by water-soluble carbon nanodots. J Phys Chem C 115:21707–21714. https://doi.org/10.1021/jp207554t

44. Chen H, Xue W, Lu C, Li H-F, Zheng Y, Lin J-M (2013) Plasmonic luminescent core–shell nanocomposites-enhanced chemiluminescence arising from the decomposition of peroxomonosulfite. Spectrochim Acta Part A Mol Biomol Spectrosc 116:355–360. https://doi.org/10.1016/j.saa.2013.07.057

45. Chen H, Li R, Li H, Lin J-M (2012) Plasmon-assisted enhancement of the ultraweak chemiluminescence using Cu/Ni metal nanoparticles. J Phys Chem C 116:14796–14803. https://doi.org/10.1021/jp303092d

46. Chen H, Lin L, Li H, Li J, Lin J-M (2015) Aggregation-induced structure transition of protein-stabilized zinc/copper nanoclusters for amplified chemiluminescence. ACS Nano 9:2173–2183. https://doi.org/10.1021/acsnano.5b00141

47. Vlessidis AG, Evmiridis NP (2009) Periodate oxidation and its contribution to instrumental methods of micro-analysis—a review. Anal Chim Acta 652:85–127. https://doi.org/10.1016/j.aca.2009.06.065

48. Li M, Lee SH, Bae ZU, Lee KP, Park YC, Lee MS (2004) Optical sensor for the determination of glucose based on KIO4 chemiluminescence detection. J Fluoresc 14:597–601. https://doi.org/10.1023/B:JOFL.0000039346.35328.d3

49. Shah SNA, Shah AH, Dou X, Khan M, Lin L, Lin J-M (2019) Radical-triggered chemiluminescence of phenanthroline derivatives: an insight into radical-aromatic interaction. ACS Omega 4:15004–15011. https://doi.org/10.1021/acsomega.9b01785

50. Zhang M, Han D, Lu C, Lin J-M (2012) Organo-modified layered double hydroxides switch-on chemiluminescence. J Phys Chem C 116:6371–6375. https://doi.org/10.1021/jp300879c

51. Shah SNA, Li H, Lin J-M (2016) Enhancement of periodate-hydrogen peroxide chemiluminescence by nitrogen doped carbon dots and its application for the determination of pyrogallol and gallic acid. Talanta 153:23–30. https://doi.org/10.1016/j.talanta.2016.02.056

52. Zheng Y, Zhang D, Shah SNA, Li H, Lin J-M (2017) Ultra-weak chemiluminescence enhanced by facilely synthesized nitrogen-rich quantum dots through chemiluminescence resonance energy transfer and electron hole injection. Chem Commun 53:5657–5660. https://doi.org/10.1039/C7CC02041D

53. Shah SNA, Khan M, Rehman ZU (2020) A prolegomena of periodate and peroxide chemiluminescence. TrAC, Trends Anal Chem 122:115722. https://doi.org/10.1016/j.trac.2019.115722

54. Li R, Chen H, Li Y, Lu C, Lin J-M (2012) Enhancing effect of alcoholic solvent on hydrosulfite-hydrogen peroxide chemiluminescence system. J Phys Chem A 116:2192–2197. https://doi.org/10.1021/jp300012t

55. Wu J, Wang X, Lin Y, Zheng Y, Lin J-M (2016) Peroxynitrous-acid-induced chemiluminescence detection of nitrite based on microfluidic chip. Talanta 154:73–79. https://doi.org/10.1016/j.talanta.2016.03.062

56. Kang J, Li X, Geng J, Han L, Tang J, Jin Y, Zhang Y (2012) Determination of hyperin in seed of Cuscuta chinensis Lam. by enhanced chemiluminescence of CdTe quantum dots on calcein/K3Fe (CN) 6 system. Food Chem 134:2383–2388. https://doi.org/10.1016/j.foodchem.2012.04.055

57. Lin Z, Xue W, Chen H, Lin J-M (2012) Classical oxidant induced chemiluminescence of fluorescent carbon dots. Chem Commun 48:1051–1053. https://doi.org/10.1039/c1cc15290d

58. Li Y, Zheng Y-Z, Zhang D-K, Li H-F, Ma Y, Lin J-M (2017) Enhanced chemiluminescence from reactions between CdTe/CdS/ZnS quantum dots and periodate. Chin Chem Lett 28:184–188. https://doi.org/10.1016/j.cclet.2016.07.020

59. Li Q, Liu F, Lu C, Lin J-M (2011) Aminothiols sensing based on fluorosurfactant-mediated triangular gold nanoparticle-catalyzed luminol chemiluminescence. J Phys Chem C 115:10964–10970. https://doi.org/10.1021/jp200711a

60. Zhou Y, Chen H, Ogawa N, Lin J-M (2011) Chemiluminescence from NaClO–H2O2 and enhanced by L-cysteine capped Mn-doped ZnS quantum-dots. J Lumin 131:1991–1997. https://doi.org/10.1016/j.jlumin.2011.04.019

61. Chen H, Lin L, Lin Z, Guo G, Lin J-M (2010) Chemiluminescence arising from the decomposition of peroxymonocarbonate and enhanced by CdTe quantum dots. J Phys Chem A 114:10049–10058. https://doi.org/10.1021/jp104060x

Chapter 2
Ultra-Weak Chemiluminescence from the Decomposition of Peroxymonocarbonate

Hui Chen, Syed Niaz Ali Shah, and Jin-Ming Lin

Abstract In this chapter, we will discuss the preparation methods for peroxymonocarbonate ions (HCO_4^-). The reaction of bicarbonate with different peroxides especially with hydrogen peroxide to form HCO_4^- at different pH solutions will be studied. The data and results will be interpreted based on kinetic and spectroscopic evidence, that how HCO_4^- ions were produced. Furthermore, the ultra-weak chemiluminescence (CL) generated from the decomposition of HCO_4^- will be discussed in detail. We will also consider the enhancement of peroxymonocarbonate ions containing CL systems with different enhancers, i.e., fluorescent compounds, metallic complexes, nanoparticles, and other molecules added into the system. The role of the generation of different free radicals and the CL mechanism revealed based on the experimental results and literature proofs will be discussed.

Keywords Bicarbonate · Peroxymonocarbonate · Ultra-weak chemiluminescence · Hydrogen peroxide · Mechanism

2.1 Introduction

As a buffer solution for the chemiluminescence (CL) medium, carbonate (CO_3^{2-}) or bicarbonate (HCO_3^-) has frequently been used. When CO_3^{2-} coexisted with a strong oxidizing agent in the basic solution, it was reported to be a luminous species. Many studies have shown that CO_3^{2-} or HCO_3^- not only acts as a buffer reagent but also as a CL sensitizer [1–4].

In their examination of the oxidation of chemical warfare agents, Drago et al. hypothesized that the HCO_3^- is an efficient activator for hydrogen peroxide (H_2O_2) [5]. Using NMR evidence, they established the existence of peroxymonocarbonate (HCO_4^-) ions generated by HCO_3^- reacting with H_2O_2. Richardson et al. explored

H. Chen
College of Materials Science and Technology, Beijing Forestry University, Beijing 100083, China

S. N. A. Shah · J.-M. Lin (✉)
Department of Chemistry, Tsinghua University, Beijing 100084, China
e-mail: jmlin@mail.tsinghua.edu.cn

the kinetics, equilibrium, and mechanism of HCO_3^- activation of H_2O_2 for sulfide oxidation and discovered HCO_4^- as a bicarbonate active species [6]. It was discovered that when H_2O_2 and HCO_3^- were combined at 25 °C in aqueous or ethanol/water solutions at neutral pH, the HCO_4^- formed in equilibrium with its reactants. An anionic peracid, HCO_4^- with no metal ions were shown to be a reasonably reactive heterolytic oxidizing agent [7]. At 25 °C, the effective equilibrium constant $K_1 = 27 \pm 1$, and the perceived equilibration rate constant was $2.4 \pm 0.1 \times 10^{-3}\,s^{-1}$. The electrode potential for the HCO_4^-/HCO_3^- couple was 1.8 ± 0.1 V (vs normal hydrogen electrode) and the half-life for production of HCO_4^- in water: ethanol (1:1.76, v/v) was roughly 300 s [6]. The HCO_3^--peroxide system's catalytic effectiveness possibly will be increased by substituting a more soluble supply of NH_4HCO_3 and ethanol for HCO_3^- and tert-butyl alcohol, respectively.

A probable CL mechanism, in which the CO_3^{2-}/HCO_3^- were tackled by $^\bullet O_2^-$ radicals, resulting in carbonate ($CO_3^{\bullet-}$) radicals was proposed in our previous studies [3, 4]. The excited triplet dimers of CO_2 molecules ((CO_2)$_2$*) were formed when $CO_3^{\bullet-}$ recombined. When this unstable intermediate released its energy by decomposing to CO_2, the CL was freed. Meanwhile, these findings led us to believe that the active species HCO_4^- exhibits CL properties comparable to peroxymonosulfate (HSO_5^-), a CL analytical reagent that was utilized several years ago [8]. It has been shown that HCO_4^-, a CO_2/HCO_3^- derived oxidant, is a two-electron oxidant, unlike the $^\bullet CO_3^-$ radical [9]. The HCO_4^- system's components are low-cost and environmentally benign. Since HCO_4^- is a strong oxidizing agent, it has been frequently employed in a range of processes, including those involving methionine [10], alkenes [7], and sulfide [6].

Toxic or environmentally hazardous byproducts were common drawbacks of many CL systems used for analysis applications. The peroxymonocarbonate system, also known as bicarbonate-activated peroxide, provided a straight forward, low-cost, and comparatively non-toxic alternative to other oxidizing agents. Because the HCO_4^- oxidizing agent was unstable and hydrolyzed promptly, producing H_2O_2 and HCO_3^-, storing HCO_4^- ions was difficult. As a result, on-line HCO_4^- preparation was expected to be the preferred method in most applications.

In this chapter, we will introduce the HCO_4^- ion as an oxidizing agent in different CL systems, which were exploited by different research groups recently. HCO_4^- ions were prepared on-line by introducing a continuous flowing stream with no gap in the channel. Simultaneously, utilizing a peristaltic pump, it was simple to move along a multichannel stream and regulate the flow rate for the proper on-line synthesis time. Using NMR, we can confirm this active carbon–oxygen intermediate was formed during the mixing of HCO_3^- and H_2O_2. The ultra-weak CL studied from the decomposition of HCO_4^- can be greatly enhanced by fluorescent compound [11], Eu(II) complex [12], $NaYF_4$:Yb^{3+}/Er^{3+} nanoparticle [13], and potassium permanganate [14]. The CL mechanism for the formation of $^1O_2$ for HCO_4^- was explored in detail. The HCO_4^- CL system is a simple, low-cost, and largely non-toxic substitute for traditional oxidizing agents that could be employed in a moderate, neutral pH environment.

2.2   On-Line Preparation of Peroxymonocarbonate

Flow injection analysis (FIA) is a sort of analysis that can be done quickly and continuously. Because storage of the unstable HCO_4^- is difficult, on-line HCO_4^- generation is to be expected the best option. The system enables continuous flow analysis to be accomplished quickly and easily by infusing into a carrier stream and performing instant discrete sampling. Due to the turbulent nature of the continuous flowing stream, distinct instant sampling results in geometrically well-defined portions of sample solution within the flowing stream. The on-line mixing is more successful when FIA presents a continuous flowing stream into the channel. Simultaneously, the peristaltic pump makes it simple to adjust the flow rate for the proper on-line preparation time.

The HCO_4^- solution was made on the spot by combining HCO_3^- and hydrogen peroxide in a three-way piece (Fig. 2.1). It comprises a two-line peristaltic pump. To create on-line HCO_4^- ions, H_2O_2 in a 1:1.76 water: ethanol solution and HCO_3^- were fed into the flow lines. The mixing time period, as well as the flow rates of HCO_3^- and H_2O_2, are critical in the on-line generation of the HCO_4^- solution. HCO_4^- ions were quantified using the intensity of CL emission. Too much or too little time did not result in the generation of enough HCO_4^- ions to cause CL emission. The lifetime of the active carbon–oxygen intermediates is also a crucial element in determining the CL signal in flow injection CL emission since transient light emission is scrutinized. The half-life of HCO_4^- ion formation in water: ethanol (1:1.76, v/v) medium has been reported to be around 300 s [6], indicating that the HCO_4^- is comparatively long-lasting in an organic solvent. The point of mixing was selected to be inside the CL cell because the HCO_4^- has such a short lifespan.

In the meantime, the quantities of mixing reagents (H_2O_2 and HCO_3^-) could have a direct impact on on-line HCO_4^- ion preparation. Gaps in the flow line can be caused by high H_2O_2 concentrations. HCO_4^- ions cannot be produced at very low H_2O_2 concentrations. The best possible concentration of H_2O_2 was observed to be 2 mol/L. Organic reagents such as acetone, acetonitrile, and ethanol, as well as carbonates like ammonium bicarbonate, $NaHCO_3$, potassium bicarbonate, Na_2CO_3, and K_2CO_3, were investigated. Table 2.1 summarizes the CL signals obtained in various mixing
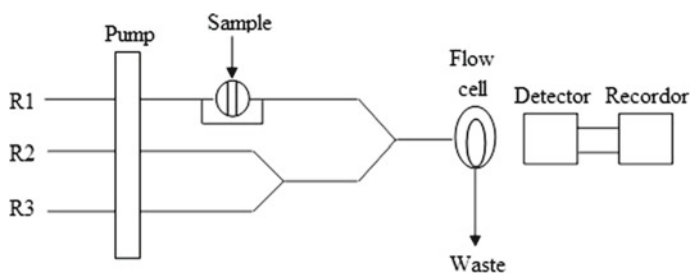

Fig. 2.1 Flow injection diagram for the HCO_4^- CL system, R_1 ethanol, R_2 H_2O_2 (in organic cosolvent), R_3 NH_4HCO_3. Copyright 2008, with permission from Elsevier Ref. [11]

Table 2.1 The influence of various organic cosolvents and CO_3^{-} salts on CL signals

Substance	NaHCO₃	KHCO₃	NH₄HCO₃	Na₂CO₃	K₂CO₃
Acetonitrile					
Acetone					
Ethanol					

Copyright 2008, with permission from Elsevier [11]

Except for the solvents and carbonate salts, all the CL readings in this table were noted under the same experimental circumstances. The X-axis represents the time scale in s and the Y-axis represents the CL strength for each CL signal (counts)

solutions. These solutions affected the CL intensity. The peak height and kinetic profile for each mixing solution were considerably different when different carbonate salts and organic solvents were used. The reaction was immediate when ethanol was there in the CL system, and all CL signals were highly crisp. The CL intensity was maximum when ethanol and ammonium bicarbonate were combined. It was discovered that ethanol can create hydrogen bonds with HCO_4^-, causing HCO_4^- to decompose quickly. Ammonium bicarbonate was employed instead of group 1 salts because of its reduced solubility in mixed solvents; the best concentration of NH_4HCO_3 for on-line HCO_4^- production was 0.05 M. Additionally, the maximum HCO_4^- was attained using a 35 cm mixing coil and a 1.1 mL min^{-1} flow rate.

HCO_3^--peroxide in water/alcohol solvents was investigated by ^{13}C-NMR using 99 percent ^{13}C-enriched $NaHCO_3$. The results of the ^{13}C-NMR spectroscopy substantially support the generation of HCO_4^- ion in the on-line flow system (Fig. 2.2) [12]. For all studies, H_2O_2 concentrations of nearly 2.0 M were used, with $[H^{13}CO_3^-] = 0.1$ M. In addition to the bicarbonate peak at 163.6 ppm, a solitary extra peak at 161.7 ppm inferred as HCO_4^- was detected. Investigation of the time-dependent peak in

Fig. 2.2 ^{13}C-NMR spectra of $NaH^{13}CO_3$ (0.05 M) in 1:1.76 (*water* ethanol, v/v) solution at 25 °C with $[H_2O_2] = 2$ M. The *times* shown were for the acquisition to be completed from the time of mixing. Copyright 2006, with permission from Wiley Ref. [12]

the ethanol: water ratio was conducted. For up to 20 min, unstable peroxymonocarbonate ions can be found. As a result, online synthesis of HCO_4^- reactive species provides a trustworthy intermediate for further research.

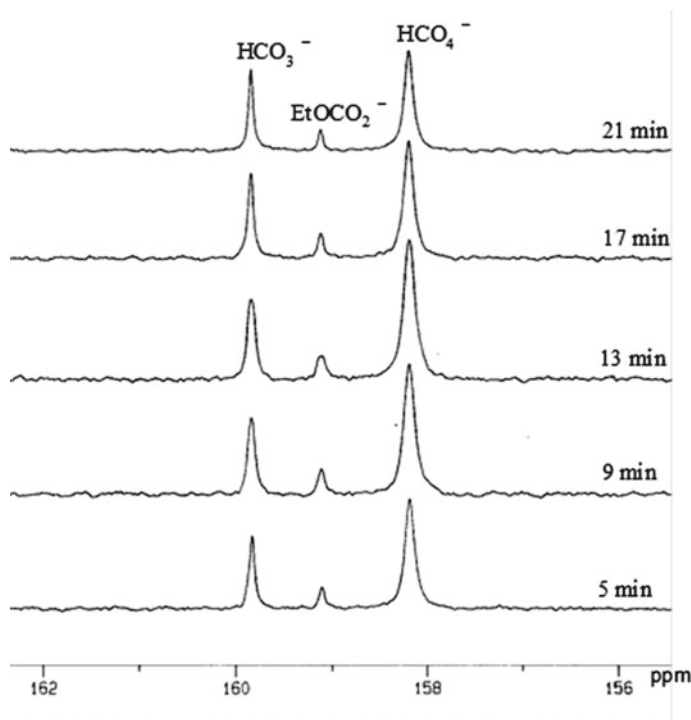## 2.3 CL Phenomenon from Peroxymonocarbonate Decomposition

2.3.1 Singlet Oxygen Produced by Peroxymonocarbonate Decomposition

It was confirmed that during its decomposition, HCO_4^- produces reactive intermediates that cause CL emission. The singlet oxygen ($^1O_2$) was initially considered based on the CL spectrum and Adam and Mehta's research [9]. The quenching effect and the boosting effect were used to see if the HCO_4^- reaction's CL emission is mediated by $^1O_2$ or not. NaN_3, a recognized scavenger of singlet oxygen [15], effectively suppressed the intense luminescence. It is well recognized that luminous reagents such as lucigenin, luminol, and cypridina luciferin analog (CLA) may react with reactive oxygen species (ROS) to produce sharp CL emissions. CLA has been utilized to determine $^1O_2$ in particular as a CL probe [16]. These findings revealed that these luminous reagents significantly increased CL intensity, particularly CLA. The CL that was detected resulted from the production of $^1O_2$. It is said that because $^1O_2$ has larger energy than ground-state triplet O_2, it can give up that energy through luminescence [17]. Several CL investigations involving $^1O_2$ have been published in the previous 30 years [18–21]. The CL wavelength of $^1O_2$ was measured at 476 nm which could explain the production of the singlet oxygen species.

HCO_4^- is an extremely active species. The homolysis of the O–O bond, according to the estimates from the thermodynamic analysis was the activation step [22]. The probable mechanism to produce active intermediates is described in Scheme 2.1. The ammonium works as a Lewis acid in this reaction, stabilizing the carbonate leaving part and facilitating the breaking of the O–O bond. Because the ammonium does not need to go through redox, the electron spin trapping (ESR)-active species created as the reaction progresses must be mostly unrelated. Ammonium peroxycarbonate complexes are involved in all of the mechanistic routes that we believe are most likely. Vibrational spectroscopy has been used to produce and analyze peroxycarbonate complexes of rhodium [23], platinum [24], and manganese [13]. In solution, the complexes are highly unstable. A perhydroxyl radical can cause radical recombination.

$$H_2O_2 + HCO_3^- \rightleftharpoons H_2O + HCO_4^- \tag{2.1}$$

$$HOOCOO^- \rightarrow CO_3^{\cdot -} + \cdot OH \tag{2.2}$$

$$H_2O_2 + HCO_3^- \rightleftharpoons H_2O + HCO_4^-$$
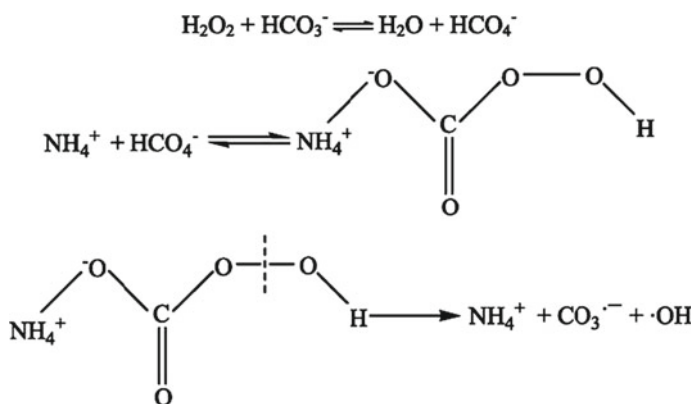
Scheme 2.1 A potential mechanism for the effective intermediate formed by the reaction of NH_4HCO_3 and H_2O_2

$$H_2O_2 + CO_3^{\cdot-} \rightarrow HCO_3^- + \cdot HO_2 \qquad (2.3)$$

$$HO_2^{\cdot} \rightarrow H^+ + O_2^{\cdot-} \qquad (2.4)$$
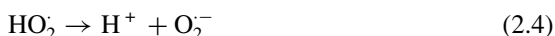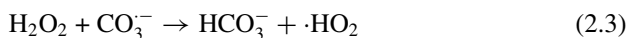
It has been demonstrated that Reactions (2.1)–(2.4) [25] are merely the initial stage in the process and that this stage is tailed by the interaction of the perhydroxyl radical ($HO_2^{\bullet}$) with the $^{\bullet}O_2^-$ and the interaction of two $HO_2^{\bullet}$ radicals, respectively [26]. The radicals created in this way may participate in the subsequent processes that result in the creation of $^1O_2$ molecules. Increased yield of $^{\bullet}O_2^-$ radical and generation of $^1O_2$ was observed as a result of an excess of H_2O_2. The existence of $^1O_2$ was also investigated utilizing a variety of approaches, including the enhancing and quenching CL methods [27–30], which were described below.

$$O_2^{\cdot-} + OH \rightarrow\,^1 O_2 + OH^- \qquad (2.5)$$

$$HO_2^{\cdot} + {}^{\cdot}O_2^- \rightarrow\,^1 O_2 + HO_2^- \qquad (2.6)$$

$$HO_2^{\cdot} + HO_2^{\cdot} \rightarrow\,^1 O_2 + H_2O_2 \qquad (2.7)$$
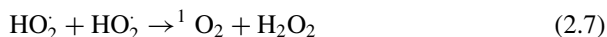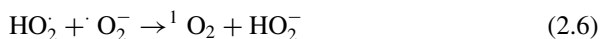
It was also demonstrated by the ESR spectrum that the creation of $^1O_2$ occurred as a result of the decomposition of HCO_4^-. When $^1O_2$ reacts with 2,2,6,6-tetramethyl-4-piperidone (TEMP), a relatively stable nitroxide adduct with a distinct spectrum is formed [31]. Because TEMP is soluble in alcohols, $^1O_2$ has a six-fold longer lifespan in alcohol than in H_2O. $^{\bullet}OH$ radical's interaction with TEMPO is inhibited. The presence of singlet oxygen was not detected in the TEMP solution (background solution). The ESR spectrum displays the specific signals of TEMPO after mixing

it with bicarbonate and H_2O_2, indicating that $^1O_2$ was generated from the HCO_4^- reaction.

Other strong methods, such as chemical trapping and mass spectrometry measurement, were used to validate the production of $^1O_2$. The produced $^1O_2$ was chemically trapped by 9,10-diphenylanthracene (DPA) [32] and electrospray ionization mass spectrometry was used to identify the consequent stable endoperoxide ($DPAO_2$). In electrospray ionization tandem MS, DPA and $DPAO_2$ were examined after the CL reaction. DPA's positive mode mass spectrum shows a significant $[M]^+$ ion at $m/z = 330$, which corresponds to molecular ion, and $DPAO_2$'s spectrum shows a strong $[M + H]^+$ ion peak at $m/z = 363$, which corresponds to the positively charged molecular ion. The $^1O_2$ derived from the H_2O_2/ClO_4^- and $H_2O_2/molybdate$ (MoO_4^-) systems were also proven using a similar manner [26, 33]. These findings are consistent with the current system. These results strongly suggest that $^1O_2$ was formed in the HCO_4^- CL reaction, implying a possible $^1O_2$-reliant mechanism.

2.3.2 CL Energy Transfer from the Decomposition of Peroxymonocarbonate

Chemiluminescence resonance energy transfer (CRET) is non-radiative energy transmission from a CL donor to a fluorophore acceptor [34]. Luminescent substrates are oxidized without the use of an excitation source, which increases sensitivity by eliminating sample autofluorescence. For the sensitive recognition of biomolecules, graphene [35], fluorescein isothiocyanate [36], and CdSe/ZnS QDs grounded CRET systems have been investigated [37, 38]. Due to the difficulty in identifying an applicable CL reaction or donor that can stimulate a fluorescent acceptor via energy transfer, only a few studies on CRET have been reported to date.

2.3.2.1 CL Energy Transfer to Fluorescent Compounds

During the mixing of HCO_3^- and H_2O_2 solutions in organic solutions, ultra-weak CL can be seen. After a sufficient number of fluorescent organic molecules, for instance, dichlorofluorescein (DCF), were added to the HCO_4^- solution, a stout CL was observed. Studies of the fluorescence, CL and UV–vis spectra, electron spin resonance (ESR), mass spectra (MS), and comparisons with H_2O_2/hypochlorite (ClO^-) and H_2O_2/MoO_4^- systems led to the discovery of the CL mechanism. The peroxy O–O bond in the HO-OCOO is homolyzed unimolecularly, which starts the process. The formation of $^\bullet O_2^-$ radical is thought to be the result of radical bond rearrangement. $^1O_2$ is produced when the superoxide ion interacts with the perhydroxyl radical. As a result of the energy transfers from $^1O_2$ to DCF, an excited energy acceptor (DCF*) was produced. Emission with a maximum wavelength of 509 nm was observed during the relaxation of the energy acceptor to its ground state.

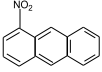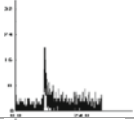Kinetics of the CL Reaction of HCO$_4$–Fluorescent Compounds
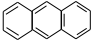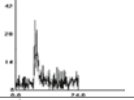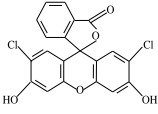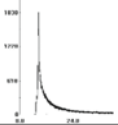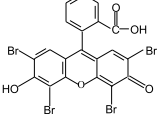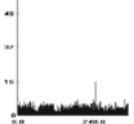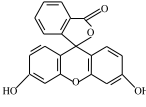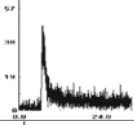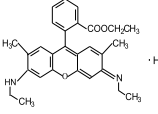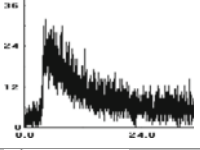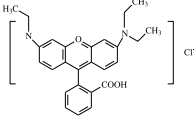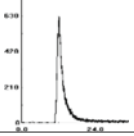
Preliminary tests using the batch approach revealed that when combining the HCO$_3{}^-$ and H$_2$O$_2$ solution in organic cosolvent (water: ethanol, 1:1.76, v/v), an ultra-weak CL was found. When fluorescent organic molecules, such as 1.0×10^{-5} M dichlorofluorescein (DCF), were added into a mixed solution of H$_2$O$_2$ (in water: ethanol, 1:1.76, v/v) and HCO$_3{}^-$, stout CL emission was seen. The presence of H$_2$O$_2$ was crucial because no CL could be observed without it. From the equilibrium of H$_2$O$_2$ and HCO$_3{}^-$ in an organic cosolvent, the HCO$_4{}^-$ was proposed as an oxidizing agent. As a result, HCO$_4{}^-$ was researched further as an oxidant. Other fluorescent organic compounds were also tried to see if CL emission was conceivable. Nine different fluorescent compounds were investigated for their effects on CL, as indicated in Table 2.2. The DCF has the greatest consequence on CL strength. When other fluorescent organic reagents were used as an enhancer, the CL emission was lower than the DCF. Their molecular architectures were found to be incapable of accepting the energy from the CL reaction. As a result, the HCO$_4{}^-$-DCF CL reaction was chosen as a standard for studying the mechanism of HCO$_4{}^-$ with fluorescent organic compounds [11].

Mechanism of Fluorescent Compound Enhanced CL

To reveal the improved CL mechanism, the CL and fluorescence spectra were also studied. In the DCF solution, there was one peak at 509 nm in fluorescence spectra. The maximum wavelength (max = 509 nm) and peak intensity barely altered after adding H$_2$O$_2$ and bicarbonate to the solution. In addition, CL spectra in HCO$_4{}^-$-DCF solution showed two peaks at 440–490 and 490–550 nm in the CL spectra (Fig. 2.3). The first peak observed at 440–490 nm matched the CL spectra of ^{1}O$_2$ (max = 476 nm) well [39]. It signifies that during the CL reaction, ^{1}O$_2$ is responsible for the emission. The second peak at 490–550 nm matched the fluorescence spectrum of DCF produced in this experiment (max = 509 nm). The CL peak detected at 509 nm was confirmed to be due to excited DCF* [40]. The energy acceptor then relaxes to the ground state, causing light emission (max = 509 nm). This also offered the CL energy transfer mechanism. The excited energy acceptor (DCF*) is formed when singlet oxygen transfers its energy to DCF.

When DCF was added to a mixture of TEMP, CO$_3{}^{2-}$, and hydrogen peroxide in an ESR experiment, the signal strength was significantly reduced. Because the energy of ^{1}O$_2$ was switched to DCF, which can be explained by the decrease of ^{1}O$_2$ in the reaction. The ^{1}O$_2$ was generated during the HCO$_4{}^-$ breakdown. The excited energy acceptor (DCF*) was formed when ^{1}O$_2$ transfered its energy to DCF. Light is emitted when the energy acceptor relaxes to the ground state.

Table 2.2 The effects of nine distinct fluorescent compounds (FOCs) on CL signal intensities in a batch manner
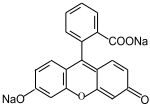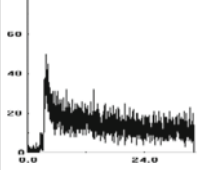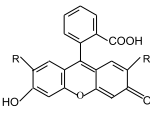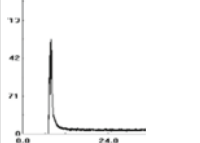
FOC	Structure	Concentration (mol/L)	S/N	Signal shape
Nitroanthracene		1×10^{-5}	25	
Anthracene		1×10^{-5}	35	
DCF		1×10^{-5}	1835	
Eosin Y		1×10^{-5}	20	
Fluorescein		1×10^{-5}	47	
Rh6G		1×10^{-5}	32	
RhB		1×10^{-5}	720	

(continued)

2.3.2.2 CL Energy Transfer to Lanthanide Complexes

Eu(II) complexes with diverse ligands have gotten a lot of attention because of their distinctive luminescence features, such as lengthy luminescence decay time and narrow emission peaks [41–43]. To explore the energy transfer pathway for HCO_4^- ions, the Eu(II)-EDTA or Eu (II)-Dipicolinate complexes were used.

Table 2.2 (continued)

FOC	Structure	Concentration (mol/L)	S/N	Signal shape
Uranine		1×10^{-5}	50	
Calcein		1×10^{-5}	1410	

Copyright 2008, with permission from Elsevier Ref. [15]

Fig. 2.3 The CL spectrum in a system of H_2O_2 (water: ethanol, 1:1.76, v/v)-bicarbonate-DCF. Copyright 2008, with permission from Elsevier Ref. [11]
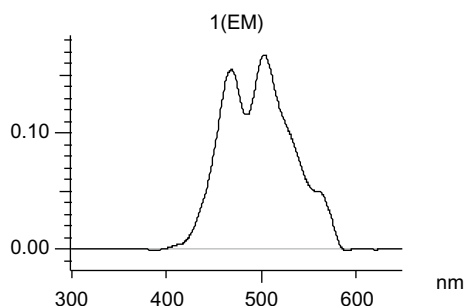
CL Kinetics of HCO_4^--Eu(II)-EDTA Complex

The flow injection technique was used to investigate the on-line synthesis of HCO_4^- in the existence of HCO_3^- and different substrates. By infusing 150 L of Eu^{2+} into an EDTA stream and mixing it with HCO_4^-, the CL signals were recorded, and the CL peak height was measured. In an initial test, the influence of the order in which the reagent solutions are mixed on the CL intensity was investigated using the batch approach (Fig. 2.4). CL emission was mild when 100 µL of 2 M H_2O_2 solution was introduced into 100 µL of 0.05 M HCO_3^-. The CL strength increased noticeably when 100 µL of 0.01 mol/L Eu^{2+}-EDTA (metal:ligand = 1:3) solution was added to 100 µL 2 M H_2O_2-0.05 M HCO_3^- in water:ethanol (1:1.76 v/v) (Fig. 2.5). The effects of Eu^{3+} and Zn^{2+} on the CL signals were scrutinized. The CL signal was unaffected by these two ions.

Fig. 2.4 Illustration of the batch method for CL of HCO_4^--Eu(II)-EDTA complex
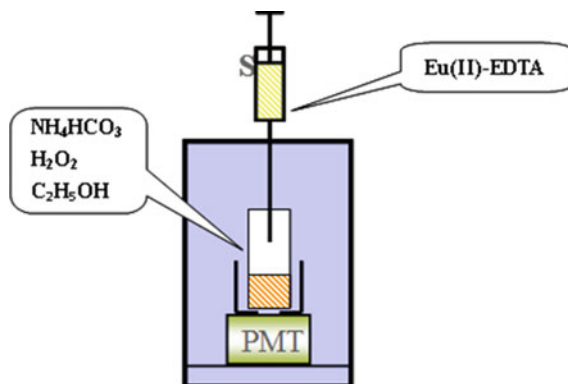
Fig. 2.5 Kinetics of chemiluminescent reactions. **a** HCO_4^- CL system; **b** HCO_4^--Eu^{2+}–EDTA CL system. *Conditions* 2 M H_2O_2, 0.05 M HCO_3^-, 0.01 M Eu^{2+}, 0.03 M EDTA. Copyright 2006, with permission from Wiley Ref. [12]
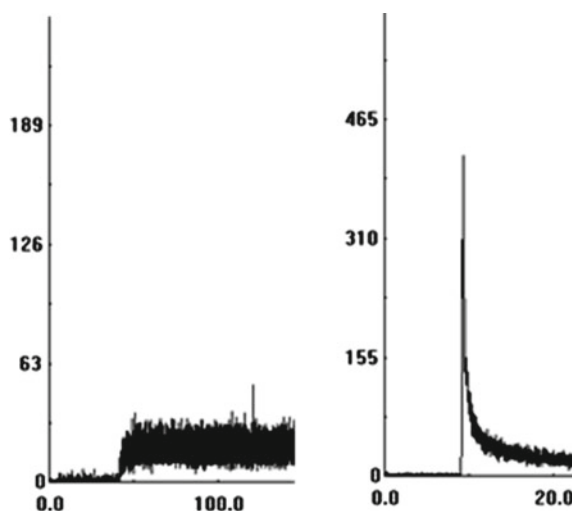
Mechanism of CL Reaction of HCO_4^--Eu^{2+}-EDTA Complex

To determine the CL mechanism, UV–visible absorption spectra for Eu^{2+} prior to and after the CL reaction, as well as the CL spectra were recorded (Fig. 2.6A). The absorption Eu^{2+} in water showed two peaks at 248 and 318 nm, due to the $4f^7 \rightarrow 4f^6 5d$ electronic transitions [44]. The Lambert–Beer law was satisfied by the Eu^{2+} solutions in the 10^{-4}–10^{-2} M concentration range when measured at 248 nm. The other constituents of the CL system analyzed, i.e., HCO_3^-, H_2O_2, and HCO_4^-, did not produce expressive signals at 248 nm, hence this wavelength was employed to study Eu^{2+} before and following the reaction. After the reaction, the peaks at 248 and 318 nm vanished from the absorption spectrum. Furthermore, the absorption spectrum of the reaction did not superimpose on the absorption spectrum of Eu^{3+}. Nonetheless, the two shapes were strikingly comparable. As a result of this, it was
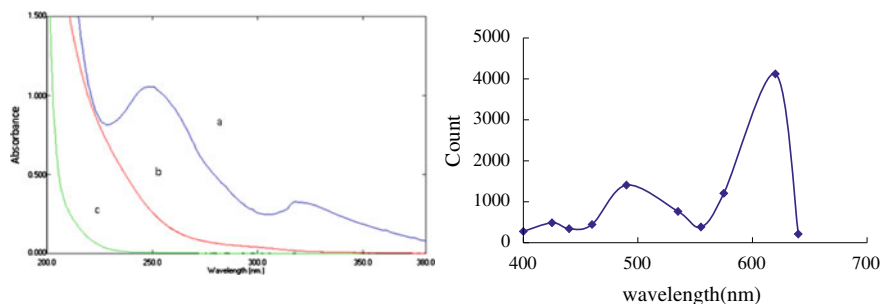
Fig. 2.6 **a** Absorption spectra of (a) Eu^{2+}, (b) Eu^{2+} after the CL reaction, and (c) Eu^{3+}; concentration of all reagents was 1×10^{-3} M. **b** The CL spectra of the HCO_4^-–Eu^{2+}–EDTA system. Copyright 2006, with permission from Wiley Ref. [12]

demonstrated that Eu^{2+} has oxidized to Eu^{3+} following the HCO_4^-–Eu^{2+}–EDTA CL reaction. The excited product in the Ru^{2+}/Ru^{3+} with 2,2'-bipyridine redox system was recognized as a metal to ligand charge transfer triplet [45], comparable to Eu^{2+}/Eu^{3+}. Elbanowsli [46] also discovered that the $[Eu^{2+}\text{-}N_3]^{2+}$ complex may take energy from $^1O_2$ dimers with ease. As a result, it was concluded that singlet oxygen is produced via the CL reaction of the HCO_4^-–Eu^{2+}–EDTA combination, which caused the CL production. ESR spin trapping, CL, and an MS approach have all been used to show that $^1O_2$ exists as an emissive species in this CL system.

For the detection of $^\bullet O_2^-$ radical and $^1O_2$, the p-methoxyphenyl Cypridina luciferin analog (MCLA) has been utilized as a CL probe [16]. MCLA considerably increased the CL intensity in a CL reaction. Sodium azide, a singlet oxygen scavenger, was also confirmed to have a quenching impact on the CL (about 13-fold). The presence of $^1O_2$ is preliminarily confirmed by these facts. The CL spectrum of this system, as determined by cutoff filters, revealed two peaks in the 400–640 nm range (Fig. 2.6b). The second peak (615 nm) is typical of Eu^{3+}. It is possible to conclude that the CL emission was caused by the Eu^{3+}ion. Lanthanide ions, particularly Eu^{2+}, Eu^{3+}, and Tb^{3+}, have been shown to have intense luminescence and have been utilized as luminescent probes, donors, and acceptors. The HCO_4^- has high activity as an active intermediate and easily oxidizes Eu^{2+} to Eu^{3+}.

$$HCO_4^- + Eu^{2+} \rightarrow {}^\bullet CO_3^- + \cdot OH + Eu^{3+} \qquad (2.8)$$

In the presence of Eu^{3+}, there was no CL, but introducing Eu^{2+} to the system resulted in a brilliant CL. This established that adding Eu^{2+} to a solution comprising HCO_4^- started the CL process. $^\bullet OH$ radicals are also produced by the HCO_4^--Eu^{2+} system. The CL system produces $^1O_2$ as a result of simultaneous HCO_4^- breakdown and radical recombination. Excited Eu^{3+} ions were produced a result of Eu^{2+} ion oxidation by peroxymonocarbonate, which produces light at 615 nm when they return to the ground state, corresponding to the transition $^5D_0$-$^7F_2$. The stability of the formed complex with the ligand and the hydration number determines the strength

of lanthanide ion emission [47, 48]. CL emission increases significantly when Eu^{2+} and EDTA were present. The dominating band in the CL spectra was attributable to Eu^{3+}, with a maximum at around 615 nm [49], indicating that these ions are the solitary cause of emission in the CL system investigated. Based on the findings, the subsequent response mechanism (Reactions 2.9–2.12) was discovered.

$$O_2\left(^1\Delta_g\right) + O_2\left(^1\Delta_g\right) \rightarrow O_2\left(^1\sum\nolimits_g^+\right) + O_2\left(^3\sum\nolimits_g^-\right) \quad K = 1.3 \times 10^3 \quad (2.9)$$

$$O_2\left(^1\sum\nolimits_g^+\right) + O_2\left(^1\Delta_g\right) + [Eu(III)(EDTA)]^-$$
$$\rightarrow 2O_2\left(^3\sum\nolimits_g^-\right) + \left[Eu(III)(EDTA)^*\right]^- \quad (2.10)$$

$$\left[Eu(III)(EDTA)^*\right]^- \rightarrow \left[Eu(III)^*(EDTA)\right]^- \quad (2.11)$$

$$\left[Eu(III)^*(EDTA)\right]^- \rightarrow [Eu(III)(EDTA)]^- + h\nu \quad (2.12)$$
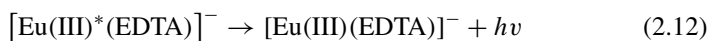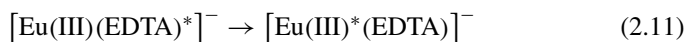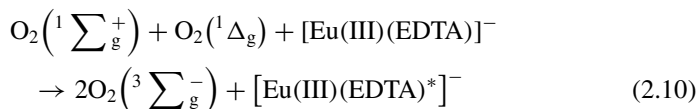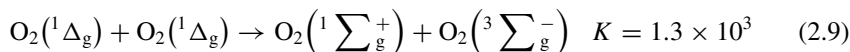
The emission of excited carbonyl groups can be attributed to a low peak intensity with a maximum emission at 500 nm [50, 51].

Energy Transfer to Eu(II)-Dipicolinate Complex

Because of the short lifetime and elevated activity of this active carbon–oxygen intermediate, as well as the unique luminescence properties of Eu^{2+} complexes, such as a long luminescence decay time and narrow emission peaks, Eu^{2+} complexes were predominantly well appropriate for an energy transfer study in the HCO_4^- CL reaction. CL released during the oxidation of Eu^{2+} complexes with organic ligands by H_2O_2 was first studied in 1983 [49]. After the complexation of Eu^{2+}, this radical-mediated process produced excited Eu^{3+} ions, and the CL intensity amplified considerably. Subsequently injecting Eu^{2+} into the HCO_4^--solution with a ligand, an ultra-weak CL is seen in an on-line reaction. The CL was influenced by the type of ligand used. We found that when dipicolinate was utilized as the ligand of Eu^{2+}, the CL intensity was the highest. The CL energy transfer reaction with HCO_4^- as the oxidizing agent was investigated, and the findings indicated that radical reactions were the most important factor in the transfer of energy in the HCO_4^- CL system. Peroxymonocarbonate and the Eu^{2+}-dipicolinate complex were examined for their energy transfer CL reaction. HCO_4^- oxidizes Eu^{2+} to Eu^{3+} while concurrently creating radicals, according to UV–visible absorption spectra, CL, ESR spin trapping procedure, and mass spectrum tests. Singlet molecular oxygen was created through bond rearrangement within radicals. The (Eu^{3+}-dipic) complex accepted the energy originating from the $^1O_2$. Radiative deactivation of the excited (Eu^{3+}-*dipic) ions resulted in the CL emission. The formation of $^1O_2$ in the reaction of HCO_4^- with the Eu^{2+}/Eu^{3+}-dipicolinate complex suggests a $^1O_2$-dependent process. CL emission

occurs when $^1O_2$ transfers its excess energy to an acceptor (Eu^{3+}-dipic) (Reaction 2.13).

$$O_2\left(^1\sum\nolimits_{g}^{+}\right) + O_2\left(^1\Delta_g\right) + \left[Eu^{3+}(dipic)\right]^{-}$$
$$\to 2O_2\left(^3\sum\nolimits_{g}^{-}\right) + \left[Eu^{3+}(dipic)^*\right]^{-} \tag{2.13}$$
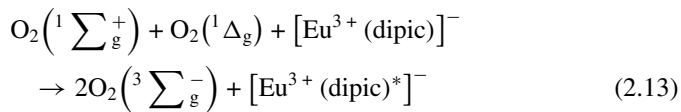
Eu^{3+} ions are the result of the oxidation of Eu^{2+} ions by peroxymonocarbonate. The Eu^{3+}-dipicolinate complex received energy from $^1O_2$ to form the excited Eu^{3+}-dipicolinate complex, which emits radiation with a wavelength of 615 nm due to the transitions $^5D_0$ -$^7F_2$ when it returns to the ground state (Reactions 2.14–2.15) [49].

$$\left[Eu^{3+}(dipic)^*\right]^{-} \to \left[Eu^{3+\,*}(dipic)\right]^{-} \tag{2.14}$$

$$\left[Eu^{3+\,*}(dipic)\right]^{-} \to \left[Eu^{3+}(dipic)\right]^{-} + h\nu \tag{2.15}$$
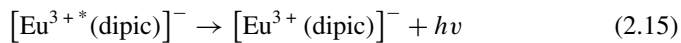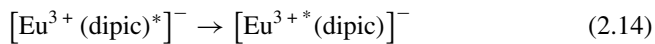
2.3.2.3 CL Energy Transfer to NaYF$_4$:Yb^{3+}/Er^{3+} NPs

CL has greatly increased in the $HCO_3{}^{-}$–NH_4OH–H_2O_2 system when $NaYF_4$:Yb^{3+}/Er^{3+} (NYF:Yb/Er) NPs with branching structure was used. Ammonia catalyzed the breakdown of $HCO_4{}^{-}$, a result of the reaction between $HCO_3{}^{-}$ and H_2O_2. It was discovered a CRET system using $HCO_4{}^{-}$ ions and NYF:Yb/Er NPs as the energy donor-acceptor pair. The improved CL was generated by the emission of NYF:Yb/Er NPs excited by the $HCO_4{}^{-}$ decomposition energy.

Kinetic Aspect of $HCO_4{}^{-}$–$NaYF_4$:Yb^{3+}/Er^{3+} NPs

The light-generating reactions were done in batches, and the recognition was done with a BPCL luminescence analyzer. The effects of adding $NaYF_4$, $HCO_3{}^{-}$, NYF:Yb/Er NPs, ammonium hydroxide, and H_2O_2 in different order were investigated. At a voltage of 1.2 kV, the CL strength was presented and integrated with a 0.1 s interval. When H_2O_2 was introduced into $HCO_3{}^{-}$ using a microliter syringe, there were two CL peaks observed. The CL count reached in 0.2 s to its first maximum value of 225, and then swiftly decreased. After 60 s, the second-highest possible count of 30 was reached. The CL lasted approximately 90 s (Fig. 2.7a, Peak 1). It was discovered that when H_2O_2 was injected into NH_4OH-$HCO_3{}^{-}$ system, the kinetic curve recorded one peak and the CL signals reached 223 counts. The light lasted around 103 s before it was completely extinguished (Fig. 2.7a, Peak 2). $NaHCO_3$, NH_4OH, and H_2O_2 did not reacted with $NaYF_4$ and NYF:Yb/Er NPs. An increased CL was produced when $NaYF_4$ or NYF:Yb/Er NPs was mingled with $HCO_3{}^{-}$ first, then H_2O_2 was added. The light lasted approximately 64 and 40 s, respectively. NYF:Yb/Er NPs enhanced
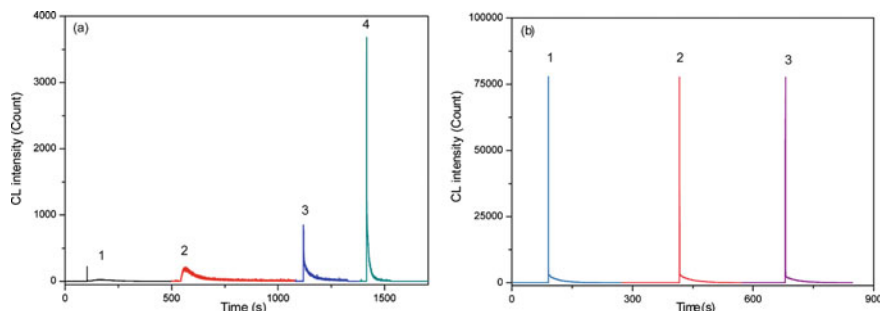
Fig. 2.7 Kinetic curves of CL systems. **a** HCO_3^-–H_2O_2 (Peak 1), HCO_3^-–NH_4OH–H_2O_2 (Peak 2), HCO_3^-–$NaYF_4$ NPs–H_2O_2 (Peak 3), HCO_3^-–NYF:Yb/Er NPs–H_2O_2 (Peak 4), and **b** HCO_3^-– NH_4OH–NYF:Yb/Er NPs–H_2O_2 (Peak 1), HCO_3^-–NH_4OH–NYF:Yb/Er NPs–Yb^{3+}–H_2O_2 (Peak 2), HCO_3^-–NH_4OH–NYF:Yb/Er NPs–Er^{3+}–H_2O_2 (Peak 3). Reprinted with permission from Ref. [13]. Copyright 2012 American Chemical Society

CL was roughly five times stronger than $NaYF_4$ NPs enhanced CL (Fig. 2.7a, Peaks 3 and 4). A considerable increase in CL was seen when NH_4OH was injected into the HCO_3^-–NYF:Yb/Er NPs first, and finally H_2O_2 was added. CL intensity was 77,366 counts, which was 344 times that of the HCO_3^-–H_2O_2 CL. The light lasted about 50 s, showing a quick CL process (Fig. 2.7b). The CL of the HCO_3^--NH_4OH-NYF:Yb/Er NPs-H_2O_2 system was unaffected by individual Yb^{3+} and Er^{3+} ions (Fig. 2.7b).

Mechanism of the Chemiluminescence

Emitting Species Studies

The effects of active oxygen radical scavengers on the CL of the HCO_3^-–NH_4OH-NYF:Yb/Er NPs-H_2O_2 (NNNH) system were examined to better understand the mechanism of the system. The NBT method was widely utilized to identify $^\bullet O_2^-$ radicals [4]. NBT can be reduced to its deep-blue diformazan form by using $^\bullet O_2^-$ [52, 53]. The hue of the solution altered from yellow to blue after 1.0×10^{-6} M NBT was added to the H_2O_2–HCO_3^-–NH_4OH–NYF:Yb/Er NPs system. The CL intensity of this system was reduced by approximately 30 fold (Table 2.3). In this case, it suggested that $^\bullet O_2^-$ radical was generated through the CL reaction. MCLA interacted with $^\bullet O_2^-$ and $^1O_2$ to produce a high-octane dioxetanone intermediate that emitted intense CL light at 465 nm [16, 54]. MCLA can increase the CL counts of the NNNH system by around five times at a concentration of 1.0×10^{-7} M (Table 2.3). It also establishes that $^\bullet O_2^-$ and $^1O_2$ exist in the CL system. DABCO is an effective $^1O_2$ quencher [55]. The deactivation of O_2 ($^1\sum_g^+$) by DABCO is primarily an electronic-to-vibrational process [56]. As demonstrated in Table 2.3, the CL signals of the NNNH system fall as the DABCO concentration rises, signifying that $^1O_2$ was formed. $^1O_2$ is scavenged by sodium azide (NaN_3) [15, 57]. The quenching impact

Table 2.3 Radical scavengers' effects on the CL of the NNNH system

Radical scavengers	Radical	Concentration (mol L^{-1})	CL intensity (count)
H_2O			77,366
NBT	$\cdot O_2{}^-$	1.0×10^{-6}	2110
MCLA	$\cdot O_2{}^-$, $^1O_2$	1.0×10^{-7}	386,675
DABCO	$^1O_2$	1.0×10^{-3}	1102
		5.0×10^{-3}	486
		1.0×10^{-2}	158
NaN_3	$^1O_2$	1.0×10^{-5}	366
Thiourea	$\cdot OH$	1.0×10^{-5}	1472
t-butanol	$\cdot OH$	0.01% (v/v)	1200
DMSO	$\cdot OH$	0.01% (v/v)	1653

Solution conditions were 0.2 M $NaHCO_3$, 0.1 M H_2O_2 and 0.5 µg/mL NYF:Yb/Er NPs. The volume of NYF:Yb/Er NPs and NH_4OH was 50 µL and that of $NaHCO_3$, H_2O_2, and radical scavenger was 100 µL, respectively

of 1.0×10^{-5} mol L^{-1} NaN_3 confirmed the production of $^1O_2$ in the investigated system (Table 2.3).

The radical scavengers i.e., thiourea, t-butanol, and DMSO are reported to be active for $^\bullet OH$ radical [58]. A considerable inhibition was seen when 1.0×10^{-5} M thiourea was introduced to the NNNH system (about 50 times, Table 2.3). The CL of the NNNH system can be strongly inhibited by t-butanol and DMSO at a volume level of 0.01 percent (v/v) (Table 2.3). All of the preceding evidence suggests that the CL reaction involves $^\bullet OH$ radical.

Spin Trapping Studies

The presence of $^1O_2$ and $^\bullet OH$ radicals was demonstrated using room-temperature ESR spectroscopy. The TEMPO adduct can be formed when TEMP reacts with $^1O_2$. It is a stable nitroxide radical with a distinctive spectrum [59–61]. The intensity change in the specific signal of TEMPO and during the first 1 min of the reaction (Fig. 2.8a), demonstrates the production of $^1O_2$ in the $HCO_3{}^-$–H_2O_2–NH_4OH system. When TEMP was added to the NNNH system, however, the EPR intensity of TEMPO was enhanced roughly thrice. A distinct drop in intensity during the first minute of the reaction was also observed, indicating that $^1O_2$ was being reduced in the NNNH system (Fig. 2.8b). The breakdown of $^1O_2$ was caused by NYF:Yb/Er NPs.

ESR spectroscopy was utilized to detect $^\bullet OH$ radical with DMPO. In the $HCO_3{}^-$-NH_4OH-H_2O_2 CL system, Fig. 2.8c depicted the signal variation of the DMPO-OH adduct during the initial time of the reaction. It proved that $^\bullet OH$ radical formed in the $HCO_3{}^-$–H_2O_2–NH_4OH system. The ESR signal of DMPO-OH increased when DMPO was added to the NNNH system (Fig. 2.8d). However, in the NNNH system, the lifespan of $^\bullet OH$ radical was shorter than in the $HCO_3{}^-$– H_2O_2–NH_4OH system. Other radicals were also produced in the NNNH system, as seen by the overlapping
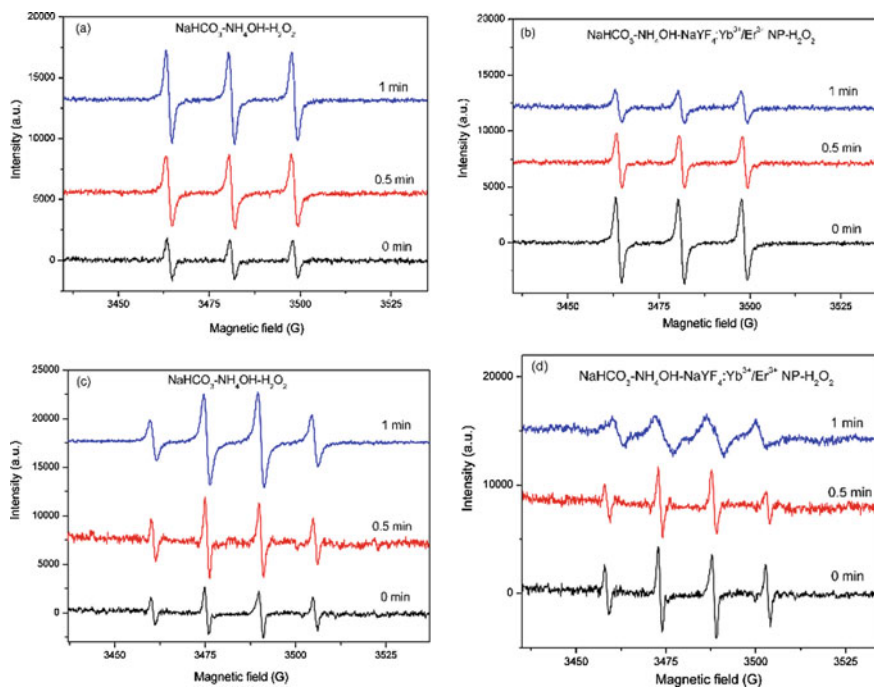
Fig. 2.8 EPR spectra of $^\bullet$OH radical and $^1O_2$. **a** $^1O_2$ and **c** $^\bullet$OH in $HCO_3{}^-$–NH_4OH–H_2O_2 system; **b** $^1O_2$ and **d** $^\bullet$OH radical in NNNH system. *Conditions* 0.1 M H_2O_2, 0.05 M TEMP, 0.05 M DMPO, 0.2 M $HCO_3{}^-$, 5.0 μmol/L NH_4OH and 0.5 μg/mL NYF:Yb/Er NPs. Reprinted with permission from Ref. [13]. Copyright 2012 American Chemical Society

EPR peak at 1 min of the reaction. These findings also suggest that $^\bullet$OH radicals be present and that the reactivity of NYF:Yb/Er NPs on its lifetime impacts it.

Spectra of CL Systems

The CL spectra in the $HCO_3{}^-$–H_2O_2–NH_4OH and NNNH systems were studied with a fluorescence spectrometer to confirm the emitting species. A Hitachi F-7000 spectrophotometer was employed to measure the CL spectrum after the Xe lamp was turned off with a flow analysis device. A CL detector, a flow cell put inside the cell holder, and two peristaltic pumps were used as part of the setup. At room temperature, all optical measurements were completed. During the CL spectrum monitoring, the emission slit was expanded to a width of 20 nm. The CL spectrum of the $HCO_3{}^-$–H_2O_2-NH_4OH system shows four peaks in the 300–700 nm range (Fig. 2.9a). The decomposition of excited $(CO_2)_2{}^*$ dimer corresponds to the peak at 441 nm [1, 62]. The generation of an oxygen molecular pair $(O_2)_2{}^*$ resulted in peaks at 480 and 580 nm [39, 63]. The peak of $^1O_2$ emission was at 634 nm [64]. They have a lot of energy and can use it to shed it through luminescence.
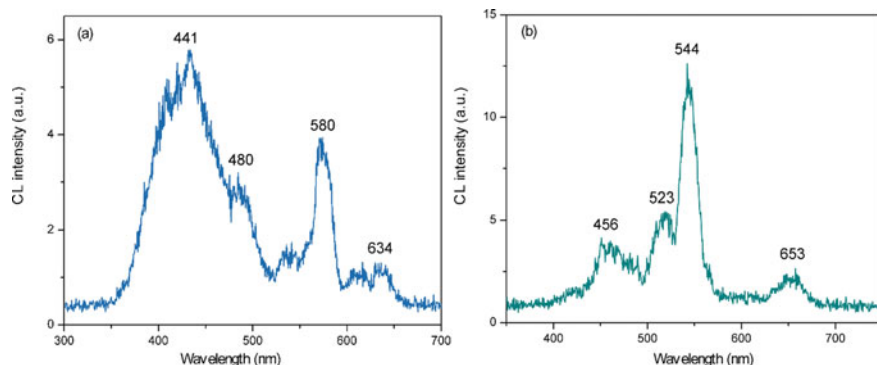
Fig. 2.9 CL spectra. **a** $HCO_3^- - H_2O_2 - NH_4OH$ system and **b** NNNH system. *Conditions* were 0.2 M HCO_3^-, 0.1 M H_2O_2, 5.0 µM NH_4OH and 0.5 µg/mL NYF:Yb/Er NPs. The flow rates were 1.0, 1.0, 1.5 and 1.5 mL/min for NH_4OH, NYF:Yb/Er NPs, HCO_3^- and H_2O_2, respectively. Reprinted with permission from Ref. [13]. Copyright 2012 American Chemical Society

The CL spectra had peaked with maxima located at 456, 523, 544, and 653 nm when NYF:Yb/Er NPs were injected into the $HCO_3^- - H_2O_2 - NH_4OH$ flow system (Fig. 2.9b). The excited state of NYF:Yb/Er NPs is most likely the CL's emitting species. The reaction of $^\bullet CO_3^-$ radicals produces a peak at 456 nm [65]. The emission peaks of $NaYF_4$:Yb/Er NPs are identical at 523, 544, and 653 nm. In the CL spectrum of the NNNH system, peaks at 580 and 634 nm from the emission of $(O_2)_2^*$ and $^1O_2$ vanished. It was hypothesized that the emission is depleted to activate the NYF:Yb/Er NPs through energy transfer.

Mechanism of the CL Reaction

Based on the radical scavenger's studies, EPR, and CL spectra of the NNNH CL system, the mechanism was determined as given by the subsequent reactions. H_2O_2 reacts with HCO_3^- to produce HCO_4^- [6, 66]. In an aqueous solution, ammonia ionizes as equilibrium Reaction 2.16, which is a Lewis acid aided O–O bond breakage by stabilizing the CO_3^{2-} leaving group in the HCO_4^- (Scheme 2.1) [11, 67]. Nuclear magnetic resonance and infrared spectra have demonstrated a comparable mechanistic mechanism for the formation of platinum and rhodium peroxycarbonate complexes. The ammonium peroxycarbonate complexes break down readily to produce $^\bullet OH$ and $^\bullet CO_3^-$ radicals (Reaction 2.17) [68].

$$NH_4OH \rightleftharpoons NH_4^+ + OH^- \tag{2.16}$$

$$\tag{2.17}$$
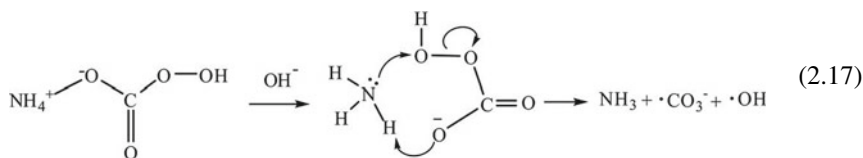
H_2O_2 reacts with $\cdot CO_3^-$ radicals to produce an $\cdot O_2^-$ radical (Reactions 2.3–2.4). The presence of OH^- ions in the equilibrium ammonia reaction sped up Reaction 7, speeding up the generation of $\cdot O_2^-$ radical with the neutralization of H^+ ions. As a result, there is a higher production of $^1O_2$ and $(O_2)_2^*$ (Reactions 2.5 and 2.18–2.19).

$$H^+ + OH^- \rightleftharpoons H_2O \tag{2.18}$$

$$2 \cdot O_2^- + 2 \cdot O_2^- + 4H_2O \rightarrow (O_2)_2^* + 2H_2O_2 + 4OH^- \tag{2.19}$$
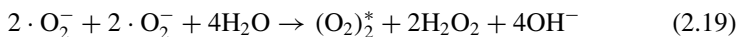
When $\cdot OH$ radicals combine with excess HCO_3^-, $HCO_3^{\cdot -}$ radicals are generated (Reaction 2.20). The intermediate $(CO_2)_2^*$ was formed via the recombination of $HCO_3^{\cdot -}$. They were unstable and degraded to CO_2 (Reactions 2.21–2.22), releasing energy and generating light at 430–460 nm [69, 70].

$$\cdot OH + HCO_3^- \rightarrow OH^- + \cdot HCO_3 \tag{2.20}$$

$$2 \cdot HCO_3 \rightarrow (CO_2)_2^* + H_2O_2 \tag{2.21}$$

$$(CO_2)_2^* \rightarrow 2CO_2 + h\nu \,(456\,nm) \tag{2.22}$$
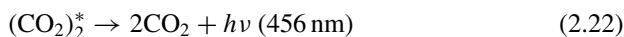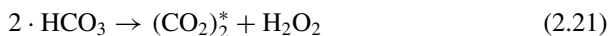
Based on the CL spectrum of the NNNH system, it was hypothesized that the excited NYF:Yb/Er NPs was formed. The FL spectra of NYF:Yb/Er NPs excited with light of 441, 480, 580, and 634 nm, respectively, were studied to prove that $^1O_2$, $(CO_2)_2^*$, and $(O_2)_2^*$ can excite NYF:Yb/Er NPs. When NYF:Yb/Er NPs were stimulated with the light of 441 and 480 nm, significant emissions at 523, 544, and 653 nm were seen (Fig. 2.10a, b). At 580 and 634 nm, the upconversion emissions of NYF:Yb/Er NPs were rather feeble (Fig. 2.10c, d). The NYF:Yb/Er NPs were activated by energy transfer via the breakdown of HCO_4^-, according to these findings. $^1O_2$ and $(O_2)_2^*$ consumption was the most common. NYF:Yb/Er NPs receive only a portion of the energy transferred by $(CO_2)_2^*$ (Reactions 2.23–2.25).

$$(CO_2)_2^* + NaYF_4{:}Yb^{3+}/Er^{3+}\,NP \rightarrow NaYF_4{:}Yb^{3+}/Er^{3+}\,NP^* + 2CO_2 \tag{2.23}$$

$$^1O_2 + NaYF_4{:}Yb^{3+}/Er^{3+}\,NP \rightarrow NaYF_4{:}Yb^{3+}/Er^{3+}\,NP^* + O_2 \tag{2.24}$$

$$(O_2)_2^* + NaYF_4{:}Yb^{3+}/Er^{3+}\,NP \rightarrow NaYF_4{:}Yb^{3+}/Er^{3+}\,NP^* + 2O_2 \tag{2.25}$$

The following is an explanation of the energy transfer mechanism. The energy was absorbed by the Yb^{3+} ion in the $^2F_{7/2}$ ground state, which is then stimulated to the $^2F_{5/2}$ level. The excited $^2F_{5/2}$ state of the Yb^{3+} ion is resonant with the Er^{3+} ion's excited $^4I_{11/2}$ state. By absorbing another photon from Yb^{3+} ($^2F_{5/2}$) the electrons of Er^{3+} are first excited from the $^4I_{15/2}$ level to the $^4I_{11/2}$ level by energy transfer, and
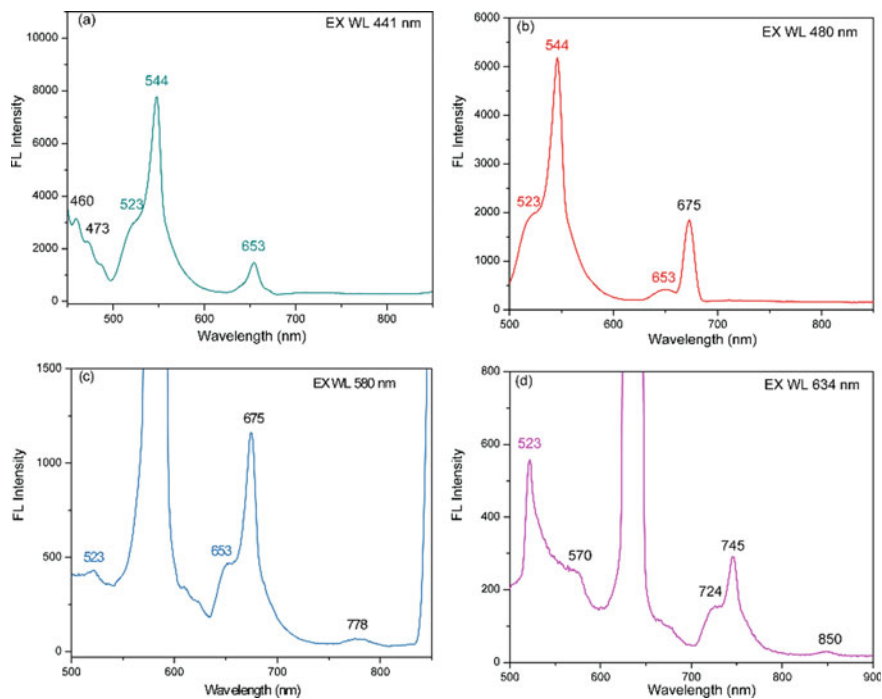
Fig. 2.10 Fluorescence spectra of NYF:Yb/Er NPs excited at different wavelengths **a** 441 nm, **b** 480 nm, **c** 580 nm and **d** 634 nm. Reprinted with permission from Ref. [13]. Copyright 2012 American Chemical Society

subsequently to the $^4F_{7/2}$ level by absorbing another photon from the $^4I_{15/2}$ level (Reactions 2.26–2.27).

$$^4I_{15/2}\left(Er^{3+}\right) + {}^2F_{5/2}\left(Yb^{3+}\right) \rightarrow^4 I_{11/2}\left(Er^{3+}\right) + {}^2F_{7/2}\left(Yb^{3+}\right) \tag{2.26}$$

$$^4I_{11/2}\left(Er^{3+}\right) + {}^2F_{5/2}\left(Yb^{3+}\right) \rightarrow^4 F_{7/2}\left(Er^{3+}\right) + {}^2F_{7/2}\left(Yb^{3+}\right) \tag{2.27}$$
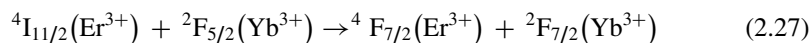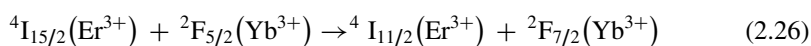
The excited electrons on the $^4F_{7/2}$ level of Er^{3+} decay to the $^2H_{11/2}$, $^4S_{3/2}$, and $^4F_{9/2}$ levels, respectively, by a nonradioactive mechanism. The $^2H_{11/2}/^4S_{3/2}/^4F_{9/2}$ $^4I_{15/2}$ transitions of Er^{3+} ion provide the amazingly enhanced CL (Reactions 2.28–2.30).

$$^2H_{11/2}(Er^{3+}) \rightarrow {}^4I_{15/2}(Er^{3+}) + h\nu \text{ (523 nm)} \tag{2.28}$$

$$^4S_{3/2}(Er^{3+}) \rightarrow {}^4I_{15/2}(Er^{3+}) + h\nu \text{ (544 nm)} \tag{2.29}$$

$$^4F_{9/2}(Er^{3+}) \rightarrow {}^4I_{15/2}(Er^{3+}) + h\nu \text{ (653 nm)} \tag{2.30}$$
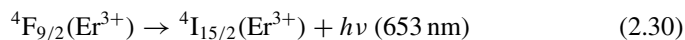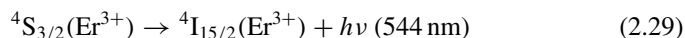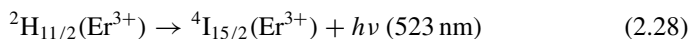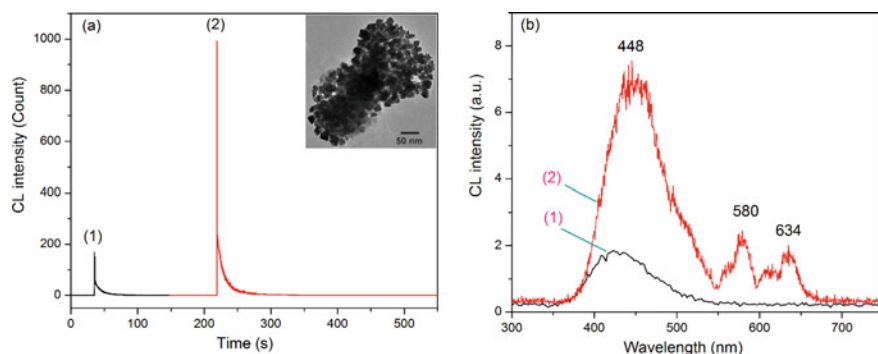
Fig. 2.11 Kinetic curves and CL spectra of NaHCO$_3$–H$_2$O$_2$–NH$_4$OH CL system with different nanoparticles. **a** Kinetic curves of short nano rod-like NYF:Yb/Er NPs (Peak 1) and branched NaYF4 NPs (Peak 2) in HCO$_3^-$–H$_2$O$_2$–NH$_4$OH CL system and TEM image of the short nano rod-like NYF:Yb/Er NPs (*inset* in a), and **b** CL spectra of nano rod-like NYF:Yb/Er NPs (Peak 1) and branched NaYF$_4$ NPs (Peak 2) in the CL system. The solution conditions were the same as those in Figs. 2.7 and 2.9. Reprinted with permission from Ref. [13]. Copyright 2012 American Chemical Society

In the ultraviolet–visible spectral band, lanthanide-doped NPs possess tiny absorption cross-sections. The CRET phenomenon, which was seen in NYF:Yb/Er NPs, is particularly remarkable. It cannot be used as an acceptor in traditional energy transfer experiments [71]. Though, in the NNNH CL system, the surface impact of the branching structure of NYF:Yb/Er NPs was crucial for the radical reactions that produced ^{1}O$_2$, (CO$_2$)$_2$*, and (O$_2$)$_2$*. This reduces the distance between the donor and the acceptor, allowing the mismatched energy levels to resonate at the same frequency. By dividing the integral area of the NYF:Yb/Er NPs emission spectrum by the integral area of the entire spectrum of the NNNH CL system, the CRET efficiency was calculated to be around 57% [38]. The efficient CRET signal was produced because NH$_3$ can constantly catalyze the HCO$_3^-$–H$_2$O$_2$ CL reaction. The CRET was made possible by the vicinity of the light source to the NPs and the high quantum yield of NYF:Yb/Er NPs. In the NaHCO$_3$–NH$_4$OH–H$_2$O$_2$ environment, the CL of short nano rod-like NYF:Yb/Er NPs and branching NaYF$_4$ NPs was studied. It was also demonstrated that the efficient CRET between HCO$_4^-$ donor and NYF:Yb/Er NPs requires a branching structure of NYF:Yb/Er NPs. Both short nano rod-like NYF:Yb/Er NPs and branching NaYF$_4$ NPs were unable to activate a CRET progression in the control experiment (Fig. 2.11).

In the control experiment, the short nano rod-like NYF:Yb/Er NPs were injected into HCO$_3^-$–NH$_4$OH–H$_2$O$_2$ CL system. The maximum value of CL intensity is much lower than that of the CL system with the same concentration of branched NYF:Yb/Er NPs, which was 169 (Fig. 2.11a, Peak 1). Besides, the CL spectrum shows only the emission from the decomposition of HCO$_4^-$ without the characteristic emission of nano rod-like NYF:Yb/Er NPs (Fig. 2.11b, Peak 1). This indicates that the nano rod-like NYF:Yb/Er NPs were unable to initiate a CRET process. The CRET was
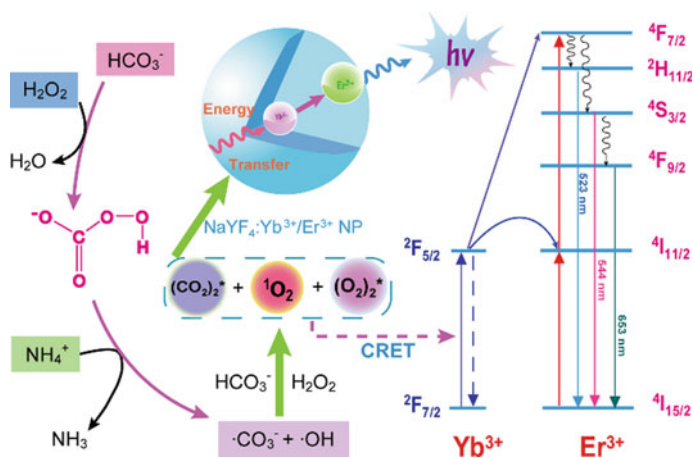
Fig. 2.12 Schematic illustration of the CRET mechanism of NNNH system. Reprinted with permission from Ref. [13]. Copyright 2012 American Chemical Society

well correlated to the branched structure of NPs which shorten the proximity between emitters and NPs by special surface adsorption. That is critical for an efficient energy transfer.

The CL of branched $NaYF_4$ NPs with branched $NaYF_4:Yb^{3+}/Er^{3+}$ NPs in the HCO_3^-–H_2O_2–NH_4OH system was also compared. The maximum CL intensity of the system with branched $NaYF_4$ NPs was only 1.3% of that with branched $NaYF_4:Yb^{3+}/Er^{3+}$ NPs. Besides, the CL spectrum displayed only the emission of the decomposition of HCO_4^- without that of branched $NaYF_4$ NPs (Fig. 2.11a, Peak 2, and Fig. 2.11b, Peak 2). Results proved that branched $NaYF_4$ NPs cannot be an acceptor for a CRET process in the CL system. The branched $NaYF_4:Yb^{3+}/Er^{3+}$ NPs was a more suitable acceptor for CRET attributed to the dopant ions used as the activator to generate efficient emissions. The mechanism of CRET is further shown in Fig. 2.12.

2.4   KMnO₄ Enhanced CL from the Decomposition of Peroxymonocarbonate

Compared to acidic potassium permanganate, fewer studies have been conducted on $KMnO_4$ CL in an alkaline medium. We found potassium permanganate can boost the CL of the HCO_3^-–H_2O_2 CL system. The CL process involving O_2 and CO_2 dimer was studied using the consequences of various surfactants and radical scavengers. The energy transfer process between rhodamine B or uranine and HCO_3^-–H_2O_2–$KMnO_4$ system was investigated.

2.4.1   Kinetics of the CL Reaction

The batch approach was used to carry out the light-producing reactions in the glass cuvette. A BPCL luminescence analyzer was used for all detections. First, 50 µL of carbonate/bicarbonate solution was added to 50 µL of $KMnO_4$ in a cuvette, and then 100 µL of H_2O_2 was infused. At -1.2 kV, the CL intensity was recorded and integrated for 0.1 s intervals.

The light emission was affected by the mixing order of the reagent solutions, resulting in distinct kinetic properties. The reaction of $NaHCO_3$, H_2O_2, and $KMnO_4$ was used to make it in a batch technique. The three distinct mixing orders were compared (Table 2.4). Only a mild and rapid CL emission was seen after injecting $KMnO_4$ solution into H_2O_2 solution. When HCO_3^- solution was injected into this mixed solution, a brighter glow appeared within 1 s and lasted for around 15 s until being completely quenched. Two peaks were found in the CL profile. When HCO_3^- solution was introduced to H_2O_2 solution initially, a weak and sluggish CL was noted. A substantial emission was seen after inserting $KMnO_4$ solution into the mixed solution, and the CL signal returned to baseline after about 25 s. There was

Table 2.4   The effect of reagent mixing order on batch CL intensity

Reagent	First injection	Intensity (count)	Second injection	Intensity (count)	Profile
H_2O_2	$KMnO_4$	32	$NaHCO_3$	227	
H_2O_2	$NaHCO_3$	53	$KMnO_4$	161	
$NaHCO_3$	$KMnO_4$	3	H_2O_2	1988	

$NaHCO_3$ 1.0 M; H_2O_2 0.5 M; $KMnO_4$ 1 mM; injection volume 100 µL

no light when $KMnO_4$ was introduced to HCO_3^- solution. The injection of H_2O_2 into the mixed HCO_3^-–$KMnO_4$ solution produced the most CL emission. There was only one CL peak found. Within 2 s, the CL intensity peaked at 1988, lasted around 24 s, and then quickly faded. In this experiment, the following mixing order was employed (Table 2.4).

2.4.2 Free Radicals and Emitting Species Studies

The consequences of various radical scavengers on the CL intensity of the HCO_3^-–H_2O_2–$KMnO_4$ system were used to further investigate the CL system's mechanism.

2.4.2.1 $^{\bullet}O_2^-$ Radical Detection

NBT is frequently utilized for the recognition of $^{\bullet}O_2^-$ radicals because it can be reduced by $^{\bullet}O_2^-$ to its deep-blue diformazan form [4, 52]. There was no color change when NBT was added to HCO_3^- or $KMnO_4$. When 1.0×10^{-5} M NBT was mixed with an HCO_3^-–H_2O_2–$KMnO_4$ solution, the color changed from yellow to blue. The peak at 259 nm vanished after injecting NBT into an HCO_3^--H_2O_2-$KMnO_4$ mixed solution. The presence of $^{\bullet}O_2^-$ radicals in the mixing solution was deduced using an assistant detection method. NBT can either increase or decrease the intensity of CL because it produces ROS in reversible reactions [53].

Cytochrome c is also a unique compound for the detection of $^{\bullet}O_2^-$ radical [72, 73]. It can be reduced by the radical ion ($^{\bullet}O_2^-$) to switch its color from red to colorless in an aqueous solution, with maximum absorption at 410 nm. Cytochrome c did not respond with either HCO_3^- or H_2O_2. However, after adding it to the HCO_3^-–H_2O_2–$KMnO_4$ solution in the reaction cuvette, the color changed to colorless. When 1.0×10^{-8} mol/L of cytochrome c was injected into an HCO_3^--H_2O_2–$KMnO_4$ mixed solution, the CL intensity increased by about two fold. The absorption at 410 nm was hastily reduced. These results demonstrated that $^{\bullet}O_2^-$ radical was generated during the CL progression.

By producing a high-octane dioxetanone intermediate, MCLA can react with ROS and generate intense CL light at 465 nm [16]. It has been used to determine $^{\bullet}O_2^-$ radical and $^1O_2$ using a CL probe [54]. MCLA increased CL intensity by 1.6 times in the HCO_3^-–H_2O_2–$KMnO_4$ system at a concentration of 1.0×10^{-6} M, and the peak of 465 nm vanished. It was also demonstrated that $^1O_2$ and $^{\bullet}O_2^-$ radical were produced and took part in the CL reaction.

2.4.2.2 $^1O_2$ Detection

To further define the formation of $^1O_2$ in this CL reaction, researchers employed 1,4-diazabicyclo [2]octane (DABCO), deuterium oxide (D_2O), and CCl_4. DABCO was

previously identified as a $^1O_2$ quencher [55]. The process is primarily an electronic-to-vibrational (e–v) one [56]. Electronic-to-vibrational energy transfer is a typical deactivation mean of O_2 $(^1\sum_g^+)$ and O_2 $(^1\Delta_g)$, in which the electronic excitation energy of the O_2 molecule is converted into vibrational energy of O_2 and quencher, and occurs in any di- or polyatomic collider in the gas or liquid phase [74]. With the addition of DABCO, the CL intensity of the HCO_3^-–H_2O_2–$KMnO_4$ system was reduced.

By comparing D_2O and CCl_4–H_2O, the creation of $^1O_2$ was proven. $^1O_2$ has a tenfold longer lifespan in D_2O than it does in H_2O [75]. Because of the differential in O–D, C–Cl, and O–H vibrations in the solvent, the lifespan in CCl_4 is 59 ms but only 3.1 s in H_2O [18]. HCO_3^-–H_2O_2–$KMnO_4$ reactions in D_2O, CCl_4, and H_2O environments had varied CL profiles. The CL signals in D_2O and CCl_4 solutions had a larger peak height than those in H_2O. These findings demonstrated that $^1O_2$ was formed in the course of the reactions.

The physical quencher for $^1O_2$ is sodium azide (NaN_3) [15, 57]. The generation of $^1O_2$ was also demonstrated through a study of the quenching influence. The CL reaction was efficiently suppressed by NaN_3, suggesting that $^1O_2$ was intricate in the CL reaction.

2.4.2.3 $^\bullet$OH Radical Detection

One of the most powerful oxidizers is the $^\bullet$OH radical, which can be effectively scavenged by thiourea [58]. At a concentration of 1.0×10^{-6} M thiourea in the CL system, it displayed considerable inhibition. With higher thiourea concentrations, the quenching effect became stronger. It was established that the reaction produced $^\bullet$OH radical.

To further describe the production of $^\bullet$OH radical, tert-butanol and dimethyl sulphoxide (DMSO) [76] was hosted in the CL system. T-butanol has a reaction constant of 6108 $M.s^{-1}$ when reacting with hydroxyl radicals [77]. T-butanol or DMSO at a concentration of 0.01% (v/v) reduced the CL intensity substantially. The reduction in the CL intensity of the system indicates the production of $^\bullet$OH radical, according to the data.

Ascorbic acid, as a traditional reducing agent, can be dehydrogenated by ROS to create dehydroascorbic acid [78], which has high reducibility. By reacting with O_2 in the solution and generating diketogulonic acid, it can further reduce CL intensity. When 1.0×10^{-5} M ascorbic acid was administered, the CL intensity was substantially reduced. The CL system was shown to be a radical reaction, according to the results.

2.4.2.4   ESR Spin Trapping Study

The free radical intermediates were detected using ESR spectroscopy. $^1O_2$ has a specific target molecule called TEMPO. It can create the adduct-TEMPO by reacting
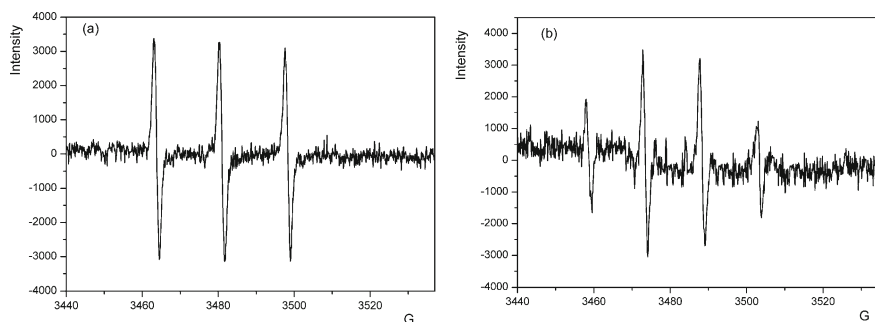
Fig. 2.13 EPR spectrum of nitroxide radicals produced by the reaction of the TEMP probe in HCO_3^--H_2O_2-$KMnO_4$ system (**a**), and EPR spectrum of $^\bullet OH$ addition to DMPO in HCO_3^--H_2O_2-$KMnO_4$ system (**b**). *Conditions* receiver gain 1.00e + 05; Mod amplitude 1G; Sweep width 100.00G; Microwave power 1.00 e + 01 mW. Copyright 2010, with permission from Springer Ref. [14]

with $^1O_2$. The stable nitroxide radical TEMPO has a distinct spectrum [79–81]. In the HCO_3^-–H_2O_2–$KMnO_4$ CL system, the particular signal of TEMPO was observed, indicating the production of $^1O_2$ (Fig. 2.13a).

$^\bullet OH$ radical was detected using ESR spectroscopy. The specific target molecule of $^\bullet OH$ [59] was 5,5-dimethyl-1-pyrroline N-oxide (DMPO). The creation of $^\bullet OH$ radical in the HCO_3^-–H_2O_2–$KMnO_4$ CL system was proven by the specific signal of the formation of DMPO-OH adduct (Fig. 2.13b).

2.4.3 Mechanism of the CL System

The CL spectrum was obtained to better understand the CL mechanism. Ten narrow band interference filters (400–640 nm) were used to obtain the CL spectrum information (Fig. 2.14a). Between the cuvette and the PMT, they were placed. With varying wavelengths, the CL signals were measured. The CL spectra had a maximum at 440 nm, according to the results. The breakdown of the excited $(CO_2)_2^*$ dimer [82] could account for the peak at 440 nm. The EHMO method calculated that the breakdown energy of the $(CO_2)_2$ dimer was 132 kcal mol/L. It was sufficient to induce emission at wavelengths greater than 220 nm [62]. The emission of $^1O_2$ results in emission at 634 nm [64], which has higher energy than ground state O_2 and can lose it through luminescence.

The CL mechanism of the HCO_3^-–H_2O_2–$KMnO_4$ system was studied using rhodamine B (RhB) and uranine (UN). All of them increased the CL's intensity. The CL spectra of the HCO_3^-–H_2O_2–$KMnO_4$–RhB or UN system revealed that RhB and UN were fluorescent substances, having emission wavelengths of 580 and 510 nm, respectively (Fig. 2.14b). When CL spectra were compared to FL spectra of RhB and UN, new luminants of the CL reaction were identified as RhB or UN
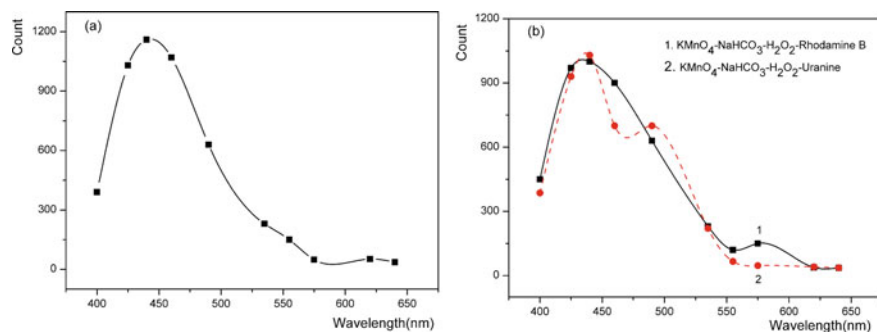
Fig. 2.14 CL spectra of HCO_3^-–H_2O_2–$KMnO_4$ system (**a**), and HCO_3^-–H_2O_2–$KMnO_4$ rhodamine B or uranine system (**b**). Copyright 2010, with permission from Springer Ref. [14]

because their peak fluorescence wavelengths were identical. When the excited RhB or UN returned to the ground state, some of the energy of $(CO_2)_2*$ and $^1O_2$ was transferred to these fluorescent substances, and fresh CL was created.

UV–Vis absorption spectroscopy was used to differentiate the change in fluorescent substance before and after the CL reaction to further confirm the emission species. The characteristic absorbance of RhB (553 nm) or UN (492 nm) was still present in the visible area of UV–vis spectra taken immediately after the reaction, whereas that of $KMnO_4$ had vanished. As a result, it was proven that the HCO_3^-–H_2O_2–$KMnO_4$–RhB or UN system did not react with RhB or UN. After absorbing energy, they were stimulated to the excited state (RhB* or UN*). The CL was brought back to the ground state by RhB* or UN*, which aided the energy transfer process.

We discovered that infusing $KMnO_4$ into an HCO_3^-–H_2O_2 mixed solution in the absence or presence of RhB or UN merely changed the fluorescence emission intensity, not the fluorescence spectra (max 580 nm, max 510 nm). In both the presence and absence of RhB or UN, the oxidation products were the same. In the HCO_3^-–H_2O_2–$KMnO_4$ system, oxidation products were the emitters. When RhB or UN was administered, the emitter transferred energy to the fluorescent substance, and the fluorescent substance became emitters. CL was produced by them. Based on these findings, Table 2.5 summarizes the mechanism of the CL reaction accelerated by RhB or UN.

2.5 Conclusions

The use of bicarbonate ions as an effective hydrogen peroxide activator was recommended for "green" processing. The production of HCO_4^- as the oxidant was corroborated by spectroscopic evidence. Ultra-weak CL produced from the decomposition of HCO_4^- was observed. When adding fluorescent compound, Eu(II) complex, $NaYF_4$:Yb^{3+}/Er^{3+} NPs, $KMnO_4$, or eosin Y-sensitized Au NPs into the system, the

Table 2.5 Chemiluminescence reactions for HCO_3^-–H_2O_2–$KMnO_4$ system

CL system	Mechanism
$NaHCO_3$–H_2O_2–$KMnO_4$	$HCO_3^- + H_2O_2 \rightleftharpoons HCO_4^- + H_2O$ (1)
	$HCO_4^- \rightarrow \cdot CO_3^- + \cdot OH$ (2)
	$H_2O_2 + \cdot CO_3^- \rightarrow HCO_3^- + HO_2\cdot$ (3)
	$HO_2\cdot \rightarrow H^+ + \cdot O_2^-$ (4)
	$\cdot O_2^- + \cdot OH \rightarrow {}^1O_2 + OH^-$ (5)
	${}^1O_2 \rightarrow {}^3O_2 + h\nu$ (6)
	$MnO_4^- + \cdot O_2^- \rightarrow MnO_4^{2-} + \cdot O_2$ (7)
	$\cdot O_2 + \cdot O_2 \rightarrow (O_2)_2^*$ (8)
	$2 \cdot O_2^- + 2 \cdot O_2^- + 4H_2O \rightarrow (O_2)_2^* + 2H_2O_2 + 4OH^-$ (9)
	$(O_2)_2^* \rightarrow 2O_2 + h\nu$ (10)
	$\cdot OH + HCO_3^- \rightarrow OH^- + \cdot HCO_3$ (11)
	$2 \cdot HCO_3 \rightarrow (CO_2)_2^* + H_2O_2$ (12)
	$(CO_2)_2^* \rightarrow 2CO_2 + h\nu$ (13)
	$(O_2)_2^* + \text{Rhodamine B} \rightarrow \text{Rhodamine B} * + 2O_2$ (14)
	$\text{Rhodamine B}* \rightarrow \text{Rhodamine B} + h\nu$ (15)
	$(O_2)_2^* + \text{Uranine} \rightarrow \text{Uranine} * + 2O_2$ (16)
	$\text{Uranine}* \rightarrow \text{Uranine} + h\nu$ (17)

CL emission was greatly improved. More applications of HCO_4^- as a possibly beneficial analytical reagent might be possible as a result of these new phenomena.

The CL mechanism for HCO_4^- was thoroughly explored. The unimolecular homolysis of the peroxo O–O bond started a mechanism reaction. The bond rearrangement within radicals is thought to produce $^\bullet O_2^-$. $^1O_2$ was formed by the reaction of the $^\bullet O_2^-$ radical with the $HO_2^\bullet$. The energy of $^1O_2$ can be transmitted to fluorescent compounds and the Eu(II) complex, forming an excited energy acceptor. The energy acceptor then relaxes to the ground state, resulting in light emission. A catalytic procedure was used to produce CL from the breakdown of HCO_4^- boosted by $KMnO_4$.

Because of its critical role as ROS in biological systems, the HCO_4^- is also of interest. Its oxidation system is simple, low-cost, and low-toxicity compared to other oxidizing agents and peroxyacids, and it can be utilized in a range of oxidation reactions that require a moderate, neutral pH.

References

1. Elbanowski M, Paetz M, Siawinski J, Cieśla L (1988) Chemiluminescence and fluorescence of the europium ions-adenine nucleotides system and its possible biological significance. Photochem Photobiol 47:463–466. https://doi.org/10.1111/j.1751-1097.1988.tb02752.x

2. Fan Z, Qingxiong L (1993) A new chemiluminescence system: MnO_4^--Na_2CO_3-KOH and its application in the determination of manganese. Talanta 40:1557–1561. https://doi.org/10.1016/0039-9140(93)80368-2

3. Lin J-M, Hobo T (1996) Flow-injection analysis with chemiluminescent detection of sulphite using Na_2CO_3 $NaHCO_3$-Cu^{2+} system. Anal Chim Acta 323:69–74. https://doi.org/10.1016/0003-2670(95)00611-7

4. Lin J-M, Yamada M (1999) Oxidation reaction between periodate and polyhydroxyl compounds and its application to chemiluminescence. Anal Chem 71:1760–1766. https://doi.org/10.1021/ac981341m

5. Drago R, Frank K, Yang Y, Wagner G (1998) Proceedings of the 1997 ERDEC scientific conference on chemical and biological defense research, p 950

6. Richardson DE, Yao H, Frank KM, Bennett DA (2000) Equilibria, kinetics, and mechanism in the bicarbonate activation of hydrogen peroxide: oxidation of sulfides by peroxymonocarbonate. J Am Chem Soc 122:1729–1739. https://doi.org/10.1021/ja9927467

7. Yao H, Richardson DE (2000) Epoxidation of alkenes with bicarbonate-activated hydrogen peroxide. J Am Chem Soc 122:3220–3221. https://doi.org/10.1021/ja993935s

8. Makita Y, Suzuki T, Yamada M, Hobo T (1994) Flow-injection determinations of cobalt (II) and iron (II) based on chemiluminescence induced by the catalytic decomposition of peroxomonosulfate. Nippon Kagaku Kaishi 701–706. https://doi.org/10.1246/nikkashi.1994.701

9. Adam A, Mehta M (1998) KH (O_2) CO_2· H_2O_2-An oxygen-rich salt of monoperoxocarbonic acid. Angew Chem Int Ed 37:1387–1388. https://doi.org/10.1002/(SICI)1521-3773(19980605)37:10

10. Richardson DE, Regino CA, Yao H, Johnson JV (2003) Methionine oxidation by peroxymonocarbonate, a reactive oxygen species formed from CO_2/bicarbonate and hydrogen peroxide. Free Radical Biol Med 35:1538–1550. https://doi.org/10.1016/j.freeradbiomed.2003.08.019

11. Lin J-M, Liu M (2009) Singlet oxygen generated from the decomposition of peroxymonocarbonate and its observation with chemiluminescence method. Spectrochim Acta Part A Mol Biomol Spectrosc 72:126–132. https://doi.org/10.1016/j.saa.2008.08.019

12. Liu M, Cheng X, Zhao L, Lin J M (2006) On-line preparation of peroxymonocarbonate and its application for the study of energy transfer chemiluminescence to lanthanide inorganic coordinate complexes. Lumin J Biol Chem Lumin 21:179–185. https://doi.org/10.1002/bio.903

13. Chen H, Li H, Lin J-M (2012) Determination of ammonia in water based on chemiluminescence resonance energy transfer between peroxymonocarbonate and branched $NaYF_4$: Yb^{3+}/Er^{3+} nanoparticles. Anal Chem 84:8871–8879. https://doi.org/10.1021/ac302300z

14. Chen H, Lu C, Li R, Guo G, Lin J-M (2010) Chemiluminescence behavior of sodium hydrogen carbonate in the potassium permanganate-hydrogen peroxide reaction. Sci China Chem 53:1784–1792. https://doi.org/10.1007/s11426-010-3158-1

15. Hosaka S, Itagaki T, Kuramitsu Y (1999) Selectivity and sensitivity in the measurement of reactive oxygen species (ROS) using chemiluminescent microspheres prepared by the binding of acridinium ester or ABEI to polymer microspheres. Luminescence 14:349–354. https://doi.org/10.1002/(SICI)1522-7243(199911/12)14:6

16. Nakano M, Sugioka K, Ushijima Y, Goto T (1986) Chemiluminescence probe with cypridina luciferin analog, 2-methyl-6-phenyl-3, 7-dihydroimidazo [1, 2-a] pyrazin-3-one, for estimating the ability of human granulocytes to generate O2−. Anal Biochem 159:363–369. https://doi.org/10.1016/0003-2697(86)90354-4

17. Khan AU, Kasha M (1963) Red chemiluminescence of molecular oxygen in aqueous solution. J Chem Phys 39:2105–2106. https://doi.org/10.1063/1.1734588

18. Adam W, Kazakov DV, Kazakov VP (2005) Singlet-oxygen chemiluminescence in peroxide reactions. Chem Rev 105:3371–3387. https://doi.org/10.1021/cr0300035

19. Shah SNA, Li H, Lin J-M (2016) Enhancement of periodate-hydrogen peroxide chemiluminescence by nitrogen doped carbon dots and its application for the determination of pyrogallol and gallic acid. Talanta 153:23–30. https://doi.org/10.1016/j.talanta.2016.02.056

20. Shah SNA, Lin J-M (2017) Recent advances in chemiluminescence based on carbonaceous dots. Adv Colloid Interface Sci 241:24–36. https://doi.org/10.1016/j.cis.2017.01.003

21. Shah SNA, Khan M, Rehman ZU (2020) A prolegomena of periodate and peroxide chemiluminescence TrAC, Trends Anal Chem 122 115722 https://doi.org/10.1016/j.trac.2019.115722

22. Koppenol W, Moreno J, Pryor WA, Ischiropoulos H, Beckman J (1992) Peroxynitrite, a cloaked oxidant formed by nitric oxide and superoxide. Chem Res Toxicol 5:834–842. https://doi.org/10.1021/tx00030a017

23. Aresta M, Tommasi I, Quaranta E, Fragale C, Mascetti J, Tranquille M, Galan F, Fouassier M (1996) Mechanism of formation of peroxocarbonates RhOOC(O)O(Cl)(P)(3) and their reactivity as oxygen transfer agents mimicking monooxygenases. The first evidence of CO(2) insertion into the O–O bond of Rh(eta(2)–O(2)) Complexes. Inorg Chem 35:4254–4260. https://doi.org/10.1021/ic951154w

24. Hayward P, Blake D, Wilkinson G, Nyman C (1970) Reactions of peroxobis (triphenylphosphine) platinum (II) and analogs with with carbon dioxide, carbon disulfide, and other unsaturated molecules. J Am Chem Soc 92:5873–5878. https://doi.org/10.1021/ja00723a010

25. Bielski BHJ, Cabelli DE, Arudi RL, Ross AB (1985) Reactivity of $HO_2/O-2$ radicals in aqueous solution. J Phys Chem Ref Data 14:1041–1100. https://doi.org/10.1063/1.555739

26. Khan AU, Kasha M (1970) Chemiluminescence arising from simultaneous transitions in pairs of singlet oxygen molecules. J Am Chem Soc 92:3293–3300. https://doi.org/10.1021/ja00714a010

27. Shah SNA, Zheng Y, Li H, Lin J-M (2016) Chemiluminescence character of ZnS quantum dots with bisulphite-hydrogen peroxide system in acidic medium. J Phys Chem C 120:9308–9316. https://doi.org/10.1021/acs.jpcc.6b01925

28. Zheng Y, Zhang D, Shah SNA, Li H, Lin J-M (2017) Ultra-weak chemiluminescence enhanced by facilely synthesized nitrogen-rich quantum dots through chemiluminescence resonance energy transfer and electron hole injection. Chem Commun 53:5657–5660. https://doi.org/10.1039/C7CC02041D

29. Dou X, Zhang Q, Shah SNA, Khan M, Uchiyama K, Lin J-M (2019) MoS_2-quantum dot triggered reactive oxygen species generation and depletion: responsible for enhanced chemiluminescence. Chem Sci 10:497–500. https://doi.org/10.1039/C8SC03511C

30. Shah SNA, Lin L, Zheng Y, Zhang D, Lin J-M (2017) Redox cycling of iron by carbon dot enhanced chemiluminescence: mechanism of electron–hole induction in carbon dot. Phys Chem Chem Phys 19:21604–21611. https://doi.org/10.1039/C7CP03724D

31. Li H-R, Wu L-Z, Tung C-H (2000) Reactions of singlet oxygen with olefins and sterically hindered amine in mixed surfactant vesicles. J Am Chem Soc 122:2446–2451. https://doi.org/10.1021/ja9917161

32. Miyamoto S, Martinez GR, Martins APB, Medeiros MH, Di Mascio P (2003) Direct evidence of singlet molecular oxygen $[O_2(^1\Delta_g)]$ production in the reaction of linoleic acid hydroperoxide with peroxynitrite. J Am Chem Soc 125:4510–4517. https://doi.org/10.1021/ja029262m

33. Aubry J, Cazin B (1988) Chemical sources of singlet oxygen. 2. Quantitative generation of singlet oxygen from hydrogen peroxide disproportionation catalyzed by molybdate ions. Inorg Chem 27:2013–2014. https://doi.org/10.1021/ic00285a001

34. Huang X, Li L, Qian H, Dong C, Ren J (2006) A resonance energy transfer between chemiluminescent donors and luminescent quantum-dots as acceptors (CRET). Angew Chem Int Ed 45:5140–5143. https://doi.org/10.1002/anie.200601196

35. Lee JS, Joung H-A, Kim M-G, Park CB (2012) Graphene-based chemiluminescence resonance energy transfer for homogeneous immunoassay. ACS Nano 6:2978–2983. https://doi.org/10.1021/nn300684d

36. Qin G, Zhao S, Huang Y, Jiang J, Ye F (2012) Magnetic bead-sensing-platform-based chemiluminescence resonance energy transfer and its immunoassay application. Anal Chem 84:2708–2712. https://doi.org/10.1021/ac202959d

37. Freeman R, Liu X, Willner I (2011) Chemiluminescent and chemiluminescence resonance energy transfer (CRET) detection of DNA, metal ions, and aptamer–substrate complexes

using hemin/G-quadruplexes and CdSe/ZnS quantum dots. J Am Chem Soc 133:11597–11604. https://doi.org/10.1021/ja202639m

38. Liu X, Freeman R, Golub E, Willner I (2011) Chemiluminescence and chemiluminescence resonance energy transfer (CRET) aptamer sensors using catalytic hemin/G-quadruplexes. ACS Nano 5:7648–7655. https://doi.org/10.1021/nn202799d

39. Wu XZ, Yamada M, Hobo T, Suzuki S (1989) Uranin sensitized chemiluminescence for alternative determinations of copper (II) and free cyanide by the flow injection method. Anal Chem 61:1505–1510. https://doi.org/10.1021/ac00189a009

40. Furukawa K, Gray E, Ogryzlo E (1970) Singlet oxygen from discharge-flow systems. Ann NY Acad Sci 171:175–187. https://doi.org/10.1111/j.1749-6632.1970.tb39322.x

41. Sabbatini N, Guardigli M, Lehn J-M (1993) Luminescent lanthanide complexes as photochemical supramolecular devices. Coord Chem Rev 123:201–228. https://doi.org/10.1016/0010-8545(93)85056-A

42. De Sa G, Malta O, De Mello DC, Simas A, Longo R, Santa-Cruz P, Da Silva JE (2000) Spectroscopic properties and design of highly luminescent lanthanide coordination complexes. Coord Chem Rev 196:165–195. https://doi.org/10.1016/S0010-8545(99)00054-5

43. Vicentini G, Zinner L, Zukerman-Schpector J, Zinner K (2000) Luminescence and structure of europium compounds. Coord Chem Rev 196:353–382. https://doi.org/10.1016/S0010-8545(99)00220-9

44. Mcclure DS, Kiss Z (1963) Survey of the spectra of the divalent rare-earth ions in cubic crystals. J Chem Phys 39:3251–3257. https://doi.org/10.1063/1.1734186

45. Glass RS, Faulkner LR (1981) Electrogenerated chemiluminescence from the tris (2, 2'-bipyridine) ruthenium (II) system. An example of S-route behavior. J Phys Chem 85:1160–1165. https://doi.org/10.1021/j150609a017

46. Elbanowski M, Staninski K, Kaczmarek M, Lis S (2001) Energy transfer in the chemiluminescent system: Eu(II)/(III)–N−3–H$_2$O$_2$. J Alloys Compd 323:670–672. https://doi.org/10.1016/S0925-8388(01)01070-2

47. Brittain HG, Choppin GR, Barthelemy PP (1992) pH-dependence of the metal ion hydration state in lanthanide complexes of polyaminopolycarboxylate ligands. J Coord Chem 26:143–153. https://doi.org/10.1080/00958979209407924

48. Elbanowski M, Lis S, Mąkowska B (1985) Fluorescence of lanthanide (III) complexes in aqueous solutions the influence of pH and solution composition. Monatshefte für Chemie/Chem Monthly 116:901–911. https://doi.org/10.1007/Bf00809183

49. Elbanowski M, Kaczmarek M, Staninski K (1998) The influence of aminopolycarboxylic acids on the chemiluminescence of the Eu (II)/Eu (III)–H$_2$O$_2$ system. J Alloys Compd 275:225–229. https://doi.org/10.1016/S0925-8388(98)00308-9

50. Lloyd R (1965) Low-level chemiluminescence from hydrocarbon autoxidation reactions. Part 1. —apparatus for studying thermal decomposition reactions and observat on benzoyl peroxide in de-oxygenated benzene. Trans Faraday Society 61:2173–2181. https://doi.org/10.1039/TF9656102173

51. Hayashi J, Yamada M, Hobo T (1991) Schiff base chemiluminescence with Fenton's reagent for the determination of primary amines and amino acids. Anal Chim Acta 247:27–35. https://doi.org/10.1016/S0003-2670(00)83048-2

52. Bielski BH, Shiue GG, Bajuk S (1980) Reduction of nitro blue tetrazolium by CO$_2$-and O2-radicals. J Phys Chem 84:830–833. https://doi.org/10.1021/j100445a006

53. Bartosz G (2006) Use of spectroscopic probes for detection of reactive oxygen species. Clin Chim Acta 368:53–76. https://doi.org/10.1016/j.cca.2005.12.039

54. Lu C, Song G, Lin J-M (2006) Reactive oxygen species and their chemiluminescence-detection methods. TrAC, Trends Anal Chem 25:985–995. https://doi.org/10.1016/j.trac.2006.07.007

55. Ouannes C, Wilson T (1968) Quenching of singlet oxygen by tertiary aliphatic amines. Effect of DABCO (1, 4-diazabicyclo [2.2. 2] octane). J Am Chem Soc 90:6527–6528. https://doi.org/10.1021/ja01025a059

56. Shikhova E, Danilov EO, Kinayyigit S, Pomestchenko IE, Tregubov AD, Camerel F, Retailleau P, Ziessel R, Castellano FN (2007) Excited-state absorption properties of platinum (II) terpyridyl acetylides. Inorg Chem 46:3038–3048. https://doi.org/10.1021/ic0618652

57. Lin J-M, Yamada M (2000) Chemiluminescent reaction of fluorescent organic compounds with KHSO5 using cobalt (II) as catalyst and its first application to molecular imprinting. Anal Chem 72:1148–1155. https://doi.org/10.1021/ac9911140

58. Wang W-F, Schuchmann MN, Schuchmann H-P, Knolle W, Von Sonntag J, Von Sonntag C (1999) Radical cations in the OH-radical-induced oxidation of thiourea and tetramethylthiourea in aqueous solution. J Am Chem Soc 121:238–245. https://doi.org/10.1021/ja983275b

59. Villamena FA, Locigno EJ, Rockenbauer A, Hadad CM, Zweier JL (2007) Theoretical and experimental studies of the spin trapping of inorganic radicals by 5, 5-dimethyl-1-pyrroline N-oxide (DMPO). 2. Carbonate radical anion. J Phys Chem A 111:384–391. https://doi.org/10.1021/jp065692d

60. Shah SNA, Dou X, Khan M, Uchiyama K, Lin J-M (2019) N-doped carbon dots/H_2O_2 chemiluminescence system for selective detection of Fe^{2+} ion in environmental samples. Talanta 196:370–375. https://doi.org/10.1016/j.talanta.2018.12.091

61. Shah SNA, Shah AH, Dou X, Khan M, Lin L, Lin J-M (2019) Radical-triggered chemiluminescence of phenanthroline derivatives: an insight into radical-aromatic interaction. ACS Omega 4:15004–15011. https://doi.org/10.1021/acsomega.9b01785

62. Bollyky LJ (1970) Chemiluminescence from the reaction of ketenes, singlet oxygen, and fluorescers. J Am Chem Soc 92:3230–3232. https://doi.org/10.1021/ja00713a077

63. Lin J, Hobo T (1995) Chemiluminescence investigation of NH_2OH-fluorescein-Cu^{2+} system and its application to copper analysis in serum. Talanta 42:1619–1623. https://doi.org/10.1016/0039-9140(95)01614-7

64. Lu C, Lin J-M (2004) Carbonate-catalyzed chemiluminescence decomposition of peroxynitrite via $(CO_2)_2*$ intermediate. Catal Today 90:343–347. https://doi.org/10.1016/j.cattod.2004.04.045

65. Cui H, Zhang Z-F, Shi M-J (2005) Chemiluminescent reactions induced by gold nanoparticles. J Phys Chem B 109:3099–3103. https://doi.org/10.1021/jp045057c

66. Bakhmutova-Albert EV, Yao H, Denevan DE, Richardson DE (2010) Kinetics and mechanism of peroxymonocarbonate formation. Inorg Chem 49:11287–11296. https://doi.org/10.1021/ic1007389

67. Lane BS, Vogt M, Derose VJ, Burgess K (2002) Manganese-catalyzed epoxidations of alkenes in bicarbonate solutions. J Am Chem Soc 124:11946–11954. https://doi.org/10.1021/ja025956j

68. Haygarth KS, Marin TW, Janik I, Kanjana K, Stanisky CM, Bartels DM (2010) Carbonate radical formation in radiolysis of sodium carbonate and bicarbonate solutions up to 250 C and the mechanism of its second order decay. J Phys Chem A 114:2142–2150. https://doi.org/10.1021/jp9105162

69. Decorpo J, Baronavski A, Mcdowell M, Saalfeld F (1972) Formation of carbon dioxide dimer in chemiluminescent reactions. J Am Chem Soc 94:2879–2880. https://doi.org/10.1021/ja00763a067

70. Sławinska D, Sławinski J (1998) Chemiluminescence of cereal products. II. Chemilumin spectra. J Biolumin Chemilumin 13:13–19. https://doi.org/10.1002/(SICI)1099-1271(199801/02)13:1%3c13::AID-BIO461%3e3.0.CO;2-F

71. Jares-Erijman EA, Jovin TM (2003) FRET imaging. Nat Biotechnol 21:1387–1395. https://doi.org/10.1038/nbt896

72. Lisdat F, Ge B, Ehrentreich-Förster E, Reszka R, Scheller F (1999) Superoxide dismutase activity measurement using cytochrome c-modified electrode. Anal Chem 71:1359–1365. https://doi.org/10.1021/ac980961k

73. Asai R, Matsukawa R, Ikebukuro K, Karube I (1999) Highly sensitive chemiluminescence flow-injection detection of the red tide phytoplankton heterosigma carterae. Anal Chim Acta 390:237–244. https://doi.org/10.1016/S0003-2670(99)00145-2

74. Schweitzer C, Schmidt R (2003) Physical mechanisms of generation and deactivation of singlet oxygen. Chem Rev 103:1685–1758. https://doi.org/10.1021/cr010371d

75. Merkel PB, Nilsson R, Kearns DR (1972) Deuterium effects on singlet oxygen lifetimes in solutions. New test of singlet oxygen reactions. J Am Chem Soc 94:1030–1031. https://doi.org/10.1021/ja00758a072

76. Herscu-Kluska R, Masarwa A, Saphier M, Cohen H, Meyerstein D (2008) Mechanism of the reaction of radicals with peroxides and dimethyl sulfoxide in aqueous solution. Chem–A Euro J 14:5880–5889. https://doi.org/10.1002/chem.200800218

77. De Witte B, Dewulf J, Demeestere K, Van Langenhove H (2009) Ozonation and advanced oxidation by the peroxone process of ciprofloxacin in water. J Hazard Mater 161:701–708. https://doi.org/10.1016/j.jhazmat.2008.04.021

78. Dai H, Wu X, Wang Y, Zhou W, Chen G (2008) An electrochemiluminescent biosensor for vitamin C based on inhibition of luminol electrochemiluminescence on graphite/poly (methyl-methacrylate) composite electrode. Electrochim Acta 53:5113–5117. https://doi.org/10.1016/j.electacta.2008.02.044

79. Lin J-M, Liu M (2008) Chemiluminescence from the decomposition of peroxymonocarbonate catalyzed by gold nanoparticles. J Phys Chem B 112:7850–7855. https://doi.org/10.1021/jp8008805

80. Zhang D, Zheng Y, Dou X, Lin H, Shah SNA, Lin J-M (2017) Heterogeneous chemiluminescence from gas-solid phase interactions of Ozone with alcohols, phenols, and saccharides. Langmuir 33:3666–3671. https://doi.org/10.1021/acs.langmuir.7b00481

81. Zhang D, Zheng Y, Dou X, Shah SNA, Lin J-M (2017) Gas-phase chemiluminescence of reactive negative ions evolved through corona discharge in air and O_2 atmospheres. RSC Adv 7:15926–15930. https://doi.org/10.1039/C6RA21683H

82. Cordes HF, Richter HP, Heller CA (1969) Mass spectrometric evidence for the existence of 1, 2-dioxetanedione (carbon dioxide dimer). Chemilumin Intermed J Am Chem Soc 91:7209–7209. https://doi.org/10.1021/ja01053a065

Chapter 3
Ultra-Weak Chemiluminescence from Decomposition of Peroxynitrous/Peroxynitrite

Hui Chen and Jin-Ming Lin

Abstract Peroxynitrite (ONOO$^-$) has been ionized from peroxynitrous acid (ONOOH) over basic solution, and ONOOH was aroused as the final product of those responses between nitrite furthermore hydrogen peroxide with the cooperation of an acidic impetus. The higher the concentration of nitrite, the higher intensity of chemiluminescence (CL) signal with the participation of a suitable surfactant (at thickness over its owing CMC) and/or a sensitizer. For instance, uranine and fluorescein all belonging to fluorescent compounds, have been shown to be powerful sensitizers (due to the rapid energy being transferred from singlet oxygen to fluorescent substances). We can use these properties to set out the nitrite in natural water samples. Bilirubin and its conjugate have the function to maximize CL emission of ^{1}O$_2$ during the decomposition of ONOO$^-$ to a micellar media that really is suitable. For the first and only time, the possibility from utilizing this exhibit CL framework for those delicate and particular mensuration of aggregate bilirubin substance clinched alongside mankind's serum was developed. We also found the supplanting from NaOH by Na$_2$CO$_3$ markedly improved the CL power owning of the decay of ONOO$^-$, and carbonate plays the role of a catalyst in the process. We also studied the CL property of carbon dots which is in the presence of peroxynitrous acid will be expected of the radiative recombination from claiming hole-injected and electron-injected carbon dots. This research provided us with new viewpoints of carbon dots.

Keywords Peroxynitrite · Peroxynitrous acid · Hydrogen peroxide · Chemiluminescence

H. Chen
College of Materials Science and Technology, Beijing Forestry University, Beijing 100083, China

J.-M. Lin (✉)
Department of Chemistry, Tsinghua University, Beijing 100084, China
e-mail: jmlin@mail.tsinghua.edu.cn

3.1   Introduction

Peroxynitrite ($ONOO^-$) as well as its corresponding peroxynitrous acid (ONOOH), play an increasingly important position in researching pathological conditions as dangerous side agents [1–3]. Peroxynitrous can generate peroxynitrite in NaOH solution and owing to the reaction of nitrite with hydrogen peroxide that has already been acidified, the peroxynitrous acid would be created. $ONOO^-$ will be a moderately sort of stable particle for basic result (pKa about 6. 8); however, when protonated to yield ONOOH, however, it promptly due to the following factors to make nitric corrosive or disintegrates along those unstable O–O links with a half-life for less than 1 s encountered with decay. In physiological pH and 37 °C, we observed chemiluminescence (CL) when the decomposition of peroxynitrite into NO- occurs. Under an appropriate surfactant (at awareness above its CMC) and a sensitizer, we also observed singlet oxygen ($^1O_2$) (the proposed CL emitter) [4, 5].

There are many methods in various literature reports about the synthesis of $ONOO^-$ [6, 7]. However, thanks to the off-line technique, ONOO generated may contain breakdown products according to literature. It is more complicate and difficult for the research results to interpret. Therefore, it is so important to synthesize $ONOO^-$ on-line. Saha et al. [8] proved an approach for synthesizing $ONOO^-$ directly, including the blending from claiming that in a modest flow system, acidified hydrogen peroxide with nitrite changes ONOOH into $ONOO^-$ under necessary conditions. However, the synthesized $ONOO^-$ need a chance to be held at −20 °C for resulting examinations. Through the above performance research, we synthesized ONOOH on-line furthermore at the same time investigated its CL decomposition system with bilirubin, carbonate, and carbon dots solution. We manufactured ONOOH in actual environments and assessed its CL destruction mechanism involving bilirubin, carbonate, and carbon dots concentrations using only a range of methodologies.

As we all know that, carbonate is a large proportion of components in a physiological circumstance, whose total concentration is pretty nearly 25 mmol L^{-1} [9]. In the introduction of carbonate liquor, $ONOO^-$ develops unstable [10, 11]. However, there is still a controversy about the mechanisms of ONOO- with carbonate fluid reaction [12–16]. Radi et al. [12], as well, for example, proposed that it may be through the formation of $ONOOCO_2^-$ intermediate. The reaction involving bicarbonate as well as ONOO- actually occurs. Hurst and co-worker [15] suggested that $ONOOCO_2^-$ is formed as an important product throughout the reaction of $ONOO^-$ with CO_2, rather than the reaction of ONOOH with bicarbonate. As a result, it may be critical to identify out just how ONOO responds with carbonate solution.

Chemiluminescence (CL) has gained popularity in recent years as a promising method. In terms of detection practical limitations and instrument relative simplicity, it has numerous significant advantages in terms of speed of analysis, reproducibility, and linear dynamic range [17], so it is often to be used in clinical laboratories on something like a constant schedule. Nitrite is and one of the widespread emission of harmful elements [18, 19]. Even if there is nitrite inside the water, it

can react with secondary and generate carcinogenic *N*-nitrosamines. Finally, this substance can seriously harm your health [20]. Secondly, while nitrite could transition oxyhaemoglobin to methemoglobin, it impedes transport of oxygen inside the bloodstream. Thus, whether in environment or human bodies, a straightforward, sympathetic, and detailed method for determination of nitrite is extremely important. Mikuska et al. [21] accounted for the determination from nitrite, dependent upon the mechanism using alkaline hydrogen peroxide for nitrite to form peroxynitrous acid [22–24], with resulting response with alkaline luminol that is to say the light emitter. We developed a flow-injection CL method for the determination of nitrite without any special CL reagent, e.g., luminol and lucigenin. This special method is realized through the decomposition of the peroxynitrite to structure NO^- ion, furthermore, singlet oxygen ($^1O_2$) which is the light-emitting species. The detection limit (S/N = 3) is 5.0×10^{-8} mol L^{-1} and the relative standard deviation for nine repeated measurements of 1.0×10^{-6} mol L^{-1} nitrite was 4.3%. The selectivity is better owing to the selective reaction of peroxynitrite.

In healthy biological individuals, the unconjugated form of bilirubin comprises approximately most of it (more than 95%), and total bilirubin concentrations in blood normally range between 3.5 and 10 mg L^{-1} [25]. If the concentration of bilirubin in the human serum or plasma is not within the normal range usually reveals the presence of a few disorders regarding the liver, extending from neonatal jaundice to infectious hepatitis [26]. Measurement of bilirubin plays an important role in diagnosing including several issues. In many medical research units around the world, the most commonly used and widely used the method used to determine bilirubin is dependent on the existence of an accelerator. However, these ways take a long time and the sensitivity is very low. The use of a flow-injection CL system to assess nitrite was accurately described owing to the rapid decomposition of $ONOO^-$ into NO^- and singlet oxygen ($^1O_2$) (the proposed CL emitter) in a suitable condition where are surfactants (concentration higher than its CMC) and sensitizers (uranium) suitable for reaction in the system. We found bilirubin and its conjugate could enhance CL emission intensity significantly which formed by a nitrite hydrogen peroxide effect proceeds in a micellar solution environment. It was commonly used to predict the total bilirubin levels of human serum with high selectivity, good recovery and precision, and wide linear dynamic range [5].

3.2 On-Line Preparation of Peroxynitrous and Nitrite Determination

Acidic medium will promote the response between nitrite and hydrogen peroxide and the final product is peroxynitrite, a compound that becomes very unstable in an acidic environment. The reaction is quenched into peroxynitrite. With peroxynitrite destruction, the feeble signal of chloride ion was captured. This CL system was created as conjunction of a flow-injection methodology for monitoring nitrite values.

The strength of chloride ion with the increase of nitrite concentration whose intensity in the range from 1.0×10^{-7} to 5.0×10^{-5} mol L^{-1}.

3.2.1 On-Line Preparation of Peroxynitrous

As shown in Fig. 3.1, The carrier stream was injected with 50 μL nitrite stock solutions or a sample solution. and mixed with the carrier stream by an injector and mixed with H_2O_2-HCl soluion through a three-way piece. It is necessary to use a 20 cm mixing coil for effective sample blending of H_2O_2–HCl solution. A cation-exchange column located after the loop valve was used for proper pre-treatment of samples. Finally, the sample–H_2O_2–HCl solution and NaOH–EDAB–uranine solution was thoroughly mixed and placed in a spiral flow CL cell with a photomultiplier tube. Record the CL signal keenly with a portable recorder.

CL is described as that of the emission of a photon from a species in an electromagnetic excited state during or after a chemical reaction. Therefore, in the CL reaction, it is crucial to adjust the appropriate combining order of the reagent solution. Because there is it may not be possible to observe or capture only weak light if the mixing orders is unsuitable. For the highest CL signal, we adopted batch method to measure various mixing orders. The results indicated that if we injected 100 μL appropriate amount of NaOH solution into H_2O_2–H_2O–NO_2^- solution, CL phenomenon would not happen. The replacement of all H_2O with 0.06 mol L^{-1} HCl solution there was a weak CL emission. This occurrence revealed that in the experimental reaction system of NO_2^- with H_2O_2, the involvement of acidic catalysts is only one element, after that, you must first add the NaOH solution if we want to generate CL signal. If NaOH
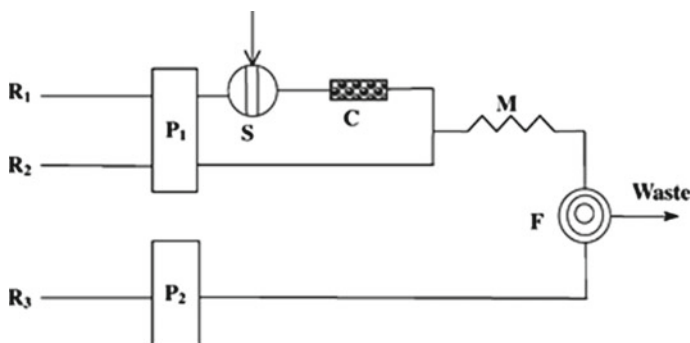
Fig. 3.1 Diffusion chemiluminescence system graphical diagram. P_1 and P_2, peristaltic pumps; M, blending coil (20 cm long); S, 50 ml sample injector; C, 5.0 mm i.d. 3.0 cm length column filled with Dowex 50 W X4 resin; F, flow cell; R_1, carrier (water) at 1.8 ml min^{-1}; R_2, carrier (water) at 1.8 ml/min; R_3, carrier (water) at 1.8 ml min^{-1}; R_4, carrier (water) at 1.8, 0.01 mol L^{-1} H_2O_2–0.06 mol L^{-1} HCl solution at 1.8 mL/min; R_3, 0.006 M EDAB–0.001 mol L^{-1} uranine in 0.15 mol L^{-1} NaOH solution at 2.5 ml/min. Copyright 2002, with permission from Elsevier [4]

solution is added first and then HCl solution is added, the receiving instrument will not record the signal of CL. Therefore, it is obviously important that the order inside which NaOH and HCl solutions are joined in the NO_2–H_2O_2 system. NaOH must be finally added to the solution system, and the order of addition must be considered from the point of view of the flow system.

CL's sensitivity does have to be strengthened. Through some controllable measures, surfactants and promoters are also necessary to improve the strength of the reaction. We studied three major compositions of EDAB and uranine with NaOH. We can find that the CL intensity would not be massively increased if EDAB and uranine just were not added to the basic solution together. The strongest CL emission would appear if such a NaOH–EDAB–uranine blending solution was poured into an H_2O_2–HCl–NO_2 system.

Finally, effect of mixing time on the reaction intensity of H_2O_2 and HCl solutions after mixing was studied. Everyone knows that H_2O_2 is a relatively stable material in acidic medium. Our experimental results showed that it would stay stable for at least 3 h if 0.01 mol L^{-1} H_2O_2 and 0.06 mol L^{-1} HCl were mixed. Control the mixing time from 10 s to 180 min the CL intensity was almost the same. Therefore, to further simplify the flow system to obtain a simpler and more stable flow system, the H_2O_2–HCl solution was added ahead of time and supplied from line R_2 (Fig. 3.1).

3.2.2 Effect of Reagents on the CL Generated from the Decomposition of Peroxynitrous

Mixtures produce peroxynitrite acid, this process requires acid as catalyst. Therefore, we cannot see any CL phenomenon in alkaline or neutral solutions. Four phenomenon HCl, H_2SO_4, H_3PO_4, and HNO_3 were compared. These four different acids could be employed as an effective catalyst for the NO_2^-–H_2O_2 catalytic reaction, but on the other hand, HCl can catalyze the strongest CL signal. The reason is presumably that Cl^- ion takes part in the reaction of H_2O_2 and HNO_2 (Reactions 3.1–3.3). When the concentration of HCl solution is 0.06 M, the strength reflected by CL signal is the strongest. This concentration is the optimum concentration in the subsequent test.

$$H^+ + HNO_2 \rightarrow H_2NO_2 \tag{3.1}$$

$$H_2NO_2 + Cl^- \rightarrow NOCl + H_2O \tag{3.2}$$

$$NOCl + H_2O_2 \rightarrow HOONO + H^+ + Cl^- \tag{3.3}$$
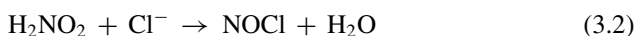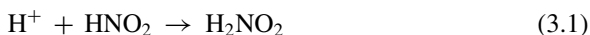
It is well understood that an arranged surfactant micelle can be utilized as a reaction medium to dramatically increase CL intensity. Critical micelle concentration (CMC) that is a certain minimum concentration. Micelles are manufactured as

amphiphilic surfactant molecules interact effectively in aqueous system. There is one big difference between local microenvironment in micellar media with that in a media that is homogeneous. Currently, the system is set up in such a way that owing to the generation of singlet oxygen is the key to the CL. Therefore, the amount of singlet oxygen produced has a significant impact on the efficiency. In order to investigate the contribution of different surfactants, they were given to the nitrite–H_2O_2 system. In the data shown in Table 3.1, there is the optimum level of concentration of each surfactant. Anionic and the concentration of non-ionic surfactants are not directly related to the CL intensity. The experimental results can be analyzed that among the eight cationic surfactants, the performance of EDAB is the best, The CL signal provided can be enhanced by 14 times. And we tested his optimal concentration. The CL intensity is straightforwardly relative to focus of EDAB in the range of 0.001–0.006 mol L^{-1}. Referring to the solubility of EDAB in water, we choose 0.006 M EDAB concentration as the most suitable concentration.

CL is usually improved by releasing power from just an excitation step to a deliberately added fluorescent compound. In this work, we compared eight fluorescent compounds to enhance the reaction intensity in CL analysis. The results were shown in Table 3.2. Fluorescein can be apparently found, eosin Y and uranine both have obviously enhanced ability for the determination of nitrite. Uranine, notably, can boost the system's CL capacity by nine times.Therefore, uranine can be used as an enhancer for strengthening weak CL. At a uranine concentration of 0.001 mol L^{-1}, the CL intensity was maximum. The CL signal was significantly lowered when uranine concentrations passed 0.001 mol L^{-1}, the reason may be the excess uranium

Table 3.1 Surfactants' impact on CL strength

Surfactant	Concentration (mM)	Relative intensity[a]
None		1.0
Cetyltrimethylammonium bromide (CTAB)	5.0 (0.9)	12.4
myristyltrimethylammonium bromide (MTAB)	7.0 (3.5)	11.0
Didodecyldimethylammonium bromide (DDDAB)	4.0 (0.18)	1.0
Octadecyldimethylammonium chloride (OTAC)	5.0	12.6
Ethyldimethylcetylammonium bromide (EDAB)	6.0	14.0
Dodecyltrimethylammonium bromide (DTAB)	18.0	6.0
Dioctadecyldimethylammonium chloride (DODAC)	1.0	1.0
Didodecyldimethylammonium bromide (DODAB)	1.0	1.0
Sodium dodecyl sulfate (SDS)	10.0 (8.0)	1.0
Triton X-100	0.1% (v/v)	1.0
Tween	0.1% (v/v)	1.0

Copyright 2002, with permission from Elsevier [4]
The values in parentheses are the critical micelle concentration (CMC)
[a] Normalized with respect to the signal in the absence of surfactant

Table 3.2 Sensitizer's impact on intensity values

Fluorescent compound (1.0 mM)	Relative CL intensity[a]
None	1.0
Uranine	9.0
Eosin Y	6.2
Fluorescein	4.4
Riboflavine	1.0
8-Hydroxyquinoline	1.0
Rhodamine B	1.0
Acridine	1.0
Brilliant Sulfoflavine	1.0

Copyright 2002, with permission from Elsevier [4]
[a] Normalized with respect to the signal in the absence of enhancer

can absorb yellow emitted light. 0.001 mol L^{-1} uranium is selected for the analysis process.

3.2.3 Quantity of Nitrite in Liquid by Using Peroxynitrite

Based on the above research, the standard curve is obtained for nitrite determination, $Y = 7.0 \times 10^6 X + 2.77$. The relative CL strength is Y, and the nitrite concentration is X. In the range of concentration of 1.0×10^{-7}–5.0×10^{-5} mol L^{-1} nitrite, a suitable calibration graph was linear. The detection limit (S/N = 3) for nitrite was 5.0×10^{-8} mol L^{-1}, 0.9995 was the reliability analysis. The population standard deviation was 4.3%.

The effects among many water interferences on the measurement of 1.0×10^{-6} mol L^{-1} nitrite were tested. The tolerance limit is $\pm 5\%$ of the peak height error. Except I^- ion, the existence of anionic ions has little effect on the strength of chloride ions. They can coexist with nitrite in solution with high concentrations. Many cationic ions, particularly cobalt (II) and chromium (III) would be lost without the employment of a cation-exchange column (III), are seriously disturbed. So rather than nitrite solution, a strong CL signal will still appear when you inject 1.0×10^{-8} mol L^{-1} cobalt (II) or chromium (III) into the flow system. CL emission from H_2O_2 breakdown driven by transition metals possibly explains this phenomenon. Therefore, the degree of this reaction might potentially be turned into a CL method. Dowex 50 W X4 resin cation-exchange column is installed behind the injector. The interference of cations on the experimental results can be removed relatively cleanly. The determination of a 10^{-6} mol L^{-1} nitrite solution is unaffected by quantities of these cationic ions less than 10^{-5} mol L^{-1}.

The proposed method is used to find out how much nitrite there is in tap water and well water relatively accurately. The technique was being used to figure out

the nitrite concentration in tap water and well waters. Well water is directly potable water from underground without pre-treatment The pore size of the newly collected sample is 0.45 μm membrane filter, stored in the refrigerator at a temperature of about 4 °C, and analyzed according to the recommended procedure within 4 h after collection. The cationic ions exchange column with glass wool at both ends eliminates interference of cations. Determination consistent with the results obtained by standard spectrophotometry [27], The sample promoting recovery from 94 to 106%. In Beijing's Haidian District, tap water seems to have a greater nitrite ratio than well water at that time.

3.3 Bilirubin-Enhanced Peroxynitrite CL by Energy Transfer

3.3.1 Mechanism of Bilirubin and Peroxynitrite

The on-line reaction of concentrated hydrochloric acid hydrogen peroxide with nitrite and peroxynitrite (ONOO) in a fluid flow from ONOOH in NaOH solution formed peroxynitrous acid (ONOOH). Weak chemiluminescence (CL) emission signals were captured while singlet oxygen ($^1O_2$) is formed during the destruction of ONOO$^-$. In a suitable micellar medium, bilirubin and its conjugates can enhance the CL emission of $^1O_2$. The ability of determining total bilirubin in human serum in a sensitive and selective manner by the existing CL system was proved for the first time, and the data were statistically compared to that same certified value. The present method has been greatly improved in overcoming the problem of bis(2,4,6-trichlorophenyl) oxalate CL highly insolubility.

The result was shown in Fig. 3.2, Dispense 50 μL of a mixed solution of NaOH, surfactant, and bilirubin into the carrier stream (water) and mix with ONOOH. It was manufactured in actual environments in a spiral diffusion CL cell by the combination of nitrite and acidified hydrogen peroxide. This flow cell was installed in a straight

Fig. 3.2 Flow-injection chemiluminescence system schematic diagram. Peristaltic pumps P_1 and P_2; S stands for NaOH/CTAB/bilirubin; KR stands for knotted reactor (10 cm); F stands for flow cell; W stands for waste. Copyright 2003, with permission from Elsevier [5]
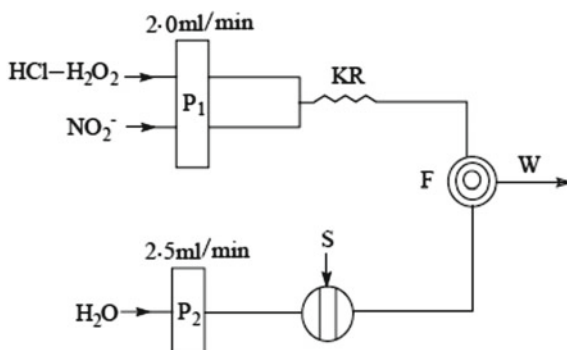
line with the photomultiplier tube of the luminometer, and the CL signal is captured by recorder. A 10 cm knotting reactor was used to mix nitrite and H_2O_2/HCl solution more fully installed in a straight line with the photomultiplier tube of the luminometer's photomultiplier tube. Recorder was being used to gather the CL signals (Shimadzu, Kyoto, Japan). A 10 cm knotted reactor was used to enhance the blending of nitrite and H_2O_2/HCl solution.

Many studies have confirmed that the decomposition of $ONOO^-$ produces $^1O_2$, the state in which molecular oxygen is excited. Two quenchers of $^1O_2$, 1,4-diazabicyclo [2,2,2,2,] octane (DABCO), and NaN_3 [28], were used. The result of our study indicated in the presence of some substances (DABCO, NaN_3), the CL strength of bilirubin with $ONOO^-$ involved on-line interaction of nitrite with acidified hydrogen peroxide. Also, with the increase of concentration, CL emission decreased. The analysis of experimental phenomena shows that $^1O_2$ had played a major role in the process of chemiexcitation. Some oxidants can convert bilirubin into biliverdin [29]. On top of that, ONOO is a potent oxidant. This result can be attributed to the oxidation of bilirubin to biliverdin by $ONOO^-$. Figure 3.3 showed the CL spectrum of $ONOO^-$ reaction with bilirubin. It is worth noting that the CL spectrum of the CL reactivity is comparable to the bilirubin fluorescence spectra of bilirubin explored by scholars [30, 31], indicating that the CL emission could have been the result of electrons radiating with the first singlet excited electronic state to the bilirubin ground state. It can be seen from the storage analysis diagram that the CL maximum wavelength of bilirubin is around 530 nm, which is recorded for the fluorescence
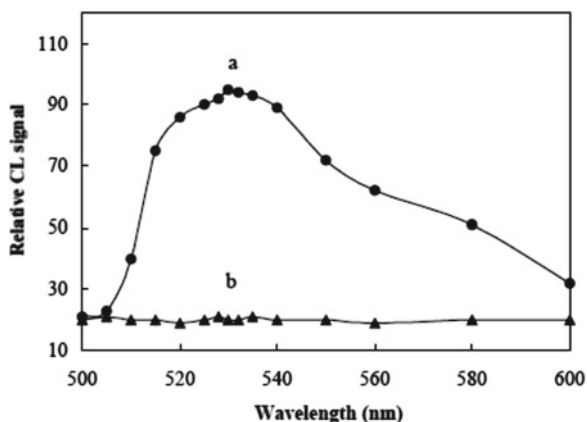
Fig. 3.3 The (**a**) peroxynitrite/bilirubin response and (**b**) blank CL spectrum. H_2O_2, HCl, nitrite, NaOH, and CTAB made up the blank solution. H_2O_2, HCl, nitrite, NaOH, and CTAB concentrations were 0.03, 0.1, 0.01, 0.12, and 0.01 mol L^{-1}, respectively. It was decided to implement the flow-injection method. H_2O_2/HCl and nitrite solution flow rates were 2.0 ml min^{-1}. The flow rate of the NaOH/CTAB/bilirubin mixing solutions was 2.5 ml min^{-1}. The excitation light was turned off, and the emission slit was widened to its widest setting of 20 nm. The sample solution for calculating the CL spectrum of bilirubin was 1.0 mg L^{-1} bilirubin standard solution. Copyright 2003, with permission from Elsevier [5]

maxima of bilirubin bonded to micelles. The difference in fluorescence maxima is attributed to the different settings in which bilirubin is conformed or ionized. [32].

3.3.2 Determination of Total Bilirubin in Human Serum by Chemiluminescence

The decomposition of $ONOO^-$ into NO^- and singlet oxygen has been known as the ONOO decomposition reaction. It is the process of excitation of CL phenomenon (recommended chloride ion as emitter). Bilirubin and its conjugates can be used as enhancers to enhance nitrite-hydrogen peroxide reaction, so as to enhance CL emission. In order to determine the optimum conditions for bilirubin, flow-injection analysis was used to measure the peak height of CL signal to noise (S/N). The reaction of nitrite and hydrogen peroxide to produce ONOOH requires acid as catalyst based on previous experimental data conclusions. The concentration of NaOH has a significant influence on the CL strength. In the absence of sodium hydroxide (NaOH), our CL device did not obtain the CL signal. A concentration of 0.12 mol L^{-1} NaOH was used as one of the best conditions for FIA–CL.

Micelles affected the single-molecule chemistry and photophysics by the way of changing microviscosity, local pH, polarity, reaction pathway, or rate of the solution system. In addition, micelles as reaction medium can improve the CL intensity. In this work, the effects of three different types of micelles on ONOO in aqueous solution were studied. Their ability to produce the highest CL strength when detecting bilirubin compared with bilirubin. The results showed that the anionic and non-ionic surfactants had no impact on CL intensity, consequently. It can be concluded that some cationic surfactants, such as CTAB and EDAB, are effective at increasing CL intensity. CTAB, in contrast, can augment the CL effectiveness of the management system by around 54 times, and the CL intensity increases nearly linearly as the CTAB concentration is low from 0.002 to 0.01 mol L^{-1}, but remains essentially constant once the CTAB levels exceed 0.01 mol L^{-1}. Therefore, the concentration is 0.01 mol·L^{-1}. Considering the solubility of CTAB in water, CTAB is selected as the best condition.

Under ideal experimental circumstances, the calibration curves were found to be linear from 13 to 110 µg·L^{-1} and $10–95 \text{ µg L}^{-1}$ for bilirubin and bilirubin ditaurite, respectively. The detection limits for bilirubin and its conjugate (S/N = 3) were determined to be 10 ng mL^{-1} and 8 ng·mL^{-1}, respectively, which are nearly five times lower than the detection limits for bilirubin in aqueous medium based on redox reactions reported by FIA–CL [33]. A continuous stream of bilirubin at 30 µg L^{-1} mean$\pm$ standard of bilirubin (R.S.D.) has been detected constantly.

The impacts of typical, as well as the selectivity of the developed approach for the detection of total bilirubin were investigated. The amounts of these interference species added to 50 µg L^{-1} bilirubin were indicative of the dilute concentrations with the NaOH/CTAB mixing solution. The findings of this experimental approach

reveal that the CL signal is stable at this moment, confirming the great selectivity of this method for bilirubin measurement.

We used this test method to establish its applicability and reliability of bilirubin and its conjugate, for instance. The total bilirubin content of certified reference human serum samples prepared using the current approach and a well clinical method were compared to assess the analytical advantage of the proposed methodology [34]. Again, for determination of total bilirubin contents in normal serum samples, the results of the two methods were very similar. Furthermore, bilirubin recovery rates in spiked serum samples ranged from 95 to 108%.

3.4 Chemiluminescence from Carbonate and Peroxynitrous Acid

Mixing acidified hydrogen peroxide and nitrite in a solution system, a weak chemi-luminescent (CL) signal can be captured due to the generation of singlet oxygen ($^1O_2$) generated when ONOOH reacted with NaOH mixed solution, while Na_2CO_3 replaced NaOH to significantly enhance the CL intensity. Carbonate species were regenerated as a result of the reaction, demonstrating that carbonate was being used as a catalyst [35]. Based on the studies of CL and fluorescence spectra, it is proposed that the reaction between carbonate and ONOOH may affect the reaction mecha-nism of CL. In conclusion, ONOOH quenching reaction can occur and ONOO$^-$ can be formed in basic media and very unstable in acidic solutions. Some scholars have proposed that the ONOO$^-$ reaction with excessive HCO_3^- culminated in bicarbonate ion radicals ($HCO_3\bullet$) via one-electron transfer. $HCO_3\bullet$ recombination can produce excited triplet dimers of two CO_2 molecules [$(CO_2)_2$] immediately. The nature of this intermediate is very unstable. When it is decomposed into CO_2, the energy is released through CL emission. The addition of uranine to a hydroxide solution increases the CL signal, which is caused by transferring energy from a moderately excited triplet dimer of two CO_2 molecules to uranine, resulting in two CL peaks.

3.4.1 Kinetics of the CL Reaction of Carbonate and Peroxynitrous Acid

In order to make the captured CL intensity high enough, the different mixing sequences of reagents were measured. Experiments showed that 100 µL of H_2O is injected into H_2O_2–HCl–NO_2^- solution, it will not produce CL phenomenon. On the other hand, replacing H_2O with NaOH solution will produce weak CL emission. On the other hand, replacing H_2O with NaOH solution would produce weak CL emission. This phenomenon is attributed to the production of $^1O_2$ (a well-known CL emitter). The addition of Na_2CO_3 resulted in a significant increase in the CL intensity.

The addition of Na_2CO_3–uranine mixing solution into H_2O_2–HCl–NO_2^- solution provided the strongest CL emission. Therefore, carbonate has a great influence on CL signal. A number of CL analyses have indeed been performed in the carbonate solution system in our previous works [34–36]. In order to explain the chemiluminescence mechanism of the current system more systematically, the following experiments were carried out.

If the aqueous solution contains a certain amount of carbonate, at the mixing interface, small volumes are frequently formed. To examine the effects of CO_2 and O_2 on the CL signal, all solutions were degassed for 10 to 15 min with bubbling N_2 gas. O_2 was introduced into Na_2CO_3 solution and bubbled together for nearly 10 min, the CL intensity remained relatively constant, indicating that the existence of O_2 has no effect on CL. The time of introducing CO_2 into the degassed Na_2CO_3 solution is 1 to 10 min, and the CL intensity decreased gradually. This phenomenon indicated a decrease of pH values (12.2–9.9), resulting in bubbling CO_2.

To determine the emission species, we also measured CL and fluorescent spectra which are shown in Fig. 3.4a, and it can be seen intuitively that the wavelength of 443 nm is the maximum value of CL spectrum. Many studies have shown that singlet oxygen ($^1O_2$) is a light-emitting species. It is known that there are several maxima in the emission spectra of $^1O_2$, i.e., 1269, 762, 634, and 381 nm [37]. Throughout this work, DABCO and NaN_3 have been shown to have no effect on CL intensity, which indicates that there is no correlation between the occurrence of CL at $^1O_2$. At the same time, many scholars have concluded that carbonate is a substance that can emit
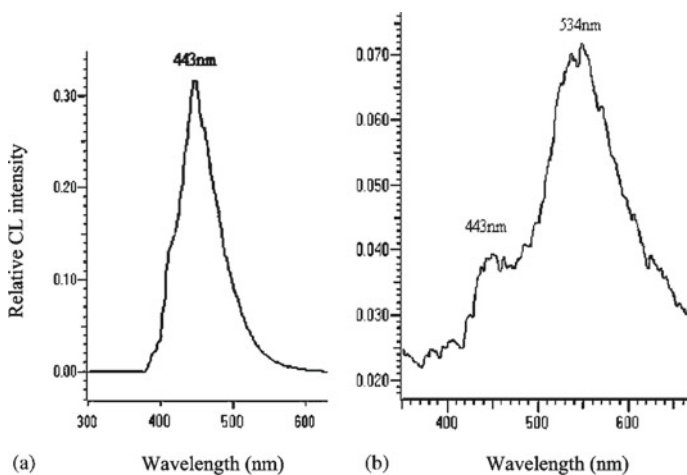
Fig. 3.4 CL spectra in Na_2CO_3 (**a**) and Na_2CO_3–uranine (**b**) solutions of both the H_2O_2–HCl–NO_2 reaction. H_2O_2, HCl, NO_2, Na_2CO_3, and uranine concentrations were 0.02, 0.1, 0.1, 0.4, and 5×10^{-7} mol L^{-1}, respectively. It was decided to implement the flow-injection method. H_2O_2–HCl solution and NO_2^- solution had flow rates of 3.0 ml/min. The flow rate of the Na_2CO_3 solution was 3.5 mL/min. The emission slit width was set to 20 nm and the excitation light was immediately turned off. Copyright 2004, with Elsevier's authorization [34]

light [38], we also recorded the CL emission band at 436–446 nm, which leads to a reduction in carbon dioxide emissions. Therefore, the CL observed in the present system may also be related to the formation of $(CO_2)_2^*$ in this reaction. The result was shown in Fig. 3.4b when uranine solution was added into H_2O_2–HCl–NO_2–Na_2CO_3 flow system, the CL spectrum had two peaks and the maximum located at 443 and 534 nm, respectively. Importantly, the first CL peak (443 nm) was the same as that obtained from the reactions of the H_2O_2–HCl–NO_2–Na_2CO_3 solutions (Fig. 3.4a).

However, after the addition of uranine, 443 nm in the spectrum was reduced. The concentration of uranine was lowered to 5×10^{-7} mol L^{-1} with 0.4 mol L^{-1} carbonate solution in order to concurrently record two CL peaks with maximum locations at 443 and 534 nm in the same spectral picture, respectively. It is found that the CL peak at 534 nm comes from uranine, this phenomenon may be caused by the chemical reaction between triplet dimer $(CO_2)_2^*$ and uranium, that is, the chemical excitation of uranium. The fluorescence spectra of uranine in Na_2CO_3 solution were also recorded. The fluorescent maximum wavelength of uranine in Na_2CO_3 solution was 534 nm, which was the same as the CL emission maximum of uranine in the spectrum. The fluorescent maximum was located at 534 nm whenever uranine–Na_2CO_3 solution was introduced to H_2O_2–HCl–NO_2^- solution (Fig. 3.5), and the fluorescent intensity of uranine was maintained unaltered. This phenomenon shows that uranium is only a sensitizer. They are not consumed in the reaction as reactants while $(CO_2)_2^*$ was a CL emitter.

Figure 3.6 shows the UV absorption of peroxynitrous acid produced by the reaction of nitrite and H_2O_2/HCl, they reacted rapidly. Due to the isomerization of peroxynitrous acid to form nitrate (solid line), there is an absorption peak at 301 nm. However, a new band appeared at 354 nm due to recombination between •NO_2 radicals to generate nitrite, but really the classic nitrate band at 301 nm remained. It shows that only nitrate (solid line) is the product of spontaneous decomposition of

Fig. 3.5 Fluorescent spectrum of uranine in H_2O_2–HCl–NO_2–Na_2CO_3 solution. The concentration of uranine was 1.0×10^{-5} mol L^{-1}. All other conditions were the same as in Fig. 3.3. Copyright 2004, with permission from Elsevier [34]
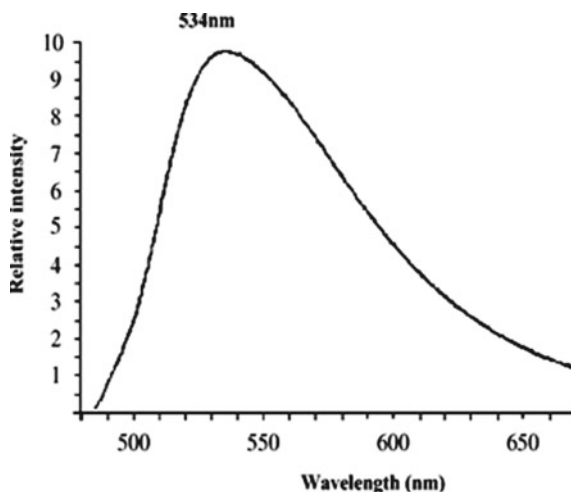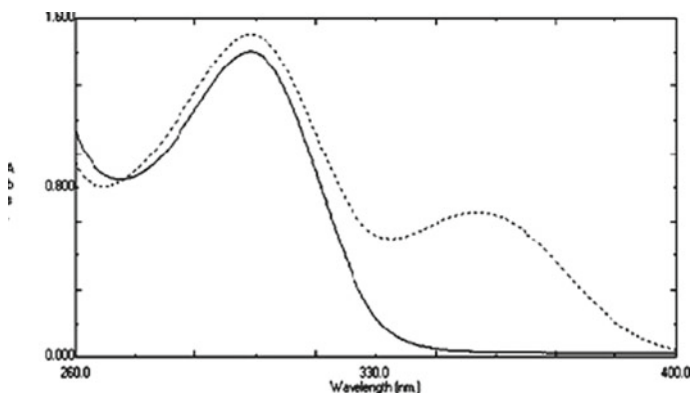
Fig. 3.6 Absorption spectra of peroxynitrous acid from the reaction of nitrite and H_2O_2–HCl in the absence (solid line) and presence (dashed line) of Na_2CO_3 solution. The concentrations of NO_2, H_2O_2, HCl, and Na_2CO_3 were 0.6, 0.7, 0.6, and 1.0 mol L^{-1}, respectively. The volume of each solution was 1.0 mL. Copyright 2004, with permission from Elsevier [34]

peroxynitrite and it reacted with carbonate solution (dotted line) to produce nitrite and nitrate at the same time.

3.4.2 Mechanism for the CL Reaction of Carbonate and Peroxynitrous Acid

The carbonate-catalyzed $ONOO^-$ chemiluminescence mechanism from our above observations, it can be inferred that the chemical decomposition is as follows. Nitrite reacts with acidified H_2O_2 to form HOONO (Reaction 3.4), which is an unstable molecule in acidic solution and can be transformed into ONOO in basic solution via a chemical reaction as a product of CO_3^{2-} to HCO_3^- protonation(Reactions 3.5 and 3.6):

$$H_2O_2 \ + \ HNO_2 \ \rightarrow \ HOONO \ + \ H_2O \tag{3.4}$$

$$CO_3^{2-} \ + \ H_2O \ \rightleftharpoons \ HCO_3^- \ + \ OH^- \tag{3.5}$$

$$ONOOH \ + \ OH^- \ \rightarrow \ ONOO^- \ + \ H_2O \tag{3.6}$$
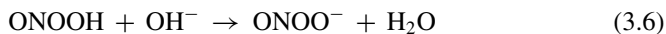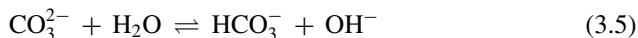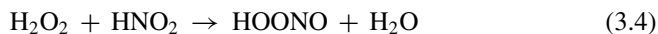
As we all know that the one-electron standard redox potentials of $ONOO^-/\bullet NO_2$ and $HCO_3\bullet/HCO_3^-$ couples are similar. Therefore, when $ONOO^-$ reacts with excess HCO_3^- thermodynamically, ONOO's one-electron oxidation of HCO_3^- releases bicarbonate radicals ($HCO_3\bullet$) according to Reaction 3.7.

$$ONOO^- + HCO_3^- + H^+ \rightarrow HCO_3 \cdot + \cdot NO_2 + OH^- \tag{3.7}$$

The experimental data of spectrophotometry show that nitrite and nitrate are produced by the polymerization of $\cdot NO_2$ radicals in aqueous solution (Reaction 3.8):

$$\cdot NO_2 + \cdot NO_2 + H_2O \rightarrow NO_2^- + NO_3^- + 2H^+ \tag{3.8}$$
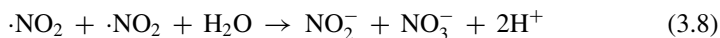
The excited triplet dimers $[(CO_2)^*{}_2]$ of two CO_2 molecules can be directly produced by the recombination of $HCO_3\bullet$ (Reaction 3.9)[39]:

$$2HCO_3^{\bullet} \rightarrow (CO_2)_2^* + H_2O_2 \tag{3.9}$$
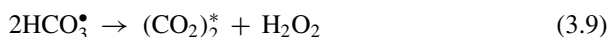
The energy is released when this unstable intermediate breaks down to CO_2. (Reaction 3.10):

$$(CO_2)_2^* \rightarrow 2CO_2 + h\nu \, (\lambda \max = 443 \, nm) \tag{3.10}$$
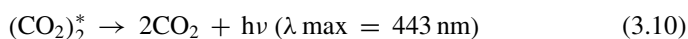
Dissolved CO_2 and carbonate can reach rapid equilibrium in the solution system and as a consequence, during the ONOOH–carbonate interaction, carbonate was regenerated, suggesting that carbonate species functions as an effective catalyst.

The extended Hückel molecular orbital (EHMO) method had been used to compute the decomposed energy of $(CO_2)^*{}_2$, when we observed that it was 132 kcal mol^{-1} [40].

$$(CO_2)_{2*} + uranine \rightarrow 2CO_2 + uranine^* \tag{3.11}$$

$$uranine^* \rightarrow uranine + h\nu(\lambda = 534 \, nm) \tag{3.12}$$
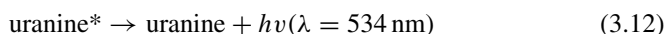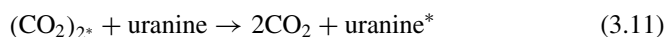
Since part of the energy from the excited triplet dimer of two CO_2 molecules is transferred to uranium (Reactions 3.11 and 3.12), the CL wavelength of 534 nm can be regarded as the result of intermolecular energy transfer (Fig. 3.4b) (Reactions 3.11 and 3.12). Therefore, the CL spectrum of H_2O_2–HCl–NO_2–Na_2CO_3 uranine solutions shows two bands.

3.5 Conclusion

In conclusion, the chemiluminescence produced by the decomposition of peroxynitrous was studied. ONOOH was used to build $ONOO^-$ in an alkaline solution. For the measurement of nitrite, an innovative flow-injection CL method was devised. It is based on the conversion of nitrite to nitric oxide by reaction. We also proved that in the presence of carbonate, the decomposition of peroxynitrite will produce

an unstable substance —excited triplet dimmers of two CO_2 molecules $[(CO_2)^*_2]$, which realized energy when decomposed into CO_2. In alkaline solution, the generated CO_2 can quickly reach equilibrium with carbonate in the system, so carbonate is regenerated through ONOOH chemical reaction with carbonate. Carbonate is an indispensable catalyst in the reaction. The CL behavior and the mechanism of carbon dots have been studied in detail, which will give us further insight into the properties of carbon dots. Furthermore, the application of CL in other fields is also promising.

References

1. Lymar SV, Jiang Q, Hurst JK (1996) Mechanism of carbon dioxide-catalyzed oxidation of tyrosine by peroxynitrite. Biochem 35:7855–7861
2. Zhu L, Gunn C, Beckman JS (1992) Bactericidal activity of peroxynitrite. Arch Biochem Biophys 298:452–457
3. Denicola A, Freeman BA, Trujillo M, Radi R (1996) Peroxynitrite reaction with carbon dioxide/bicarbonate: kinetics and influence on peroxynitrite-mediated oxidations. Arch Biochem Biophys 333:49–58
4. Lu C, Qu F, Lin J-M, Yamada M (2002) Flow-injection chemiluminescent determination of nitrite in water based on the formation of peroxynitrite from the reaction of nitrite and hydrogen peroxide. Anal Chim Acta 474:107–114
5. Lu C, Lin J-M, Huie CW (2004) Determination of total bilirubin in human serum by chemiluminescence from the reaction of bilirubin and peroxynitrite. Talanta 63:333–337
6. Khan AU, Kovacic D, Kolbanovskiy A, Desai M, Frenkel K, Geacintov NE (2000) The decomposition of peroxynitrite to nitroxyl anion (NO⁻) and singlet oxygen in aqueous solution. Proc Natl Acad Sci 97:2984–2989
7. Mahoney LR (1970) Evidence for the formation of hydroxyl radicals in the isomerization of pernitrous acid to nitric acid in aqueous solution. J Am Chem Soc 92:5262–5263
8. Saha A, Goldstein S, Cabelli D, Czapski G (1998) Determination of optimal conditions for synthesis of peroxynitrite by mixing acidified hydrogen peroxide with nitrite. Free Radic Biol Med 24:653–659
9. Gow A, Duran D, Thom SR, Ischiropoulos H (1996) Carbon dioxide enhancement of peroxynitrite-mediated protein tyrosine nitration. Arch Biochem Biophys 333:42–48
10. Goldstein S, Czapski G (1995) The reaction of no-center-dot with o-2(center-dot-) and HO₂-center-dot-a pulse-radiolysis study. Free Radic Biol Med 19:505–510
11. Lemercier JN, Padmaja S, Cueto R, Squadrito GL, Uppu RM, Pryor WA (1997) Carbon dioxide modulation of hydroxylation and nitration of phenol by peroxynitrite. Arch Biochem Biophys 345:160–170
12. Radi R, Cosgrove TP, Beckman JS, Freeman BA (1993) Peroxynitrite-induced luminol chemiluminescence. Biochem J 290:51–57
13. Merényi G, Lind J, Goldstein S (2002) The rate of homolysis of adducts of peroxynitrite to the co double bond. J Am Chem Soc 124:40–48
14. Hodges GR, Ingold KU (1999) Cage-escape of geminate radical pairs can produce peroxynitrate from peroxynitrite under a wide variety of experimental conditions. J Am Chem Soc 121:10695–10701
15. Lymar SV, Hurst JK (1995) Rapid reaction between peroxynitrite ion and carbon dioxide: implications for biological activity. J Am Chem Soc 117:8867–8868
16. Lymar SV, Hurst JK (1998) CO_2-catalyzed one-electron oxidations by peroxynitrite: properties of the reactive intermediates. Inorg Chem 37:294–301
17. Dodeigne C, Thunus L, Lejeune R (2002) Chemiluminescence as diagnostic tool. A review. Talanta 51:415–439

18. Wolff IA, Wasserman AE (1972) Nitrates, nitrites and nitrosoamine. Science 177:15–19
19. Masuda M, Mower HF, Pignatelli B, Celan I, Friesen MD, Nishino H, Ohshima H (2000) Formation of N-nitrosamines and N-nitramines by the reaction of secondary amines with peroxynitrite and other reactive nitrogen species: somparison with nitrotyrosine formation. Chem Res Toxicol 13:301–308
20. Choi KK, Fung KW (1980) Determination of nitrate and nitrite in meat products by using a nitrate ion-selective electrode. Analyst 105:241–245
21. Mikuska P, Vecera Z, Zdrahal Z (1995) Flow-injection chemiluminescence determination of ultra low concentrations of nitrite in water. Anal Chim Acta 316:261–268
22. Anbar M, Taube H (1954) Interaction of nitrous acid with hydrogen peroxide and with water. J Am Chem Soc 76:6243–6247
23. Khan AU (1995) Quantitative generation of singlet oxygen from acidified aqueous peroxynitrite produced by the reaction of nitric oxide and superoxide anion. J Biolum Chemlum 10:329–333
24. Edwards JO, Plumb RC (1994) The chemistry of peroxynitrites. Prog Inorg Chem 41:599–635
25. Chowdhury JR, Wolkoff AW, Ariasin IM, Scriver CR, Beaudet AL, Sly WS, Valle D (1989) The Metabolic Basis of Inherited Inherited Diseases. New York, pp 1367–1408
26. Wu N, Wang TS, Hartwick RA, Huie CW (1992) Separation of serum bilirubin species by micellar electrokinetic chromatography with direct sample injection. J Chromatogr 582:77–85
27. Wei FS (1998) Analytical Methods for the Examination of Water and Wastewater, 3rd edn. Chinese Environment and Science Press, Beijing, p 260
28. Lin J-M, Yamada M (2000) Chemiluminescent reaction of fluorescent organic compounds with $KHSO_5$ using cobalt (II) as catalyst and its first application to molecular imprinting. Anal Chem 72:1148–1155
29. van Norman JD, Szentirmay R (1974) Chemistry of bilirubin and biliverdin in N, N-dimethylformamide. Anal Chem 46:1456–1464
30. Chen RF (1974) Fluorescence stopped-flow study of relaxation processes in binding of bilirubin to serum albumins. Arch Biochem Biophys 160:106–112
31. Aiken JH, Huie CW (1991) Detection of bilirubin using surfactant fluorescence enhancement and visible laser fluorometry. Anal Lett 24:167–180
32. Cu A, Bellah G, Lightner DA (1975) Fluorescence of bilirubin. J Am Chem Soc 97:2579–2580
33. Palilis LP, Calokerinos AC, Grekas N (1996) Chemiluminescence arising from the oxidation of bilirubin in aqueous media. Anal Chim Acta 333:267–275
34. Lu C, Lin J-M (2004) Carbonate-catalyzed chemiluminescence decomposition of peroxynitrite via $(CO_2)_2^*$ intermediate. Catal Today 90:343–347
35. Lin J-M, Hobo T (1996) Flow-injection analysis with chemiluminescent detection of sulphite using Na_2CO_3-$NaHCO_3$-Cu^{2+} system. Anal Chim Acta 323:69–74
36. Lu C, Lin J-M, Huie CW, Yamada M (2004) Chemiluminescence study of carbonate and peroxynitrous acid and its application to the direct determination of nitrite based on solid surface enhancement. Anal Chim Acta 510:29–34
37. Wu XZ, Yamada M, Hobo T, Suzuki S (1989) Uranine sensitized chemiluminescence for alternative determinations of copper(II) and free cyanide by the flow injection method. Anal Chem 61:1505–1510
38. Lin J-M, Yamada M (1999) Oxidation reaction between periodate and polyhydroxyl compounds and its application to chemiluminescence. Anal Chem 71:1760–1766
39. Wierzchowski J, Slawinska D, Slawinski J (1986) Carbonate and superoxide ion-radicals as intermediates in the chemiluminescence of the ferricyanide-hydrogen peroxide redox system. Z Phys Chem Neue Folge 148:197–214
40. Bollyky LJ (1970) Chemiluminescence from the reaction of ketenes, singlet oxygen, and fluorescers. J Am Chem Soc 92:3230–3232

Chapter 4
Ultra-Weak Chemiluminescence System of Reactive Nitrogen Species

Zhen Lin and Jin-Ming Lin

Abstract Reactive nitrogen species are a class of reactive molecules with oxidant. The chapter introduced some reactive nitrogen species, containing nitrogen dioxide, nitric oxide, peroxynitrous acid, and peroxynitrite. The chemiluminescence properties of the reactive nitrogen species have been reviewed and their applications have been mentioned.

4.1 Introduction

Reactive nitrogen species are a class of molecules with oxidant. Reactive nitrogen species contained nitric oxide (NO), dinitrogen trioxide (N_2O_3), nitrogen dioxide (NO_2), peroxynitrous acid (ONOOH), peroxynitrite ($ONOO^-$) as well as other types of chemically nitrogen-contained reactive-free radicals.

NO as a free radical, is the most famous reactive nitrogen species, which acts as an important intermediate in many chemical reactions. In vivo, NO is cellular signaling molecule participating in many physiological processes. For example, NO diffuses freely across cell membranes to relax smooth muscle cells and to dilate the blood vessels. NO is also involved in the modulation of nerve cells and defense functions of immune system. Discovery of key roles of NO led to Nobel Prize-winning research in related areas and NO was proclaimed as "Molecule of the Year" in 1992 [1]. Due to its short lifetime and its high oxidant ability, its formation and decomposition mechanism have aroused great attention.

In vivo, NO is synthesized within cells by NO synthase from arginine with the aid of oxygen and NADPH. NO synthase converts L-arginine to L-citrullin (Fig. 4.1). NO

Z. Lin
College of Pharmaceutical Science, Fujian Medical University, Fuzhou 350122, China

J.-M. Lin (✉)
Department of Chemistry, Tsinghua University, Beijing 100084, China
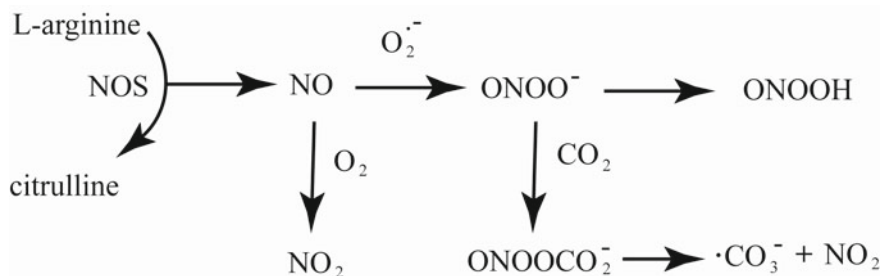e-mail: jmlin@mail.tsinghua.edu.cn

Fig. 4.1 Reactions leading to the generation of NO and related reactive nitrogen species [2, 5]

is highly reactive and easily oxidized to NO_2. NO reacted with superoxide to produce $ONOO^-$ [2]. $ONOO^-$ is not a radical but an oxidant and nitrating agent. $ONOO^-$ can damage various molecules in cells, including amino acid, DNA, lipid as well as proteins. It should be noted that the reactions of $ONOO^-$ with these substrates cannot compete with the reaction of $ONOO^-$ with CO_2 under physiological conditions because of the rapid reaction between $ONOO^-$ and CO_2 ($K = 3 \times 10^4 \, M^{-1} \, s^{-1}$). The product of the reaction is $ONOOCO_2^-$ [3, 4], which then decomposes to carbonate radical ($\cdot CO_3^-$) and NO_2 (as shown in Fig. 4.1) [5]. From this route, CO_2 modulates the reactivity of $ONOO^-$ [6, 7].

The conjugate acid of $ONOO^-$ is $ONOOH$, which is a reactive nitrogen-containing species and has a half-life lower than 1 s. $ONOOH$ may directly oxidize the substrates. $ONOOH$ may also decompose into reactive species with high activity which subsequently oxidize the substrates [8].

Most reactive nitrogen species owned short life and easily interacted with other compounds. Chemiluminescence (CL) produced light through a chemical reaction. Excited species with short lifetime are generated and deactivated to their ground state with light-emitting. Hence, CL is a satisfactory tool for the investigation of the reactive nitrogen species. To our best known, the CL phenomena happened between some reactive nitrogen species, which gave us new insight into these species. The chapter reviews the CL characteristics of the reactive nitrogen species and introduces some important applications of the CL phenomena.

4.2 CL from the Reaction Between NO and O_3

NO, as a relatively unstable molecular, could react with the ozone to produce oxygen and NO_2, with the emission of light [9]. The intensity of the CL is proportional to the concentration of NO, if the volume of the sample gas and excess ozone are controlled, which could be developed as a real-time determination method for gaseous NO.

$$NO + O_3 \rightarrow O_2 + NO_2* \rightarrow NO_2 + \text{ light} \tag{4.1}$$

Biological NO is easy to be oxidized to NO_2^- or NO_3^-. In this case, NO can be determined indirectly through NO_2^- or NO_3^-. NO_3^- could be reduced by nitrate reductase to NO_2^-, which is further reduced to NO by reaction with iodide under acidic conditions. Both NO_2^- and NO_3^- can also be reduced to NO with acidic vanadium (III) [10]. Under the catalysis of metal, other oxides of nitrogen (NO, NO_2, NO_3, HNO_3, N_2O_5, $CH_3COO_2NO_2$) can also be converted to NO and were detected by the CL method [11, 12]. Hence, the total amount of nitrogen [13] was detected by the CL method.

Based on the CL reaction between NO and ozone, a CL detector is developed for nitrogen-contained compounds determination. In recent years, some researchers considered that CL nitrogen detector is a very promising alternative to traditional detectors (mass spectrometry, flame ionization detector, and nitrogen phosphorus detector) for specific organic nitrogen compounds. It is because that the CL reaction between the NO and O_3 enabled the detection of the nitrogen species selectively.

Particularly, with the help of well-known separation methods, such as capillary electrophoretic system [14, 15], gas chromatography [16–18], and ion chromatography [19], the CL nitrogen detector can be applied to various complex samples. Sokolowski et al. [14] connected the capillary electrophoretic system to a CL nitrogen detector via a pneumatic nebulizer interface. Organic nitrogen compounds are combusted at high temperature to nitrogen oxide, which is oxidized by excess ozone to excited state NO_2^*. The CL emission passed through a high-pass optical fiber was detected by a photomultiplier. Mohammad et al. [15] also used capillary electrophoresis-CL nitrogen detector system to detect *p*-aminosalicylic acid and L-phenylalanine.

$$C_xH_yN_z + (x + 1/4y + 1/2z)O_2 \rightarrow zNO + xCO_2 + y/2\, H_2O\,[14] \qquad (4.2)$$
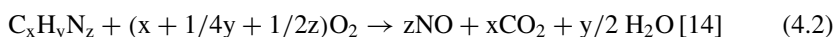
Özel et al. [16] developed a nitrogen CL detector for a gas chromatography to determine organic nitrogen. The gas chromatography is highly selective, sensitive, and has well response to individual organic compounds. The pyrolyzer in the system converts the analytes in the gas chromatograph column effluent into the corresponding CL species. With the use of proper sample pre-treatment technology, such as solid-phase extraction, the interferences are eliminated and the method could be used for the detection of organic nitrogen in complex atmospheric aerosol samples. Gas chromatography with a nitrogen CL detection system could determine six specific mutagenic and carcinogenic nitrosamines in grilled lamb and vegetables [17]. Lucy et al. [19] combined CL nitrogen detection with ion chromatography for the detection of nitrogen-containing ions, including nitrite, nitrate, cyanide, tetradecyltrimethylammonium, and ammonium with equimolar response.

It should be mentioned that the relationship between the structure of compounds and the CL response is the main concern for the nitrogen CL detection system. Yan et al. [20] used the CL nitrogen detector for the high-throughput screening

technologies. The compound structure dependence of this detector was investigated and demonstrated that compounds with adjacent nitrogen atoms connected by a double bond had a response of 0.5/nitrogen atom. Structurally similar calibration compounds are suggested to be used in this type of analysis.

4.3   CL Induced by ONOOH

ONOOH, as a kind of nitrogen-containing hydroperoxide is a strong acid. Its pKa is 6.5–6.8. The formation of ONOOH by $NaNO_2$ and H_2O_2 in acid medium has been ascertained. Its decomposition mechanism is controversial. One view is concerned about whether the formation of $^1O_2$ from the decomposition of ONOOH. The other opposing view is focusing on its homolysis pathway.

Khan et al. [21] synthesized $ONOO^-$ by mixing NO and $\cdot O_2^-$ at pH 13, after protonation of $ONOO^-$ at 7.0 to ONOOH. ONOOH decomposed into $^1O_2$ and HNO. The generation of $^1O_2$ was confirmed by electron paramagnetic resonance with 9, 10-diphenylanthracene (DPA) as the trapping reagent. HNO loses protons and forms the nitroxyl anion (NO^-). Nitrosylhemoglobin (HbNO) in methemoglobin (MetHb) solution trapped NO^-. Furthermore, Khan et al. [22]confirmed the presence of $^1O_2$ by light emission located at 1280 nm in ONOOH system. However, Martinez et al. [23] investigated the radials in MetHb and hydrogen peroxide (H_2O_2)–free $ONOO^-$ system by UV–visible and electron paramagnetic resonance(EPR) experiments. They claimed that contamination with H_2O_2 gave rise to ferryl hemoglobin and no light emitted from $^1O_2$ at 1270 nm. The $^1O_2$ was produced from the reaction between excess H_2O_2 and ONOOH rather than from the decomposition of $ONOO^-$.

Thermochemical estimation, spin method including EPR and chemically induced dynamic nuclear polarization (CIDNP) [24] claimed the homolysis of ONOOH to generate $\cdot OH$ and $\cdot NO_2$ radicals. However, the yield of the radicals could not be quantified, which reduced its convincing and the non-radical decomposition could not be fully excluded. The newly investigation claimed that ONOOH homolysis along the O–O bond to generate a geminate pair of $\cdot OH$ and $\cdot NO_2$ radicals. Roughly, 30% of the geminate pair diffuses out of the solvent cage to generate free radicals and the remainder collapses to nitric acid [25].

The CL characteristic of ONOOH has obtained great attention nowadays. Starodubtseva et al. [26] reported the CL emission from the acid solution of $NaNO_2$ and H_2O_2. The production of cis-ONOOH, tran-ONOOH, activated ONOOH (ONOOH*). ONOOH* rearranged to HNO_3 with energy releasing in the form of CL emission.

ONOOH acted as not only an oxidant, but also a peroxidizing reagent, which reacted with many compounds to generate CL emission. Liang et al. [27] reported that chloroquine interacted with ONOOH in sulfuric acid medium with CL emission, which intensity was in proportion with the concentration of chloroquine and the method could be developed as determination method for chloroquine. In the

system, ONOOH turned chloroquine to 4-quinolinone in excited states and 4-hydroxyquinoline. Both two products contributed to the CL emission. Liang's group [28] further found that tryptophan in pharmaceutical preparations and human serum reacted with ONOOH and decomposed to dioxetane, which is the CL emitter. The above CL system could be applied to tryptophan detection. The same group also found that berberine [29] and fluoroquinolones [30], including ciprofloxacin, norfloxacin, and ofloxacin, were oxidized by ONOOH to produce CL. Pipemidic acid [31] could accept the energy transferred from excited state ONOOH.

4.4   CL from ONOO⁻

In vivo, $ONOO^-$ is formed from NO and $\cdot O_2^-$ in a diffused-controlled process. In the laboratory, $ONOO^-$ can be obtained from many pathways, such as nitrosation of H_2O_2 by S-nitrosothiols (RSNO) [32, 33], the ozonation of azide [34], or the decomposition of 3-morpholinosydnonimine (SIN-1). Mostly, $ONOO^-$ is prepared by rapid mixing of H_2O_2 with HNO_2 in mildly acid conditions. Alkaline solution was added following to convert ONOOH to $ONOO^-$.

4.4.1   CL from ONOO⁻ and H₂O₂

It has been reported that $ONOO^-$ reacts with H_2O_2 to release $^1O_2$ [35]. The transition of the oxygen in excited states to the triplet oxygen in ground state is accompanied by the CL emission. A liquid nitrogen-cooled germanium diode confirmed the CL emission in 1270 nm resulting from the production of $^1O_2$. The research illustrated the cytotoxicity mediated by $ONOO^-$ and H_2O_2. Alvarez et al. [36] also claimed that the reaction between $ONOO^-$ and H_2O_2 produced oxygen and slowed down the decomposition of the $ONOO^-$. They proposed that, at acidic pH, an activated intermediate of ONOOH was responsible for H_2O_2 oxidation. At alkaline solution, a stabilizing complex between H_2O_2 and *trans*-$ONOO^-$ was involved.

4.4.2   CL from ONOO⁻ Decomposition

Our group [37] reported for the first time that CL emission had been observed during $ONOO^-$ decomposition. The production of $^1O_2$ during the decomposition of $ONOO^-$ caused the CL. Fluorescence compounds, such as fluorescein, acted as the energy acceptor of $^1O_2$. Ethyldimethylcetylammonium bromide greatly enhanced the CL emission, based on which, a method for nitrite detection had been developed. According to the similar CL reaction, Wang et al. [38] established a sequential injection CL system for the detection of trace amounts of nitrite in water samples.

We further found that bilirubin and its conjugate could enhance the CL emission during the process of $ONOO^-$ decomposition. Bilirubin and its decomposed product were supposed as the energy acceptors and became the CL emitter. The CL system could be developed for bilirubin content detection [39]. Besides bilirubin and its conjugate, Sharov et al. found coumarin 525 and chlorophyll-α strongly enhanced the CL from the $ONOO^-$. An electronically excited intermediate of $ONOO^-$ was produced with a certain yield [40].

Some nitrogen-contained compounds could also be indirectly determined by the $ONOO^-$ CL system. Wang et al. [41] used triehanolamine (TEA) solution to absorb NO_2 in air. NO_2 was then converted into nitrite, which reacted with H_2O_2 to form ONOOH. The alkaline solution changed ONOOH to $ONOO^-$ accompanied with CL emission. Wang et al. [42] further found that cetyltrimethyl ammonium bromide(CTAB) could enhance the CL system.

4.4.3   CL from the Reaction Between $ONOO^-$ and CO_2

The concentrations of CO_2 are relatively high in vivo (interstitial fluids ($30\ mmol \cdot L^{-1}$) and intracellular ($12\ mmol \cdot L^{-1}$))). Lymar and Hurst firstly reported that $ONOO^-$ reacted rapidly with CO_2 ($K = 3 \times 10^4\ M^{-1}\ s^{-1}$) to form $ONOOCO_2^-$ [3]. Hence, the reaction of $ONOO^-$ with CO_2 should be the predominant pathway for $ONOO^-$ in vivo.

The decomposition mechanism for $ONOOCO_2^-$ has gained great attention. Meli et al. [43, 44] reported that the reaction of $ONOO^-$ with CO_2 in alkaline solution form a transient maximum absorption at 640 nm and attributed the absorption to $ONOOCO_2^-$. The result from Denicola et al. group [45] also claimed that $ONOO^-$ rapidly reacted with carbon dioxide to yield $ONOOCO_2^-$. $ONOOCO_2^-$ could take part in nitration and oxidation processes. While Goldstein et al. argued with this conclusion. They used cutoff filters to exclude the absorption at 640 nm. Alternatively, the $\cdot CO_3^-$ with a maximum of 600 nm had been observed. The absorption reported at 640 nm was interfered by NO or ferrocyanide, which indicated that $ONOOCO_2^-$ did not accumulate and the reaction of $ONOO^-$ and CO_2 formed 33% $\cdot CO_3^-$ and NO_2 [46].

Our group [47] observed the CL from the reaction between $ONOO^-$ and CO_2 locating at 416–460 nm. which was assigned to the CO_2 in excited state ((CO_2)*). Uranine could enhance the CL emission and act as the energy acceptor [48]. Yang et al. [49] observed the weak CL emission from the mixing of $ONOO^-$ with dihydralazine sulfate (DHZS). Carbonate had positive influence on the CL emission. It was postulated that the $\cdot CO_3^-$ generated from the decomposition of $ONOOCO_2^-$ acted as a potent one-electron oxidant and performed a one-electron oxidation of DHZS to produce electronically excited phthalate that gave out CL emission.
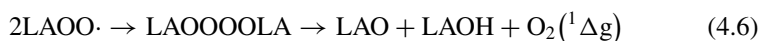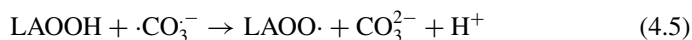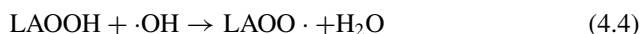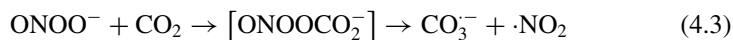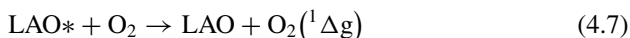
4.4.4 CL from ONOO⁻ Oxidation

$ONOO^-$ could oxidize single molecular, amino acids, proteins, lipid as well as intact cells to generate CL. Massari et al. [55] reported nucleophilic addition of $ONOO^-$ to glyoxal in normally aerated phosphate buffer produced $^1O_2$ ($^1\Delta g$) with light emission at 1270 nm. Furthermore, CL intensity was increased in D_2O and suppressed by $^1O_2$ quencher (NaN_3, L-His). The chemical trapping product of the $^1O_2$ by anthracene-9, 9, 10-endoperoxide derivative, 10-divinylsulfonate, was detected by HPLC/MS/MS. The above results all confirmed the generation of $^1O_2$ in $ONOO^-$-glyoxal system. $ONOO^-$ is also reported to promote the aerobic oxidation of 3-methyl-2,4-pentanedione (MP) and isobutanal (IBAL) in phosphate buffer (pH 7.2) [56]. $ONOO^-$ is the oxidizing agent. Triplet acetone is formed in the oxidation process and acts as the energy donor accounting for the CL emission.

Bovine serum albumin (BSA), especially fatty acid-containing BSA reacts with $ONOO^-$ to produce CL emission [57]. Most of the light is ranging from 500 to 600 nm, which is similar to tryptophan and tyrosine in excited state. The same research group [58] further found that tryptophan was the amino acid which emitted the most light during oxidation. Hence, it can be induced that tryptophan is one amino acid responsible for the CL emission during protein oxidation.

Pholasin is a monomeric glycoprotein and has been used as an indicator for monitoring the loss of plasma antioxidants. Koppenol [59] studied its CL with $ONOO^-$ and investigated the effects of O_2, CO_2, and some antioxidants on the CL to illustrate the CL mechanism. A first oxidation product or the reversible formation of a protein-$ONOO^-$ intermediate may be involved in the CL reaction.

$ONOO^-$ affects series of biological functions through lipid peroxidation [60, 61]. Miyamoto et al. [62] investigated the CL interaction between $ONOO^-$ and lipid hydroperoxide. Linoleid acid hydroperoxide (LAOOH) or ^{18}O-labeled LAOOH ($LA^{18}O^{18}OH$) was used as the model. Chemical trapping technologies, HPLC/MS analysis, and spectral measurements were all employed to confirm the potential CL emission species. $^1O_2$ was supposed for the CL emitting. The OH· and $CO_3^{·-}$ formed from $ONOO^-$ related species oxidized the LAOOH to LAOO· (Reactions 4.3–4.5), the self-reaction of which generated predominantly O_2 ($^1\Delta g$) [63] (Reactions 4.6 and 4.7).

$$ONOO^- + CO_2 \rightarrow \left[ONOOCO_2^-\right] \rightarrow CO_3^- + \cdot NO_2 \qquad (4.3)$$

$$LAOOH + \cdot OH \rightarrow LAOO \cdot + H_2O \qquad (4.4)$$

$$LAOOH + \cdot CO_3^- \rightarrow LAOO \cdot + CO_3^{2-} + H^+ \qquad (4.5)$$

$$2LAOO \cdot \rightarrow LAOOOOLA \rightarrow LAO + LAOH + O_2(^1\Delta g) \qquad (4.6)$$

$$LAO* + O_2 \rightarrow LAO + O_2(^1\Delta g) \tag{4.7}$$

Besides proteins and lipid, CL from the $ONOO^-$ in cell has also been investigated. In cells, $ONOO^-$ was formed through the reaction between NO and $\cdot O_2^-$. Groot et al. [64] observed the NO and $\cdot O_2^-$ induced luminol CL in rate kupffer cells and found that the CL was doubled by the addition of L-arginine and significantly reduced by inhibitors of L-arginine-dependent NO formation. The discovery raised our concern with the NO-related CL determination in cells or proteins [65].

4.4.5 Nanoparticle-Based CL from ONOOH and ONOO⁻ System

Nanometer-sized particles have attracted great attention, due to their special physical and chemical characteristics, such as quantum size effect and high surface energy, which are different from bulk materials. The application of nanoparticles in CL research is a hot topic in the present years. Nanoparticles in CL system could act as the catalyst that accelerated the CL reaction, as the energy acceptor that enhanced the CL intensity, or as luminophore that participated in the CL reaction. Nanoparticles improved the sensitivity and extended the application of CL in related areas.

Gold nanoparticles are a class of nanoparticles that are widely explored in CL systems. To prevent the aggregation problem of gold nanoparticles, Lu et al. [66] capped the gold nanoparticles with non-ionic fluorosurfactant (FSN) molecules. The FSN capped gold nanoparticles exhibited enhanced effect on the carbonate and ONOOH CL system. From the CL spectra, it could be induced that FSN capped gold nanoparticles increased the production of carbon dioxide dimer $((CO_2)_2^*)$ in excited states, whose CL emission band located ranging from 430 to 450 nm and acted as the CL emitter in the CL system.

Besides gold nanoparticles, CdTe as one kind of semiconductor nanocrystals also exhibited a significant sensitized effect on CL from ONOOH-Na_2CO_3 system [67]. The main CL emission overlapped with the FL spectrum of CdTe nanoparticles, which suggested that the CdTe nanoparticles acted as the energy acceptor receiving the energy from $(CO_2)_2^*$. The energy releasing from the excited state of CdTe nanoparticles to their basic state caused the CL emission.

Although semiconductor nanocrystals, such as CdTe, have excellent CL-enhanced properties, their toxicity has been the focus of the attention. The exploring of the new and benign nanoparticles with the similar characteristic has been the main challenging. Photoluminescent carbon dots were of particular interest due to their excellent optical properties and low toxicity. We first found the CL-enhanced properties in ONOOH system [68]. ONOOH that formed by on-line mixing of NO_2^- and acidified H_2O_2 could directly induce the CL from the carbon dots. The CL intensity exhibited linearly with nitrite concentration in certain range, which was developed as a determination method for nitrite in river water, pond water, and pure milk. The radiative

electron–hole annihilation between hole-injected and electron-injected carbon dots caused the CL emission, which extended the range the nanoparticles that could be applied in the CL system.

Carbon dots could also enhance the CL from $NaNO_2$–H_2O_2–Na_2CO_3 system [69]. $(CO_2)_2^*$ is suggested to donate its energy to carbon dots. Carbon dots in excited state were formed and released their energy to ground state with CL emission The carbon dots-$NaNO_2$–H_2O_2–Na_2CO_3 system has been developed for nitrite sensing and used for nitrite detection in tap water.

$ONOO^-$ can be concentrated onto the Mg–Al–carbonate layered double hydroxides (Mg–Al–CO_3 LDHs) surface by electrostatic attraction. Hence, Mg–Al–CO_3 LDHs catalyze the CL emission from ONOOH. The inhibition of ascorbic acid on the CL system enabled the determination for ascorbic acid ranging from 5.0 to 5000 nmol L^{-1}. This method could be used for ascorbic acid detection in commercial liquid fruit juices [70]. The proposed LDHs-catalyzed $ONOO^-$ extended the range of the material that could be utilized in CL field.

4.5 The Application of the CL from Nitrogen Species

4.5.1 Determination of Some Nitrogen-Contained Compounds in Different Matrix [71]

Considering the importance of reactive nitrogen species in various physiological and pathological events, their determination and their relationship with biological events are of remarkable interest. A new generation of fluorescent probes that are specific and sensitive for their respective reactive nitrogen species have been used. For example, some organic or metal-based probes could interact with oxidized NO [55]. $ONOO^-$ could oxidize fuorogenic probes [72], such as 4, 5-diaminofluorescein diacetate (DAF-2DA), dihydrodichlorofluorescein (DCFH), and dihydrorhodamine-123 (DHR-123) to fluorescent dye. The increase in fluorescence response has been widely employed to monitor $ONOO^-$. Li et al. [73] used $ONOO^-$ to oxidize colorless *o*-phenylenediamin to produce a colored product. There is a linear relationship between the absorbance and the concentration of $ONOO^-$ in a certain range. However, the synthesis of the probe is the main difficulty of the method. The sensitivity and the interference from the matrix are the main problems of the fluorescence method [74]. Huang et al. [75] developed a novel CL method by using folic acid as the CL probe, which was oxidized by the $ONOO^-$ to generate CL emission. The CL intensity was in proportion to the concentration of $ONOO^-$ in a certain range with satisfied recoveries. Compared with the fluorescent probe, folic acid as the CL probe not only has a low detection limit but also owns high stability as is easily prepared.

Besides this, the CL reaction between NO_2 and luminol can be developed for the detection nitric dioxide in gaseline. $ONOO^-$-luminol CL system could be used for the direct detection of reactive nitrogen species in experimental autoimmune uveitis

[76]. The CL reaction between NO and O_3 can be not only applied to the detection of NO in gas phase, but also for the determination of NO in vivo [77]. Fluorescein could enhance the CL from Na_2SO_3-$ONOO^-$ system [78]. Furthermore, the CL intensity of the reaction was linear with the concentration of $ONOO^-$. Based on this, a flow injection CL method for $ONOO^-$ detection had been developed.

4.5.2 Evaluation of the Oxidation Stress in Cells or Organs

Traditionally, the methods for detecting oxidative stress are through measuring end product of tissue injury. However, there are many intermediates in these reactions could not be detected with the present method. CL, as a useful tool, could monitor the electronically excited species through their light-emitting and evaluate the oxidation stress in cells or organs as noninvasive technique without adding reagents that could interfere with the process. Yao [79] has established a flow injection CL method to investigate the possible mechanism for NO and oxidative stress-induced pathophysiological variance in acute myocardial infarction development. $ONOO^-$-induced oxidative stress has been investigated in red blood cells by luminol-dependent CL [80]. Addition of $ONOO^-$ obviously increased the CL emission, while glutathione ethyl ester, an antioxidant, partially reduced the CL intensity.

4.5.3 Investigation of the Mediators of Some Diseases

The nitrogen species-related CL method could be used to investigate the mediators of some diseases [81]. Tecder-Ünal et al. [82] employed $ONOO^-$-induced CL system, to study the effect of $ONOO^-$ (both endogenous and exogenous) on the reperfusion arrhythmias in anaesthetized rats, and illustrated that $ONOO^-$ was the key factor. Haklar et al. [83]detected changes in NO and other ROS by measuring CL and to investigate the role of L-arginine and some related species in a rate mesenteric ischaemia–reperfusion model. Braga et al. [84] also used the $ONOO^-$-based CL system to study the influences of budesonide on $\cdot O_2^-$, NO, and $ONOO^-$ production during the respiratory burst of human neutrophils.

Potdar et al. [85] developed an integrated CL and computational approach to gain a quantitative understanding of the interactions of some nitrogen species in high glucose-exposed endothelial cells using a CL analyzer. The research is significant for the understanding of the endothelial cell (EC) dysfunction and illustrating the mediators of many diabetes-related pathogenesis. Gross et al. [86] directly characterized the NO production in human macrophagic cells phagocytizing opsonized zymosan. The result revealed that inducible NO synthase (iNOS) activity is involved in CL emission.

References

1. Cech TR, Bennett D, Jasny B et al (1992) The molecule of the year. Science 258:1861
2. Koppenol W, Moreno J, Pryor WA et al (1992) Peroxynitrite, a cloaked oxidant formed by nitric oxide and superoxide. Chem Res Toxicol 5:834–842
3. Lymar SV, Hurst JK (1995) Rapid reaction between peroxonitrite ion and carbon dioxide: implications for biological activity. J Am Chem Soc 117:8867–8868
4. Merényi G, Lind J (1997) Thermodynamics of peroxynitrite and its CO_2 adduct. Chem Res Toxicol 10:1216–1220
5. Zhang H, Squadrito GL, Pryor WA (1997) The mechanism of the peroxynitrite–carbon dioxide reaction probed using tyrosine. Nitric Oxide 1:301–307
6. Squadrito GL, Pryor WA (2002) Mapping the reaction of peroxynitrite with CO_2: energetics, reactive species, and biological implications. Chem Res Toxicol 15:885–895
7. Chen S, Hoffman MZ (1973) Rate constants for the reaction of the carbonate radical with compounds of biochemical interest in neutral aqueous solution. Radiat Res 56:40–47
8. Goldstein S, Czapski G (1995) Direct and indirect oxidations by peroxynitrite. Inorg Chem 34:4041–4048
9. Fontijn A, Sabadell AJ, Ronco RJ (1970) Homogeneous chemiluminescent measurement of nitric oxide with ozone. Implications for continuous selective monitoring of gaseous air pollutants. Anal Chem 42:575–579
10. Braman RS, Hendrix SA (1989) Nanogram nitrite and nitrate determination in environmental and biological materials by vanadium (III) reduction with chemiluminescence detection. Anal Chem 61:2715–2718
11. Anderson L, Fahey D (1990) Studies with nitryl hypochlorite: thermal dissociation rate and catalytic conversion to nitric oxide using an NO/O_3 chemiluminescence detector. J Phys Chem 94:644–652
12. Fahey D, Eubank C, Hübler G et al (1985) Evaluation of a catalytic reduction technique for the measurement of total reactive odd-nitrogen NOy in the atmosphere. J Atmos Chem 3:435–468
13. Fahey D W (1991) Application of the NO/O chemiluminescence technique to measurements of reactive nitrogen species in the stratosphere. Measurement of Atmospheric Gases, 21–23 January 1991, Los Angeles, California, pp 212–223
14. Sokolowski AD, Vigh G (1999) Coupling of a gas-phase chemiluminescence nitrogen detector and a capillary electrophoretic system. Anal Chem 71:5253–5257
15. Mohammad A, Fujinari E, Okorodudu A et al (2000) Apparatus and method for interfacing capillary electrophoresis and chemiluminescence nitrogen detection for the analysis of nitrogen-containing compounds. J Chromatogr A 868:121–125
16. Özel MZ, Hamilton JF, Lewis AC (2011) New sensitive and quantitative analysis method for organic nitrogen compounds in urban aerosol samples. Environ Sci Technol 45:1497–1505
17. Kocak D, Ozel M, Gogus F et al (2012) Determination of volatile nitrosamines in grilled lamb and vegetables using comprehensive gas chromatography-nitrogen chemiluminescence detection. Food Chem 135:2215–2220
18. Yan X (2002) Sulfur and nitrogen chemiluminescence detection in gas chromatographic analysis. J Chromatogr A 976:3–10
19. Lucy CA, Harrison CR (2001) Chemiluminescence nitrogen detection in ion chromatography for the determination of nitrogen-containing anions. J Chromatogr A 920:135–141
20. Yan B, Zhao J, Leopold K et al (2007) Structure-dependent response of a chemiluminescence nitrogen detector for organic compounds with adjacent nitrogen atoms connected by a single bond. Anal Chem 79:718–726
21. Khan AU, Kovacic D, Kolbanovskiy A et al (2000) The decomposition of peroxynitrite to nitroxyl anion (NO^-) and singlet oxygen in aqueous solution. Proc Natl Acad Sci U S A 97:2984–2989
22. Khan AU (1995) Quantitative generation of singlet ($^1\Delta_g$) oxygen from acidified aqueous peroxynitrite produced by the reaction of nitric oxide and superoxide anion. J Biolumin Chemilumin 10:329–333

23. Martinez GR, Di Mascio P, Bonini MG et al (2000) Peroxynitrite does not decompose to singlet oxygen ($^1\Delta_g O_2$) and nitroxyl (NO^-). Proc Natl Acad Sci U S A 97:10307–10312
24. Butler A, Rutherford T, Short D et al (1997) Tyrosine nitration and peroxonitrite (peroxynitrite) isomerisation: 15N CIDNP NMR studies. Chem Commun 669–670
25. Goldstein S, Lind J, Merényi G (2005) Chemistry of peroxynitrites as compared to peroxynitrates. Chem Rev 105:2457
26. Starodubtseva M, Cherenkevich S, Semenkova G (1999) Investigation of the interaction of sodium nitrite with hydrogen peroxide in aqueous solutions by the chemiluminescence method. J Appl Spectrosc 66:473–476
27. Liang YD, Song JF, Yang XF et al (2004) Flow-injection chemiluminescence determination of chloroquine using peroxynitrous acid as oxidant. Talanta 62:757–763
28. Liang YD, Song JF (2005) Flow-injection chemiluminescence determination of tryptophan through its peroxidation and epoxidation by peroxynitrous acid. J Pharm Biomed Anal 38:100–106
29. Liang YD, Yu CX (2013) Determination of berberine in pharmaceutical preparations using acidic hydrogen peroxide–nitrite chemiluminescence system. Drug Tes Anal 5:150–155
30. Liang YD, Song JF, Yang XF (2004) Flow-injection chemiluminescence determination of fluoroquinolones by enhancement of weak chemiluminescence from peroxynitrous acid. Anal Chim Acta 510:21–28
31. Liang YD, Song JF, Tian T (2004) Determination of pipemidic acid based on flow-injection chemiluminescence due to energy transfer from peroxynitrous acid synthesized on-line. Anal Bioanal Chem 380:918–923
32. Coupe PJ, Williams DLH (2001) Formation of peroxynitrite at high pH and the generation of S-nitrosothiols from thiols and peroxynitrous acid in acid solution. J Chem Soc Perkin Trans 2:1595–1599
33. Coupe PJ, Williams DLH (1999) Formation of peroxynitrite from S-nitrosothiols and hydrogen peroxide. J Chem Soc Perkin Trans 2:1057–1058
34. Uppu RM, Squadrito GL, Cueto R et al (1996) Synthesis of peroxynitrite by azide-ozone reaction. Methods Enzymol 269:311–321
35. Di Mascio P, Bechara EJH, Medeiros MHG et al (1994) Singlet molecular oxygen production in the reaction of peroxynitrite with hydrogen peroxide. FEBS Lett 355:287–289
36. Alvarez B, Denicola A, Radi R (1995) Reaction between peroxynitrite and hydrogen peroxide: formation of oxygen and slowing of peroxynitrite decomposition. Chem Res Toxicol 8:859–864
37. Lu C, Qu F, Lin J-M et al (2002) Flow-injection chemiluminescent determination of nitrite in water based on the formation of peroxynitrite from the reaction of nitrite and hydrogen peroxide. Anal Chim Acta 474:107–114
38. Wang Y, Fan S (2005) Determination of nitrite in water samples by sequential injection analysis with chemiluminescence detection on chip flow cell. Guang Pu Xue Yu Guang Pu Fen Xi 25:184–187
39. Lu C, Lin JM, Huie CW (2004) Determination of total bilirubin in human serum by chemiluminescence from the reaction of bilirubin and peroxynitrite. Talanta 63:333–337
40. Sharov V, Driomina E, Wingerath T et al (1998) Electronically excited intermediate from peroxynitrite: evaluation by chemiluminescence and by the isomerization of β-carotene. J Photochem Photobiol B 47:142–147
41. Wang Y, Fan SH, Wang SL (2005) Chemiluminescence determination of nitrogen oxide in air with a sequential injection method. Anal Chim Acta 541:129–134
42. Wang Y, Fan SH (2005) Determination of nitrogen oxide in air by sequential injection analysis with chemiluminescence detection. Metall Anal (China) 25:1–5
43. Meli R, Nauser T, Koppenol WH (1999) Direct observation of intermediates in the reaction of peroxynitrite with carbon dioxide. Helv Chim Acta 82:722–725
44. Meli R, Nauser T, Latal P et al (2002) Reaction of peroxynitrite with carbon dioxide: intermediates and determination of the yield of $CO_3^{\bullet-}$ and $NO_2^{\bullet}$. J Biol Inorg Chem 7:31–36
45. Denicola A, Freeman BA, Trujillo M et al (1996) Peroxynitrite reaction with carbon dioxide/bicarbonate: kinetics and influence on peroxynitrite-mediated oxidations. Arch Biochem Biophys 333:49

46. Goldstein S, Czapski G, Lind J et al (2001) Carbonate radical ion is the only observable intermediate in the reaction of peroxynitrite with CO_2. Chem Res Toxicol 14:1273–1276
47. Lu C, Lin J-M, Huie CW et al (2004) Chemiluminescence study of carbonate and peroxynitrous acid and its application to the direct determination of nitrite based on solid surface enhancement. Anal Chim Acta 510:29–34
48. Lu C, Lin J-M (2004) Carbonate-catalyzed chemiluminescence decomposition of peroxynitrite via $(CO_2)_2$* intermediate. Catal today 90:343–347
49. Yang XF (2008) Chemiluminescence investigation of carbon dioxide-enhanced oxidation of dihydralazine sulfate by peroxynitrite and its application to pharmaceutical analysis. Anal Chim Acta 616:190–195
50. Radi R, Cosgrove T, Beckman J et al (1993) Peroxynitrite-induced luminol chemiluminescence. Biochem J 290:51–57
51. Carreras MC, Pargament GA, Catz SD et al (1994) Kinetics of nitric oxide and hydrogen peroxide production and formation of peroxynitrite during the respiratory burst of human neutrophils. FEBS Lett 341:65
52. Dai K, Vlessidis AG, Evmiridis NP (2003) Dialysis membrane sampler for on-line flow injection analysis/chemiluminescence-detection of peroxynitrite in biological samples. Talanta 59:55–65
53. Németh A, Stadler K, Jakus J et al (2012) Pitfalls of peroxynitrite determination by luminescent probe in diabetic rat aorta. React Kinet Mech Catal 106:1–10
54. Pueyo ME, Arnal JF, Rami J et al (1998) Angiotensin II stimulates the production of NO and peroxynitrite in endothelial cells. Am J Physiol Cell Physiol 274:214–220
55. McQuade LE, Lippard SJ (2010) Fluorescent probes to investigate nitric oxide and other reactive nitrogen species in biology (truncated form: fluorescent probes of reactive nitrogen species). Curr Opin Chem Biol 14:43–49
56. Knudsen FS, Penatti CAA, Royer LO et al (2000) Chemiluminescent aldehyde and beta-diketone reactions promoted by peroxynitrite. Chem Res Toxicol 13:317–326
57. Watts B, Barnard M, Turrens JF (1995) Peroxynitrite-dependent chemiluminescence of amino acids, proteins, and intact cells. Arch Biochem Biophys 317:324–330
58. Pollet E, Martínez JA, Metha B et al (1998) Role of tryptophan oxidation in peroxynitrite-dependent protein chemiluminescence. Arch Biochem Biophys 349:74
59. Glebska J, Koppenol WH (2005) Chemiluminescence of Pholasin caused by peroxynitrite. Free Radical Biol Med 38:1014–1022
60. Gadelha FR, Thomson L, Fagian M et al (1997) Ca^{2+}-independent permeabilization of the inner mitochondrial membrane by peroxynitrite is mediated by membrane protein thiol cross-linking and lipid peroxidation. Arch Biochem Biophys 345:243
61. van der Veen RC, Roberts LJ (1999) Contrasting roles for nitric oxide and peroxynitrite in the peroxidation of myelin lipids. J Neuroimmunol 95:1–7
62. Miyamoto S, Martinez GR, Martins APB et al (2003) Direct evidence of singlet molecular oxygen $[O_2 (^1\Delta_g)]$ production in the reaction of linoleic acid hydroperoxide with peroxynitrite. J Am Chem Soc 125:4510–4517
63. Mendenhall GD, Sheng XC, Wilson T (1991) Yields of excited carbonyl species from alkoxyl and from alkylperoxyl radical dismutations. J Am Chem Soc 113:8976–8977
64. Wang JF, Komarov P, Sies H et al (1991) Contribution of nitric oxide synthase to luminol-dependent chemiluminescence generated by phorbol-ester-activated Kupffer cells. Biochem J 279:311
65. Castro L, Alvarez MN, Radi R (1996) Modulatory role of nitric oxide on superoxide-dependent luminol chemiluminescence. Arch Biochem Biophys 333:179–188
66. Li J, Li Q, Lu C et al (2011) Determination of nitrite in tap waters based on fluorosurfactant-capped gold nanoparticles-enhanced chemiluminescence from carbonate and peroxynitrous acid. Analyst 136:2379–2384
67. Zhang H, Zhang L, Lu C et al (2011) CdTe nanocrystals-enhanced chemiluminescence from peroxynitrous acid-carbonate and its application to the direct determination of nitrite. Spectrochim Acta, Part A 85:217–222

68. Lin Z, Xue W, Chen H et al (2011) Peroxynitrous-acid-induced chemiluminescence of fluorescent carbon dots for nitrite sensing. Anal Chem 83:8245–8251
69. Lin Z, Dou X, Li H et al (2015) Nitrite sensing based on the carbon dots-enhanced chemiluminescence from peroxynitrous acid and carbonate. Talanta 132:457–462
70. Wang Z, Teng X, Lu C (2012) Carbonate interlayered hydrotalcites-enhanced peroxynitrous acid chemiluminescence for high selectivity sensing of ascorbic acid. Analyst 137:1876–1881
71. Tarpey MM, Fridovich I (2001) Methods of detection of vascular reactive species nitric oxide, superoxide, hydrogen peroxide, and peroxynitrite. Circ Res 89:224–236
72. Roychowdhury S, Luthe A, Keilhoff G et al (2002) Oxidative stress in glial cultures: detection by DAF-2 fluorescence used as a tool to measure peroxynitrite rather than nitric oxide. Glia 38:103–114
73. Li DJ, Wang LL, Zeng X et al (2004) Spectrophotometric determination of peroxynitrite using o-phenylenediamine as a probe. Anal Lett 37:2949–2963
74. Planchet E, Kaiser WM (2006) Nitric oxide (NO) detection by DAF fluorescence and chemiluminescence: a comparison using abiotic and biotic NO sources. J Exp Bot 57:3043–3055
75. Huang JC, Li DJ, Diao JC et al (2007) A novel fluorescent method for determination of peroxynitrite using folic acid as a probe. Talanta 72:1283–1287
76. Bae SR, Wu GS, Sevanian A et al (2007) Direct detection of reactive nitrogen species in experimental autoimmune uveitis. Korean J Ophthalmol KJO 21:21–27
77. Murrant CL, Reid MB (2001) Detection of reactive oxygen and reactive nitrogen species in skeletal muscle. Microsc Res Tech 55:236–248
78. Shi J, Ma HM, Wang RY et al (2011) Determiantion of peroxynitrite by flow injection chemiluminescence. Chin J Spectro Lab 28:192–195
79. Yao D, Vlessidis AG, Evmiridis NP et al (2004) Possible mechanism for nitric oxide and oxidative stress induced pathophysiological variance in acute myocardial infarction development: a study by a flow injection–chemiluminescence method. Anal Chim Acta 505:115–123
80. Kanski J, Koppal T, Butterfield DA (1999) Investigation of peroxynitrite induced oxidative stress in red blood cells monitored by luminol-dependent chemiluminescence. Anal Lett 32:1183–1192
81. Barnard ML, Robertson B, Watts B et al (1997) Role of nitric oxide and superoxide anion in spontaneous lung chemiluminescence. Am J Physiol Lung Cell Mol Physiol 272:262–267
82. Tecder-ünal M, Kanzyk Y (2004) Peroxynitrite in reperfusion arrhythmias and its whole blood chemiluminescence results. Pharmacol Res 49:7–16
83. Haklar G, Ulukaya-Durakbaś Ç, Yüksel M et al (2007) Oxygen radical and nitric oxide in rat mesenteric ischaemia-reperfusion:modulation by L-arginine and NG-nitro-L-arginine methyl ester. Clin Exp Pharmacol Physiol 25:908–912
84. Braga PC, Dal Sasso M, Culici M et al (2005) Budesonide reduces superoxide and peroxynitrite anion chemiluminescence during human neutrophil bursts. Pharmacology 75:179–186
85. Potdar S, Kavdia M (2009) NO/peroxynitrite dynamics of high glucose-exposed HUVECs: chemiluminescent measurement and computational model. Microvasc Res 78:191–198
86. Gross A, Dugas N, Spiesser S et al (1998) Nitric oxide production in human macrophagic cells phagocytizing opsonized zymosan: direct characterization by measurement of the luminol dependent chemilurninescence. Free Radical Res 28:179–191

Chapter 5
Ultra-Weak Chemiluminescence from Decomposition of Peroxomonosulfate

Hui Chen and Jin-Ming Lin

Abstract Whether or not molecular mass aliphatic dicarboxylic acids have an influence on the HSO_5^-–Co^{2+} chemiluminescence (CL) system has been considered. Aliphatic dicarboxylic acids were found to have a positive impact on the CL attached to HSO_5^-–Co^{2+} system. In addition, CL intensities improved steadily as the chain length of dicarboxylic acid carbon increased. The mechanism of CL showed that the presence of peroxo-diacide should be beneficial to the improvement of CL, which finally degraded into dicarboxylic acid and original oxygen. In the peroxomonosulphate system, the CL phenomena of lanthanide ions (Ln) and their coordinated complexes have been observed, as well as the energy transfer mechanism in this process have been studied. When Eu(III) or Tb(III) was mixed into the peroxomonosulfate solution system, a strong, crisp CL signal appeared. Because of the 2,6-pyridinedicarboxylic acid (DPA) ligand and hexadecyltrimethyllammonium chloride micelles, the strength of CL was significantly improved. Singlet oxygen was produced through decomposition of peroxymonosulfate catalyzed by Ln (III) ion. The lanthanide ions were the luminescence transmitter, which had an energy transfer.

Keywords Chemiluminescence · Peroxomonosulfate · Dicarboxylic acids · Cobalt (II) · Singlet oxygen · Peroxodiacide · Flow-injection analysis

5.1 Introduction

Peroxymonosulphurous acid (H_2SO_5, PMS, Caro's acid) is a stronger oxidant than peroxydiacid ($H_2S_2O_8$) and may be thought of as a hydrogen peroxide replacement in which one of the hydrogen atoms is replaced by a sulfur oxygen anion group. When the temperature is 15 °C, the first-order ionization constant (chemical kinetics) is less

H. Chen
College of Materials Science and Technology, Beijing Forestry University, Beijing 100083, China
e-mail: chenhui@bjfu.edu.cn

J.-M. Lin (✉)
Department of Chemistry, Tsinghua University, Beijing 100084, China
e-mail: jmlin@mail.tsinghua.edu.cn

than zero, the second-order ionization constant (chemical kinetics) is equal to 9.88 ± 0.1, and the electrode potential $E = 1.82$ V versus HSO_4^-, PMS is very easy to react. When the PH of aqueous solution is around 7, PMS decomposes rapidly, resulting in many inorganic reagents being easily oxidized and most organic compounds being attacked [1, 2]. Therefore, the Baeyer–Villiger reaction often uses PMS as a powerful inorganic acid and a more strong oxidant to convert ketones into esters. The inorganic salt of PMS, potassium peroxomonosulfate ($KHSO_5$), is an inexpensive and readily accessible potassium carotate. The product of 86% hydrogen peroxide reaction with concentrated sulfuric acid is neutralized with K_2CO_3 to obtain $KHSO_5$, which is a triple salt potassium peroxomonosulphate ($2KHSO_5 \cdot KHSO_4 \cdot K_2SO_4$) [3]. In many oxidation reactions, $KHSO_5$ can also act as an oxidant, such as the oxidation of alcohols, ketones, carboxylic acids, olefins, phenols, amines, and sulfides [4]. HSO_5^- decomposes rather fast in a $pH = pKa_2$ [5] solution to produce singlet oxygen. In the chemiluminescence (CL) of singlet oxygen($^1O_2$), this requirement mentioned above is critical. On the contrary, HSO_5^- is stable in acidic or alkaline solutions.

It was created as a prospective CL analytical technique based on the CL phenomena in transition metal-catalyzed decompositions of peroxymonosulfate ion and sensitized by fluorescent organic chemicals. This technique can be used to determine transition metals, such as cobalt (II), iron (II), and vanadium (IV) ions, as well as fluorescent organic compounds such as dansyl amino acids, fluorescent dyes, and polycyclic aromatic hydrocarbons. This CL approach was used in liquid chromatography for post-column detection and has been integrated with high-sensitivity molecular imprinting [6–8]. In addition, it is also used to determine the folic acid in its urine metabolism and the humic in native water [9, 10].

Low CL emission was seen in the existence of trace quantities of transition metal ions like Co (II) and Fe (II) when HSO_5^- interacted with the transition metal ions [8]. Co (II) was shown to be the best transition metal ion for activating PMS to produce radicals such as $SO_5^{\cdot-}$, $SO_4^{\cdot-}$ and $\cdot OH$. These radicals were previously identified by radiolysis using optical pulses, which is important in CL reactions [11]. Hydrocarbons, such as low molecular weight aliphatic monocarboxylic acids (formic, acetic, propionic, butyric, and valerian), have considerably promoted CL emissions from $HSO_5^- – Co^{2+}$, as shown in our early research. [3]. Lanthanide-sensitized luminescence features a significant Stokes shift, narrow emission bands of 1–20 nm half-width, and a long emission lifetime, which makes it ideal for time-resolved luminescence experiments without interference [12].

In this study [13, 14], the CL phenomena of low molecular weight aliphatic dicarboxylic acids in the $HSO_5^- – Co^{2+}$ system were researched, and then the CL phenomena of Eu(II) and Eu(II)-EDTA in the peroxymonocrbonate system were investigated.

5.2 Enhanced CL of Peroxomonosulfate-Cobalt (II)-Dicarboxylic Acids System

5.2.1 Dynamic Profile of Peroxomonosulfate-Cobalt (II) CL

The HSO_5^-–Co^{2+}- dicarboxylic acids CL system's chemiluminescent dynamic profile was reported (Fig. 5.1). The HSO_5^-–Co^{2+}–CL signal was defined as a benchmark CL intensity because no other reagents were used. When $CoSO_4$ was introduced into the HSO_5 solution, little luminescence was produced, as displayed by the CL's kinetic curve. A high CL was reported when low molecular weight aliphatic dicarboxylic acid was added to the HSO_5^-/Co^{2+} solution combination. From Fig. 5.1, the maximal intensity of the complete CL was determined to be about 2 s, suggesting that the reaction of HSO_5^- with Co^{2+} was a rapid CL process. The duration of the CL signals, on the other hand, was greatly extended, reaching six times the 50 s duration of the blank signal, and the CL intensity was also considerably boosted, going from one hundred and eighteen to around twelve hundred counts.
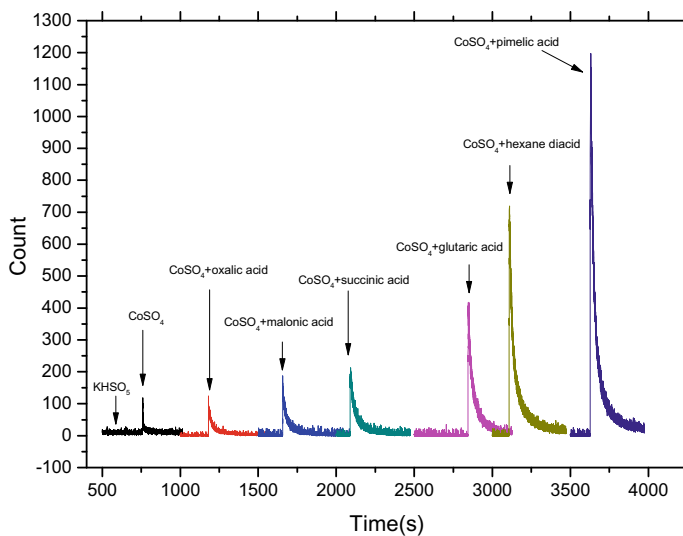
Fig. 5.1 CL profiles for $KHSO_5$, $CoSO_4$, and aliphatic dicarboxylic acids in a dynamic state. $KHSO_5$, $CoSO_4$, and dicarboxylic acids had concentrations of 1.0×10^{-2}, 1.0×10^{-2} and 1.0×10^{-3} mol L^{-1}, respectively. $KHSO_5$, $CoSO_4$, and dicarboxylic acids were all administered in 50 μL volumes. Copyright 2010, with permission from Wiley [13]

5.2.2 Flow-Injection CL of Peroxomonosulfate-Cobalt (II)

5.2.2.1 Design of Flow-Injection CL System

A reasonable incorporating method (i.e., incorporating order and incorporating time interval) of reagents, as well as the speeds of the CL reaction, should be used, as they were critical for the design of the flow-injection CL system and, as a result, had a significant impact on the CL intensity. Distinct CL strengths are influenced by different mixing paths and CL reaction paces in general. On the means of irrational mixture or the speeds of CL reaction, an intensity of CL zero or extremely low is occasionally observed. Because the light emission from the CL reaction is very transient, the velocity of the CL reaction was a significant factor in determining the sensitivity of the CL flow-injection system. In batches, the intensity-time profile of this CL system was evaluated to find the intensity of the CL with the highest sensitivity. The CL reaction of HSO_5^- and Co^{2+} solution was found to be extremely rapid, with the CL intensity peaks two seconds after the reaction begins and decays to datum line after five seconds. Additional research found that the reagents should be combined in the following order: first, $KHSO_5$ should be mixed with $CoSO_4$ solution, and then the sample should be placed in the flow CL cell. As exhibited in Fig. 5.2, the experimental requirements for the HSO_5^- –Co^{2+} CL system have been optimized. Various mixing tube lengths were used to determine the CL intensity. The results demonstrated that as the length of the mixing tuberose, the CI intensity reduced considerably (Fig. 5.2A). This was most likely owing to the catalytic breakdown of peroxymonosulfate, which necessitated a maximum length reduction of the mixing tube. Finally, the mixing tube was built to contain a solution of peroxymonosulphate and cobalt (II) at the CL cell's intake. The influence of flow rate on each stream was investigated between 0.1 and 1.5 mL min^{-1}, with the selected succinic acid concentration set to 1.0×10^{-6} mol L^{-1}; the result is shown in Fig. 5.2B. The HSO_5^-–Co^{2+} CL system's experimental needs have been optimized, as illustrated in Fig. 5.2. Different mixing tube lengths were used to measure CL intensity. The CI intensity reduced considerably as the mixing tube length grew, according to the findings (Fig. 5.2A). It was most likely caused by the catalytic breakdown of peroxymonosulfate, which meant severing as much of the mixing tube as possible. Lastly, at the CL cell's input, the mixing tube was constructed using peroxymonosulphate and cobalt (II). The influence of velocity rate was investigated for each stream within the area of 0.1–1.5 mL min^{-1}, with the succinic acid that has been chosen at 1.0×10^{-6} mol/L; the results are given in Fig. 5.2B.

Increased outflows of $KHSO_5$ and $CoSO_4$ from 0.1 to 0.6 mL min^{-1} resulted in an increase in CL intensity. CL intensity steadily decreased within a range of not more than 0.6 mL/min. The best of the flows studied, the load-carrying flow rate, followed a similar trend at 0.6 ml/min. As a consequence, the optimum throughput of the HSO_5^-/Co^{2+} CL system for all flows was 0.6 mL·min^{-1}. The effects of $KHSO_5$ and $CoSO_4$ concentrations ranging from 5.0×10^{-4}–1.0×10^{-2} mol L^{-1} were investigated (results were shown in Fig. 5.2c, d). When $KHSO_5$ and $CoSO_4$ concentrations
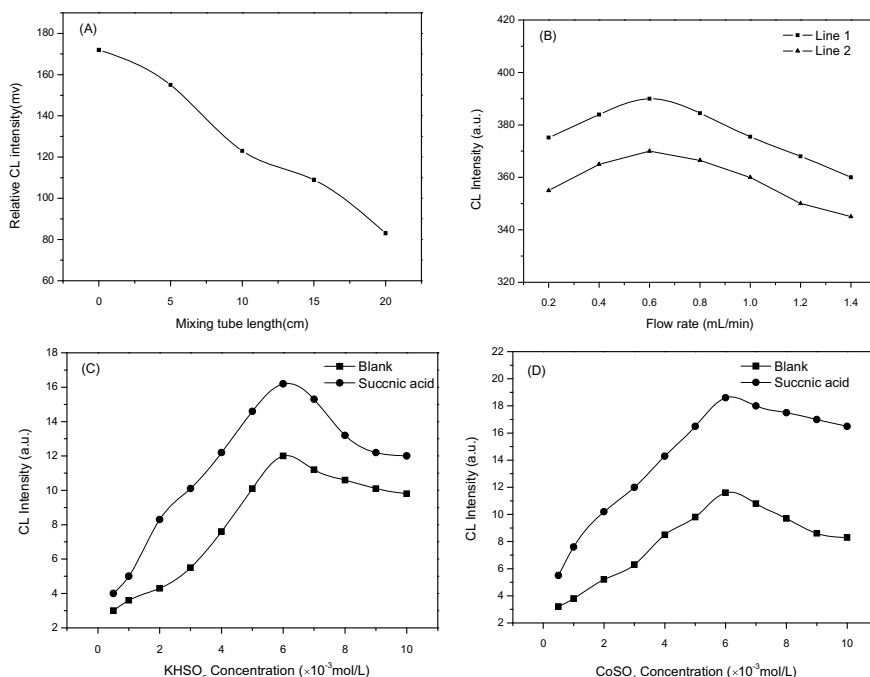
Fig. 5.2 Experiment conditions are being tweaked. **a** The effect of mixing tube length on $KHSO_5$ and CoSO4 concentrations: 1.0×10^{-2} mol L^{-1} $KHSO_5$ and 1.0×10^{-2} mol L^{-1} $CoSO_4$. **b** Flow rate effect: 5.0×10^{-3} mol L^{-1} $KHSO_5$ and $CoSO_4$, 1.0×10^{-4} mol L^{-1} succinic acid; Line 1, flow rate effect of $KHSO_5$ and $CoSO_4$, 1.0 mL min^{-1} carrier stream; Line 2, flow rate effect of $KHSO_5$ and $CoSO_4$, 1.0 mL min^{-1} carrier stream (**c**) Effect of $KHSO_5$ concentration: 1.0×10^{-4} mol L^{-1} succinic acid, 1.0×10^{-2} mol·$L^{-1}CoSO_4$; $KHSO_5$ and $CoSO_4$ flow rates, 0.6 mL·min^{-1}. **d** Effect of $CoSO_4$ concentration: 1.0×10^{-4} mol L^{-1} succinic acid, 4.0×10^{-2} mol L^{-1} $KHSO_5$; flow rates of $KHSO_5$ and $CoSO_4$ are 0.6 mL min^{-1}. Copyright 2010, with permission from Wiley [13]

were raised from 5.0×10^{-4} mol L^{-1} to 6.0×10^{-3} mol·L^{-1}, the CL intensity grew consistently; however, when the concentrations were increased above 6.0×10^{-3} mol L^{-1}, the CL intensity gradually decreased. In the case of $KHSO_5$ and $CoSO_4$, a final concentration of 6.0×10^{-3} mol L^{-1} was selected.

5.2.2.2   Flow-Injection CL Under the Optimum Conditions

Oxalic acid, malonic acid, succinic acid, glutinic acid, hexane diacid, and pimelic acid were all studied with the use of the FIA method. Figure 5.3 depicts the CL system's FIA CL signals after being supplied with aliphatic dicarboxylic acids under ideal conditions. Aliphatic dicarboxylic acid CL intensities increased as the carbon chain length increased in the $HSO_5{}^-$–Co^{2+} system.
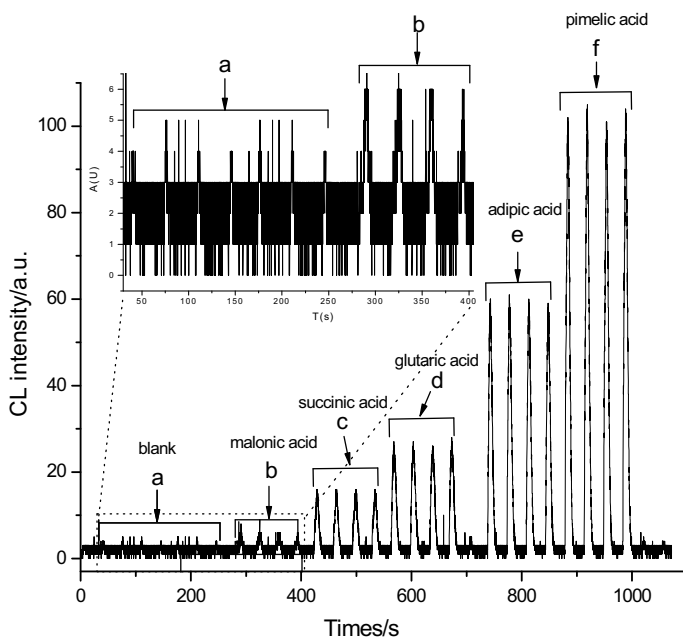
Fig. 5.3 CL signals for oxalic acid (**a**), malonic acid (**b**), succinic acid (**c**), glutaric acid (**d**), hexane diacid (**e**), and pimelic acid (f). KHSO₅, CoSO₄, and aliphatic dicarboxylic acids were used at concentrations of 6×10^{-3}, 6.0×10^{-3} and 1.0×10^{-4} mol L^{-1}, respectively. KHSO₅ solution, CoSO₄ solution, and carrier (water) all flowed at 0.6 mL/min. Copyright 2010, with permission from Wiley [13]

5.2.2.3   Effects of Organic Solvents

A number of organic solvents such surfactant micelles and water-miscible organic solvents, have abolished CL signals from the HSO_5^-–Co^{2+} system, as we previously reported [8]. Certain organic solvents were investigated in the current investigation (Fig. 5.4). Methanol demonstrated the most inhibitory effects on the CL system of HSO_5^--Co^{2+} dicarboxylic acids of all the solvents tested. Methanol's suppressive profile in the CL system after addition of hexane diacid was shown in Fig. 5.4a. With seven dicarboxylic acids added, Fig. 5.4b depicted all of the suppressive influences of methanol on the CL system (effects data of other solvents on the CL system not shown). As demonstrated in Fig. 5.4c, the CL signals of the HSO_5^-–Co^{2+} system were not considerably altered when low polar solvents (n-hexane and chloroform) were added; however, when solvents with dielectric constants more than 20 were introduced, the CL intensity decreased dramatically.
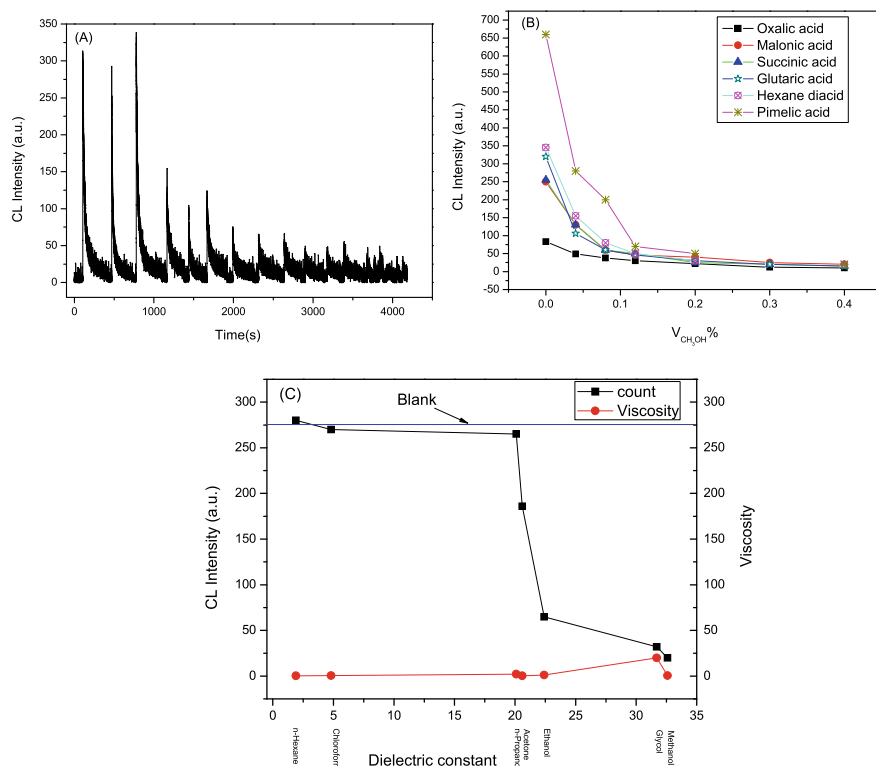
Fig. 5.4 Effect of organic solvent. **a** CL profiles in batch studies: 0, 0.04, 0.08, 0.12, 0.2 and 0.4% Methanol (V/V), 1×10^{-2} mol L^{-1} KHSO$_5$, 1×10^{-2} mol L^{-1} CoSO$_4$ and 1×10^{-3} mol L^{-1} hexane diacid. **b** Effect of methanol concentration: 1×10^{-2} mol·L^{-1} KHSO$_5$, 1×10^{-2} mol·L^{-1} CoSO$_4$, 1×10^{-3} mol·L^{-1} dicarboxylic acid. **c** Line 1: effects of organic solvents with different polarities, 1×10^{-2} mol·L^{-1} KHSO$_5$, 1×10^{-2} mol L^{-1} CoSO$_4$, 1×10^{-3} mol L^{-1} dicarboxylic acid; Line 2: viscosities of variant organic solvents. Copyright 2010, with permission from Wiley [13]

5.2.2.4   Quenching Effect on the CL System

The mechanism of HSO$_5{}^-$ interacting with Co^{2+} has been widely researched. Simple oxygen (^{1}O$_2$), an excited state of molecular oxygen, is commonly accepted to play an important part in CL processes. In the presence of traces of Co^{2+}, pure oxygen was created during the breakdown of HSO$_5{}^-$. The known extinction of ^{1}O$_2$, NaN$_3$, was utilized to confirm the function of ^{1}O$_2$. The effective CL quench effect of NaN$_3$ is shown in Fig. 5.5. In the disintegration of HSO$_5{}^-$, the presence of ^{1}O$_2$ was clearly demonstrated. To validate the generation of ^{1}O$_2$ in this CL reaction, the CL spectra and the electron spin resonance (ESR) spin-trapping method were used.
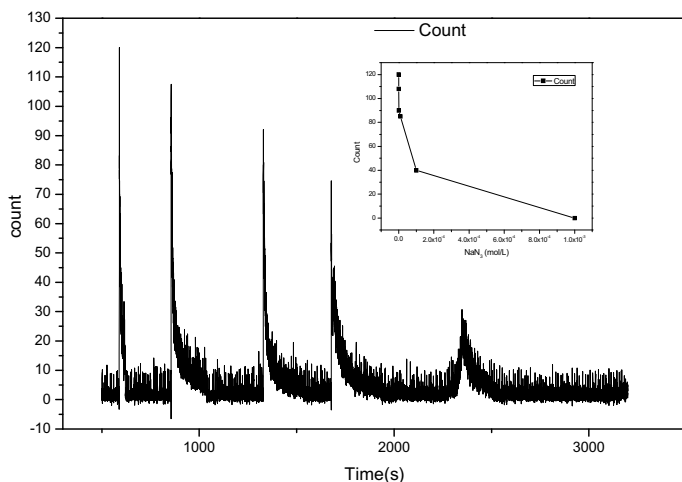
Fig. 5.5 Effect of NaN$_3$ on the CL signals. Batch method: 50 µL of 1.0×10^{-2} mol L^{-1} KHSO$_5$ solution was injected into 50µL of 1.0×10^{-2} mol L^{-1} CoSO$_4$ solution containing NaN$_3$. Copyright 2010, with permission from Wiley [13]

5.2.3 Proposed CL Mechanism

The exact TEMPO signals produced by the TEMP reaction with a single oxygen were shown in Fig. 5.6. Spectrum No. 2 demonstrated the formation of singlet oxygen in the KHSO$_5$–CoSO$_4$ CL system, whereas spectrum No. 3 and No. 4 showed the suppressing effect of 0.1 and 0.02% (V/V) methanol, respectively, and spectrum No.5 revealed the CL system boosting impact of 1.0×10^{-3} mol L^{-1} hexane diacid. The findings strongly suggest that during CL reactions, pure oxygen was created.

Many transition metal ions have been shown to perform a catalytic role in a variety of chemical processes [15]. Co (II) was the best catalyst for peroxymonosulfate among these transitional metallic ions [11]. There was also a report on the catalytic yield of Co (II) for the breakdown of peroxymonosulfate [16, 17].

The effects of several organic solvents were explored to acquire a better understanding of the CL mechanism of the HSO$_5^-$-Co^{2+}-dicarboxylic acid system. The outcomes are depicted in Fig. 5.4. Previously, it was found that the aqueous-phase OH attack on one of the H-atoms attached to the carbon atom of methanol was dominating (with a yield of 93%, Reaction 5.1) [18]. One of the results of this radical reaction was an organic radical, which was rapidly oxidized by O$_2$ to form hydroxymethyl peroxy radical (Reaction 5.2). The action of the peroxy radical was more ambiguous. A slow unimolecular decomposition resulting in formaldehyde had been observed (Reaction 5.3) [19]. Following that, ongoing reactions (Reactions 5.4 and 5.5) produced O$_2$, which eventually reacted with the hydroxymethyl radical (Reaction 5.2). Because the hydroxyl radical was a major contributor to CL emission (Reactions 5.12 and 5.15), the CL signals of the HSO$_5^-$–Co^{2+} system would be
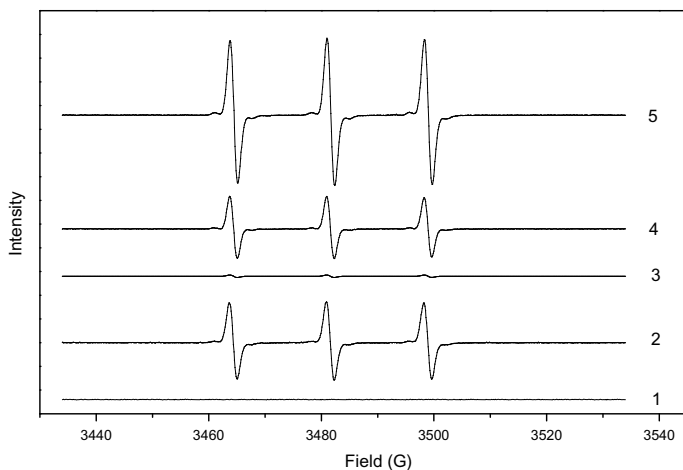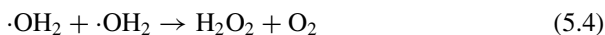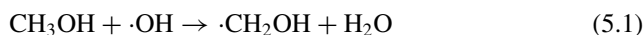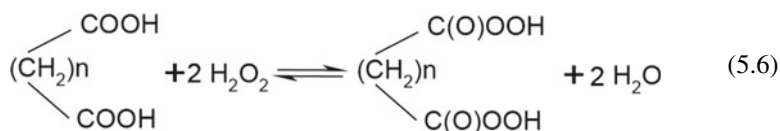
Fig. 5.6 ESR spectra of singlet oxygen by reaction of TEMP with the CL system. Spectrum 1, blank (H_2O); spectrum 2, $KHSO_5$–$CoSO_4$ CL system; spectrum 3, 0.1% (V/V) methanol added in $KHSO_5$–$CoSO_4$ CL system; spectrum 4, 0.02% (V/V) methanol added in $KHSO_5$-$CoSO_4$ CL system and spectrum 5, 1×10^{-3} mol·L^{-1} hexane diacid added in $KHSO_5$-$CoSO_4$ CL system. Conditions: receiver gain $= 8.00e + 04$; Modulation amplitude $= 1.04G$; Sweep width $= 100.00G$; Microwave frequency $= 9.7500$ GHz. Copyright 2010, with permission from Wiley [13]

reduced by methanol's consumption of hydroxyl radicals. Furthermore, with more methanol added, the suppression would be more severe.
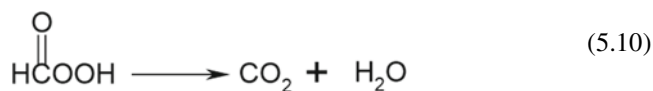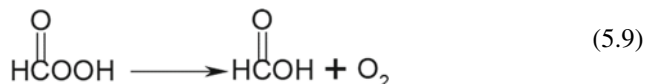
$$CH_3OH + \cdot OH \rightarrow \cdot CH_2OH + H_2O \tag{5.1}$$

$$\cdot CH_2OH + O_2 \rightarrow \cdot OOCH_2OH \tag{5.2}$$

$$\cdot OOCH_2OH \rightarrow HCHO + \cdot HO_2 \tag{5.3}$$

$$\cdot OH_2 + \cdot OH_2 \rightarrow H_2O_2 + O_2 \tag{5.4}$$

$$2H_2O_2 \rightarrow 2H_2O + O_2 \tag{5.5}$$

The CL signal in the HSO_5^-–Co^{2+} CL system was greatly improved by the addition of dicarboxylic acid, as shown in Fig. 5.4. According to reports, the aliphatic acid could combine with hydrogen peroxide to form a peroxo-diacid in an equilibrium mechanism. (Reaction 5.6) [20].

$$\underset{\text{COOH}}{\overset{\text{COOH}}{(CH_2)n}} \quad +2\,H_2O_2 \; \rightleftharpoons \; \underset{\text{C(O)OOH}}{\overset{\text{C(O)OOH}}{(CH_2)n}} \quad +2\,H_2O \qquad (5.6)$$

HSO_5^- could potentially act as an oxidant, supplying hydroxyl radicals in the same way that hydrogen peroxide (Reactions 5.7 and 5.8) did [4].

$$HSO_5^- \rightarrow SO_4^- + \cdot OH \qquad (5.7)$$

$$H_2O_2 \rightarrow \cdot OH + \cdot OH \qquad (5.8)$$

As a result, HSO_5^- might oxidize dicarboxylic acid to peroxo-diacid, a changeable and easily decomposable compound [21]. Despite the fact that peroxy-formic acid might be degraded in two ways (Reactions 5.9 and 5.10), there were no visible carbon dioxide peaks in the CL spectra to confirm carbon dioxide production [3].
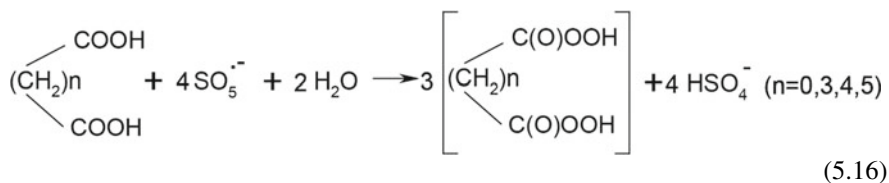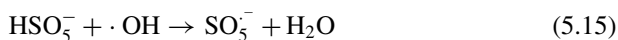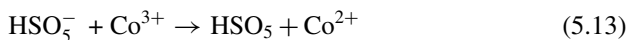
$$H\overset{O}{\overset{\|}{C}}OOH \longrightarrow H\overset{O}{\overset{\|}{C}}OH + O_2 \qquad (5.9)$$

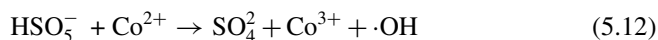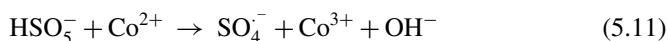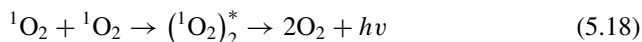$$H\overset{O}{\overset{\|}{C}}OOH \longrightarrow CO_2 + H_2O \qquad (5.10)$$

In a nutshell, the extinguishing impact of NaN_3 on O_2 (Fig. 5.6), the ESR spectra of TEMPO (Fig. 5.6) and the distinctive peaks of oxygen in the CL spectra all demonstrated that oxygen was generated in the CL reaction.

Methanol absorbed the hydroxyl radical that would have quenched the CL reaction in Reaction 5.1 when it was introduced to the CL system. However, the quench was not complete due to the presence of the $SO_5^{\cdot-}$ radical. The combination of HSO_5^- with Co (II) produced the $SO_5^{\cdot-}$ radical (Reactions 5.13, 5.14, and 5.15). Meanwhile, in Reactions 5.12–5.15, the hydroxyl radical may be involved in the formation of the $SO_5^{\cdot-}$ radical, which aided in the development of peroxo-diacid. HSO_5^-, like Co (II) in the CL reactions, was important in the training of the $SO_5^{\cdot-}$ radical. HSO_5^- oxidized Co^{2+} to produce $SO_4^{\cdot-}$ radical and Co^{3+}, as indicated in Reaction 5.11, since the oxidation potential of peroxomonosulfate (1.82 V) was slightly greater than that of Co^{3+} ($E_{Co^{3+}/Co^{2+}} = 1.802$ V) [8]. Co (II), as one of the effective metal ion-catalysts [22], was simulated again through the interaction of HSO_5^- and Co^{3+} (Reaction 5.13). Dicarboxylic acids can be easily oxidized by the $SO_5^{\cdot-}$ radical to create peroxo-diacid (Reaction 5.16). The peroxo-diacid behaved identically to formic acid (Reaction 5.9), i.e., it decomposed simultaneously into the original dicarboxylic acid and singlet oxygen (Reaction 5.17). Then a singlet oxygen molecule pair, $(^1O_2)_2^*$, was formed with a higher energy than the triple oxygen in its ground state [23, 24]. $(^1O_2)_2^*$ declined fast to O_2 in roughly 1×10^{-8} s, with transition from an enthusiastic to a grounded energy state. The CL signal was created by the

CL emission from the decay, which exhibited VIS emission bands of 545, 580, 634, and 703 nm. (Reaction 5.18) [25].

As shown in the CL dynamic profiles (Fig. 5.3), the duration of CL strengthened by increasing the length of the carbon chain. The improvement in CL, to a certain extent, was strongly associated with the carbon numbers of the dicarboxylic acid. As reported, the CL intensity of the HSO_5^--Co^{2+}-dicarboxylic acid system was determined by the decomposition rate of the dicarboxylic acid. On the other hand, the rate of decomposition of dicarboxylic acid was accelerated by increasing the length of the carbon chain [25]. Consequently, the intensity of the CL rose in lockstep with the length of the carbon chain. Based on the preceding explanation, the CL mechanism of the HSO_5^-–Co^{2+}-dicarboxylic acid system may be summarized as illustrated in Reactions (5.11–5.18): CL duration was increased by lengthening the carbon chain, as seen by the CL dynamic profiles (Fig. 5.2). To a degree, the dicarboxylic acid's carbon numbers were substantially linked to the improvement in CL. The rate of dicarboxylic acid breakdown determined the CL intensity of the HSO_5^-–Co^{2+}-dicarboxylic acid system, as previously reported. Meanwhile, extending the carbon chain length accelerated the decomposition of dicarboxylic acid [25]. As a result, as the carbon chain length rose, the CL intensity increased as well. Figure 4 shows the results. According to the explanation above, the CL mechanism of the HSO_5^--Co^{2+}-dicarboxylic acid system can be characterized as the following Reaction (5.11–5.18):

$$HSO_5^- + Co^{2+} \rightarrow SO_4^- + Co^{3+} + OH^- \tag{5.11}$$

$$HSO_5^- + Co^{2+} \rightarrow SO_4^2 + Co^{3+} + \cdot OH \tag{5.12}$$

$$HSO_5^- + Co^{3+} \rightarrow HSO_5 + Co^{2+} \tag{5.13}$$

$$HSO_5^- + SO_4^- \rightarrow SO_5^- + HSO_4^- \tag{5.14}$$

$$HSO_5^- + \cdot OH \rightarrow SO_5^- + H_2O \tag{5.15}$$

$$\tag{5.16}$$

$$\tag{5.17}$$

$$^1O_2 + {}^1O_2 \rightarrow \left({}^1O_2\right)_2^* \rightarrow 2O_2 + h\upsilon \qquad (5.18)$$
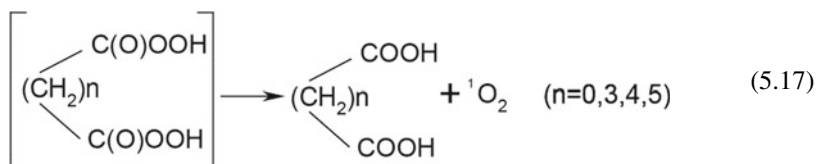
5.3 Lanthanide Ions-Enhanced Peroxomonosulfate CL by Energy Transfer

5.3.1 Batch and Flow-Injection Chemiluminescence of Peroxomonosulfate

Even though they are luminous, lanthanide ions are easily bridged by nonradiative processes when the energy difference between the lowest outgoing state and the ground manifold is minimal. With energy differences of roughly 12150, 32000, and 14800 cm^{-1}, respectively, Eu(III), Gd(III), and Tb(III) are the best ions [26, 27]. In the peroxymonosulfate (PMS) system, the dynamic profile of chemiluminescence (CL) of typical lanthanide ions, Eu(III), Gd(III), and Tb(III), is illustrated in Fig. 5.7. The kinetic curve indicated very sharp and powerful CL signals when the Ln (III) solutions were added to the PMS solution. Unlike the former, even at high concentrations, the Gd(III) signal was feeble. The BPCL photomultiplier detects wavelengths between 400 and 650 nm. Tb(III) has the highest CL intensity because its structured luminescence is virtually visible (highest energy band, 490 nm; highest intensity band, 545 nm) [28, 29]. Gd(III) has a major emission band of around 310 nm that derives from $^6P_{7/2} \rightarrow {}^8S_{7/2}$, resulting in essentially little CL signal in the PMS system. Because of its improved repeatability, the flow-injection chemiluminescence (FI-CL) system was created based on the results of batch CL. Flow rates of 1.5 mL min^{-1} for carrier stream and 0.5 mL min^{-1} for 0.02 mol L^{-1} peroxymonosulfate solution were

Fig. 5.7 Lanthanide ion chemiluminescence profiles in a batch system. 50μL Ln(III) solution was mixed into 0.02 mol·L^{-1} PMS solution of the same volume. In the figure, the Ln(III) concentrations are listed. Copyright 2009, with permission from Wiley [14]
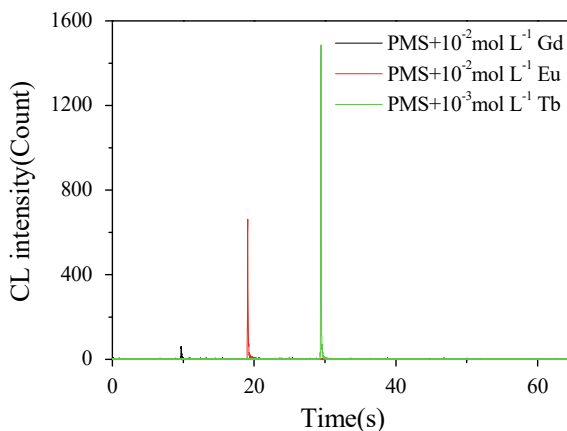
chosen as the FI-CL optimal conditions based on CL intensity for 5.0 mmol·L^{-1} Eu(III) or 1.0 mmol·L^{-1} Tb(III).

5.3.2 CL Enhancement by Ligands and Surfactants

Although lanthanide ions generate very feeble luminescence, in complexes with encapsulating ligands, a powerful luminescence of the ion may be achieved by the "antenna effect," which is characterized as a light conversion process including different absorbing (ligand) and emitting (metal ion) components [30–32]. The high coordination number is caused by the ionic nature of the lanthanide-ligand interaction, which is produced by the screening of 4f orbitals and the element's comparatively large radius. Although lanthanide ions can only generate mild luminescence, the "antenna effect" allows for intense luminescence of the ions in the complex of lanthanide ions and encapsulating ligands. The antenna effect is a term that refers to the process of light conversion that involves absorption, energy transmission, and emission. This process entails some absorption (ligand) and emission (metal ion) components. In complexes including both lanthanide ions and their enclosing ligands, the "antenna effect," which is characterized as a light conversion process comprising an absorption-energy transfer-emission sequence, may create a strong luminescence of the ion [30–32].

Table 5.1 exhibited the influence of batch chemiluminescent ligands on the CL intensity of lanthanide ions in the current system.

In the PMS system, almost all lanthanide coordinate complexes produced greater CL signals than their ions in the selected aromatic and aliphatic ligands, and the chemiluminescence of Ln(III)-2,6-pyridinedicarboxylic acid (DPA) complexes was greatest. From Fig. 5.8, when the molar ratio of Ln(III) to DPA was 1:1, the CL emission was at its highest. The stability of the compound produced with the ligand

Table 5.1 Effect of different ligands on the CL signals (count) in batch experiments ($n = 2$)

Ligand	PMS + Eu-ligand[a]	PMS + Tb-ligand
No ligand	16 ± 3	75 ± 6
2,6-Pyridinedicarboxylic acid	114 ± 21	922 ± 137
Phthalic acid	30 ± 4	191 ± 31
Ethylenediamine	30 ± 8	99 ± 16
Citric acid	42 ± 6	112 ± 3
EDTA	41 ± 7	224 ± 43

Copyright 2009, with permission from Wiley [14]
[a]The concentrations of PMS, Ln(III), and ligand were 0.01, 1.0×10^{-4}, and 1.0×10^{-4} mol·L^{-1}, respectively, in the reaction mixtures. Fifty microliters of Ln(III)-ligand mixing solution were injected into a volume of HSO$_5^-$ solution equal to that of the mixing solution

Fig. 5.8 Various DPA to
Ln(III) ratios have different
effects on CL intensity in the
FI–CL system. PMS, Eu(III),
and Tb(III) concentrations
were 0.02, 0.005 and
0.001 mol·L^{-1}, respectively.
Copyright 2009, with
permission from Wiley [14]
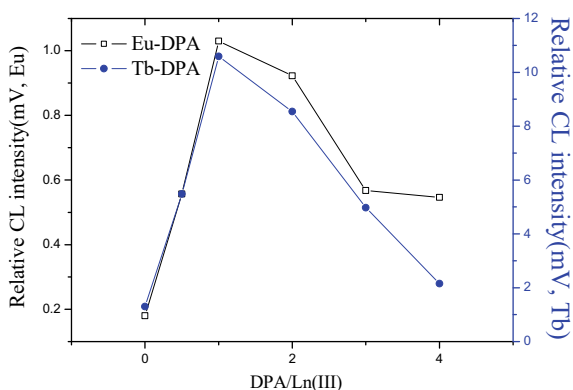
and the hydration number of the lanthanide ion influenced the intensity of coordinated lanthanide CL emission [33].

Surfactant molecules with hydrophobic tails and hydrophilic head groups tend to dynamically interact in aqueous solution to produce micelles when the surfactant concentration exceeds their critical concentration of micelles. Micelles have been shown to alter the chemistry and photophysics of molecules by changing microviscosity, local pH, polarity, reaction route or pace, and so on. [34, 35]. Micelle as a reaction medium may boost the severity of CL in some CL systems because the local microenvironment in micellar settings differs dramatically from that in homogeneous environments [36].

Various surfactants were introduced to the reaction system, including cationic, anionic, and non-ionic ones, to study how they affected the CL intensity. It was necessary to prepare each concentration of surfactants at a level above the micelle critical concentration. Only the CL signals of Ln(III) coordinate complexes were effectively enhanced by CTAC micelles, while the CL signals of Ln(III) were not enhanced, as shown in Table 5.2. A study was conducted to determine the effect of CTAC concentration on relative CL intensity. The concentrations of CTAC used were from 0.0008 to 0.005 mol·L^{-1}. The CL intensity increased with increasing CTAC concentration from 0.0008 to 0.003 mol·L^{-1}, as seen in Fig. 5.9, but remained rather steady at concentrations greater than 0.003 mol·L^{-1}.

The fluorescence lifetimes of lanthanide ions, their coordinate complexes, and complexes in CTAC micelles were determined using a time-resolved fluorescence spectrometer, as shown in Table 5.3. DPA and CTAC micelles enhance the fluorescence lifetimes of Ln(III) and their coordinate complexes, while also increasing the luminescence intensity of Ln(III) and their coordinate complexes.

As demonstrated in Table 5.4, further surprising findings may be obtained by evaluating the data in Tables 5.1, 5.4 and 5.3. The CL intensity ratio of Eu(III)-DPA to Eu(III) in the PMS system is less than that of Tb, and the same is true for Ln(III)-DPA to Ln(III)), but in the PMS system CL intensity ratio of Eu(III)-DPA/CTAC to Eu(III)-DPA is much greater than that of Tb, and Ln(III)-DPA/CTAC to Ln(III)-DPA also have the same characteristics. The findings explain why the enhancement

Table 5.2 In batch tests, the effect of various surfactants on CL signals (Count) ($n = 2$)

Surfactant[a]	Conc. (mol L^{-1})	PMS + Eu[b]	PMS + Eu-DPA	PMS + Tb	PMS + Tb-DPA
Without	0	14 ± 4	68 ± 8	65 ± 2	406 ± 56
SDS	0.05	ND	30 ± 3	ND	ND
SDBS	0.005	ND	ND	ND	ND
Tween 85	1% (v/v)	12 ± 1	13 ± 4	11 ± 5	63 ± 21
Triton X-100	1% (v/v)	ND	11 ± 3	ND	29 ± 6
CTAC	0.005	15 ± 4	1856 ± 93	19 ± 2	2284 ± 264
CTOH	0.005	12 ± 2	48 ± 2	17 ± 2	34 ± 7

Copyright 2009, with permission from Wiley [14]
[a]SDS, Sodium dodecyl sulfate; SDBS, Sodium dodecylbenzenesulfonate; CTAC, Hexade-cyltrimethylammonium chloride; CTOH, Hexadecyltrimethylammonium hydroxide
[b]PMS, Ln(III), and DPA were used at concentrations of 0.01, 1.0×10^{-4}, and 1.0×10^{-4} mol L^{-1}, respectively. Injection of 50 µL of Ln(III)-ligand in surfactant solution into the same volume of HSO$_5^-$ solution was performed

Fig. 5.9 The FI-CL system's CL intensity is affected by the concentrations of CTAC. The PMS concentration was 0.02 mol·L^{-1}, and the Ln(III) and DPA concentrations were shown in the figure. Copyright 2009, with permission from Wiley [14]
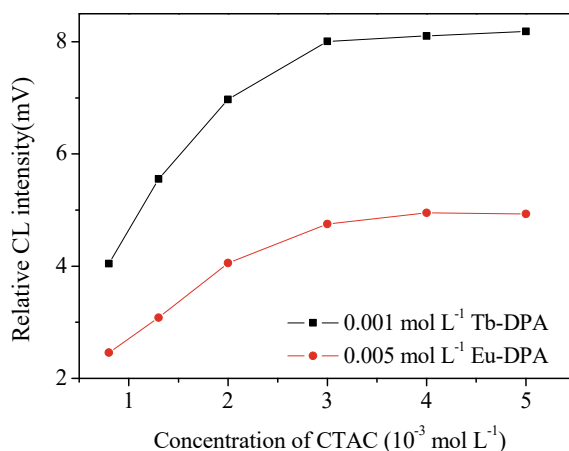

Table 5.3 The fluorescence lifetimes of lanthanide ions, their coordinate complexes, and the complexes in CTAC micelles have been measured in this study

Reagent	τ_{Eu} (ms)	τ_{Tb} (ms)
Ln(III)	0.093	0.219
Ln(III)-DPA	0.202	0.731
Ln(III)-DPA/CTAC	4.619	0.943

Copyright 2009, with permission from Wiley [14]
CTAC, Ln(III), and DPA were used at concentrations of 0.003, 5.0×10^{-5} and 5.0×10^{-5} mol·L^{-1}, respectively. Excitation wavelength: 285 nm (Eu, * 300 nm), 270 nm (Tb); emission wavelength, 616 nm (Eu, * 614 nm), 490 nm (Tb); fit parameters: Fit = A + Bexp(-t/τ)

Table 5.4 Comparisons of fluorescence lifetimes and CL enhancement

CL intensity ratio	Eu	Tb
$CL_{Ln\text{-}DPA}/CL_{Ln}$	7.125	12.29
$\tau_{Ln\text{-}DPA}/\tau_{Ln}$	2.172	3.338
$CL_{Ln\text{-}DPA/CTAC}/CL_{Ln\text{-}DPA}$	27.29	5.626
$\tau_{Ln\text{-}DPA/CTAC}/\tau_{Ln\text{-}DPA}$	22.86	1.290

Copyright 2009, with permission from Wiley [14]

of DPA on Eu(III) CL is greater than that of Tb(III), whereas the enhancement of CTAC micelles on Tb(III) coordinate complexes CL is more than that of Eu(III). The fluorescence lifetimes of Ln(III) in the media are related to the degree of improvement in DPA and CTAC on Ln(III) CL.

5.3.3 Chemiluminescence and Energy Transfer Mechanism

In a batch experiment, Table 5.5 demonstrates the effect of the $^1O_2$ quenchers 1,4-diazabicyclo[2.2.2]octane (DABCO) and sodium azide (NaN_3) [24, 37] on the CL signal. With increasing concentrations of DABCO and NaN_3, PMS/Eu(III) and PMS/Tb(III) signals were all decreased. When the concentration of (NaN_3) exceeded 0.01 mol·L^{-1}, the CL signal disappeared. The excited state of molecular oxygen was called singlet oxygen and may be the cause of the CL seen in the system.

The spin-trapping approach using electron spin resonance added to the evidence for the formation of $^1O_2$ in the system. According to Reaction 5.19, when $^1O_2$ reacts with 2,2,6,6-tetramethyl-4-piperidone (TEMP), 2,2,6,6-tetramethyl-4-piperidone-N-oxide (TEMPO) is formed, which is a stable nitroxide radical with a distinctive spectrum [38, 39].

Table 5.5 Effect of singlet oxygen quenchers on the CL signal (count) in batch experiments ($n = 2$)

Quencher	Conc. (mol·L^{-1})	PMS[a] + 10^{-2} mol·L^{-1} Eu	PMS + 10^{-3} mol·L^{-1} Tb
Without	0	649 ± 19	1538 ± 73
DABCO	10^{-4}	514 ± 15	1194 ± 213
DABCO	10^{-3}	440 ± 87	830 ± 55
DABCO	10^{-2} M	193 ± 30	282 ± 16
NaN_3	10^{-4} M	287 ± 21	946 ± 28
NaN_3	10^{-3} M	36 ± 6	104 ± 9
NaN_3	10^{-2} M	ND	ND

Copyright 2009, with permission from Wiley [14]
[a]PMS has a content of 0.02 mol L^{-1}. Each reagent contains 50 μL

$$(5.19)$$
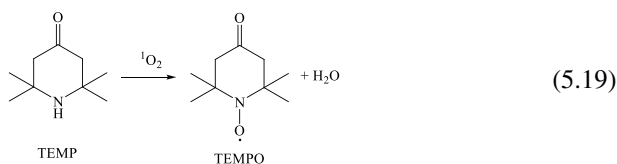
2,2,6,6-Tetramethyl-4-piperidone was dissolved in ethanol at acceptable concentrations because TEMP is soluble in alcohols, the lifespan of $^1O_2$ is enhanced sixfold when compared to H_2O, and an interaction between ·OH and TEMPO is reduced [33, 40]. The TEMPO signals were detected in the PMS/Eu(III) and PMS/Tb(III) systems by measuring the resulting hyperfine coupling constants, despite the fact that no signal was detected in the TEMP background, as shown in Fig. 5.10. During the PMS/Ln(III) CL procedure, the generation of $^1O_2$ also benefited from electron spin resonance data.

Numerous studies have shown that a transition metal with a different valence (Eu or Tb in our work) promoted activating the PMS through Reactions (5.20–5.22), resulting in the generation of various radicals such as $SO_5^{·-}$, $SO_4^{·-}$ and ·OH [22, 41, 42].

$$HSO_5^- + M^{n+} \rightarrow M^{(n+1)+} + SO_4^{·-} + OH^- \qquad (5.20)$$

$$HSO_5^- + M^{n+} \rightarrow M^{(n+1)+} + SO_4^{2-} + ·OH \qquad (5.21)$$
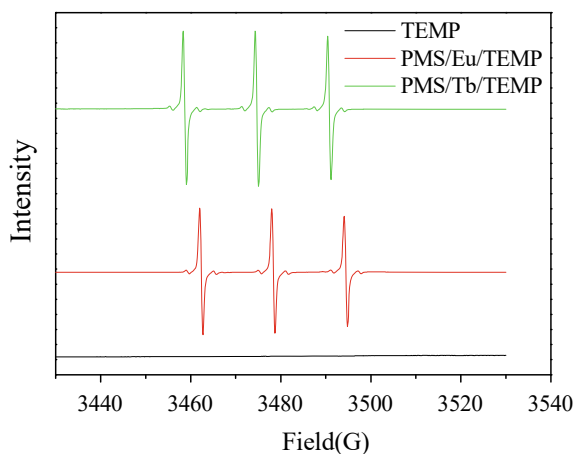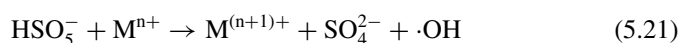
Fig. 5.10 ESR spectra of TEMP adduct with $^1O_2$ produced in the PMS/Ln(III) system. PMS, Ln(III), and TEMP concentrations were 0.005, 0.0025 and 0.05 mol·L^{-1}. Experimental condition: Microwave frequency of 9.764 GHz; microwave power of 5.048 mW; field modulation amplitude of 0.0001; field modulation frequency of 100 kHz; receiver gain of 40. Copyright 2009, with permission from Wiley [14]

$$HSO_5^- + M^{(n+1)+} \rightarrow SO_5^{\cdot-} + M^{n+} + H^+ + e^- \qquad (5.22)$$
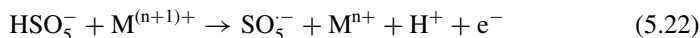
Following Reactions 5.14, 5.15, and 5.23 [17, 23], singlet oxygen will produce higher energy than ground state triplet oxygen.

$$HSO_5^- + SO_4^{\cdot-} \rightarrow SO_5^{\cdot-} + HSO_4^- \qquad (5.14)$$

$$HSO_5^- + \cdot OH \rightarrow SO_5^{\cdot-} + H_2O \qquad (5.15)$$

$$2SO_5^{\cdot-} + H_2O \rightarrow 2HSO_4^- + 1.5\,^1O_2 \qquad (5.23)$$
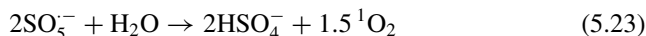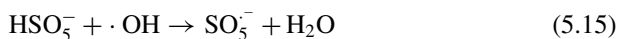
Researchers examined Ln(III) fluorescence spectra in different media with CL spectra in peroxymonosulfate systems in order to compare emitting species and better understand the mechanism throughout the CL process. Line-like emission bands were maintained even if the FL intensity of Ln(III) changed in various media because the outer $5s^2 5p^6$ filled subshells shielded 4f electrons from interactions, as demonstrated in Fig. 5.11a, b. In the coordination complex between Eu(III)-DPA and micelles system, $^5D_0 \rightarrow {}^7F_1$ of Eu(III) is responsible for the strong fluorescence emission band of 595 nm, and $^5D_0 \rightarrow {}^7F_2$ of Eu(III) is responsible for the strong fluorescence emission band of 617 nm, respectively. $^5D_4 \rightarrow {}^7F_6$ (490 nm), $^5D_4 \rightarrow {}^7F_5$ (545 nm), $^5D_4 \rightarrow {}^7F_4$ (585 nm), and $^5D_4 \rightarrow {}^7F_3$ (623 nm) are displayed in the visible spectrum and belong to Tb(III)-DPA and the coordinate complexes in micelles emission, both correspond to the Tb(III) transition from the $^5D_4$ state. The most visible lines were discovered at wavelengths of 490 and 545 nm [43, 45].

Sharp filters were used to measure the chemiluminescence spectra of the current system, as illustrated in Figs. 5.11b and 5.12b. In the PMS system, at about 620 nm, the CL strong maximum spectra of the Eu(III), Eu(III)-DPA, and the coordination
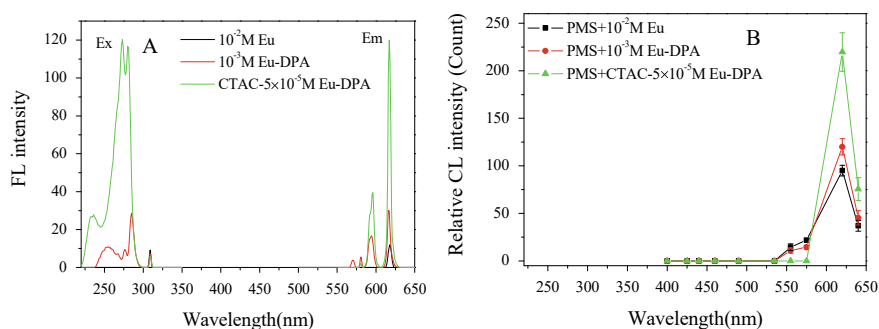

Fig. 5.11 The FL (**a**) and CL (**b**) spectra of Eu(III) are compared in various media. On the fluorescence equipment, the excitation and emission slits are 2.5 nm wide, and the scanning speed is 300 nm·min^{-1}. Eu(III) and DPA concentrations are presented in the figures, as are PMS and CTAC concentrations of 0.02 and 0.003 mol·L^{-1} (M), respectively. Copyright 2009, with permission from Wiley [14]
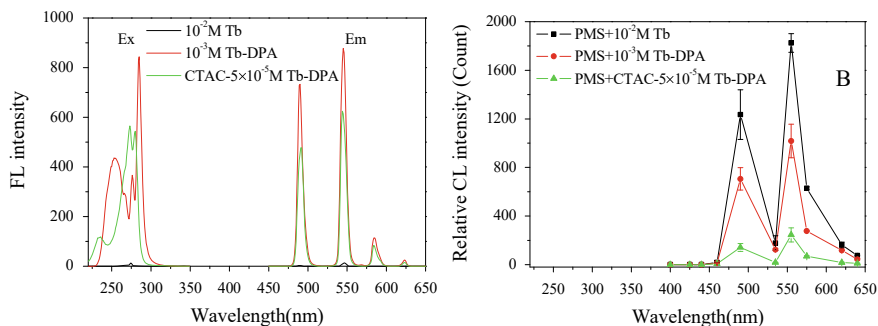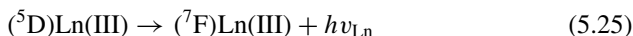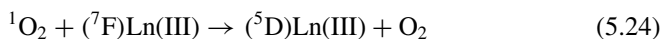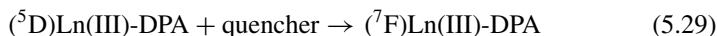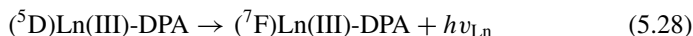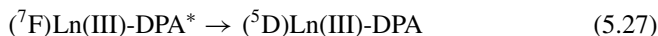
Fig. 5.12 The FL (**a**) and CL (**b**) spectra of Tb(III) in different mediums are compared. The Tb(III) and DPA concentrations were listed in the figures. Copyright 2009, with permission from Wiley [14]

complexes in micelles were seen, which corresponded to the conversion $^5D_0 \rightarrow {}^7F_2$ of Eu(III). Tb(III), Tb(III)-DPA, and the coordinate complexes in micelles in the PMS system had CL strong maximum spectra at ~490 nm and ~550 nm, which could be due to $^5D_4 \rightarrow {}^7F_6$ and $^5D_4 \rightarrow {}^7F_5$ transition of Tb(III).In the fluorescence and chemi-luminescence emission processes, the above tests indicated that lanthanide trivalent ions were the only luminescence emitters. Lanthanide trivalent ions were excited to the 5D state by absorption of energy from singlet oxygen in the PMS/Ln(III) CL system, and then produced characteristic emission by returning the ground manifold, as described in Reactions (5.24 and 5.25) [36, 46]:

$$^1O_2 + (^7F)Ln(III) \rightarrow (^5D)Ln(III) + O_2 \tag{5.24}$$

$$(^5D)Ln(III) \rightarrow (^7F)Ln(III) + h\nu_{Ln} \tag{5.25}$$

However, as compared to the low CL intensity, the aforesaid energy transfer was relatively inefficient. Ligands may receive energy from singlet oxygen through the antenna effect and excite the Ln(III) through intramolecular energy transfer in the coordinate complexes, resulting in a significant increase in CL, as seen in following Reactions (5.26–5.29):

$$^1O_2 + (^7F)Ln(III)\text{-}DPA \rightarrow (^7F)Ln(III)\text{-}DPA^* + O_2 \tag{5.26}$$

$$(^7F)Ln(III)\text{-}DPA^* \rightarrow (^5D)Ln(III)\text{-}DPA \tag{5.27}$$

$$(^5D)Ln(III)\text{-}DPA \rightarrow (^7F)Ln(III)\text{-}DPA + h\nu_{Ln} \tag{5.28}$$

$$(^5D)Ln(III)\text{-}DPA + quencher \rightarrow (^7F)Ln(III)\text{-}DPA \tag{5.29}$$

CTAC micelles have a beneficial effect on the fluorescence lifetimes of Ln(III) and their coordinate complexes in the PMS/Ln(III)-DPA/CTAC CL system, which improves the CL intensity of Ln(III) and their coordinate complexes. Through the report, it can be speculated that the reason why micelles can increase the CL strength in the system is that it can increase the efficiency of intermolecular energy transfer [46], eliminate the quenching effect of water [14], and increase the lifetime of singlet oxygen (approximately water Ten times) [40, 47].

5.4 Conclusions

The research on CL mechanism of $KHSO_5$ system is very valuable. Aliphatic dicarboxylic acids are beneficial to enhance the CL signal in the $KHSO_5$-$CoSO_4$ system, such as oxalic acid, malonic acid, succinic acid, glutaric acid, adipic acid, and pimelic acid. The production of peroxo-diacid may help increase the CL phenomenon of dicarboxylic acid. Dicarboxylic acid was previously in an unstable excited state and eventually decomposed into dicarboxylic acid and singlet oxygen. In addition, according to the evaluation of the decomposition rate, the strength of CL increases with the increase of the carbon chain length, and the two show a stable positive correlation. When the dimer $({}^1O_2)_2{}^*$ produced by singlet oxygen decays into triplet oxygen (a ground state substance), the CL emission is recorded. in this process. It was found that methanol can scavenge hydroxyl radicals in the $KHSO_5$-$CoSO_4$ system, thereby effectively limiting CL emissions. In the study to explore the CL phenomenon of Ln(III) and the enhancement of DPA and CTAC micelles, batch and flow-injection CL methods were used, and it was found that the fluorescence lifetime of Ln(III) in different media affects its enhancement degree. The CL phenomenon found in the system may be due to the comparison of fluorescence and CL spectra, which led to the production of singlet oxygen and the energy transfer process.

References

1. Yusuf G, Adewuyi SOO (2003) Aqueous absorption and oxidation of nitric oxide with oxone for the treatment of tail gases: process feasibility, stoichiometry, reaction pathways, and absorption rate. Ind Eng Chem Res 42:4084–4100
2. Ball DL, Edwards JOI (1956) The kinetics and mechanism of the decomposition of Caro's acid I. J Am Chem Soc 78:1125–1129
3. Wang M, Zhao LX, Lin J-M (2007) Chemiluminescence of the peroxomonosulphate-cobalt (II)-aliphatic monocarboxylic acids system. Luminescence 22:182–188
4. Richard JK, Albert MS (1960) The oxidation of organic substances by potassium peroxymonosulfate. J Org Chem 25:1901–1906
5. Betterton EA, Hoffmann MR (1990) Kinetics and mechanism of the oxidation of aqueous hydrogen sulfide by peroxymonosulfate. Environ Sci Technol 24:1819–1824
6. Makita Y, Umebayashi H, Suzuki T, Masuda A, Yamada M, Hobo T (1993) New analytical chemiluminescence system using peroxymonosulfate as oxidant. Chem Lett 22:1575–1578

7. Tsukada S, Miki H, Lin J-M, Suzuki T, Yamada M (1998) Chemiluminescence from fluorescent organic compounds induced by cobalt(II) catalyzed decomposition of peroxomonosulfate. Anal Chim Acta 371:163–170
8. Lin J-M, Yamada M (2000) Chemiluminescent reaction of fluorescent organic compounds with $KHSO_5$ using cobalt(II) as catalyst and its first application to molecular imprinting. Anal Chem 72:1148–1155
9. Zhang B-T, Zhao L, Lin J-M (2008) Determination of folic acid by chemiluminescence based on peroxomonosulfate-cobalt(II) system. Talanta 74:1154–1159
10. Magdaleno GB, Coichev N (2005) Chemiluminescent determination of humic substances based on the oxidation by peroxymonosulfate. Anal Chim Acta 552:141–146
11. Roebke W, Renz M, Henglein A (1969) Pulsradiolyse der anionen $S_2O_8^{2-}$ und HSO_5^- in Wässriger Lösung. Int J Radiat Phys Chem 1:39–44
12. Georges J (1993) Lanthanide-sensitized luminescence and applications to the determination of organic analytes-a review. Analyst 118:1481–1486
13. Zhou Y, Ogawa N, Lin J-M (2011) Enhanced chemiluminescence of peroxomonosulfate-cobalt (II) system in the presence of dicarboxylic acids. Luminescence 26:280–288
14. Zhang BT, Lin J-M (2010) Chemiluminescence and energy transfer mechanism of lanthanide ions in different media based on peroxomonosulfate system. Luminescence 25:322–327
15. Lu C, Song GQ, Lin J-M (2006) Reactive oxygen species and their chemiluminescence-detection methods. Trends Anal Chem 25:985–995
16. Anipsitakis GP, Stathatos E, Dionysiou DD (2005) Heterogeneous activation of oxone using Co_3O_4. J Phys Chem B 109:13052–13055
17. Muller JG, Zheng P, Rokita SE, Burrows CJ (1996) DNA and RNA modification promoted by [Co $(H_2O)_6$] Cl_2 and $KHSO_5$: Guanine selectivity, temperature dependence, and mechanism. J Am Chem Soc 118:2320–2325
18. Asmus KD, MÖckel H, Henglein A, (1973) Pulse radiolytic study of the site of hydroxyl radical attack on aliphatic alcohols in aqueous solution. J Phys Chem 77:1218–1221
19. Bothe E, Schulte FD (1978) $HO_2^\cdot$ elimination from α-hydroxyalkylperoxyl radicals in aqueous solution. Photochem Photobio 28:639–644
20. Silbert LS, Siegel E, Swern D (1962) Peroxides IX. New method for the direct preparation of aromatic and aliphatic peroxy acids. J Org Chem 27:1336–1342
21. Koubek E, Haggett ML, Battaglia CJ, Ibne M, Pyun HY, Edwards JO (1963) Kinetics and mechanism of the spontaneous decompositions of some peroxoacids, hydrogen peroxide and t-butyl hydroperoxide. J Am Chem Soc 85:2263–2268
22. Maruthamuthu P, Neta P (1977) Radiolytic chain decomposition of peroxomonophosphoric and peroxomonosulfuric acids. J Phys Chem 81:937–940
23. Zhang Z, Edwards JO (1992) Chain lengths in the decomposition of peroxomonosulfate catalyzed by cobalt and vanadium. Rate law for catalysis by vanadium. Inorg Chem 31:3514–3517
24. Ouannes C, Wilson T (1968) Quenching of singlet oxygen by tertiary aliphatic amines. Effect of DABCO (1, 4-diazabicyclo [222] octane). J Am Chem Soc 90:6527–6528
25. Stephens ER, Hanst PL, Doerr RC (1957) Infrared spectra of aliphatic peroxyacids. Anal Chem 29:776–777
26. Liu G, Jacquier B (2005) Spectroscopic properties of rare earths in optical materials. Tsinghua University Press, Beijing, pp 462–499
27. Teotonio TES, Brito HF, Felinto MCFC, Thompson LC, Young VG, Malta OL (2005) Preparation, crystal structure and optical spectroscopy of the rare earth complexes ($RE^{3+}=$ Sm, Eu, Gd and Tb) with 2-thiopheneacetate anion. J Mol Struct 751:85–94
28. Prodi L, Maestri M, Ziessel R, Balzani V (1991) Luminescent europium (3+), terbium (3+) and gadolinium (3+) complexes of a branched-triazacyclononane ligand containing three 2, 2'-bipyridine units. Inorg Chem 30:3798–3802
29. Blasse G (1984) Handb Phys Chem Rare Earths 4:237–274
30. Fratini A, Richards G, Larder E, Swavey S (2008) Neodymium, gadolinium, and terbium complexes containing hexafluoroacetylacetonate and 2,2'-bipyrimidine: structural and spectroscopic characterization. Inorg Chem 47:1030–1036

31. Sabbatini N, Guardigli M, Lehn J-M (1993) Luminescent lanthanide complexes as photochemical supramolecular devices. Coord Chem Rev 123:201–228
32. Vicentini G, Zinner LB, Zukerman-Schpector J, Zinner K (2000) Luminescence and structure of europium compounds. Coord Chem Rev 196:353–382
33. Liu M, Zhao L, Lin J-M (2006) Chemiluminescence energy transfer reaction for the on-line preparation of peroxymonocarbonate and Eu(II)-dipicolinate complex. J Phys Chem A 110:7509–7514
34. Dan N, Lau ML, Grayeski ML (1991) Micellar-enhanced aqueous peroxyoxalate chemiluminescence. Anal Chem 63:1766–1771
35. Chen Y, Rosenzweig Z (2002) Luminescent CdSe quantum dot doped stabilized micelles. Nano Lett 2:1299–1302
36. Lin J-M, Yamada M (2003) Microheterogeneous systems of micelles and microemulsions as reaction media in chemiluminescent analysis. TrAC-Trends Anal Chem 22:99–107
37. Engl R, Kilger R, Maier M, Scherer K, Abels C, Baumler W (2002) Singlet oxygen generation by 8-methoxypsoralen in deuterium oxide: relaxation rate constants and dependence of the generation efficacy on the oxygen partial pressure. J Phys Chem B 106:5776–5781
38. Yamakoshi Y, Umezawa N, Ryu A, Arakane K, Miyata N, Goda Y, Masumizu T, Nagano T (2003) Active oxygen species generated from photoexcited fullerene (C60) as potential medicines: O_2^- versus O_2. J Am Chem Soc 125:12803–12809
39. Li H-R, Wu L-Z, Tung C-H (2000) Reactions of singlet oxygen with olefins and sterically hindered amine in mixed surfactant vesicles. J Am Chem Soc 122:2446–2451
40. Rodgers MAJ (1983) Solvent-induced deactivation of singlet oxygen: additivity relationships in nonaromatic solvents. J Am Chem Soc 105:6201–6205
41. Anipsitakis GP, Dionysiou DD (2003) Degradation of organic contaminants in water with sulfate radicals generated by the conjunction of peroxymonosulfate with cobalt. Environ Sci Technol 37:4790–4797
42. Anipsitakis GP, Dionysiou DD (2004) Radical generation by the interaction of transition metals with common oxidants. Environ Sci Technol 38:3705–3712
43. Dong Y-B, Wang P, Ma J-P, Zhao X-X, Wang H-Y, Tang B, Huang R-Q (2007) Coordination-driven nanosized lanthanide "molecular lantern" with tunable luminescent properties. J Am Chem Soc 129:4872–4873
44. Wang P, Ma J-P, Dong Y-B, Huang R-Q (2007) Tunable luminescent lanthanide coordination polymers based on reversible solid-state ion-exchange monitored by ion-dependent photoinduced emission spectra. J Am Chem Soc 129:10620–10621
45. Horrocks WD, Sudnick DR (1979) Lanthanide ion probes of structure in biology lassssssssssser-induced luminescence decay constants provide a direct measure of the number of metal-coordinated water molecules. J Am Chem Soc 101:334–340
46. Escabi-Perez JR, Nome F, Fendler JH (1977) Energy transfer in micellar systems steady state and time resolved luminescence of aqueous micelle solubilized naphthalene and terbium chloride. J Am Chem Soc 99:7749–7754
47. Martinez LA, Martínez CG, Klopotek BB, Lang J, Neuner A, Braun AM, Oliveros E (2002) Nonradiative and radiative deactivation of singlet molecular oxygen ($O_2(a1\Delta g)$) in micellar media and microemulsions. J Photochem Photobiol B 58:94–107

Chapter 6
Ultra-Weak Chemiluminescence from Reaction of Sulfite and Hydrogen Peroxide

Hui Chen and Jin-Ming Lin

Abstract The chemiluminescence (CL) response combining hydrogen peroxide (H_2O_2) as well as sodium bisulfite ($NaHSO_3$) was investigated. In this CL system, The significant facilitators were the hydroxyl radical ($\cdot OH$) and the sulfite radical ($\cdot SO_3{}^-$). The inhibitory efficiency effects of radical scavengers such as thiourea, chloride ion, nitro blue formazan chloride (NBT), and 5,5-dimethyl-1-pyrroline N-oxide (DMPO) have indeed been validated. Single oxygen ($^1O_2$) and agitated sulfur dioxide ($SO_2{}^*$) emitted species associated with the $NaHSO_3-H_2O_2$ CL system. Alcoholic solvent, particularly n-butanol, has increased ultra-weak CL emission over 40 times. The strong stimulating effect of alcohol solvent is due to the establishment of solvent tank in the system, which can speed up the reaction on the one hand and protect the classification of quenching with water on the other hand. The discharge of ultra-low CL was also increased 70 times by 10 pmol benzo[a]pyrene-7, 10-quinone (7, 10-BaPQ). Radical collectors and the electron spin resonance (ESR) profile were being used to evaluate the $NaHSO_3$-7, 10-BaPQ-H_2O_2 system intermediates. In the $NaHSO_3$-7, 10-BaPQ-H_2O_2 system, hydroxyl radicals ($\cdot OH$), superoxide anionic radicals ($\cdot O_2{}^-$), as well as sulfite radicals ($\cdot SO_3{}^-$) were synthesized. On the basis of this mechanism, a highly sensitive manner for deciding 7, 10-BaPQ was first proposed. Carbon nanodots were upgraded in this ultra-low CL reaction of hydrogen peroxide and sodium thiosulfate, and the mechanism was better understood in detail.

Keywords Sulfite · Bisulfite · Sulfur dioxide · Hydrogen peroxide · 1-Hydroxypyrene chemiluminescence · Airborne particulates · Benzo[a]pyrene-7 · 10-quinone

H. Chen
College of Materials Science and Technology, Beijing Forestry University, Beijing 100083, China
e-mail: chenhui@bjfu.edu.cn

J.-M. Lin (✉)
Department of Chemistry, Tsinghua University, Beijing 100084, China
e-mail: jmlin@mail.tsinghua.edu.cn

6.1 Introduction

The oxidation of sulfite (SO_3^{2-}) has been investigated for more than 50 years [1–4]. Hydrogen peroxide (H_2O_2) is a powerful oxidant capable of converting SO_3^{2-} to lead to SO_4^{2-}. Sulfite oxidation, according to Hoffman, occurs due to its rapid nucleophilic shift of HSO_3^- by H_2O_2, at which time peroxomonosulfurous acid was likely framed in 1975. Peroxomonosulfurous acid goes through a speed rearrangement to produce SO_4^{2-} ion [5, 6]. In particular, Halperin et al. revealed SO_3^{2-} oxidation with H_2O_2 through the use of the peroxomonosulfurous acid intermediates. They studied the marked H_2O_2 response and concluded each H_2O_2 particle transfers two oxygen atoms to the SO_3^{2-} ion [7, 8] On the contrary, The radical oxidation of SO_3^{2-} by H_2O_2 was predicted by multiple organizations. In the $SO_3^{2-}-H_2O_2$ reaction, radical sulfite ($\cdot SO_3^{2-}$) and radical hydroxyl ($\cdot OH$) were cultivated. Electronic spin resonance (ESR) spectra identified the radicals $\cdot SO_3^-$ and $\cdot OH$. The mechanism of SO_3^{2-} oxidized by H_2O_2 is unknown at this point.

In 1975, Stauff and colleagues observed an ultra-low CL emission while SO_3^{2-} was oxidized with H_2O_2. And then, multiple types of CL systems gathered from SO_3^{2-} oxidation have been corroborated [13−16]. They maintained that oxidation of SO_3^{2-} yielded the $\cdot SO_3^-$ radical, which was then dimerized to actually produce the $S_2O_6^{2-}$ ion in most situations. The emitter was stimulated sulfur dioxide (SO_2^*), which was framed by the breakdown of the $S_2O_6^{2-}$ ion. CL emissions derived from oxidation of SO_3^{2-} were very low-lying as a consequence of the low-lying quantum efficiency of SO_2^* emissions. SO_2^* emission wavelength measurement is extremely difficult.

Surfactant nanoemulsions have always been implemented to enhance the CL emission [19−21]. Emitting species and radicals may be sheltered by micelles surfactants. But besides that, reactantions were captivated to the surface of microemulsions, contributing to increased reactant concentrations on the surface. The CL intensity remains constant as the concentrations of reactants climb, which is really just another strong motivation to strengthen CL strength. While compared to pure water, a number of reagents were more soluble in microcapsules [22].

In our research [23], we successfully identified that singlet oxygen ($^1O_2$) was cultivated and during oxidation of SO_3^{2-} by H_2O_2. Two distinct $^1O_2$ scavengers can emit $^1O_2$ over more than a number of years (DABCO and NaN_3). Apart from that, $^1O_2$ has also been tracked down by ESR spectrum. $SO_3^{2-}-H_2O_2$ reacted radically, as evidenced by the increasing ascorbic acid refrain. The reaction of $SO_3^{2-}-H_2O_2$ yielded radicals like as $\cdot OH$, $\cdot SO_3^-$, and $\cdot O_2^-$. To encourage the creation of radicals, various forms of extreme criticism have been employed. The CL emission derived from $SO_3^{2-}-H_2O_2$ was very feeble. We keep under observation that the emission of ultra-low CL was increased by 40-fold by *n*-butanol. An alcoholic solvent with a carbon number of 1–5 has been compared. CL intensity was found to increase as carbon numbers increased. The reinforcement effect may be the same as that of surfacing micelles. In pure water, *n*-butanol can develop surfactant micelles that

resemble solvent cages, which protect radicals while also releasing species in the CL reaction.

For the first time, the ultra-weak CL reaction process on the influence of carbon nanotubes was evaluated by applying hydrogen peroxide and sodium bisulfite. The intensity of H_2O_2–HSO_3– CL emissions were found to be significantly improved by carbon nanodots. The CL intensity was multiplied by about 60. Positively charged carbon nanodots ($CD^{\bullet +}$) and negatively charged carbon nanodots ($CD^{\bullet -}$) are annihilated by electron transfer, resulting in delighted state carbon nanodots (CD^*). To investigate intermediates, circumferential scavengers such as nitro blue tetrazolium chloride (NBT), sodium azide, thiourea, 5,5-dimethyl-1-pyrroline N-oxide, and ascorbic acid had been used. The inter-median radicals produced at the same time as the CL reaction. For the production of $CD^{\bullet +}$ and $CD^{\bullet,-}$, radicals such as hydroxide ($\cdot OH$), sulfate anionic radical ($SO_4^{\bullet -}$), superoxide anionic radical ($\cdot O^{2-}$), and sulfur trioxide anionic radical ($\cdot SO_3^{-}$) were noteworthy. The results of the CL emission spectra, absorption spectra, and electron spin resonance (ESR) spectra were being used to estimate the mechanism for continued to improve CL.

Polycyclic aromatic hydrocarbon (PAH) is a major series of environmentally harmful organic compounds, which are formed by the burning of fossil fuels, industry waste, automobile exhausts, and tobacco smoke [24–27]. The downfall PAH degradation yields hydroxylated PAHs, nito-PAHs, and PAH quinones, among several other chemical pollutants [28–31]. PAH quinones are a category of hazardous compounds that yields reactive oxygen species (ROS) whenever they move forwards through their redox period in the female body [32–34]. Adverse health effects such as aging, cancer, and inflammation have all been linked to ROS production [35, 36]. Apart from that, PAHS quinones can form covalent enzyme complexes with proteins with the enzyme's functional groups, attempting to destroy the enzyme's activity [37, 38]. Therefore, a conscious and reliable approach for the assurance of quinone PAHs in the environment is required. Four- and five-cycle PAH quinones just are not measurable while also LC–MS/MS. PAH and subsequent behind were mainly evaluated using HPLC with brightness. Sad to say, PAH quinones have no shadow properties. Thus, derivatization is demanded for HPLC-fluorescence determination. Chemiluminescence is an authoritative method by reason of excitation light is not necessary in relation to fluorescence. Low baseline signal of chemiluminescence results in higher awareness. To complete PAH compounds with high acuity and understanding, HPLC with peroxyoxalate or luminol CL system with online post-column ultraviolet irradiation was being used [39]. But exacting conditions make the approaches not appear to be pertinent for environmental fragments. In our work [40], this NaHSO$_3$–H_2O_2 CL system had been used to strengthen an ultra-sensitive CL methodology to investigate 7, 10-BaPQ. Although 7, 10-BaPQ showed no brilliance discharge, a strong CL emission was realized when H_2O_2 was infused into NaHSO$_3$-7, 10-BaPQ mixture solutions. 7, 10-BaPQ can be disclosed with no bypass or reduction of this approach. The proposed method is straightforward and saves time in comparison to other reports. The level of 7, 10-BaPQ concentrations was more easily spotted. For only the first time, the prospective method has been successfully applied to recognize the concentrations of 7, 10-BaPQ in atmospheric pollutants.

6.2 Chemiluminescent Study of Sulfite-Hydrogen Peroxide System

NaHSO$_3$ was oxidized by H$_2$O$_2$ through peroxomonosulfurous acid intermediate, which then broke down to produce ·OH and ·SO$_3^-$ radicals. ^{1}O$_2$ was also spouting species besides SO$_2^*$. The CL emission took away NaHSO$_3$–H$_2$O$_2$ reaction can be greatly increased by alcoholic solvent (exclusively *n*-butanol) enormously. When *n*-butanol was arranged in 50% methanol or 50% ethanol, the stimulant force was no longer present. The fact determined the construction of solvent cage in pure water, which can protect the spouting species taken away from quenching by water.

6.2.1 Kinetic of Sulfite-Hydrogen Peroxide System

In a 3 mL quartz glass cuvette, the CL kinetics contour was required using that UPLC ultra-weak chemiluminescence analyzer (Institute of Biophysics, Chinese Academy of Science, Beijing, China) (Fig. 6.1a). The great voltage was 1.2 kV. On a PC that has a data-acquisition interface, the item was listed. The BPCL program would be used for data collection and processing. The CL emission spectrum has been estimated in the same apparatus with the addition of some cut-off filters before PMT.

We utilized a high-performance liquid system with three pressure transducers, model LF-800 (SJ-1221, Atto, Japan). Flow-injection CL signal quantification (Microtec NITI-On, Funabashi, Japan). A model LF-800 flow-injection system (Microtec NITI-On, Funabashi, Japan) with three mixed convection pumps is being used to measure the CL signal of flow injection (SJ-1221, Atto, Japan). Three flow pipelines constitute the flow-injection CL system (Fig. 6.1b). Water was taken as an aid for H$_2$O$_2$. Organic solvent solutions were blended with H$_2$O$_2$ in the mixing coil. The carrier (water) of H$_2$O$_2$, organic solvent, and NaHSO$_3$ were aroused into the flow cell before PMT. A six-valve injector had been used to convey the H$_2$O$_2$. The LF-800 analyzer was being used to retrieve the CL flag. As a function of CL strength, the
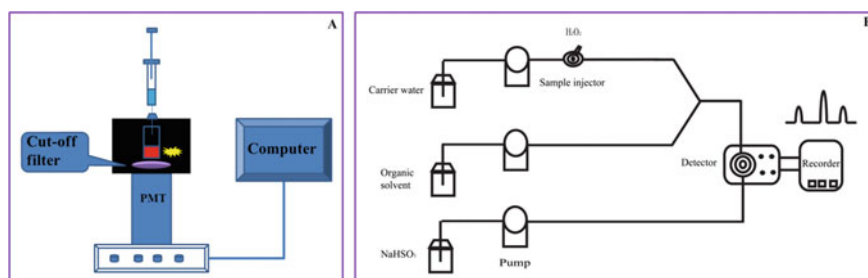
Fig. 6.1 BPCL and flow-injection CL instrument schematic. Copyright 2012 American Chemical Society, reprinted with permission from Ref. [23]
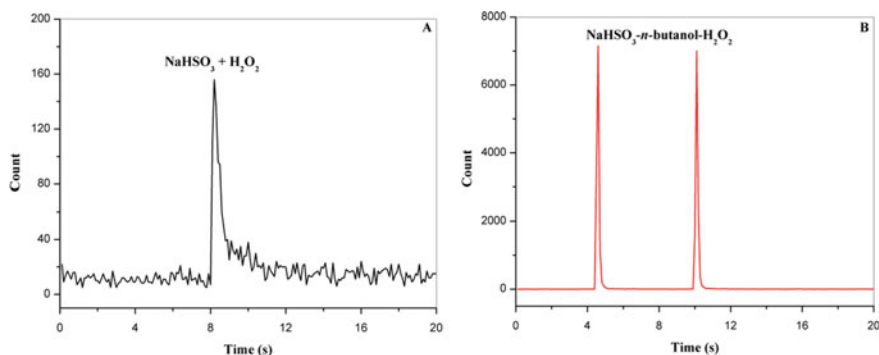
Fig. 6.2 Chemiluminescence emission is recorded. H_2O_2 solution was injected into NaHSO$_3$ solution (**a**) and NaHSO$_3$-*n*-butanol (0.08 basis points in water) combined solution (**b**). 0.1 mol L^{-1} NaHSO$_3$; 0.5 mol L^{-1} H_2O_2; 100 µl input volume. Copyright 2012 American Chemical Society, reprinted with permission from Ref. [23]

maximum height of the signal level was measured. The CL system's kinetic bend is crucial for understanding the responses. Figure 6.2a illustrates a typical CL response bend (CL intensity versus time profile) of the NaHSO$_3$–H_2O_2 system. An ultra-weak CL emission, which got its largest value in 0.1 s, was recognized when H_2O_2 was infused into NaHSO$_3$ solution. The ultra-weak CL emission could be increased by adding alcoholic solvent with the carbon number taken away from two to five. Associating order of CL reagents played a significant role in CL emission. Therefore, various mixing orders of NaHSO$_3$, H_2O_2, and alcoholic solvent were surveyed. When alcoholic solvent reacting with only NaHSO$_3$ or H_2O_2, no CL emission was recognized. Furthermore, during the injection of *n*-butanol into the NaHSO$_3$–H_2O_2 mixture, no CL indicator was listed. The reaction rate of NaHSO$_3$–H_2O_2 was increased through the enhancement of alcoholic solvent.

6.2.2   Possible Mechanism for Sulfite-Hydrogen Peroxide System

In order to investigate the detail of the CL reality, the intermediates in the system were identified by different free radical scavengers. The outcomes were presented in Table 6.1. Ascorbic acid is an economical reactive oxygen species (ROS) scavenger [41, 42]. When ascorbic acid is present, the CL emission drops dramatically, indicating that the CL reaction has taken a radical turn. The availability of superoxide anion (ROS) such as the ·OH and $·O_2{}^-$ ions have been maintained in the system. The radicals $·SO_3{}^-$ and ·OH was employed in the first stage of the process. The restriction forces of DMPO would be used to prove the generation of $·SO_3{}^-$ and ·OH [43, 44]. Thiourea is a unique ingredient scavenger with ·OH radicals [45]. A strong inhibitory

Table 6.1 The $NaHSO_3$–H_2O_2 system[a] was affected by free radical scavenging

Radical scavengers	Intermediates	Concentration (mol L^{-1})	Inhibition ratio (%)[b]
Without scavenger	–	–	0
Ascorbic acid	$\cdot OH, \cdot O_2^-$	0.01	100
DMPO	$\cdot SO_3^-, \cdot OH$	0.05 (v/v)	50
Thiourea	$\cdot OH$	0.01	100
Br^-	$\cdot OH$	0.01	50
Cl^-	$\cdot OH$	0.01	35
NBT	$\cdot O_2^-$	0.01	90
NaN_3	$^1O_2$	0.01	50
DABCO	$^1O_2$	0.05	30

Reprinted with permission from Ref. [23], Copyright 2012 American Chemical Society
[a]Concentrations of $NaHSO_3$ and H_2O_2 were 0.2 and 0.5 mol L^{-1}, injection volume was 100 μL, radical scavengers were 50 μL; 7, 10-BaPQ was 10 pmol
[b]Average value of three times

force of thiourea designated the survival of radical $\cdot OH$. Inhibition of Br^- and Cl^- further proved the formation of $\cdot OH$ radicals.

NBT was regarded as $\cdot O_2^-$ radical scavengers [46, 47]. The addition of NBT inhibited CL release (90%), confirming that $\cdot O_2^-$ plays an important role in CL release process.

Within the inorganic CL system, $^1O_2$ was a common emission species. So that the creation of $^1O_2$, NaN_3, and DABCO, which can scavenge $^1O_2$ skillfully, were occupied [48, 49]. The findings appeared to demonstrate that $^1O_2$ survived.

The ESR spectrum was a conscious approach to diagnose radicals. Due to the short lifetime of free radicals, the spin capture technique is a fundamental approach to determine free radicals. In this research in the course of this research, DMPO and TEMP were accustomed to trap $\cdot OH$ and $^1O_2$ [50–52]. The spectra apparently displayed the existence of $\cdot OH$ and $^1O_2$ (Fig. 6.3).

In the system, CL emissions of $NaHSO_3$-n-butanol-H_2O_2 have been estimated to diagnose emission species. The superlative wavelength was placed around 490 nm, which belonged to the $^1O_2$ [53]. The largest summit, 400 nm to 600 nm, was at SO_2^* (Fig. 6.4).

Based on the CL emission spectrum, the radical collector experimental consequences, and the ESR spectra, the CL mechanism of the reaction system was proposed. In the $NaHSO_3$–H_2O_2 reaction system, the manufacturing of the $\cdot OH$ radical was an essential part. (Reaction 6.1). It could be evidenced via the extinction influence of thiourea, CL^-, and Br^-. Furthermore, $\cdot OH$ radical has also been identified by ESR spin-trapping technique (Fig. 6.3A).
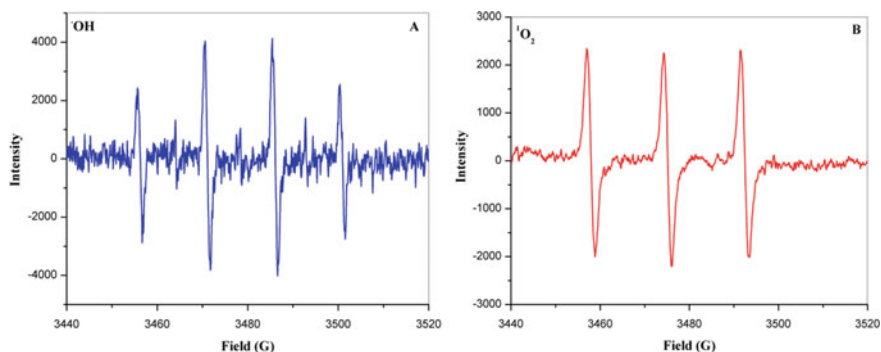
$$H_2O_2 + HSO_3^- \rightleftharpoons \underset{O}{\overset{^-O}{\bigvee}} S - O \!\mid\! - OH \rightarrow \cdot OH + \cdot SO_3^- \qquad (6.1)$$
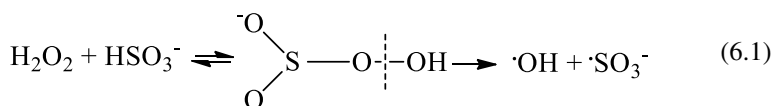
Fig. 6.3 Singlet oxygen and hydroxyl radical ESR spectra. (**a**) ·OH radical ESR spectrum in HSO_3^--n-butanol-H_2O_2 solution. $^1O_2$ ESR spectrum in HSO_3^--n-butanol-H_2O_2 solution (**b**). TEMP was employed directly without dilution in DMPO 0.2 mol·L^{-1} conditions. The H_2O_2 and NaHSO$_3$ concentrations were the same as in Fig. 6.2. **a** 30 µL NaHSO$_3$ + 30 µL DMPO + 30 µL n-butanol + 30 µL H_2O_2 **b** 50 µL NaHSO$_3$ + 50 µL n-butanol + 3µ L TEMP + 50 µL H_2O_2. Copyright 2012 American Chemical Society, reprinted with permission from Ref. [23]
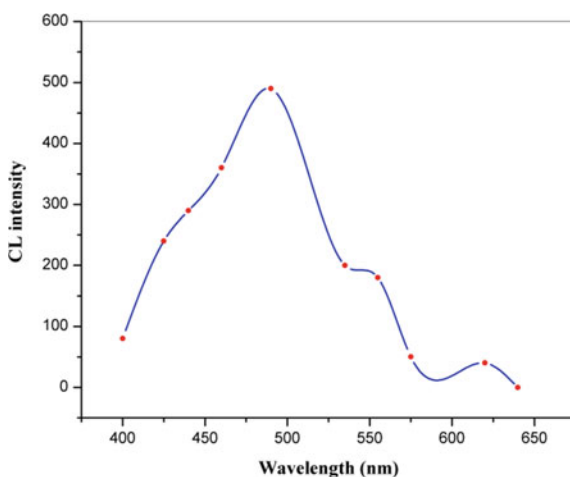
Fig. 6.4 Emission wavelength of NaHSO$_3$-n-butanol-H_2O_2 CL system. The concentrations of H_2O_2 and NaHSO$_3$ were similar to volumes of NaHSO$_3$, n-butanol, and H_2O_2 100 µL correspondingly, n-butanol was 0.08% (v/v). The NaHSO$_3$-n-butanol-H_2O_2 CL system's emission wavelength. H_2O_2 and NaHSO$_3$ concentrations were comparable to those that can be seen in Fig. 6.2. Volumes of NaHSO$_3$, n-butanol, and H_2O_2 were both 100 µL, without n-butanol accounting for 0.08% (v/v). Copyright 2012 American Chemical Society, reprinted with permission from Ref. [23]

The ·OH radical, which is a strong oxidant, interacted with HSO$_3^-$ to produce ·SO$_3^-$ radical is forming at a rapid rate (Reaction 6.2) [54, 55].

$$\cdot OH + HSO_3^- \rightarrow \cdot SO_3^- + H_2O$$
$$k = 4.5 \times 10^9 \, M^{-1} \, s^{-1} \tag{6.2}$$
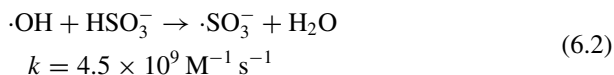
The $\cdot SO_3^-$ radical can dimerize to $S_2O_6^{2-}$, which can then decompose to SO_2^*. With the degradation of SO_2^*, the CL emission was noticed (Reactions 6.3–6.5). The CL quantum yield was bottom; accordingly, the CL emission was extremely powerless.
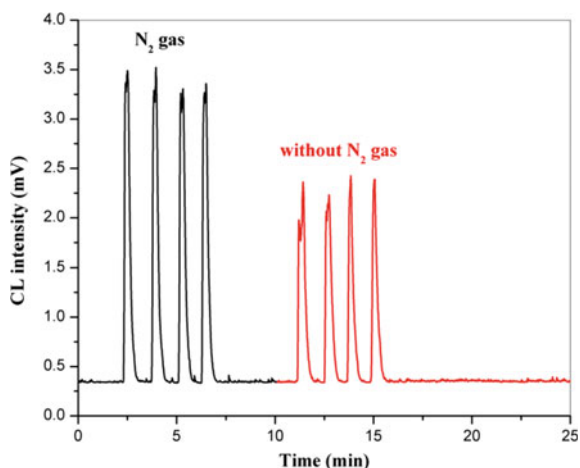
$$\cdot SO_3^- + \cdot SO_3^- \rightarrow S_2O_6^{2-} + H_2O \tag{6.3}$$

$$S_2O_6^{2-} \rightarrow SO_4^{2-} + SO_2^* \tag{6.4}$$

$$SO_2^* \rightarrow SO_2 + h\nu \tag{6.5}$$
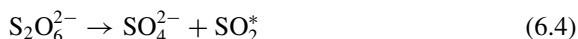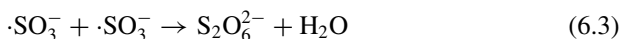
Dissolved oxygen is a crucial factor that can cause CL emission to be disrupted. For thirty minutes, ultra-pure nitrogen (N_2) was pumped into the CL system to completely remove the dissolved oxygen in the CL solution. After 30 min of N_2 gas, CL emissions increased by 30%. (Fig. 6.5). This gradual impact is demonstrated in the following reaction. The peroxymonosulfate radical($^-O_3SOO\cdot$) was formed when the $\cdot SO_3^-$ radical interacted quickly with dissolved oxygen (Reaction 6.6) [56, 57].

$$\cdot SO_3^- + O_2 \rightarrow \cdot SO_5^-$$
$$k = 1.5 \times 10^9 \, M^{-1} \, s^{-1} \tag{6.6}$$
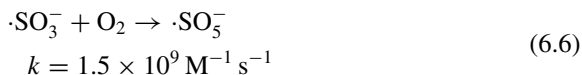
Peroxymonosulfate radical is a powerful oxidant, which can oxidize HSO_3^- to generate $\cdot SO_4^-$ (Reaction 6.7). Dithionate ion was assembled by the dimerization of

Fig. 6.5 CL emission before and after N_2 gas for 30 min. **a** N_2 gas 30 min. **b** Without N_2 gas

$\cdot SO_4^-$ radical (Reaction 6.8).

$$\cdot SO_5^- + HSO_3^- \rightarrow \cdot SO_4^- + HSO_4^-$$
$$k = 1.3 \times 10^7 \, M^{-1} \, s^{-1} \tag{6.7}$$

$$\cdot SO_4^- + \cdot SO_4^- \rightarrow S_2O_8^{2-} \tag{6.8}$$
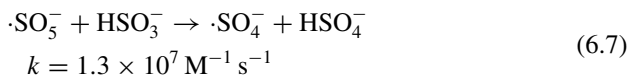
With the occurrence of the Reactions 6.6, 6.7, and 6.8, the concentrations of $\cdot SO_3^-$ radical shortened, resulting in an inhibiting impact on CL emission from $SO_2{}^*$.

In the CL system, $^1O_2$ is likewise a spouting species. The inhibitory action of DABCO, NaN_3, and the ESR spectrum have all confirmed the presence. The reactions that result in the production of $^1O_2$ are as follows (Reactions 6.9–6.11) [58, 59].

$$\cdot SO_3^- + H_2O_2 \rightarrow HSO_3^- + HO_2^{\cdot-} \tag{6.9}$$

$$HO_2^{\cdot-} + OH \rightarrow H_2O + {}^1O_2$$
$$k = 7.1 \times 10^9 \, M^{-1} \, s^{-1} \tag{6.10}$$

$$^1O_2 \rightarrow {}^1O_2 + h\nu \tag{6.11}$$
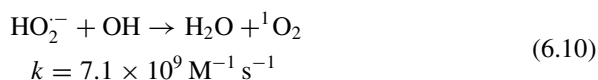
6.2.3   Alcoholic Solvent Enhances the Effect of NaHSO₃−H₂O₂ on the NaHSO₃−H₂O₂ System

$NaHSO_3$–H_2O_2 CL emissions were especially depressed owing to the bottom quantum performance of $^1O_2$ and $SO_2{}^*$. Nonetheless, when *n*-butanol was added, CL strength increased nearly 60 times. Alcohols with diverse carbon atoms were added into CL system and their effects were compared. The consequences were exhibited in Table 6.2.

In terms of CL emission, alcohols with a carbon number of 2–5 have obvious advancement effect on CL emission. The rise of carbon number makes CL strength become higher and higher. In the case of the same number of carbons, alcohols with carbon branches reduce CL strength than alcohols without carbon branches (Table 6.2). To explain this interesting phenomenon, kinetic bulge of the CL system with extension of different alcoholic solvents were identified. The consequences were appearance in Fig. 6.6.

From the kinetic curves (Figs. 6.2 and 6.6), It is conspicuous that the addition of alcohols makes the reaction in CL system faster, which brings as a result to the growth of CL intensity. In an aqueous solution, the alcoholic solvent can form solvent chambers similar to surfactant micelles. Many scholars at home and abroad have reported why surfactant micelles can boost CL intensity. Many publications have hypothesized that the surfactant micelle can boost CL intensity for a range

Table 6.2 Different organic compounds' influences on CL emission

Organic compound	V (%)[a]	Carbon number	CL intensity (mV)[b]
None			3.2
Methanol	20	1	3.3
Ethanol	0.04	2	3.5
n-Propanol	0.04	3	16
iso-Propanol	0.04	3	4.0
n-Butanol	0.08	4	125
iso-Butanol	0.4	4	100
tert-Butanol	20	4	21
Pentanol	0.08	5	80

Copyright 2012 American Chemical Society, reprinted with permission from Ref. [23]
[a] Alcoholic solvent volume was selected at the ratio in which the CL emission was increased most
[b] Average value of three times
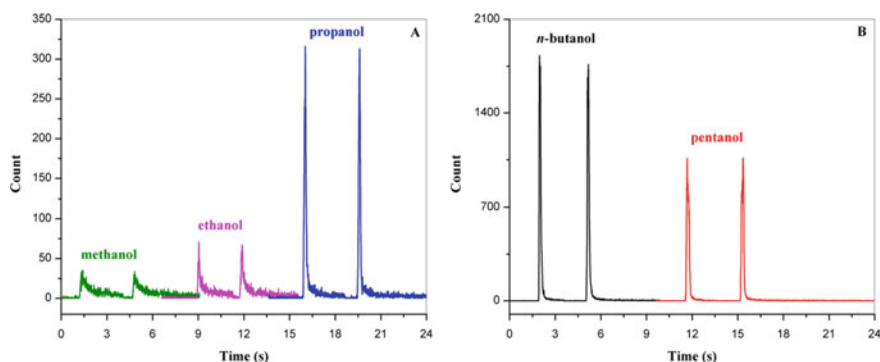
Fig. 6.6 CL kinetics curve with extension of distinct alcoholic solvents (0.06% in water). Reprinted with permission from Ref. [23], Copyright 2012 American Chemical Society

of factors. For the following reasons, first of all, solubilizing surfactant micelles is a predominant component for the improvement influence. Compared with pure water, some organic CL reagents are more easily soluble in surfactant micelles. After that, the surfactant's electrostatic interaction lured counter-ions to the microspheres surface, contributing to increased CL reagent concentrations. The increase in CL reagent concentration is due to the electrostatic effect, which can attract counter-ions to the surface of micelles, resulting in this phenomenon. The surfactant micelles cage guards free radical intermediates and emitting species from water quenching. For an alcoholic solvent, the third reason is no longer feasible. The intermediates, $^1O_2$, and SO_2^* can be maintained by the solvent cage, caused by an increase in CL intensity. The intermediate, $^1O_2$, and SO_2^* can be surrounded by the gradually formed

solvent cage, so the strength of CL increases under the protection of the solvent cage. This plunge can be proven by measuring the strengthening force of *n*-butanol in the pure water solution with 50% methanol/water or 50% ethanol/water mixing solution. In pure water, *n*-butanol improved CL intensity by 60 times, but no augmentation effect was observed when *n*-butanol was dissolved with 50% methanol/water or ethanol/water (Fig. 6.7). This is because *n*-butanol does not form a solvent cage in 50% methanol/water or 50% ethanol/water, while in solution, because of the hydrophobicity of *n*-butanol, a solvent cage is formed in pure water.

6.3 Determination of 1-Hydroxypyrene Particulates in the Air Combined with Tremendous -Performance Liquid Chromatography

7, 10-BaPQ (10 pmol) improves the emission of ultra-low LC for 70 times that originate from the $NaHSO_3$–H_2O_2 system. The intermediates of this system are proved by radical scavengers and ESR spectrum. A forceful CL signal at 440 nm confirms the formation of semiquinone, which is formed by the reaction of $\cdot O_2^-$ radical reacted with 7, 10-BaPQ. A high-sensitivity CL approach has been entrenched on the basis of this operation. 7, 10-BaPQ particulates in the air were determined and confirmed with the results of HPLC-APCI/MS and HPLC–UV.

6.3.1 CL Phenomenon

The intensity of the chemiluminescence relative to the temporal patterns is important for studying the details of the reaction mechanism. Figure 6.8a illustrates the kinetic bend of the $NaHSO_3$–H_2O_2 CL reaction. $NaHSO_3$ reacts rapidly with H_2O_2. When H_2O_2 was introduced into $NaHSO_3$, there was an ultra-weak CL emission that lasted less than 2 s. When H_2O_2 is injected into $NaHSO_3$, ultra-short CL emission occurs (Fig. 6.8a). The CL intensity of $NaHSO_3$–H_2O_2 was expanded 70 times after attachment of 10 pmol 7, 10-BaPQ (Fig. 6.8b). On the other hand, the contour of kinetics bend of $NaHSO_3$–H_2O_2 was not altered by adding 7, 10-BaPQ. No CL emission was detected when 7, 10-BaPQ reacted with only $NaHSO_3$ or H_2O_2. Furthermore, no signal was listed when 7, 10-BaPQ was added into the mixture of $NaHSO_3$-H_2O_2.

Oxidation of sulfite has been investigated by many researchers. Through research, Hoffman came to the conclusion that sulfite oxidation occurs through the rapid nucleophilic replacement of HSO_3^- by H_2O_2 [5, 6]. In this trial, intermediate peroxomonosulfuric acid was accomplished. Radical mechanism has also been reported by Shi, who has detected the $\cdot OH$ radical and $\cdot SO_3^-$ radical generated in the reaction of and $NaHSO_3$ by ESR spin-trapping method [11]. Recently, Xue reported oxidation of HSO_3- with H_2O_2 to give peroxomonosulphurous acid, which broke down to give

Fig. 6.7 Blank was NaHSO$_3$–H$_2$O$_2$ system. *n*-butanol was 0.08% in **a** water, **b** 50% methanol/water mixture **c** 50% ethanol/water. Copyright 2012 American Chemical Society, reprinted with permission from Ref. [23]
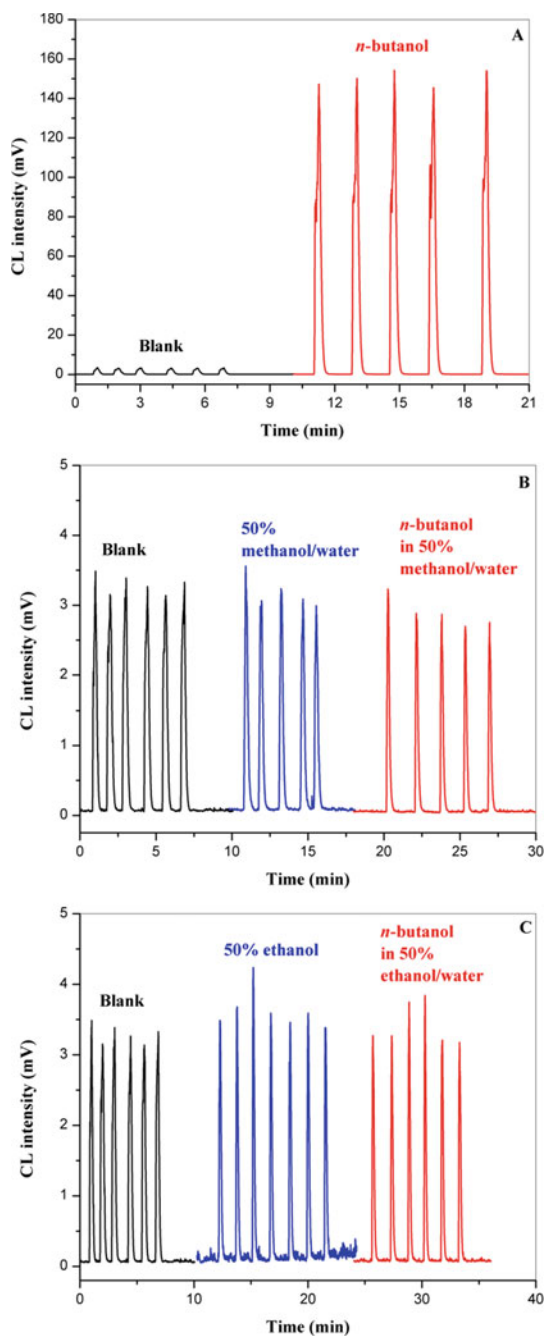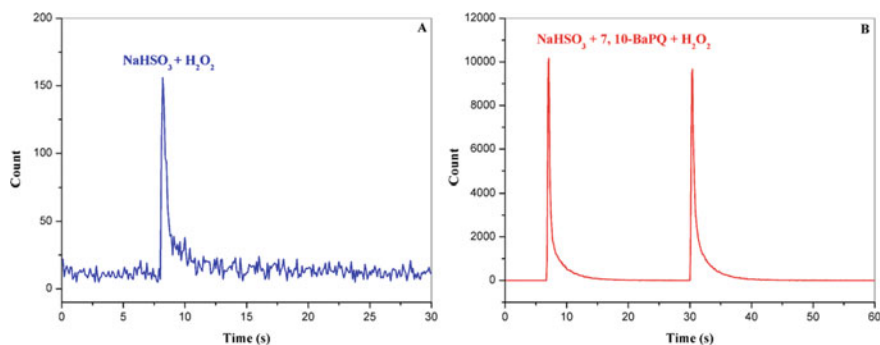
Fig. 6.8 The CL intensity and time distribution of the reaction of **a** NaHSO$_3$–H$_2$O$_2$ and **b** NaHSO$_3$-7, 10-BaPQ-H$_2$O$_2$, NaHSO$_3$, 0.1 mol L^{-1}; H$_2$O$_2$, 0.15 mol L^{-1}; dose volume was 100 µL. Copyright 2012 American Chemical Society, reprinted with permission from Ref. [40]

·OH and ·SO$_3$$^-$. In this research, different radical scavengers were applied to study the mechanism of NaHSO$_3$-7, 10-BaPQ-H$_2$O$_2$ system. The mechanism of NaHSO$_3$-7, 10-BaPQ-H$_2$O$_2$ system was researched by using different free radical scavengers. The outcome was exhibited in Table 6.3.

Ascorbic acid is an effective active oxygen-free radical (·OH, O$_2$$^{·-}$) scavenger [42]. The CL intensity dropped to zero with the extension of ascorbic acid. It was reported that OH radical was produced during the radical reaction between NaHSO$_3$ and H$_2$O$_2$ [58]. Thiourea has been ordinarily used as ·OH radical collectors. The inhibition of chloride ion strength by thiourea confirmed the formation of hydroxyl radicals. Besides, electron spin resonance (ESR) spectra further confirmed the existence of OH radicals.

The inhibition effect of DMPO on ·SO$_3$$^-$ radical confirmed the production of ·SO$_3$$^-$ radical in the reaction system (Reaction 6.12) [60].

$$DMPO + ·SO_3^- \rightarrow DMPO/ · SO_3 \tag{6.12}$$
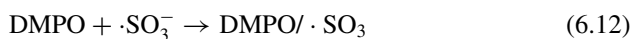
Table 6.3 Radical scavengers' effect on the NaHSO$_3$-7, 10-BaPQ-H$_2$O$_2$ system[a]

Radical scavengers	Concentration (mol L^{-1})	CL intensity[b] of NaHSO$_3$-H$_2$O$_2$-7, 10-BaPQ
Blank	–	10,000
ascorbic acid	0.01	30
thiourea	0.01	800
NBT	0.01	15
DMPO	0.05% (v/v)	6500

Copyright 2012 American Chemical Society, reprinted with permission from Ref. [40]
[a]Concentrations of NaHSO$_3$ and H$_2$O$_2$ were 0.2 and 0.5 mol L^{-1}, injection rate was 100 µL, radical scavengers were 50 µL; 7, 10-BaPQ was 10 pmol
[b]Average value of three times

·SO$_3^-$ radical stacked with excess H$_2$O$_2$ to give HO$_2$·$^-$. NBT is ·O$_2^-$ radical scavenger (Reaction 6.13) [46, 47]. When NBT was added to NaHSO$_3$-7, 10-BAPQ-H$_2$O$_2$, the CL strength depreciated to zero. Consequently, we can conclude ·O$_2^-$ radical was generated in this system, which played a crucial role in CL emission.

$$NBT^{2+} + ·O_2^- \rightarrow ·NBT^+ + O_2 \tag{6.13}$$
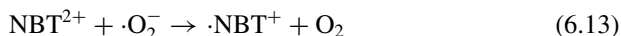
6.3.2 CL Mechanism

Based on the study of intermediates in this system, mechanism of this CL system can be speculated as the following reactions and graphically the technique of the CL system can be inferred by using the following reaction operation and diagram demonstrated in Scheme 6.1.

First of all, HSO$_3^-$ replied with H$_2$O$_2$ by nucleophilic displacement to found an intermediate acid peroxomonosulphous, which shooked-up to generated ·OH and ·SO$_3^-$ radical. ·OH radical as a forceful oxidant counter with HSO$_3^-$ to deliver ·SO$_3^-$ radical at a speedy rate. ·SO$_3^-$ radical was oxidized by H$_2$O$_2$ to deliver ·O$_2^-$ radical, which is an essential radical in the CL system. Besides, a few groups have recorded the oxidation of quinone to semiquinone by ·O$_2^-$ radical (Reaction 6.14) [61–64]. The release of CL was recorded with the disintegration of excited semiquinone [65–67]. After reaction with NaHSO$_3$-H$_2$O$_2$ system, more than 80% of 7, 10-BaPQ goes back to its initial structure. Following the reaction, two weak peaks developed in the chromatogram, in the NaHSO$_3$-H$_2$O$_2$ system, which can be bred by the reaction of semiquinone with other radicals or ions. Several PAH quinones (1, 4-benzoquinone, 1, 4-naphthoquinone, 1, 4-anthraquinone, 1, 4-chrysenequinone), whose structures are the same as 7, 10-BaPQ, which were also appended into the NaHSO$_3$–H$_2$O$_2$ system. The increase in benzene cycling resulted in an increase in CL intensity. On the other hand, the CL intensity of these PAH quinones were yet extremely devalued than 7, 10-BaPQ.
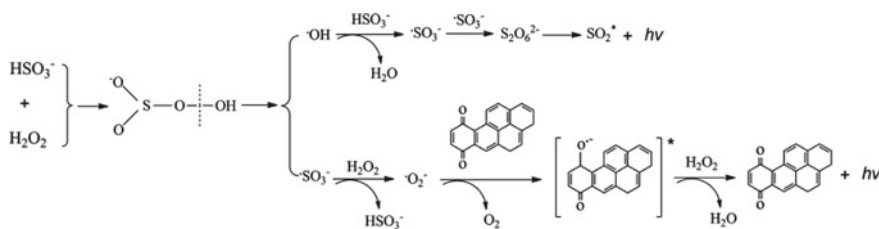
Scheme 6.1 NaHSO$_3$-7, 10-BaPQ-H$_2$O$_2$ CL system mechanism

Fig. 6.9 CL emission spectra of the 10-BaPQ-H_2O_2 CL system with $NaHSO_3$-7. **a** The $NaHSO_3$–H_2O_2 system's emission spectrum. **b** The $NaHSO_3$-7, 10-BaPQ-H_2O_2 system's emission spectrum. Copyright 2012 American Chemical Society, reprinted with permission from Ref. [40]

$$(6.14)$$
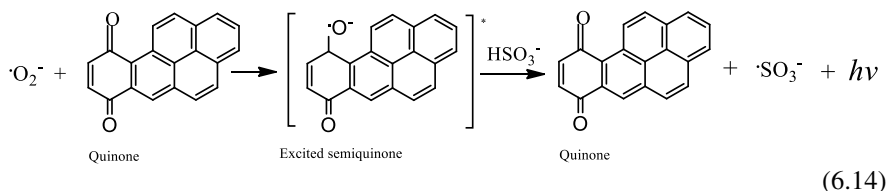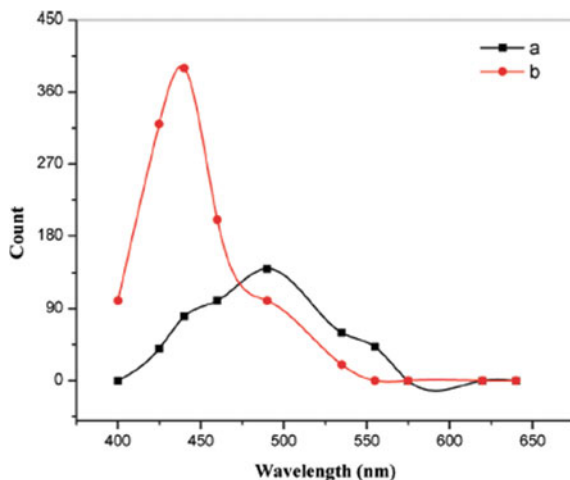
In addition, the $NaHSO_3$–H_2O_2 due to the dynamic one generation of excited sulfur dioxide (SO_2^*). $\cdot SO_3^-$ radical dimerized to deliver $S_2O_6^{2-}$ ion. SO_2^* was formed by the dissipation of $S_2O_6^{2-}$ ion [14, 68].

The spectrum of CL emissions has played a crucial role in the identification of emitter species in the CL system. Therefore, CL emission spectra of $NaHSO_3$–H_2O_2 were measured by a cut-off filter (400–640 nm). A single climax with a maximum of around 440 nm arose in the spectrum of $NaHSO_3$-7, 10-BaPQ-H_2O_2 system (Fig. 6.9) that may belong to the passionate semiquinone.

6.3.3 10-BaPQ in Airborne Particulates Determination

The CL system has been developed as an ultra-sensible post-column detection system for the judgment of 7,10-BaPQ in airborne particles. The $NaHSO_3$−7, 10-BaPQ-H_2O_2 CL systems are enormously affected by organic dissolution. Then various comparisons were made between methanol and acetonitrile. It was discovered that a basic separation of 7,10-BaPQ of the intervention compounds and the highest height is achieved when 80% (v/v) methanol/water is used. Figure 6.10a illustrates a

Fig. 6.10 a In
HPLC-NaHSO$_3$–H$_2$O$_2$
system, typical
chromatogram of standard
7,10-BaPQ (1.5 pmol per
injection). **b** HPLC-CL
(7,10-BaPQ, 1.0 ×
10^{-8} mol L^{-1}) and
HPLC–UV (7,10-BaPQ, 1.0
× 10^{-6} mol L^{-1})
chromatograms of
7,10-BaPQ. **c** 7,10-BaPQ
chromatograms in HPLC-CL
and LC–MS/MS
(7,10-BaPQ, 1.0 ×
10^{-7} mol L^{-1}). Reprinted
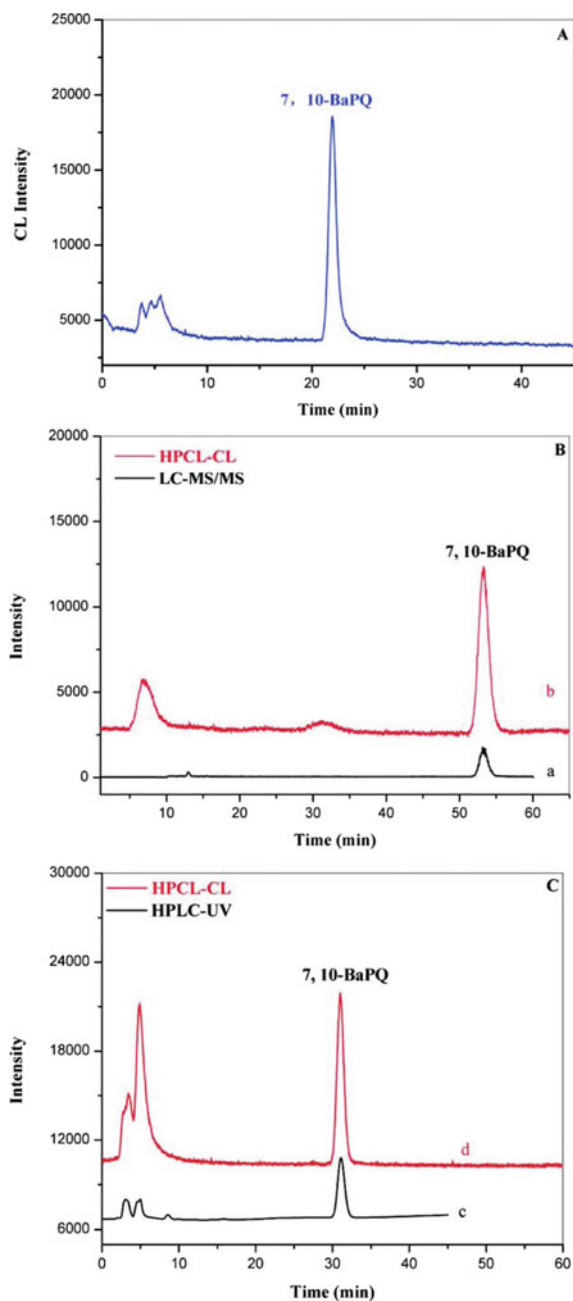with permission from [40],
copyright 2012 American
Chemical Society

Table 6.4 Precision of the method for determining 7, 10-BaPQ in airborne particulates and 7, 10-BaPQ recovery in airborne particulates

Intra-day ($n = 3$)			Inter-day ($n = 3$)		
Added (pmol)	0	15.0	50.0	0	15.0	50.0
Found (pmol)	3.90	19.3	53.7	3.90	18.5	54.1
Recovery (%)[a]	–	102.7	99.6	–	97.3	100.4
RSD (%)	7.80	4.80	4.80	5.70	1.60	1.00

Copyright 2012 American Chemical Society, reprinted with permission from Ref. [40]
[a]Expressed as (found amount—non-spiked amount)/added amount

typical chromatogram of standard 7,10-BaPQ in optimum circumstances. The consequence displays that under optimal conditions, Fig. 6.10a demonstration the typical chromatogram of standard 7,10-BAPQ.

The prospective approach was assessed from a diameter, sensitivity, and rigor perspective. Calibration curves were acknowledged by ensuring a dose between 50 fmol and 20 pmol per injection with a standard 7, 10-bapq solution. A highly linear relation between maximum crest and concentrations was earned (12 calibration points; $R_2 = 0.9995$). The slope and intercept of the calibration curve;s regression equation were 1.22×10^{12} and -463, respectively. The detection limit of 7,10-BaPQ was 30 fmol per injection (S/N = 3) [69]. What is more, the suggested HPLC-CL method for differentiating 7,10-BaPQ was 2 orders of magnitude superior to the LC–MS-MS method and 3 orders of magnitude superior to the HPLC–UV method. (Fig. 6.10b, c). The precision and precision of the recommended approach for the determination of 7,10-BaPQ was researched by rising airborne particles to two different levels of 7,10 BaPQ standard solutions. The outcome are demonstrated in Table 6.4.

BaP is a major pollutant that is ubiquitous in the atmosphere, the sea, rivers, and the ground. In environment, BaP was decomposed by solar irradiation, bacteria, and chemical reactions, which led to the generation of various BaP derivatives, such as nitro BaP, hydroxyl BaP, and BaP quinones. Three major quinone BaP isomers, 1, 6-, 3, 6-, and 6, 12-BaPQ, were determined in airborne particles. However, 7, 10-BaPQ has never been reported in airborne particulates because of the lower concentration and lack of sensitive methods. Determination of particulate 7,10- bapq in air. Benzene[a]pyrene (BaP), one of the largest PAHs pollutants in the surroundings is highly carcinogenic and mutagenic. BaP quinones were formed when BaP reacted with some reactive oxygen species in airborne particles. The toxicity of these BaPQs is more advanced than BaP. Consequently, it is urgent to control the concentration of these QAPs. On the other hand, universal approach, LC–MS/MS, GC–MS/MS, HPLC–UV, and HPLC-fluorescence, which are difficult to identify the BaPQs due to their sensitivity, are not large enough for practical use, particularly for 7,10-BaPQ.
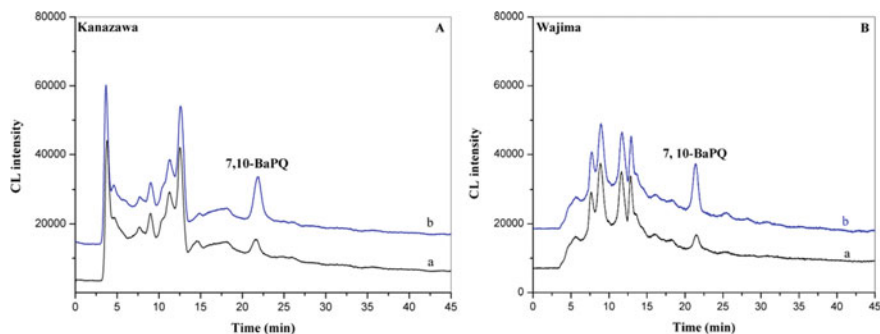
Fig. 6.11 7, 10-BaPQ chromatograms in airborne particles (**a**) and airborne particulates spiked with 1.5 pmol 7, 10-BaPQ (**b**). Copyright 2012 American Chemical Society, reprinted with permission from Ref. [40]

The recommended HPLC-CL approach was used for the successful steadfastness of 7,10-BaPQ in airborne particles.

In Kanazawa, Japan in December 2010 and Wajima, Japan in October 2007, average concentrations of 7,10-BaPQ were 2.0 and 1.6 pg m^{-3}, respectively. In Fig. 6.11a, b, chromatograms of airborne particles may be seen.

6.4 Conclusions

An ultra-feeble chemiluminescence emission was observed when $NaHSO_3$ reacting with H_2O_2. $NaHSO_3$ was discovered to still be oxidized with H_2O_2 through the use of peroxomonosulfuric acid, which then decomposed to construct radicals $\cdot OH$ and $\cdot SO_3^-$. Aside from SO_2^*, $^1O_2$ was also spewing species. The alcoholic solvent has the opportunity to significantly boost CL emission from the $NaHSO_3$-H_2O_2 reaction (especially *n*-butanol). When *n*-butanol was arranged in 50% methanol or 50% ethanol, the heightening effect was dead and gone. Ultra-weak chemiluminescence can also be greatly improved by benzo[a]pyrene-7, 10-quinone (7, 10-BaPQ). The enhancing effect was ascribed to the oxidation of 7, 10-BaPQ by superoxide radicals generated in $NaHSO_3$-H_2O_2 system. Based on this mechanism, an ultra-sensitive approach for determination of 7, 10-BaPQ was developed for the first time. In the H_2O_2–$NaHSO_3$ aqueous system, we also distinguished the mechanism for elevating carbon points LC. In the reaction period of HSO_3^- and H_2O_2, $\cdot OH$, $SO_4^{\cdot-}$, $\cdot SO_3^-$ and $\cdot O_2^-$ were manufactured.

References

1. Fridovich I, Handler P (1960) Detection of free radicals in illuminated dye solutions by the initiation of sulfite oxidation. J Biol Chem 235:1835–1838
2. Backstrom HLJ (1927) The chain-reaction of negative catalysis. J Am Chem Soc 49:1460–1472
3. Alyea HN, Backstrom HLJ (1929) The inhibition action of alcohols on the oxidation of sodium sulfite. J Am Chem Soc 51:90–109
4. Fuller EC, Crist RHJ (1941) The rate of oxidation of sulfite ions by oxygen. J Am Chem Soc 63:1644–1650
5. Hoffmann MR, Edwards JO (1975) Kinetics of the oxidation of sulfite by hydrogen peroxide in acidic solution. J Phys Chem 79:2096–2098
6. Macardle JV, Hoffmann MR (1983) Kinetics and Mechanism of the oxidation of aquated sulfur dioxide by hydrogen peroxide at Low pH. J Phys Chem 87:5425–5429
7. Halperin J, Taube H (1952) The Transfer of oxygen atoms in oxidation-reduction reactions. III.The reaction of halogenates with sulfite in aqueous solution. J Am Chem Soc 74:375–380
8. Halperin J, Taube H (1952) The transfer of oxygen atoms in oxidation-reduction reactions. IV. The reaction of hydrogen peroxide with sulfite and thiosulfate, and of oxygen, manganese dioxide and of permanganate with sulfite. J Am Chem Soc 74:380–382
9. Ranguelova K, Mason RP (2009) New insights into the detection of sulfur trioxide anion radical by spin trapping: radical trapping versus nucleophilic addition. Free Radical Biol Med 47:128–134
10. Ozawa T, Hanaki A (1987) Spin-trapping of sulfite radical anion SO_3^-, by a water soluble nitrosol-aromatic spin-trap. Biochem Biophys Res Commun 142:410–416
11. Shi X (1994) Generation of SO_3^-, and OH radicals in SO_3^- reactions with inorganic environmental pollutants and its implications to SO_3^{2-} toxicity. J Inorg Biochem 56:155–165
12. Stauff J, Jaeschke W (1975) A chemiluminescence technique for measuring atmospheric trace concentrations of sulfur dioxide. Atmos Environ 9:1038–1039
13. Kerezsi I, Lente G, Fabian I (2005) Highly efficient photoinitiation in the Cerium(III)-catalyzed aqueous autoxidation of Sulfur(IV). An example of comprehensive evaluation of photoinduced chain reacions. J Am Chem Soc 127:4785–4793
14. Katom M, Yamada M, Suzuki S (1984) Flavin mononucleotide sensitized and polyoxyethylene (20) sorbitan triolate micelle-enhanced gas/solution chemiluminescence for direct continuous monitoring of sulfur dioxide in the atmosphere. Anal Chem 56:2529–2534
15. Li B, Deng Q, Lv J, Zhang Z (2006) Homogeneous chemiluminescence system in neutral and near neutral aqueous solution with ClO_2 as oxidant and its analytical application. Anal Chim Acta 560:128–133
16. Huang Y, Zhang C, Zhang X, Zhang Z (1999) Chemiluminescence of sulfite based on auto-oxidation sensitized by rhodamine 6G. Anal Chim Acta 391:95–100
17. Sun C, Liu B, Li J (2008) Sensitized chemiluminescence of CdTe quantum-dos on Ce(IV)-sulfite and its analytical applications. Talanta 75:447–454
18. Li Y, Lu J (2007) Direct chemiluminescence determination of ibuprofen by the enhancement of the $KMnO_4$-sulphite reaction. Luminescence 22:326–330
19. Lin J-M, Yamada M (2003) Microheterogeneous systems of micelles and microemulsions as reaction media in chemiluminescent analysis. Trends Anal Chem 22:99–107
20. Hinze WL, Riehl TE, Singh HN, Baba Y (1984) Micelle-enhanced chemiluminescence and application to the determination of biological reductants using lucigenin. Anal Chem 56:2180–2191
21. Lu C, Qu F, Lin J-M, Yamada M (2002) Flow-injection chemiluminescent determination of nitrite in water based on the formation of peroxynitrite from the reaction of nitrite and hydrogen peroxide. Anal Chim Acta 424:107–114
22. Liang SX, Li H, Lin J-M (2008) Reaction mechanism of surfactant-sensitized chemiluminescence of bis(2,4,6-trichlorophyenyl) oxalate and hydrogen peroxide induced by gold nanoparticles. Luminescence 23:381–385

23. Li R, Chen H, Li Y, Lu C, Lin J-M (2012) Enhancing effect of alcoholic solvent on hydrosulfite-hydrogen peroxide chemiluminescence system. J Phys Chem A 116(9):2192–2197

24. Yang Y, Vanmetre PC, Mahler BJ, Wilson JT, Ligouis B, Muhitrazzaque M, Schaeffer DJ, Werth CJJ (2010) Influence of coal-tar sealcoat and other carbonaceous materials on polycyclic aromatic hydrocarbon loading in an urban watershed. Environ Sci Technol 44:1217–1223

25. Castro D, Slezakova K, Delerue-Matos C, Alvim-Ferraz M, Morais S, Pereira M (2011) Polycyclic aromatic hydrocarbons in gas and particulate phases of indoor environments influenced by tobacco smoke: Levels, phase distributions, and health risks. Atmos Environ 45:1799–1808

26. Marr LC, Grogan LA, WÖhrnschimmel HY, Molina LT, Molina MJ (2004) Vehicle traffic as a source of particulate polycyclic aromatic hydrocarbon exposure in the Mexico city metropolitan area. Environ Sci Technol 38:2584–2592

27. Wang J, Levendis YA, Richter H, Howard JB, Carlson J (2001) Polycyclic aromatic hydrocarbon and particulate emissions from two-stage combustion of polystyrene: the effect of the primary furnace temperature. Environ Sci Technol 35:3541–3552

28. Kishikawa N, Morita S, Wada M, Ohba Y, Nakashima K, Kuroda N (2004) Determination of hydroxylated polycyclic aromatic hydrocarbons in airborne particulates by high performance liquid chromatography with fluorescence detection. Anal Sci 20:129–132

29. Kameda T, Akiyama A, Toriba A, Tang N, Hayakawa K (2011) Atmospheric formation of hydroxynitropyrenes from a photochemical reaction of particle-associated 1-nitropyrene. Environ Sci Technol 45:3325–3332

30. Kojima Y, Inazu K, Hisamatsu Y, Okochi H, Baba T (2010) Influence of secondary formation on atmospheric occurrences of oxygenated polycyclic aromatic hydrocarbons in airborne particles. Atmos Environ 44:2873–2880

31. Walgraeve C, Demeestere K, Dewulf J, Zimmermann R, Langenhove HV (2010) Oxygenated polycyclic aromatic hydrocarbons in atmospheric particulate matter: Molecular characterization and occurrence. Atmos Environ 44:1831–1846

32. Zhao Y, Xia Q, Yin JJ, Yu H, Fu P (2011) Photoirradiation of polycyclic aromatic hydrocarbon diones by UVA light leading to lipid peroxidation. Chemosphere 85:83–91

33. Motoyama Y, Bekki K, Chung S, Tang N, Kameda T, Toriba A, Taguchi K, Hayakawa K (2009) Oxidative stress more strongly induced by ortho- than para quinoid polycyclic aromatic hydrocarbons in A549 cells. J Health Sci 55:845–850

34. Bolton JL, Thacher GRJ (2008) Potential mechanisms of estrogen quinone carcinogenesis. Chem Res Toxicol 21:93–101

35. Ma B, Carr BA, Krolikowski P, Chang F (2007) Cytotoxicity of a quinone-containing cockroach sex pheromone in human lung adenocarcinoma cells. Chem Res Toxicol 20:72–78

36. Terashima I, Suzuki N, Shibutani S (2001) Mutagenic properties of estrogen quinone-derived DNA adducts in simian kidney cells. Biochemistry 40:166–172

37. Kumagai Y, Nakajima H, Midorikawa K, Homma-Takeda S, Shimojo N (1998) Inhibition of nitric oxide formation by neuronal nitric oxide synthase by quinones: nitric oxide synthase as a quinone reductase. Chem Res Toxicol 11:608–613

38. Taguchi K, Kumagai Y, Endo A, Kikushima M, Ishii Y, Shimojo N (2001) Ohenanthraquinone affects endothelial nitric oxide synthase activity though modification of the thiol group: an alterlnative inhibition mechanism. J Health Sci 47:571–574

39. Ahmed S, Kishikawa N, Ohyama K, Maki T, Kurosaki H, Nakashima K, Kuroda N (2009) An ultrasensitive and highly selective determination method for quinones by high-performance liquid chromatography with photochemically initiated luminol chemiluminescence. J Chromatogr A 1216:3977–3984

40. Li R, Kameda T, Toriba A, Hayakawa K, Lin J-M (2012) Determination of benzo[a]pyrene-7,10-quinone in airborne particulates by using a chemiluminescence reaction of hydrogen peroxide and hydrosulfite. Anal Chem 84:3215–3221

41. Chen H, Lin L, Lin Z, Guo G, Lin J-M (2010) Chemiluminescence arising from the decomposition of peroxymonocarbonate and enhanced by CdTe quantum dots. J Phys Chem A 114:10049–10058

42. Liang S, Zhao LX, Zhang BT, Lin J-M (2008) Experimental Studies on the chemilumines-cence reaction mechanism of carbonate/bicarbonate and hydrogen peroxide in the presence of cobalt(II). J Phys Chem A 112:618–623

43. Shi X, Dalal N, Kasprzak KS (1994) Enhanced generation of hydroxyl radical and sulfur trioxide anion radical from oxidation of sodium sulfite, nickel(ll) sulfite, and nickel subsulfide in the presence of nickel (II) complex. Environ Health Persp 102:91–96

44. Khan N, Wilmot CM, Rosen GM, Demidenko E, Sun J, Joseph J, Ohara J, Kalyanaraman B, Swartz HM (2003) Spin traps: in vitro toxicity and stablity of radical adducts. Free Radical Biol Med 34:1473–1481

45. Tsai CH, Stern A, Chiou JF, Chen CL, Liu TA (2001) Rapid and specific detection of hydroxyl radical using an ultraweak chemiluminescence analyzer and a low-level chemilu-minescence emitter: application to hydroxyl radical-scavenging ability of aqueous extracts of food constituents. J Agri Food Chem 49:2137–2141

46. Lin J-M, Yamada M (1999) Oxidation reaction between periodate and polyhydroxyl compounds and its cpplication to chemiluminescence. Anal Chem 71:1760–1766

47. Bleiskl BHJ, Shiue GG, Bajuk S (1980) Reduction of nitro blue tetrazolium by CO_2^- and O_2^- Radicals. J Phys Chem 84:830–833

48. Naito K, Tachikawa T, Cui SC, Sugimoto A, Fujitsuka M, Majima J (2006) Single-molecule detection of airborne singlet oxygen. J Am Chem Soc 128:16430–16431

49. Massari J, Takikawa R, Medias DB, Angeli JPF, Mascio PD, Assuncao NA, Bechara EJH (2011) Generation of singlet oxygen by the glyoxal-peroxynitrite system. J Am Chem Soc 51:20761–20768

50. Chen H, Lin L, Lin Z, Lu C, Guo G, Lin J-M (2011) Flow-injection analysis of hydrogen peroxide based on carbon nanospheres catalyzed hydrogen carbonate-hydrogen peroxide chemiluminescent reaction. Analyst 136:1957–1964

51. Chen H, Li R, Lin L, Guo G, Lin J-M (2010) Determination of L-ascorbic acid in human serum by chemiluminescence based on hydrogen peroxide–sodium hydrogen carbonate-CdSe/CdS quantum dots system. Talanta 81:1688–1696

52. Li H, Wu LZ, Tung CH (2000) Reactions of singlet oxygen with olefins and sterically hindered amine in mixed surfactant vesicles. J Am Chem Soc 122:2446–2451

53. Adam W, Kazakov DV, Kazakov VP (2005) Singlet-oxygen chemiluminescence in peroxide reactions. Chem Rev 105:3371–3387

54. Neta P, Huie RE, Ross AB (1988) Rate constants for reactions of inorganic radicals in aqueous solution. J Phys Chem Ref Data 17:1028–1284

55. Robert E, Neta P (1987) Rate constants for some oxidations of S(IV) by radicals in aqueous solutions. Atmos Environ 21:1743–1747

56. Brandt C, Eldik R (1995) Transition metal-catalyzed oxidation of sulfur(lV) oxides atmospheric-relevant processes and mechanisms. Chem Rev 119–190

57. Das TN (2001) Reactivity and role of SO_5^- radical in aqueous medium chain oxidation of sulfite to sulfate and atmospheric sulfuric acid generation. J Phys Chem A 105:9142–9155

58. Xue W, Lin Z, Chen H, Lu C, Lin J-M (2011) Enhancement of ultraweak chemiluminescence from reaction of hydrogen peroxide and bisulfite by water-soluble carbon nanodots. J Phys Chem C 115:21707–21714

59. Villamena FA, Hadad CM, Zweier JL (2003) Kinetic study and theoretical analysis of hydroxyl radical trapping and spin adduct decay of alkoxycarbonyl and dialkoxyphosphoryl nitrones in aqueous media. J Phys Chem A 107:4407–4414

60. Mottey C, Mason R (1988) Sulfate anion free radical formation by the peroxidation of (Bi)sulfite and its reaction with hydroxyl radical scavengers. Arch Biochem Biophys 267:681–689

61. Bielski BHJ, Cabelii DE, Arudi RE (1985) Reactivity of HO_2^-/O_2^- radicals in aqueous solution. J Phys Chem Ref Data 14:1041–1100

62. Garg S, Rose AL, Waite T (2007) Production of reactive oxygen species on ohotolysis of dilute aqueous quinone solutions. Photochem Photobio 83:904–913

63. Samoilova RI, Crofts AR, Dikanov SA (2011) Reaction of superoxide radical with quinone molecules. J Phys Chem A 115:11589–11593

64. Kawashima T, Ohkubo K, Fukuzmi S (2011) Stepwise vs. concerted pathways in scandium ion-coupled electron transfer from superoxide ion to p-benzoquinone derivatives. Phys Chem Chem Phys 13:3344–3352
65. Stauff J, Bartolmes P (1970) Chemiluminescence on oxidative formation of triplet states of anthrasemiquinone and anthraquinone-2-sulfonate. Angew Chem Internat Edit 9:307–308
66. Slawinska D (1978) Chemiluminescence and the formation of singlet oxygen in the oxidation of certain polyphenols and quinones. Photochem Photobio 28:453–458
67. Chen X, Zhao L, Wang X, Lin J-M (2007) Sensitive monitoring of humic acid in various aquatic environments with acidic cerium chemiluminescence detection. Anal Sci 23:1189–1193
68. Yu X, Bao J (2009) Determination of norfloxacin using gold nanoparticles catalyzed cerium(IV)-sodium sulfite chemiluminescence. J Lumin 129:973–978
69. Koebera R, Niessner R, Bayona JM (1997) Comparison of liquid chromatography-mass spectrometry interfaces for the analysis of polar metabolites of benzo[a]pyrene. Fresenius J Anal Chem 359:267–273

Chapter 7
Ultra Weak Chemiluminescence from Fenton's Reaction

Hui Chen and Jin-Ming Lin

Abstract Chemiluminescence (CL) was employed to investigate the *ortho*-chlorophenol being degraded by Fenton's reagent. Absent specific CL reagents, a slight CL emission could be emitted out the blend of ferrous ion and hydrogen peroxide under ambient temperature. Adding *ortho*-chlorophenol to the mixture led to an increase in CL intensity. Temperature also strongly increased the CL intensity, as the temperature reached 65 °C. CL spectroscopy, gas chromatography-mass spectrometry, and electron spin resonance spectroscopy were adopted to research the CL mechanism of the system composed of H_2O_2–Fe^{2+} and *ortho*-chlorophenol or *ortho*-chlorophenol free. In addition, how the CL intensity was affected by a variety of radical scavengers, surfactants, and fluorescent compounds was also assessed. Moreover, a mechanism is put forward for autonomous catalytic oxidation. From the findings, it was indicated that singlet oxygen was the major emission body in H_2O_2–Fe^{2+} system. The H_2O_2–Fe^{2+}-*ortho*-chlorophenol regime generated strong CL because of the singlet oxygen and electronically excited quinones. Formation of benzenediol-like intermediates in the process of phenol oxidation strongly facilitated the Fenton reaction and caused enhanced CL intensity, which was the new method to study the oxidation mechanism of certain organic pollutants by Fenton reagents.

Keywords Chemiluminescence · Fenton reagent · Hydrogen peroxide · Organic pollutant · Chlorophenol

H. Chen
College of Materials Science and Technology, Beijing Forestry University, Beijing 100083, China
e-mail: chenhui@bjfu.edu.cn

J.-M. Lin (✉)
Department of Chemistry, Tsinghua University, Beijing 100084, China
e-mail: jmlin@mail.tsinghua.edu.cn

7.1 Introduction

Phenolic compounds were commonly found in waste incineration, uncontrolled use of agrochemicals and pre-emergent herbicides, and in wastewater from some food processors. The U.S. EPA classifies certain phenolic compounds in 65 priority pollutants because they are not easily degradable and harmful to human beings [1]. Therefore, removing these phenolics or converting them to biodegradable substances is quite necessary.

There are three techniques to degrade phenolics provided by chemical, biological, and thermal treatments [2]. However, the biological treatment is susceptible to the conditions and is not suitable for the degradation of high concentrations of phenols [3]. Biological treatment of synthetic wastewater containing *para*-chlorophenol uses a rotating brush biofilm reactor. Some harmful compounds are released during the heat treatment process [4]. Fortunately, there is an excellent alternative to an innovative technique called Advanced Oxidation Processes (AOPs) for the removal of organic contaminants because of the strength of their oxidant powder. Fenton reagent, an important paramount technology in AOPs, had developed for more than a century since first reported in 1894 [5]. A set of reactions concerning hydrogen peroxide and ferrous iron is included. Fenton-like systems (Cu^{2+}/H_2O_2) and photo-Fenton are also highly efficient in degrading organic pollution [6, 7]. Nowadays, a novel type of AOP has been named as electro-Fenton, which generates H_2O_2 by electrode reduction of O_2, which combines with ferrous ions to become Fenton reagent [8]. In the Fenton reaction, H_2O_2 is decomposed by Fe^{2+} to a hydroxyl radical, which is of high reactivity (E^θ 2.8 v) and could oxidize a variety of organic compounds. In recent decades, its possible utilization in detoxifying wastewater, destructing organic pollutants, and improving biodegradability of wastewater has received increasing attention [9].

The reason why concerning *ortho*-chlorophenol was its high toxicity and the need to remove it out of the environment. Decomposition of *ortho*-chlorophenol by Fenton reagent has been extensively published [10, 11]. Huang et al. [12] studied the catalytic decomposition of H_2O_2 and *ortho*-chlorophenol with various iron oxides, with the aim of studying how hydrogen peroxide reacted with organic compounds. A procure that 2, 4-dichlorophenol degraded by Nafion-Fe with H_2O_2 was discussed by Sabhi et al. [13]. The parameters which affected reaction, for example, pH value, temperature, the ratio of the oxidant to the substrate, were introduced in several reports [14, 15]. Whereas, the mechanism of phenol degradation is too complicated to be further understood at present.

Chemiluminescence (CL), involving energy and electron transfer, provides practical messages about transient intermediates. In the current study [16], CL was used to investigate the mechanisms involved in the degradation of *ortho*-chlorophenol. The CL mechanisms of H_2O_2–Fe^{2+} system and H_2O_2–Fe^{2+}-*ortho*-chlorophenol system were investigated based on bulk experiment, flow injection (FI), the CL spectra, gas chromatography-mass spectrometry (GC–MS), and electron spin resonance spectrum (ESR). In addition, the influence from several radical scavengers, surfactants,

and fluorescent compounds on CL intensity was analyzed, revealing the mechanisms of the CL phenomenon, which was significant for understanding Fenton's process.

7.2 Apparatus and Procedure

In-batch CL trials were performed on a BPCL luminescence analyzer (Institute of Biophysics, Chinese Academy of Sciences, China) equipped with a PC 2000 computer. The mobile injection CL analyzer system employed is diagrammed in Fig. 7.1. It was comprised of two peristaltic pumps (SJ-1211, Atto, Japan), a 0.15-mL loop injector, a CL cell, and an ultra weak luminescence analyzer (Model LF-800, Microtec Niti-On, Japan). The solutions were all delivered by peristaltic pumps and blended in CL cell near the photomultiplier tube. Signals were logged by an IBM-compatible computer with a data-capture port.

The FL-7000 spectrophotometer (Hitachi, Japan) was employed to perform CL emission spectroscopy. The ESR spectral features measured for the spin adducts of the radicals were obtained on a Bruke EPR ELEXSY 500 spectrometer with a microwave power of 12.72 mW and modulation amplitude of 2.00 G.

A Shimadzu GCMS-QP2010 (Shimadzu, Japan) system equipped with a 30 m long, 0.25 mm I.D., 0.1 μm film thickness DB-5MS capillary column was used for detecting breakdown products. The carrier gas was helium which had a flow rate of 1.5 ml min^{-1}. 1 μl of solution was charged in the split/unsplit inlet at 220 °C during the unsplit mode, i.e., no split in one min and an overall flow rate of 12.0 mL/min. The interface temperature of GC–MS was set to 230 °C. The temperature of the oven was programmed to ramp up from 50 °C, first holding 50 °C for two min, increasing to 200 °C at 10 °C min^{-1}, then to 300 °C at 40 °C/min, and maintaining 300 °C for two minutes. Data acquisition and analysis were based on full scan mode.
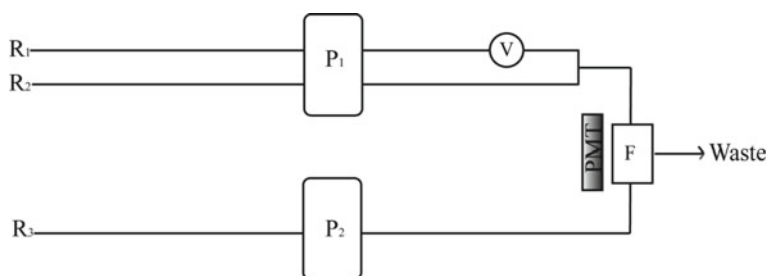
Fig. 7.1 Schematic diagram of the mobile injection CL system. P_1 and P_2 peristaltic pumps; *V* six-way valve injector; *F* flow cell; R_1, R_2, and R_3 solution delivering lines. Copyright 2012, with permission from Elsevier Ref. [16]

7.3   Chemiluminescent Kinetic Study

Some details about the mechanism resulted from the batch study. As Fig. 7.2A(a) showed, low-intensity CL emission was seen in the blend of ferrous and H_2O_2 solution. By contrast, a high CL emission intensity of 2.6×10^3 occurred with the addition of H_2O_2 to a solution of ferrous iron and *ortho*-chlorophenol, indicating a critical correlation between o-chlorophenol and CL reactions [Fig. 7.2A(b)].

Besides, how various blending sequences on reagent solutions affected CL kinetics was also explored in order to better understand the CL properties. CL with an intensity of 1.6×10^3 was recorded when the ferrous solution was combined with H_2O_2

Fig. 7.2 CL signals with a batch system and mobile injection. **A** batch CL signals with H_2O_2 injected into ferrous solution (**a**) and the blend of ferrous solution and *ortho*-chlorophenol (**b**). **B** The kinetic spectra when *ortho*-chlorophenol was injected into the mixture of ferrous solution and H_2O_2. *ortho*-chlorophenol, 1.0×10^{-3} mol L^{-1}; Fe^{2+}, 1.0×10^{-2} mol L^{-1}; H_2O_2, 1.0 mol L^{-1}. **C** The CL of the mobile injection system. (a) H_2O_2 was injected into a ferrous solution by a 6-valve nozzle. (b) The ferrous solution was introduced via a six-valve injector into H_2O_2. (c) *Ortho*-chlorophenol was injected through a six-valve injector to blend with ferrous solution and H_2O_2. Copyright 2012, with permission from Elsevier Ref. [16]
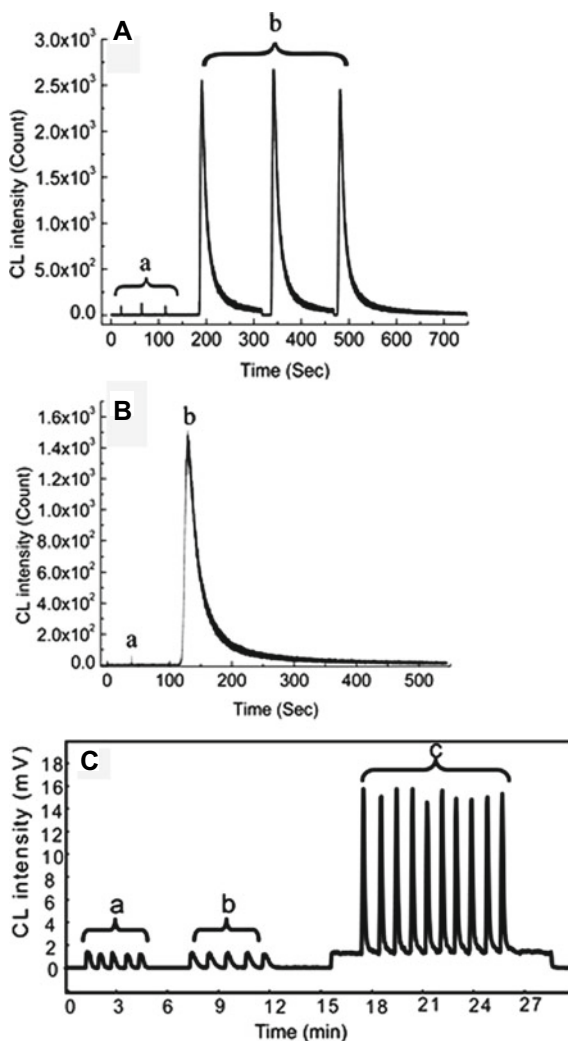
in advance and then *ortho*-chlorophenol was added afterward [Fig. 7.2B(b)], being greater than the Fe^{2+}–H_2O_2 system emission without *ortho*-chlorophenol [Illustration of Fig. 7.2B(a)]. Nevertheless, the CL intensity in such a situation was significantly smaller than when introducing H_2O_2 to the blend of *ortho*-chlorophenol and ferrous solution [Fig. 7.2A(b)]. It could be explained by the consumption of H_2O_2 by the ferrous solution when the solutions were premixed.

It is possible that this chemiluminescence phenomena originate from the formation of singlet oxygen ($^1O_2$) and electronically excited quinone. The proposed mechanism was as shown below. At the initial step, hydroxyl radicals were generated from H_2O_2–Fe^{2+} (Reaction 7.1) [17]. $HO_2\cdot$ was then formed by the reaction of the generated hydroxyl radical with Fe^{3+} (Reaction 7.2) [17].

$$Fe^{2+} + H_2O_2 \rightarrow Fe^{3+} + OH\cdot + OH^- \tag{7.1}$$

$$Fe^{3+} + H_2O_2 \rightarrow Fe^{2+} + HO_2\cdot + H^+ \tag{7.2}$$

$$Fe^{2+} + OH\cdot \rightarrow Fe^{3+} + OH^- \tag{7.3}$$
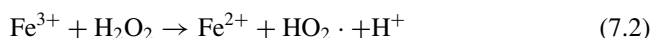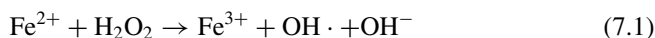
$HO_2\cdot$ decomposed to $\cdot O_2^-$ (Reaction 7.4) [18]. $\cdot O_2^-$ generated singly linear oxygen by reacting with hydroxyl radicals or $HO_2\cdot$, which was one of the CL emitters during the CL reactions (Reactions 7.5 and 7.6) [19, 20]. The combination of $HO_2\cdot$ also generated singlet oxygen (Reaction 7.7). When H_2O_2 was mixed with a solution of ferrous ions prior to the injection of *ortho*-chlorophenol, the Fenton reaction happened. Therefore, the available radicals of the organic compound could be inferred. Under such circumstances, the CL intensity was not so strong as in the case of the injection of H_2O_2 into the blend of *ortho*-chlorophenol and ferrous solution.

$$HO_2\cdot \rightarrow \cdot O_2^- + H^+ \tag{7.4}$$

$$\cdot O_2^- + OH\cdot \rightarrow {}^1O_2 + OH^- \tag{7.5}$$

$$\cdot O_2^- + HO_2\cdot \rightarrow {}^1O_2 + HO_2^- \tag{7.6}$$

$$HO_2\cdot + HO_2\cdot \rightarrow {}^1O_2 + H_2O_2 \tag{7.7}$$
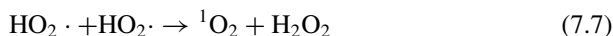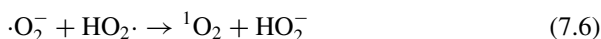
In terms of the crucial function of the *ortho*-chlorophenol to CL was due to its reducing power and the exited intermediates. Hydroquinone was formed by the attack of the formed hydroxyl radical on *ortho*-chlorophenol (Reaction 7.8). Hydroquinone could rapidly decrease ferric ions to ferrous ions and hasten the Fenton's reaction (Reaction 7.9) [21]. Electronically excited quinones with CL emission were formed by the reaction between semi-quinone and hydroxyl radicals (Reaction 7.10) [22, 23].

$$\text{(7.8)}$$

$$\text{(7.9)}$$

$$\text{(7.10)}$$
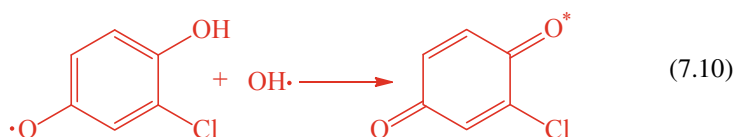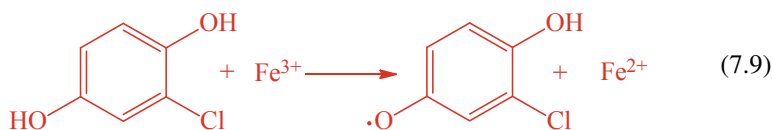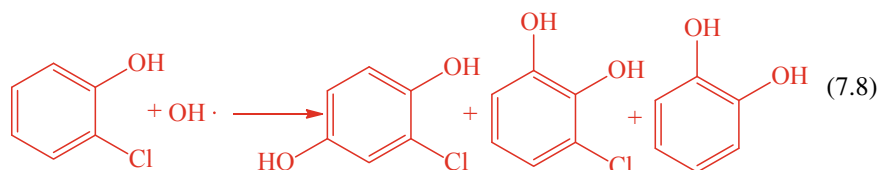
At high ferrous concentrations, photons were emitted in the CL reaction quickly. However, if the ferrous concentration was above 0.1 mol L^{-1}, CL signal became weakened. The reason was that ferrous ions could react much more to hydroxyl radical (Reaction 7.3), affecting the hydroxyl radical reacting with other species. The photon emission was slow if the ferrous concentration was 1.0×10^{-3} mol L^{-1}. The result revealed that the effectiveness of free ferrous ions was sensitive to the production of hydroxyl radicals, which limited the breakdown of organic matter. Because the reaction rate of Reaction (7.2) was slower compared to the reaction rate of Reaction 7.1, the reduction reaction can regenerate ferrous ions slower (0.001–0.01 (mol $L^{-1})^{-1}$ s^{-1} vs. 51 (mol $L^{-1})^{-1}$ s^{-1}) [24]. Thus, the kinetic curves were presented as curves using low concentrations of ferrous ions.

The highest CL intensity was observed at pH 2.8. The optimized pH range for the degradation of *ortho*-chlorophenol was reported to be 3–4 [25]. It was presumed that the degradation of chlorophenol may affect the CL intensity.

7.3.1 CL-FI System

The H_2O (carrier), H_2O_2, and ferrous solutions were transported through lines R_1, R_2, and R_3, separately (Fig. 7.1). The intensity of CL produced by blending H_2O_2 with the ferrous solution was 1.5 mV, measured by a luminescence analyzer. The lines for H_2O_2 and the ferrous solution can be switched since the observed LC intensity was nearly the same [Fig. 7.2C(b)]. When *ortho*-chlorophenol was introduced into the H_2O_2–Fe^{2+} system, a significantly higher CL strength of up to 15 mV was measured [Fig. 7.2C(c)], providing further evidence of the increased impact by *ortho*-chlorophenol to the CL as a result of the Fenton's reaction.

7.3.2   Effect of Iron on CL

The CL strengths of the various salts used are listed in the order of $(NH_4)_2Fe(SO_4)_2 \approx FeSO_4 > FeCl_2 > FeCl_3 > NH_4Fe(SO_4)_2$. It was because the ferric ion should first respond with H_2O_2 to regenerate ferrous ions that gave rise to produce the hydroxyl radical (see Reactions 7.1 and 7.2). Since the reaction rate of Reaction 7.2 was 0.001–0.01 [$(mol·L^{-1})^{-1}$ s^{-1}] which was much slower than the rate of Reaction 7.1. The ferrous ion reacted rapidly but regenerated slowly, resulting in a slower Fenton reaction rate. Hence, $(NH_4)_2Fe(SO_4)_2$ with low background noise and high signal was chosen for the following tests.

7.3.3   Effect of Temperature on CL

Activation energy values in Reaction 7.1 have been reported as few kilocalories. The influence of temperature has received little consideration. But we have noted here that temperature could affect the reaction. The CL intensity increased with higher temperature when hydrogen peroxide was added in the blend of ferrous ions solution and *ortho*-chlorophenol (Fig. 7.3). The enhancement of CL intensity was due to a great generation of hydroxyl radical at higher temperatures, which was important for the decomposition of *ortho*-chlorophenol. Similarly, Lopez et al. reported a similar conclusion that the degradation of 4-chloro-3-methylphenol was strongly influenced by temperature s [26].

Fig. 7.3   The effect of temperature on the CL when hydrogen peroxide was added to the blend of ferrous ion solution and *ortho*-chlorophenol. *ortho*-chlorophenol, 5.0×10^{-4} mol L^{-1}; Fe^{2+}, 1.0×10^{-2} mol L^{-1}; H_2O_2, 1.0 mol L^{-1}. Copyright 2012, with permission from Elsevier Ref. [16]
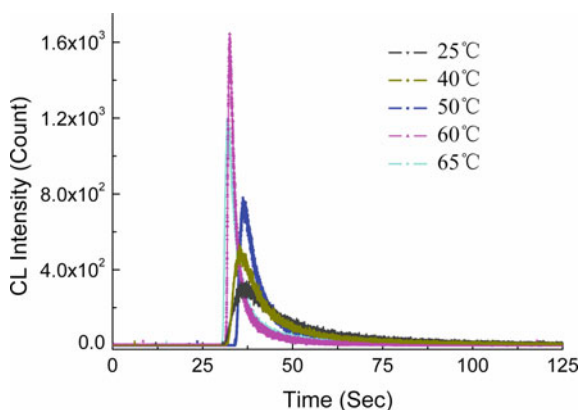
7.3.4   Impact of Radical Scavengers on CL

In the metal-containing system, the addition of hydrogen peroxide gave rise to a lot of radical reactions. To better understand the mechanism of the CL system, how some free radical scavengers affected the CL intensity was investigated. There are few organic solutions, namely methanol [27], ethanol, propanol, *tert*-butanol [15, 28, 29], that have been investigated to prevent the potential reaction of hydroxyl radicals. In this study, organic solutions used as radical scavengers were discovered to have an inhibitory influence on the CL of the Fe^{2+}–H_2O_2-*ortho*-chlorophenol system. Some other organic compounds, which included acetonitrile, CH_3Cl, and cyclohexane, had little effect on the CL intensity. *Tert*-butanol highly suppressed the CL strength in all organic compounds, resulting from its maximum reactivity toward the hydroxyl radical.

The involvement of hydroxyl radicals in the CL reaction was further confirmed by the observation that CL was inhibited when thiourea or mannitol, two important scavengers of hydroxyl radicals, were introduced into the CL reaction [30].

Format increased the strength up to 10.1-fold at a concentration of 1.0 mol/L. The two-fold doubling of the $\cdot O_2^-$ generation efficiency and the increase in CL intensity is explained by the reaction of the formate ion with hydroxyl radicals followed by the reaction with O_2 to form $\cdot O_2^-$ radicals [31].

Sodium azide was alleged to be a bursting agent for singly linear oxygen (Reaction 7.11) [32]. When 1.0×10^{-3} to 0.1 mol L^{-1} of sodium azide was introduced into the system, the CL intensity was greatly reduced [33].

$$N_3^- + {}^1O_2 \rightarrow N_3^- + {}^3O_2 \tag{7.11}$$

The iron ions are a central part of Fenton's reaction. Many ligands like PO_4^{3-} and malonic acid were introduced into the reaction both weakening the CL reaction.

7.3.5   Impact of MCLA and GSH on CL Intensity

MCLA was selected to be the superoxide anion probe because it was sensitive to superoxide anions in non-alkaline situations [34]. As the concentration of MCLA increased, the CL intensity increased, which indicated the existence of superoxide anion in the system.

Quinones have been studied to participate in 1, 4-reduction addition reactions with SH-containing compounds (Reaction 7.12). Brunmark discovered that glutathione has a bursting influence on the photoemission produced by H_2O_2 and *para*-benzoquinone [22, 23]. The peak slowed down when the glutathione concentration rose to 1.0×10^{-2} mol L^{-1}. Presumably, the peaks generated in the quinone excited state were influenced by glutathione, suggesting the formation of an excited quinine-like intermediate in H_2O_2–Fe^{2+}-*ortho*-chlorophenol system.

$$+ GS^- \longrightarrow \tag{7.12}$$
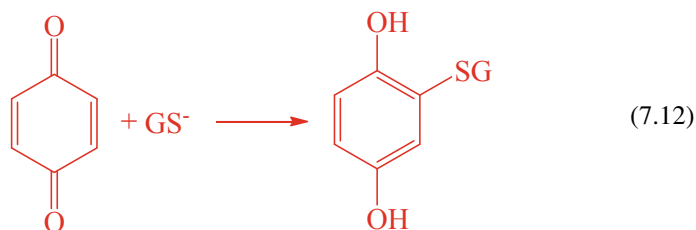
7.3.6   ESR Spin Trapping Method

Electron spin resonance (ESR) is employed to detect presence of hydroxyl radicals. DMPO underwent double bonding reaction with radicals and was converted into DMPO radical adducts by hyperfine splitting [35, 36]. As diagrammed in Fig. 7.4A,

Fig. 7.4 **A** ESR spectra of DMPO/ ·OH generated from the mixture of DMPO with Fe^{2+}–H_2O_2-*ortho*-chlorophenol; **B** ESR spectra of TEMP/$^1O_2$ generated from the mixture of TEMP with and Fe^{2+}–H_2O_2-*ortho*-chlorophenol (**a**) and Fe^{2+}–H_2O_2 (**b**). Reactions were proceeded at room temperature with pH 7.0 in phosphate buffer (0.1 mol L^{-1}). The reaction mixture consisted of 2.5 × 10^{-2} mol L^{-1} DMPO, 2.5 × 10^{-3} mol L^{-1} Fe^{2+}, 0.25 mol L^{-1} H_2O_2 and 2.5 × 10^{-4} mol L^{-1} *ortho*-chlorophenol. Copyright 2012, with permission from Elsevier Ref. [16]
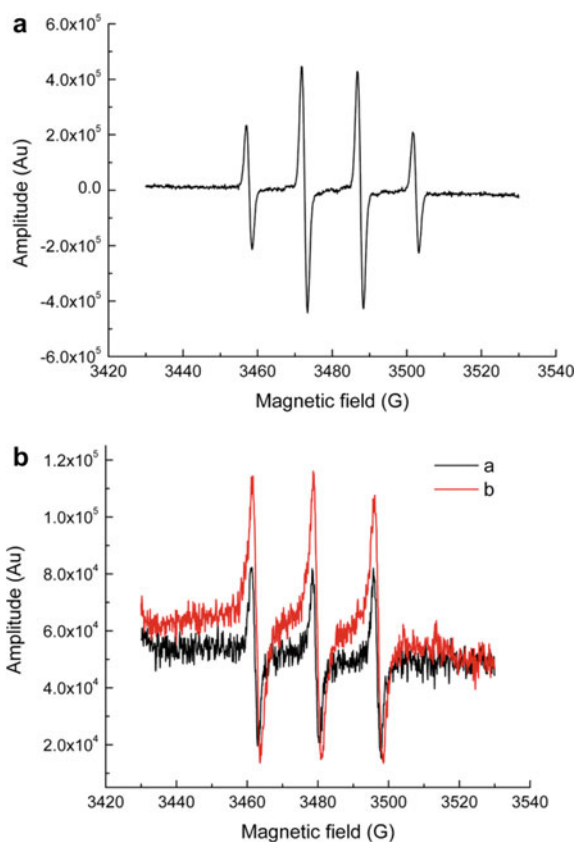
the addition of DMPO to the Fe^{2+}–H_2O_2-*ortho*-chlorophenol system resulted in a four-line signal, at a peak ratio of 1:2:2:1 and hyperfine coupling constant ($\alpha_N = 15.0$ G, $\alpha_H = 15.0$ G), in good agreement with the spectra of the DMPO-OH adduct.

ESR spin trapping and TEMP were used to indirectly detect singlet oxygen. 2,2,6,6-Tetramethyl-4-piperidone interacted with singlet oxygen to form an adduct of 4-oxo-TEMPO [37]. TEMP mixing with Fe^{2+}–H_2O_2 resulted in ESR spectra leading to a trilinear signal, in good agreement to that of the 4-oxo-TEMPO (Fig. 7.4B). The trilinear signal of the Fe^{2+}–H_2O_2-*ortho*-chlorophenol system indicated the production of a relatively low content of singlet oxygen (Fig. 7.4C) in the existence of *ortho*-chlorophenol. This was probably the consumption of hydroxyl radicals during hydroquinone formation. Enhancement of CL intensity by *ortho*-chlorophenol was affected by the excited quinone.

7.3.7 Survey of CL Reaction Decomposition Products by GC–MS

GC coupled with MS was used to characterize the breakdown products to further study the CL reactions. The intermediate components, concluding 2-chloro-1,4-benzoquinone, 2-chlorobenzene-1,4-diol and 3-chlorobenzene-1,2-diol, were identified (Fig. 7.5). Although both -OH and -Cl groups in *ortho*-chlorophenol have the ability to be oriented at both the *ortho* and *para*-positions, the substitution of o-chlorophenol relies on the orientation ability of the -OH group, as it dominates. Consequently, the major substitution compounds were 2-chlorobenzene-1, 4-diol, and 3-chlorobenzene-1, 2-diol. It was reported that the detected compounds participated in the iron redox cycle [27, 38, 39]. 2-chlorobenzene-1,4-diol was converted to 2-chloro-1,4-benzoquinone undergoing oxidation by iron ions and hydroxyl radicals [27]. 3-Chlorobenzene-1, 2-diol did not turn into 3-chloro-1, 2-benzoquinone, which may result from the small amount or short-term lifetime.

Fig. 7.5 GC–MS was used to determine the degraded intermediates in Fenton oxidation of *ortho*-chlorophenol and the GC chromatograms obtained. **a** 2-chloro-1, 4-benzoquinone; **b** 2-chlorobenzene-1, 4-diol; **c** 3-chlorobenzene-1, 2-diol. Copyright 2012, with permission from Elsevier Ref. [16]
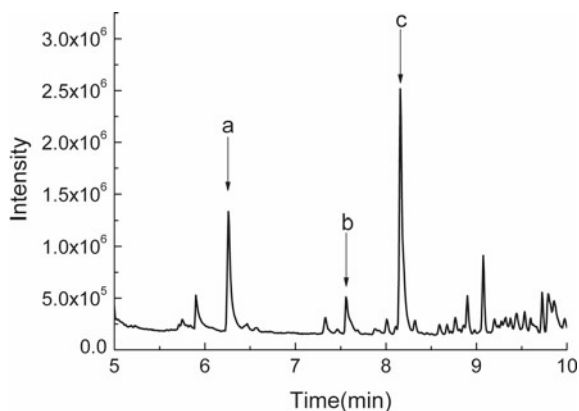
7.3.8   Survey on the Degradation of **ortho-***Chlorophenol by Fluorescence Spectrophotometry and CL Emission Spectroscopy*

A fluorometric method was applied to determine the decomposition of *ortho*-chlorophenol by treatment with Fenton's reagent. 251 and 302 nm were the highest excitation and emission wavelengths of *ortho*-chlorophenol. The blend of ferrous solution and *ortho*-chlorophenol did not alter the fluorescence intensity of *ortho*-chlorophenol.

Addition of H_2O_2 to the mixture of *ortho*-chlorophenol and ferrous solution resulted in a decrease in fluorescence intensity with increasing time of blending, providing strong evidence of the decomposition of *ortho*-chlorophenol by the oxidation of Fenton's reagent (Fig. 7.6).

Fluorescence spectrophotometry was used to test the CL spectrum of this system to study CL emitting species. The characteristic band of emission spectrum of this system was a broadband of 480–540 nm, centered at 500 nm. It was speculated that it was produced by electron-excited quinone and singlet oxygen [23, 31]. Rhodamine 6G in the H_2O_2–Fe^{2+}-*ortho*-chlorophenol system shifted the largest emission wavelength from 500 to 555 nm, the largest emission wavelength of Rhodamine 6G (Fig. 7.7b). A decrease in the intensity of CL near 500 nm was a strong evidence of energy transfer from the excited intermediate, which was itself a feeble emitter, to the fluorescent compounds having a good quantum yield [40].

Fig. 7.6 Fluorescence spectra were used to investigate the decomposition of *ortho*-chlorophenol with increasing time (along the direction of the *arrow*). *ortho*-chlorophenol, 3.5×10^{-5} mol L^{-1}; Fe^{2+}, 2.5×10^{-4} mol L^{-1}; H_2O_2, 1.0×10^{-4} mol L^{-1}. Copyright 2012, with permission from Elsevier Ref. [16]
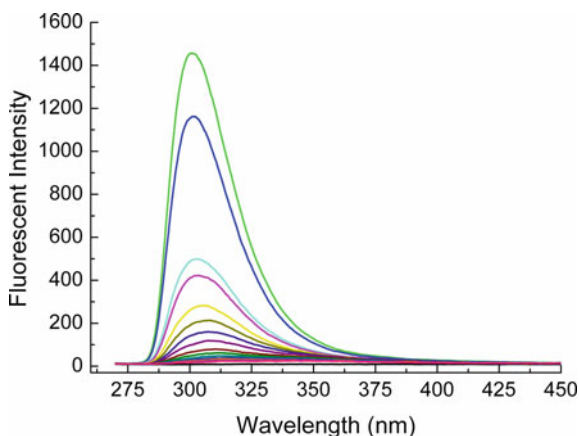
Fig. 7.7 CL spectra of H_2O_2–Fe^{2+}-*ortho*-chlorophenol system (**a**) and H_2O_2–Fe^{2+}-*ortho*-chlorophenol-rhodamine system 6G (**b**). *ortho*-chlorophenol, 1.0×10^{-3} mol L^{-1}; Fe^{2+}, 1.0×10^{-2} mol L^{-1}; H_2O_2, 1.0 mol L^{-1}; rhodamine 6G, 1.0×10^{-4} mol L^{-1}. Copyright 2012, with permission from Elsevier Ref. [16]
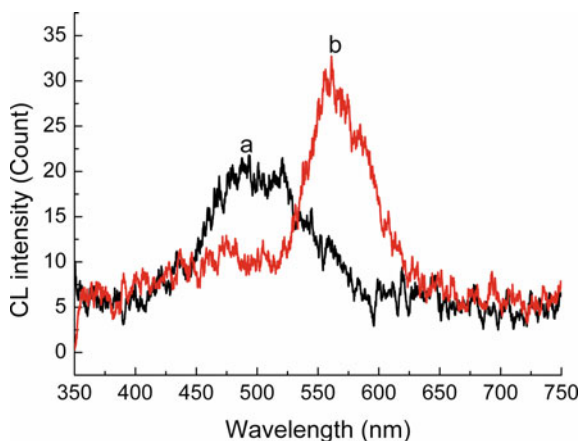
7.3.9 Probable Mechanism of CL Reaction

On the basis of the foregoing results, the CL emission mechanism for the H_2O_2–Fe^{2+} system including and excluding *ortho*-chlorophenol was represented as Fig. 7.8 (Reaction 7.1). The hydroxyl radicals formed by the blend of H_2O_2 and ferrous solution (Reaction 7.1) interacted with Fe^{3+} to form $HO_2\cdot$ (Reaction 7.2). After $HO_2\cdot$ decomposing to $\cdot O_2^-$, $\cdot O_2^-$ reacted with hydroxyl radical or $HO_2\cdot$ to generate single-linear oxygen. The single-linear was among the CL emitters during the CL reaction period (Reactions 7.5 and 7.6), which could also be generated by combinations of $HO_2\cdot$ (Reaction 7.7). It was shown that for the influence of various radical scavengers (thiourea, formate, sodium azide) on the CL system, hydroxyl radicals, singlet oxygen, and superoxide anion were the participating substances in the CL reaction. ESR spectroscopy was utilized with further confirmation of the existence of hydroxyl radicals and single-linear state oxygen within this H_2O_2–Fe^{2+} system.
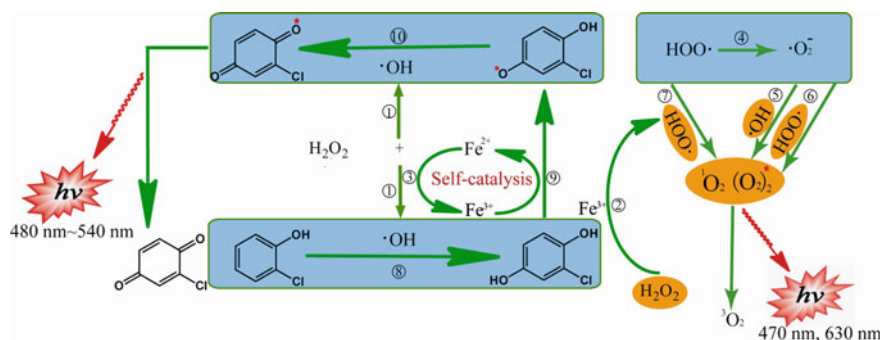
Fig. 7.8 A probable mechanism for the auto-catalytic CL oxidation of *ortho*-chlorophenol by Fenton's reagent. Copyright 2012, with permission from Elsevier Ref. [16]

Cationic surfactants, like DTAB, MTAB, CTAB, CTAC, DDDAB, somewhat strengthened the CL signal due to the concentration of $\cdot O_2^-$ around the posi-micelles surface, which favored the single-linear state oxygen formation, thus leading to higher CL intensity. In addition, micelles may offer protection for the exiting singlet state. MCLA increased CL intensity by 56 times, confirming that superoxide anions were involved in CL reactions.

The interaction between p-benzoquinone and H_2O_2 produced the activated trilinear state 2-hydroxy-p-benzoquinone, whose degradation was followed by photoemission. Typically, the oxidation of semiquinone by hydroxyl radicals could lead to producing electronically excited quinones [41, 42]. As a result, the reason for the improved CL of H_2O_2–Fe^{2+} system and *ortho*-chlorophenol was the becoming of the electronically excited quinone (Reaction 7.10 in Fig. 7.8). Maximum photoemission intensity during the attenuation of the excited trilinear quinone to its ground state was in the range of 480–540 nm. It was consistent with the pattern of the CL spectrum of the H_2O_2-Fe^{2+}-*ortho*-chlorophenol system centered at 500 nm [19].

7.4   Conclusions

The CL produced by the blend of ferrous ions and hydrogen peroxide was enhanced by *ortho*-Chlorophenol. The existence of hydroxyl radicals and electronically excited quinones was demonstrated by the action of free radical scavengers. By performing ESR spectroscopy, the findings demonstrated the existence of hydroxyl radicals and singlet oxygen in the two systems. CL spectra and reaction product measurements showed the single-linear state oxygen and electronically excited quinone are the dominant emitters of H_2O_2–Fe^{2+}-*ortho*-chlorophenol system. The CL approach was an interesting way to investigate the oxygenation of *ortho*-chlorophenol by Fenton reagents. Studies on how CL is applied are being conducted in our lab.

References

1. Keith LH, Telliard WA (1979) Priority pollutants. Environ Sci Technol 13(4):416–423
2. Zazo JA, Casas JA, Mohedano AF, Gilarranz MA, Rodrguez JJ (2005) Chemical pathway and kinetics of phenol oxidation by Fenton's reagent. Environ Sci Technol 39(23):9295–9302
3. Eker S, Kargi F (2006) Biological treatment of para-chlorophenol containing synthetic wastewater using rotating brush biofilm reactor. J Hazard Mater 135:365–371
4. Benitez FJ (2000) Contribution of free radicals to chlorophenols decomposition by several advanced oxidation processes. Chemosphere 41:1271–1277
5. Fenton HJH (1894) Oxidation of tartaric acid in presence of iron. J Chem Soc Trans 65:899–911
6. Nieto-Juarez JI, Pierzchła K, Sienkiewicz A, Kohn T (2010) Inactivation of MS_2 coliphage in Fenton and Fenton-like systems: role of transition metals, hydrogen peroxide and sunlight. Environ Sci Technol 44(9):3351–3356

 7. Pérez-Moya M, Graells M, del Valle LJ, Centelles E, Mansilla HD (2007) Fenton and photo-Fenton degradation of 2-chlorophenol: multivariate analysis and toxicity monitoring. Catal Today 124:163–171
 8. Brillas E, Sires I, Oturan MA (2009) Electro-Fenton process and related electrochemical technologies based on Fenton's reaction chemistry. Chem Rev 109(12):6570–6631
 9. Kremer ML (2003) The Fenton reaction. Dependence of the rate on pH. J Phys Chem A 107(11):1734–1741
10. Pignatello JJ (1992) Dark and photoassisted Fe^{3+}-catalyzed degradation of chlorophenoxy herbicides by hydrogen peroxide. Environ Sci Technol 26(5):944–951
11. Walling C (1998) Intermediates in the reactions of Fenton type reagents. Accounts Chem Res 31(4):155–157
12. Huang HH, Lu MC, Chen JN (2001) Catalytic decomposition of hydrogen peroxide and 2-chlorophenol with iron oxides. Water Res 35(9):2291–2299
13. Sabhi S, Kiwi J (2001) Degradation of 2,4-dichlorophenol by immobolized iron catalysis. Water Res 35(8):1994–2002
14. Elias RJ, Waterhouse AL (2010) Controlling the Fenton reaction in wine. J Agr Food Chem 58(3):1699–1707
15. Rivas FJ, Beltrán FJ, Frades J, Buxeda P (2001) Oxidation of *p*-hydroxybenzoic acid by Fenton's reagent. Water Res 35(2):387–396
16. Lin Z, Chen H, Zhou Y, Ogawa N, Lin J-M (2012) Self-catalytic degradation of ortho-chlorophenol with fenton's reagent studied by chemiluminescence. J Environ Sci 24:550–557
17. Walling C (1975) Fenton's reagent revisited. Accounts Chem Res 8:125–131
18. Bielski BHJ, Cabelli DE, Arudi RL, Ross AB (1985) Reactivity of HO_2/O_2^- radicals in aqueous solution. J Phys Chem Ref Data 14(4):1041–1100
19. Khan AU, Kasha M (1970) Chemiluminescence arising from simultaneous transitions in pairs of singlet oxygen molecules. J Am Chem Soc 2(11):3293–3300
20. Lin J-M, Liu ML (2008) Chemiluminescence from the decomposition of peroxymonocarbonate catalyzed by gold nanoparticles. J Phys Chem B 112(26):7850–7855
21. Chen F, Ma WH, He JJ, Zhao JC (2002) Fenton degradation of malachite green catalyzed by aromatic additives. J Phys Chem A 106(41):9485–9490
22. Brunmark A (1989) Formation of electronically excited states during the interaction of *p*-benzoquinone with hydrogen peroxide. J Bioluminescence Chemiluminescence 4:219–225
23. Brunmark A, Cadenas E (1987) Electronically excited state generation during the reaction of *p*-benzoquinone with H_2O_2. Free Radical Bio Med 3:169–180
24. Walling C, Goosen A (1973) Mechanism of the ferric ion catalyzed decomposition of hydrogen peroxide. Effect of organic substrates. J Am Chem Soc 95(9):2987–2991
25. De AK, Chaudhuri B, Bhattacharjee S (1999) A kinetic study of the oxidation of phenol, *o*-chlorophenol and catechol by hydrogen peroxide between 298 and 333 K: the effect of pH, temperature and ratio of oxidant to substrate. J Chem Technol Biot 74:162–168
26. Lopez A, Mascolo G, Detomaso A, Lovecchio G, Villani G (2005) Temperature activated degradation (mineralization) of 4-chloro-3-methyl phenol by Fenton's reagent. Chemosphere 59:397–403
27. Rodríguez J, Parra C, Contreras D, Freer J, Baeza (2001) Dihydroxybenzenes: driven Fenton reactions. Water Sci Technol 44(5):251–256
28. Chen RZ, Pignatello JJ (1997) Role of quinone intermediates as electron shuttles in Fenton and photoassisted fenton oxidations of aromatic compounds. Environ Sci Technol 31(8):2399–2406
29. Du YX, Zhu MH, Lei LC (2006) Role of the intermediates in the degradation of phenolic compounds by Fenton-like process. J Hazard Mater B 136:859–865
30. Liang SX, Zhao LX, Zhang BT, Lin J-M (2008) Experimental studies on the chemiluminescence reaction mechanism of carbonate/bicarbonate and hydrogen peroxide in the presence of cobalt(II). J Phys Chem A 112(4):618–623
31. Lin J-M, Yamada M (1999) Oxidation reaction between periodate and polyhydroxyl compounds and its application to chemiluminescence. Anal Chem 71(9):1760–1766

32. Lunar L, Sicilia D, Rubio S, Pérez-Bendito D, Nickel U (2002) Degradation of photographic developers by Fenton's reagent: condition optimization and kinetics for metol oxidation. Water Res 34(6):1791–1802
33. Wang M, Zhao LX, Lin J-M (2007) Chemiluminescence of the peroxomonosulphate-cobalt (II)-aliphatic monocarboxylic acids system. Luminescence 22:182–188
34. Hosaka S, Itagaki T, Kuramitsu Y (1999) Selectivity and sensitivity in the measurement of reactive oxygen species (ROS) using chemiluminescent microspheres prepared by the binding of acridinium ester or ABEI to polymer microspheres. Luminescence 14:349–354
35. Kim JK, Metcalfe IS (2007) Investigation of the generation of hydroxyl radicals and their oxidative role in the presence of heterogeneous copper catalysts. Chemosphere 69:689–696
36. Cheng S, Fung W, Chan K, Shen PK (2003) Optimizing electron spin resonance detection of hydroxyl radical in water. Chemosphere 52:1797–1805
37. Lion Y, Delemlle M, Vorst A (1976) New method for detecting singlet oxygen. Nature 263:442–443
38. Duesterberg CK, Waite TD (2007) Kinetic modeling of the oxidation of p-hydroxybenzoic acid by Fenton's reagent: implications of the role of quinones in the redox cycling of iron. Environ Sci Technol 41(11):4103–4110
39. Iwahashi H, Morishita H, Ishii T, Sugata R, Kido R (1989) Enhancement by catechols of hydroxyl-radical formation in the presence of ferric ions and hydrogen peroxide. J Biochem 105(3):429–434
40. Magde D, Rojas GE, Seybold PG (1999) Solvent dependence of the fluorescence lifetimes of xanthene dyes. Photochem Photobiol 70(5):737–744
41. He DY, Zhang ZJ, He C (2006) Investigation on the interaction between dihydroxybenzene and Fe^{3+}-H_2O_2-Rh6G system based on enhancing chemiluminescence. Luminescence 21:15–19
42. Lasovsky J, Hrbac J, Sichertova D, Bednar P (2007) Oxidation and chemiluminescence of catechol by hydrogen peroxide in the presence of Co(II) ions and CTAB micelles. Luminescence 22:501–506

Chapter 8
Ultra Weak Chemiluminescence Enhanced by Noble Metal Nanoparticle

Wenjuan Zhou and Chao Lu

Abstract Noble metal nanomaterials (NMNs) with fascinating physical and chemical properties are optimal foundation for design and also customizing nanoscale frameworks for particular technical applications. Especially, successfully regulating the size, morphology, composition, hybrid as well as microstructure of NMNs play an essential function on disclosing their brand-new or improved features and also application capacities, such as energy catalysis, analytical sensing, and biomedicine. NMNs-involved chemiluminescence (CL) has actually come to be a new and expanding area of interest in the last few years. The advancement of NMNs-involved CL systems and their application in chemical and biological analysis has been reviewed in this chapter. Additionally, application of various NMNs, including gold nanoparticles, platinum nanoparticles, silver nanoparticles and bimetallic nanoparticles in various CL systems has been emphasized. Moreover, the key challenges in this field and proposed possible solutions has been discussed for efficient and wider applications of CL analytical technology.

Keywords Chemiluminescence · Gold nanoparticles · Platinum nanoparticles · Silver nanoparticles · Bimetallic nanoparticles

8.1 Introduction

Nanoscale noble metals usually exhibit special optical, electrical, magnetic, and chemical properties, which depend on their size and morphology. The noble metal nanomaterials (NMNs) have gotten extraordinary interest in fundamental research as well as potential applications in nanotechnology and biotechnology [1–3]. The properties of nanomaterials are certainly related to many factors, including their size, morphology, composition, hybrid as well as microstructures, which are often used to

W. Zhou
Department of Chemistry, Capital Normal University, Beijing 100048, China

C. Lu (✉)
College of Chemistry, Beijing University of Chemical Technology, Beijing 100029, China
e-mail: luchao@mail.buct.edu.cn

expose and regulate the function of nanomaterials [4–6]. NMNs (e.g., Au, Ag, and Pt) can exhibit optical properties similar to molecules, such as ultraviolet absorption and fluorescence emission. Interestingly, these optical properties of NMNs tend to be highly dependent on their size. Therefore, the size regulation of NMNs offers good opportunities for their potentials in photonics, catalysis, photography, and imaging applications [7]. Owing to their high specific surface area, quantum size effect, and high surface energy, NMNs exhibit excellent catalytic performance for redox reaction, endowing their ability to amplify some weak chemiluminescence (CL) emission. Accordingly, CL analysis based on NMNs shows unique advantages and potentials in many fields, including food safety, environmental analysis, and life sciences [8–10].

Over 40 years, liquid-phase CL has been developed greatly. However, liquid-phase CL systems are often limited to molecules, ions, and simple aggregates [11–13]. In recent years, liquid-phase CL of nanoparticles has attracted extensive interest due to the superior sensitivity and stability [14]. Among them, CL reactions involving metal nanoparticles are undoubtedly one kind of the most studied systems. Metal nanoparticles play a variety of roles in CL reactions, including as reactants, catalysts, and luminophors [15]. In this chapter, we reviewed the development and analytical applications of NMNs-involved CL systems in recent years. The CL systems involving gold nanoparticles, platinum nanoparticles, silver nanoparticles, and bimetallic nanoparticles has been discussed in categories. Finally, this chapter prospected the application potentials of NMNs-involved CL systems in more extensive fields.

8.2 Gold Nanoparticles-Involved CL System

8.2.1 Gold Nanoparticles-Involved Luminol CL System

In 2005, gold nanoparticles (AuNPs) were first applied for signal enhancement in luminol–H_2O_2 CL system [16] in which AuNPs act as catalysts, and the luminescent substance was still the excited state product (3-aminophthalate anion). In alkaline aqueous solution, the CL mechanism of luminol–H_2O_2 can be summarized as follows: Luminol radicals generated by oxidation are further oxidized to form an important intermediate hydroxyl hydroperoxide, which decompose to generate excited 3-aminophthalate anion, and then produce CL emission. More reactive oxygen species (ROS) generation during the luminol oxidation would promote the CL reaction. By the addition of AuNPs into the luminol–H_2O_2 system, the weak CL signal was significantly enhanced with the same emitting species, indicating strong catalytical effect of AuNPs toward the CL reaction of luminol–H_2O_2. Thanks to abundant active sites on the AuNP surface, AuNPs can catalyze the homolysis of H_2O_2 to generate hydroxyl radicals (•OH) with higher oxidation ability, and then oxidize luminol to produce significantly higher CL intensity (Fig. 8.1) [16].

$$H_2O_2 \quad + \quad OH^- \longrightarrow \quad HO_2^- \quad + \quad H_2O$$
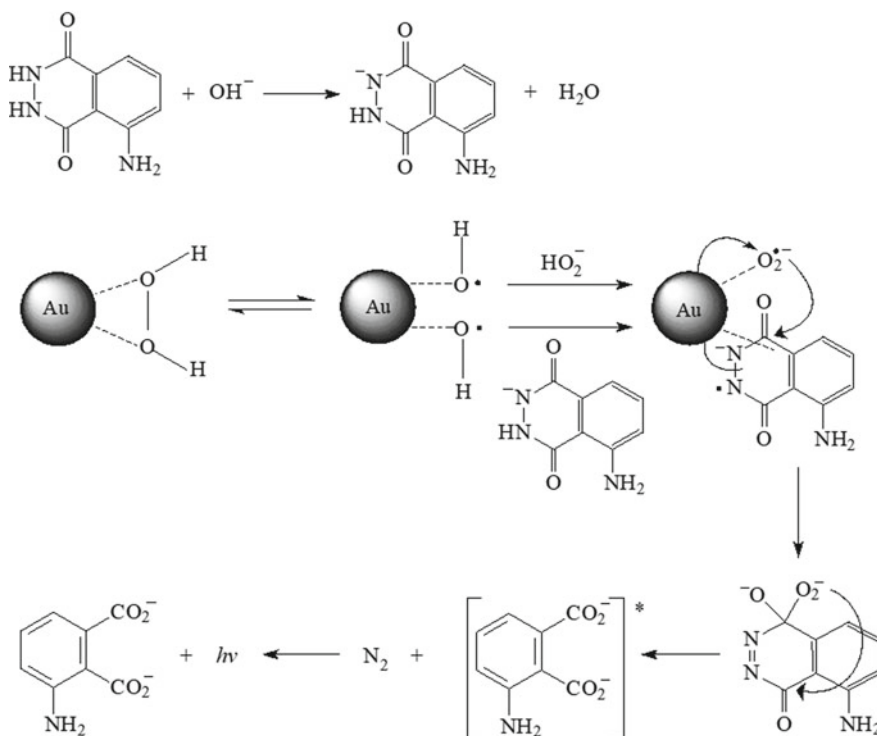
Fig. 8.1 CL mechanism for the AuNP-catalyzed luminol$-H_2O_2$ reaction. Reprinted with permission from Ref. [16]. Copyright 2005 American Chemical Society

Thereafter, analytical applications of the AuNP-catalyzed luminol–H_2O_2 CL were explored extensively for various analytical applications [17–28]. When some substances which can react with H_2O_2 to produce the state of excite substances or reactive intermediates were existed, the emission of CL system of AuNP-catalyzed luminol–H_2O_2 would be increased. From this, sensitive CL detection of fluoro-quinolones derivatives and Cu(II) has been achieved [17, 18]. The surface charge of AuNPs (which can be altered by changing protecting agents, adding salt or amino compounds) was found to affect their catalytic performance toward luminol–H_2O_2 CL reaction [19–22]. CL determination of DNA hybridization was also realized on the base of its promoting effect on salt-induced aggregation of AuNPs [19]. In a similar way, a CL method for determining C-reactive protein has been established using the AuNP-catalyzed luminol–H_2O_2 system [20]. By contrast, analytical methods based on analyte-induced inhibition of the AuNP-enhanced CL have been developed and used more widely. The quenching mechanism includes the following two aspects: (1) competitive adsorption between analytes (*e.g.*, estrogens, L-cysteine) and H_2O_2

on the AuNP surface [23, 24]; (2) AuNPs aggregation induced by analyte (e.g., hexythiazox, propranolol, heparin) [25–27].

In addition to determining the substances that can enhance/inhibit CL emission, the AuNP-catalyzed luminol–H_2O_2 CL platform can also be used for the determination of enzyme-generated H_2O_2, among which glucose has been usually determined based on the glucose oxidase method. A flow biosensor was constructed to determine glucose by immobilizing AuNPs, horseradish peroxidase, and glucose oxidase on the inside surface of the CL flow cell [28]. To facilitate the recovery of biological molecules (such as enzymes, etc.), magnetic particles (MP) has been used as the immobilization matrix [29].

Benefiting from the large specific surface area, AuNPs can function as nanocarriers to enrich a large number of luminol molecules in very small volumes. Luminol-labeled AuNPs have been developed and used for the ultrasensitive CL-based bio/chemical analysis [30, 31]. Furthermore, synergistic catalytic effect of two or more nanomaterials endowed the nanohybrids with outstanding performance in the luminol–H_2O_2 system. An in situ synthesis method for the AuNPs/metal–organic gels hybrids has been developed. Trace amounts of organophosphorus pesticides were succesfully detected using the nanohybrid-enhanced luminol–H_2O_2 CL system (with 1 nM detection limit) [32].

After the report about the enhancement effect of spherical AuNPs toward luminol–H_2O_2 CL system, Lu group has successfully opened a new way to the application of the AuNPs with triangular and rod-like shapes to increase the luminol–H_2O_2 CL [33, 34]. In comparison with the spherical AuNPs, the gold nanorods stabilized by cetyltrimethylammonium bromide showed higher catalytic activity to the CL reaction of luminol–H_2O_2. By the addition of aminothiols, the catalytic effect of gold nanorods was found to be greatly reduced, due to the Au–S bond formation at the gold nanorod ends. Based on the aminothiol-induced CL inhibition toward the gold nanorod-catalyzed luminol–H_2O_2 system, a highly sensitive and selective method has been established to determine glutathione in *Saccharomyces cerevisiae*. Lu et al. [33] synthesized triangular AuNPs protected by non-ionic surfactants using trisodium citrate as reducing agent. Compared with spherical AuNPs, the synthesized triangular AuNPs had higher surface electron density, larger specific surface area, and lower activation energy, thus having a better enhancement effect on the luminol–H_2O_2 CL [34]. Similarly, thiol-containing compounds could bond to the AuNP surface through the formation of the Au–S bond, thus reducing active sites on the triangular AuNP surface for the formation of ROS intermediates, resulting in a CL decrease (Fig. 8.2) [35]. Accordingly, the triangular AuNP-catalyzed luminol–H_2O_2 CL system was utilized to detect captopril in human urine samples.

Effective combination of highly sensitive CL with highly selective physical or chemical methods has always been caused extensive concern. High performance liquid chromatography (HPLC), as an effective separation technology, could be coupled with sensitive CL detection system to construct a HPLC-CL method, which combined high selectivity of HPLC with high sensitivity of CL technique. An on-line HPLC detector was developed by Lu et al. based on the CL response of the AuNP-catalyzed luminol–H_2O_2 system with high sensitivity [36–41]. A simple HPLC-CL
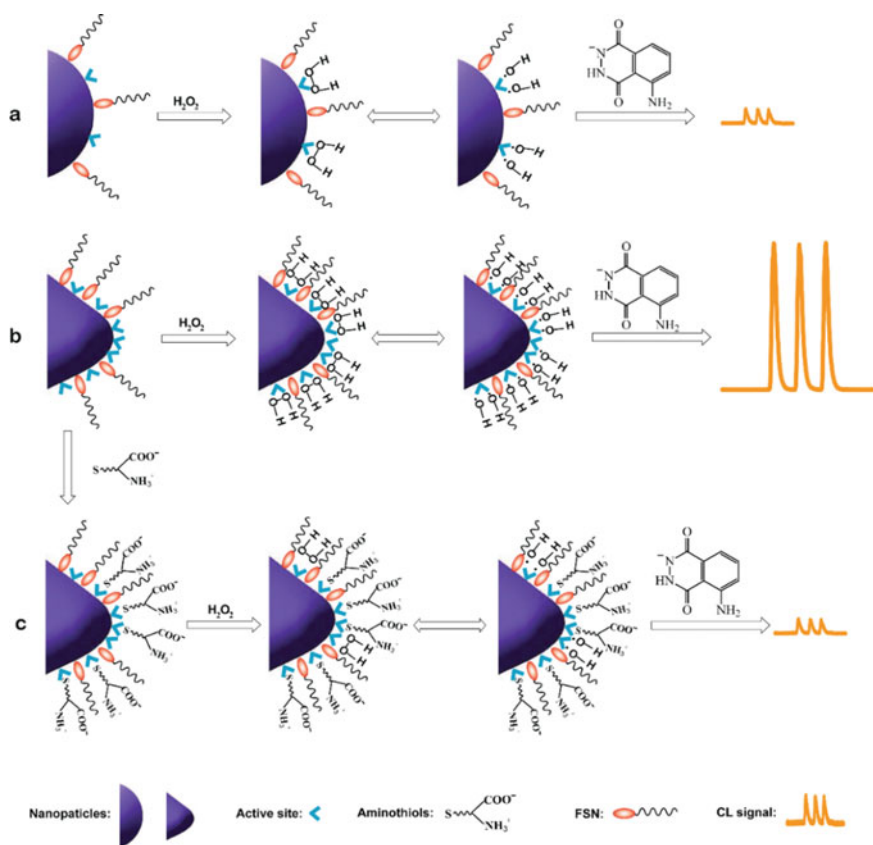
Fig. 8.2 Schematic diagram of enhanced CL of luminol−H_2O_2 catalyzed by **a** spherical AuNPs and **b** triangular AuNPs, and **c** the possible mechanism for the aminothiols-inhibited CL of the triangular AuNP-catalyzed luminol–H_2O_2 CL system. Reprinted with permission from Ref. [35]. Copyright 2011 Elsevier B.V.

method has been proposed to simultaneously detect the disulfides and thiols in biological fluids, using triangular AuNPs as postcolumn CL reagents [36–38]. In addition to chromatography, other separation methods such as capillary electrophoresis (CE) are also used in combination with CL. Liu et al. [42, 43] developed selective and sensitive methods for the quantitation of uric acid, norfloxacin, and epinephrine by using AuNP-enhanced CL detection for CE.

As a weak oxidant, silver nitrate ($AgNO_3$) can oxidize luminol to produce very weak CL emission at 425 nm, which can be significantly enhanced by the AuNPs [44]. A mechanism of the AuNP-enhanced luminol–$AgNO_3$ CL is proposed in Fig. 8.3 [44]. $AgNO_3$ was catalytically reduced to silver atoms and deposited on the AuNP surface to form an Au/Ag core-shell structure. In the meantime, luminol was oxidized to produce intense CL. In comparison with AuNPs, the Au/Ag core–shell structure
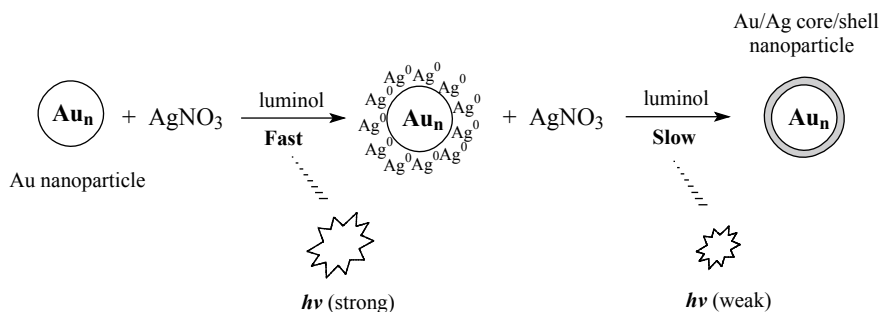
Fig. 8.3 CL mechanism of the AuNP-catalyzed luminol–$AgNO_3$ system. Reprinted with permission from Ref. [44]. Copyright 2008 American Chemical Society

showed a weaker catalytic performance, leading to a decrease in CL intensity along with the silver deposition on the AuNP surface.

In the presence of monoamine, its complete reaction with $AgNO_3$ would inhibit the oxidation of luminol and promote the silver deposition on the AuNP surface, resulting in a decreased CL. Accordingly, AuNP-catalyzed luminol–$AgNO_3$ system has been successfully applied to determine monoamine neurotransmitters coupled with HPLC [45]. On the bases of specific interaction between aptamer and bisphenol A (BPA), cationic AuNP-enhanced luminol–$AgNO_3$ CL system was utilized to selectively and sensitively detect BPA in the soil [46]. This analytical method with no chromatographic separation showed a better practicality in the developing world for the measurement of environmental pollutants.

Based on the catalysis of Hg^{2+} ions toward the $HAuCl_4$/NH_2OH reaction and the T–Hg^{2+}–T coordination chemistry, Lu et al. proposed an ultrasensitive CL sensor to determine Hg^{2+} ions [47]. AuNPs were formed on the DNA duplex-like structure, thus triggering the CL reaction of luminol–$AgNO_3$. Notably, the effects of Hg^{2+} ions on the CL of AuNP-catalyzed luminol–$AgNO_3$ system may be completely opposite when the surface molecules of AuNPs are different [48, 49]. As for the luminol-capped AuNPs, Hg^{2+} ions would be adsorbed onto the AuNP surface as a result of the affinity of AuNPs toward Hg^{2+} [48]. The catalytic activity of AuNPs would be greatly inhibited in the presence of Hg^{2+}, thus leading to CL quenching. Fan et al. found that Hg^{2+} ions enabled the recovery of the ethylenediamine-quenched CL of the AuNP-catalyzed luminol–$AgNO_3$ system due to its special binding with the amino group in ethylenediamine [49]. Hence, a turn-on CL method has been developed and applied to quantitatively detect Hg^{2+}.

Cobalt (II) compounds that have been usually utilized as efficient catalysts for the CL system of luminol–H_2O_2 can also be applied in luminol–$AgNO_3$–AuNPs system. Vitamin B12 (VB12), a cobalt (Co(II))-containing complex with a tetrapyrrole ring, has been determined by using AuNP-catalyzed luminol–$AgNO_3$ system based on the catalytic activity of cobalt (II) liberated from VB12 by acidification [50]. Another strategy based on the specific reaction between $O_2^{\bullet-}$ with Mn^{2+} was proposed to enhance CL signals of the luminol–$AgNO_3$–AuNPs system [51]. More stable and

active H_2O_2 than $O_2^{\bullet-}$ could be generated in the luminol–AgNO$_3$–AuNPs system by the addition of Mn^{2+}, thereby enhancing the CL and could be utilized to detect Mn^{2+} in water samples.

As an excellent nano-catalyst, AuNPs has been used in the luminol–ferricyanide CL system [52, 53]. Cui's group demonstrated that small-sized AuNPs (<5 nm) had an inhibition effect on the luminol–ferricyanide CL. However, the CL emission could be enhanced by the large-sized AuNPs (>10 nm) [52]. Figure 8.4 showed the mechanisms for the size-dependent AuNP-induced CL inhibition and enhancement [15, 52]. During the CL reaction, small-sized AuNPs were partially oxidized by ferricyanide, resulting in the competitive consumption of ferricyanide with luminol, which inhibited the formation of the luminol radicals and lead to decreased CL signals. By contrast, large-sized AuNPs could enhance CL signal by promoting electron transfer in the CL reaction of luminol. Both reduction ability and catalytic activity of AuNPs would be changed with the change of their size, thus the effects of AuNPs on the
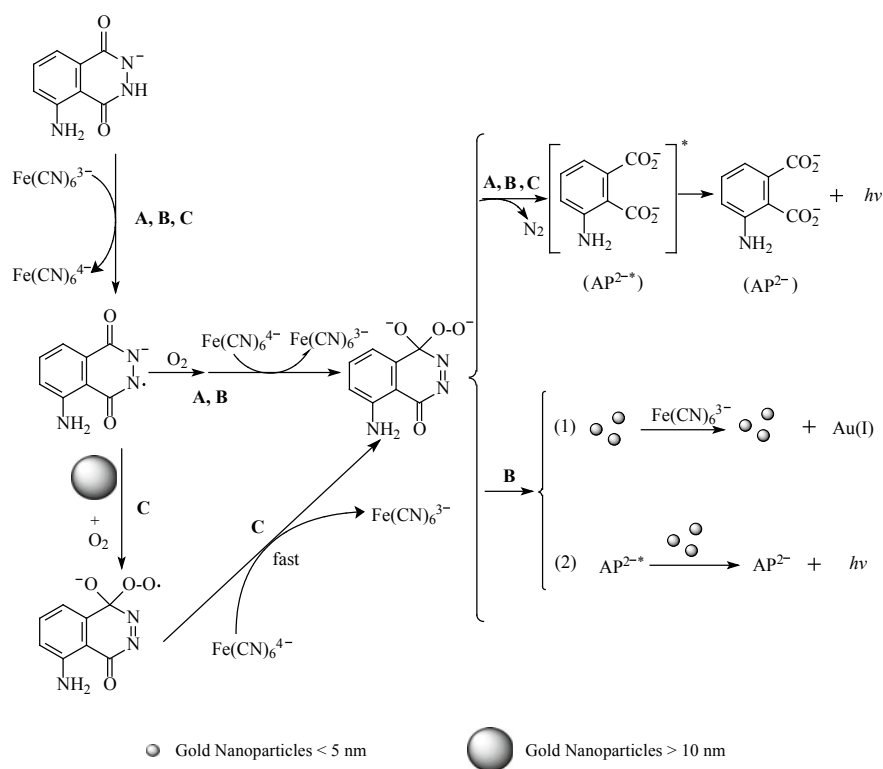
Fig. 8.4 Possible schematic mechanism for the influence of AuNPs with different sizes on the CL of luminol–ferricyanide system. **A** three major steps of the luminol–ferricyanide CL system; **B** the inhibition of the luminol–ferricyanide CL by small-sized AuNPs (<5 nm); **C** the enhancement of the luminol–ferricyanide CL by large-sized AuNPs (>10 nm). Reprinted with permission from Ref. [15]. Copyright 2011 Elsevier Ltd.

CL reaction closely depend on their size. When more ROS are produced in the reaction system, the CL signal will be enhanced. For instance, strong CL emission was obtained by addition of ascorbic acid into the luminol–ferricyanide–AuNPs system. AuNPs could catalyze the oxidation of ascorbic acid, then the generated free radical of ascorbic acid reacted with dissolved oxygen to form $O_2^{\bullet-}$, and then oxidized luminol to produce strong CL emission [53]. This ascorbic acid-enhanced CL system can be used to construct a highly sensitive analysis platform to determine vitamin C in food or healthcare products.

In alkaline solution, AuNPs are capable of catalyzing the reaction of periodate with oxygen to produce more $O_2^{\bullet-}$ radicals [54–56]. Luminol was oxidized by superoxide radicals to produce strong CL. Moreover, citrate ligands on the AuNP surface could be replaced by the generated $O_2^{\bullet-}$, which would promote the formation of the singlet oxygen molecular pairs. At the same time, the gold atoms on the AuNP surface reacted with $O_2^{\bullet-}$ to form the excited gold (I) complex. CL occurred when these excited intermediates returned to the ground state (Fig. 8.5) [56]. The presence of polyphenol could quench the CL of luminol–$NaIO_4$–AuNPs system. Based on the polyphenol-induced CL inhibition, a flow-injection CL method has been developed to determine catechol [54]. The analytical applications of AuNP-catalyzed luminol–$NaIO_4$ CL system for some other analytes, such as mefenamic acid and alkaline earth metals, are also elucidated [55, 56].

The behavior of AuNPs in the luminol–H_2O_2 CL reaction with some other oxidants has been investigated [57–60]. As a result of the catalyzation of hydrazine oxidation by AuNPs, more amount of H_2O_2 could be generated in the solution. Meanwhile, AuNPs could also catalyze the CL reaction of luminol–H_2O_2. Therefore, CL signals of the luminol–hydrazine system could be greatly increased by AuNPs [57]. In addition, catalyzing effect of AuNPs on the CL of luminol–*N*-bromosuccinimide system was investigated, where *N*-bromosuccinimide was used as an oxidant [58]. It was found that the CL of luminol–*N*-bromosuccinimide system could also be enhanced by AuNPs. In the presence of timolol maleate, the CL signal was further increased. Figure 8.6 showed the possible CL mechanism. In the reaction system, •OH and $O_2^{\bullet-}$ were generated from the AuNP-catalyzed reduction of dissolved oxygen [58]. Luminol was then oxidized by these ROS intermediates, resulting in strong CL. When there were no AuNPs in the system, the amount of N-bromosuccinimide was decreased due to the reaction between timolol maleate and N-bromosuccinimide, finally resulting in a slight decrease in CL intensity. In the presence of AuNPs, nitroxide radical (NO•) was formed through the reaction of the secondary amine in timolol and the generated H_2O_2. Peroxynitrite ($ONOO^-$) was then formed, which could oxidize luminol to produce intense CL.

Strong CL emission from luminol can also be triggered by oxidizing agent-attached AuNPs without the addition of H_2O_2 [59, 60]. For instance, the networked AuNPs prepared using HCO_4^- as a reducing agent can directly induce the strong CL from luminol, which might be ascribed to the AuNP-catalyzed generation of more amount of ROS intermediates ($CO_3^{\bullet-}$ and •OH radicals) and AuNP-promoted electron-transfer processes [59]. More recently, iodine (I_2) and polyvinyl pyrrolidone

(1)

(2) $IO_4^- + O_2 + 2OH^- \longrightarrow 2O_2^{\cdot-} + IO_3^- + H_2O$

(3)

$+ \quad h\nu \ (425 \ nm)$

(4) $4O_2^{\cdot-} + 4H_2O \xrightarrow{\text{gold nanoparticles}} (O_2)_2^* + 2H_2O_2 + 4OH^-$

(5) $(O_2)_2^* \longrightarrow 2O_2 + h\nu$

(6) $Au_n + O_2^{\cdot-} \longrightarrow Au_{n-1}[Au^I(O_2)]^{-*} \longrightarrow Au_{n-1}[Au^I(O_2)]^- + h\nu$
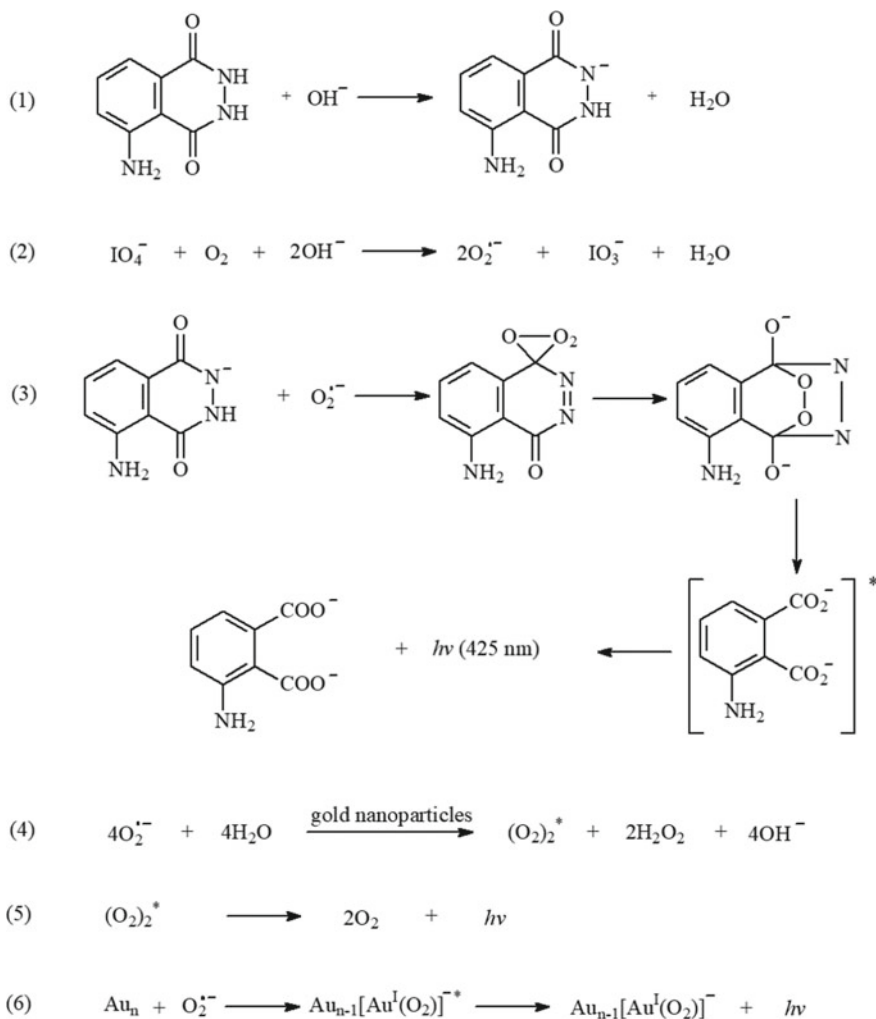
Fig. 8.5 Possible CL mechanism for the AuNP-catalyzed luminol–NaIO$_4$ system. Reprinted with permission from Ref. [56]. Copyright 2010 Elsevier B.V.

(PVP) capped AuNPs was fabricated through NaBH$_4$ reduction of Au^{3+} in the presence of complex PVP–I$_2$ [60]. Owing to the excellent catalytic activity of AuNPs, luminol reacted with the I$_2$ chemisorbed on the AuNP surface to produce intense CL.
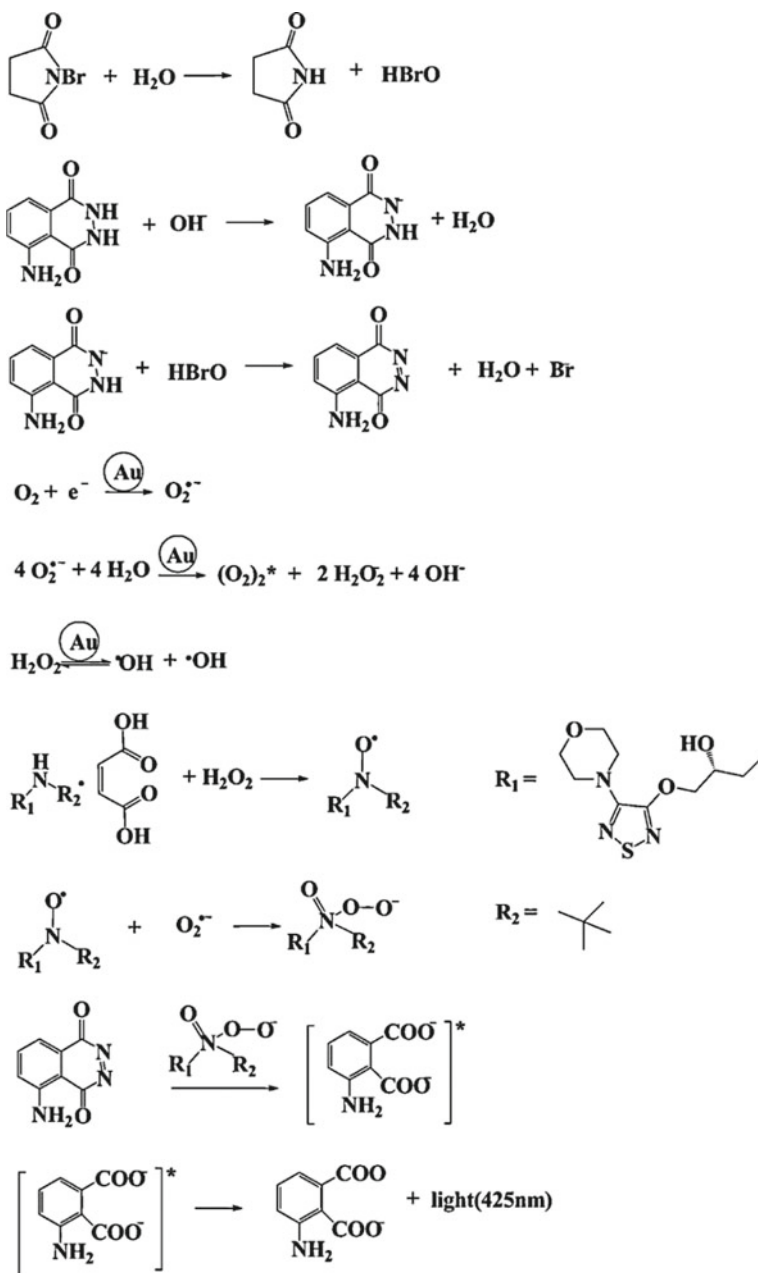
Fig. 8.6 Possible CL reaction mechanism for the luminol–*N*-bromosuccinimide system. Reprinted with permission from Ref. [58]. Copyright 2012 Elsevier B.V.
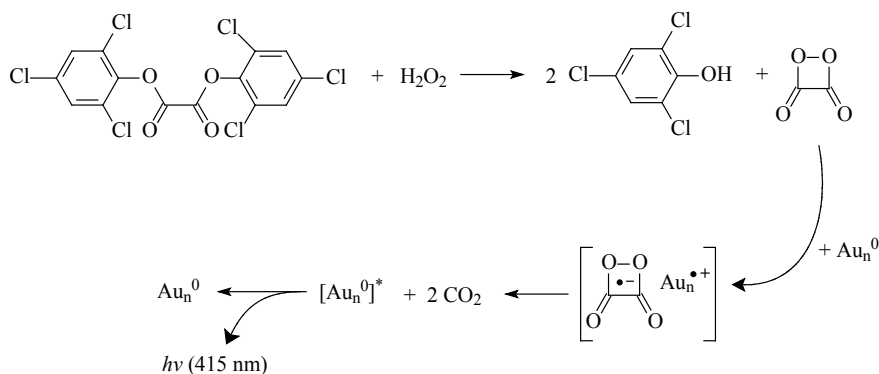
Fig. 8.7 CL mechanism for TCPO–H$_2$O$_2$–AuNPs system. Reprinted with permission from Ref. [61]. Copyright 2005 American Chemical Society

8.2.2 Gold Nanoparticles-Involved TCPO CL System

A CL emission ($\lambda_{max} = 416$ nm) from AuNPs itself can be induced by the TCPO–H$_2$O$_2$ reaction [61, 62]. Figure 8.7 showed the possible CL mechanism [61]. 1,2-Dioxetanedione, an energy-rich intermediate, was formed in the TCPO–H$_2$O$_2$ reaction. A charge-transfer complex would be yielded between AuNPs and 1,2-dioxetanedione. Then, the excited AuNPs were formed through the energy transferring from the 1,2-dioxetanedione on the AuNP surface to the gold core. By immobilization of AuNPs, carbon-nanotubes, and glucose oxidase in a nafion film, Chaichi et al. [63] constructed a biosensor for glucose detection based on the CL emission from enzymatically generated H$_2$O$_2$. Recently, a nanosensor based on the TCPO–H$_2$O$_2$–AuNPs CL system was constructed for the detection of thiram residues [64]. After interacting with thiram which has a large amount of sulfhydryl groups, the formation of intense Au–S bonds would induce the aggregation of AuNPs. The changing in surface energy level of the AuNPs thereby affect their optical properties, and indirectly quenching the CL of the AuNPs-involved TCPO–H$_2$O$_2$ system.

8.2.3 Gold Nanoparticles-Involved ROS CL System

Reactive oxyanion intermediates such as $CO_3^{\bullet-}$ and $O_2^{\bullet-}$ radicals generated in ROS-related CL systems might displace the citrate-passivating ligands on the AuNP surface. Molecular dimers would be formed by the reaction between adjacent radicals adsorbed on the AuNP surface. Cui et al. found that CL could be produced in the AuNP-involved KIO$_4$–Na$_2$CO$_3$/NaOH system [65]. Three emission bands at 490–500 nm, 430–450 nm, and 380–390 nm were observed, which may be originated from the singlet oxygen molecular pairs, carbon dioxide dimers, and excited

intermediate gold(I) complexes generated on the AuNP surface. It provided a new perspective on the CL reactions on the AuNP surface, which could be expected to be applied to biosensing and immunoassay.

HCO_4^- as an anionic ROS, could also be adsorbed on the AuNP surface. Partial electron transfer between the AuNPs and HCO_4^- would occur. Lin and his co-authors explored the effect of colloidal AuNPs with different sizes on the HCO_4^-–eosin Y CL system [66]. AuNPs with a size of 50 nm showed the strongest catalytical effect on the CL reaction of HCO_4^-–eosin Y. Figure 8.8 showed the CL mechanism. The AuNPs acted as a Lewis acid to facilitate the generation of $CO_3^{\bullet-}$ and •OH through the homolysis of HCO_4^-. $O_2^{\bullet-}$ and $^1O_2$ were formed in the system through internal bond rearrangement and interaction of radicals. Excited eosin Y was formed by receiving the energy of $^1O_2$, and emitted light when it returned to the ground state.

$$(3) \quad H_2O_2 + CO_3^{\bullet-} \rightarrow HCO_3^- + HO_2^\bullet$$

$$(4) \quad HO_2^\bullet \rightarrow H^+ + O_2^{\bullet-}$$

$$(5) \quad O_2^{\bullet-} + \bullet OH \rightarrow {}^1O_2 + HO^-$$

$$(6) \quad HO_2^\bullet + O_2^{\bullet-} \rightarrow {}^1O_2 + HO_2^-$$

$$(7) \quad HO_2^\bullet + HO_2^\bullet \rightarrow {}^1O_2 + H_2O_2$$

$$(8) \quad {}^1O_2 + \text{eosin Y} \rightarrow \text{eosin Y*} + O_2$$

$$(9) \quad \text{eosin Y*} \rightarrow \text{eosin Y} + h\nu$$
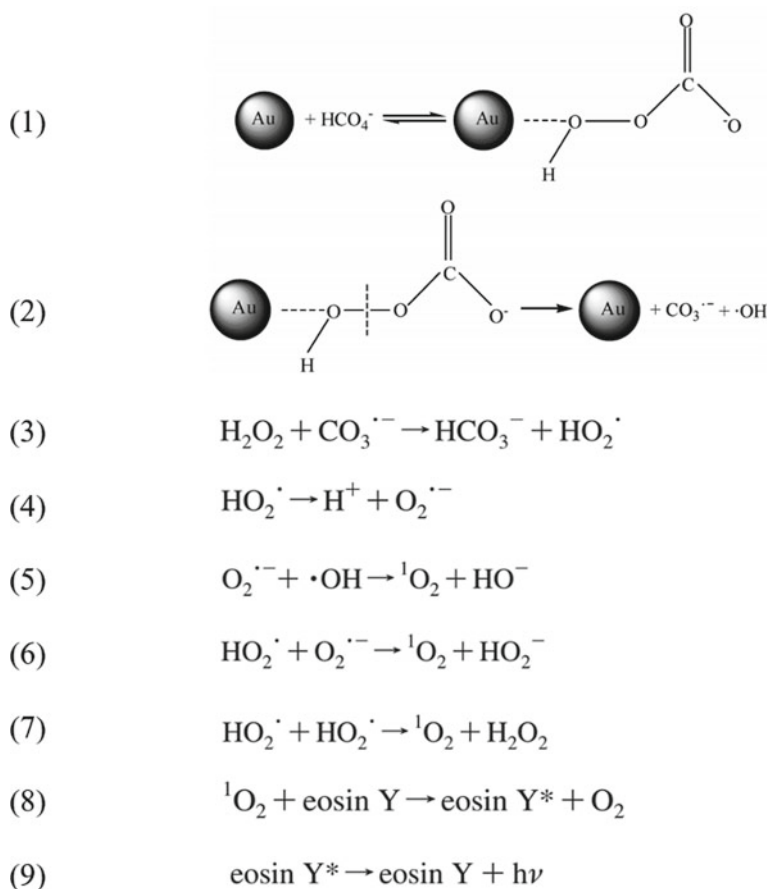
Fig. 8.8 CL mechanism for AuNP-involved HCO_4^-–eosin Y system. Reprinted with permission from Ref. [66]. Copyright 2008 American Chemical Society

In the absence of any other CL reagents, strong CL emission can be produced by direct reaction of HCO_4^- with $AuCl_4^-$ [67]. HCO_4^- acted a reducing agent in the $AuCl_4^- - HCO_4^-$ reaction to form AuNPs, and then homolysis of HCO_4^- occurred in O–O bond. The surface gold atoms were oxidized by the generated $CO_3^{\bullet -}$ adsorbed on the AuNP surface to generate excited Au(I) complexes intermediates, which could emit light. BPA was found to inhibit the $AuCl_4^- - HCO_4^-$ CL, and the degree of signal inhibition could indicate the content of BPA. Harsh conditions were needed for preparing AuNPs by on-line reduction of $HAuCl_4$ by HCO_4^-. On the other hand, very low concentration of AuNPs can be produced, resulting in an unsatisfactory detection limit (80 nM). Instead of the on-line synthesized AuNPs, nonionic fluorosurfactant molecules (FSN)-capped AuNPs, which was more stable than the citrate-capped AuNPs, were used in the $Co^{2+} - HCO_4^-$ CL system [68]. Compared with the AuNPs synthesized on line, the FSN-capped AuNPs owned high reproducibility and stability, and a lower detection limit (10 nmol·L^{-1}) for BPA was obtained.

Based on acceleration of the homolysis of the peroxo O–O bond by AuNPs, the application of AuNPs in H_2O_2-related ROS CL systems has been investigated [69]. FSN-capped AuNPs were used in the H_2O_2–Co^{2+}–$NaHCO_3$ and H_2O_2–Co^{2+}–NaOH CL systems. The introduction of FSN-capped AuNPs could increase in CL intensity in both systems, and two emission bands were observed at 430–450 nm and 490–550 nm. When FSN-capped AuNPs with a diameter of 14 nm were added into H_2O_2–Co^{2+}–NaOH solution, •OH radicals were generated from the decomposition of H_2O_2 on the AuNP surface. In alkaline solutions, a series of reactions initiated by •OH radicals promote the formation of $(O_4)^*$, forming a CL band at 490–550 nm.

In addition, $O_2^{\bullet -}$ radicals formed by the reaction of •OH radical with HO_2^- oxidized gold on the AuNP surface to produce excited Au(I) complexes, which emitted light at 430–450 nm. In the H_2O_2–Co^{2+}–$NaHCO_3$ system, •OH was generated through the reaction between HCO_4^- with Co^{2+}, followed by the $(O_4)^*$ generation in the same way with H_2O_2–Co^{2+}–NaOH system. On the other hand, •OH reacted with CO_3^{2-} to generate $CO_3^{\bullet -}$ adsorbed on the AuNP surface, thus forming the excited $(CO_2)_2^*$, which produced light emission at 430–450 nm. Due to the protection of the FSN ligand toward the gold core, FSN-capped AuNPs showed great potentials for the construction of sensitive CL systems at a wide pH range or high salt concentration. For instance, the FSN-capped AuNPs (pH = 10.2) were applied as a sensitizer in the CO_3^{2-}–ONOOH CL system at high salt condition (the concentration of Na_2CO_3 was 0.3 M) [70]. The CL mechanism can be summarized as shown in Fig. 8.9 [70]. When NaOH was added dropwise into the AuNP colloidal solution, gold complexes would be formed on the AuNP surface. The hydrophilic heads of FSN molecules could be adsorbed on AuNP surface to form a micelle layer, which was able to stabilize active intermediates in the CL reaction, thus improving the CL quantum yield. The FSN ligands on the AuNP surface could be displaced by $CO_3^{\bullet -}$ generated by the reaction of •OH and CO_3^{2-}. The adjacent $CO_3^{\bullet -}$ interact to form $(CO_2)_2^*$, thus producing CL emission at 430–450 nm.

The strategy of using AuNPs to enhance CL has also been applied in some other weak CL systems [71, 72]. Yu et al. proposed AuNP could strongly improve the
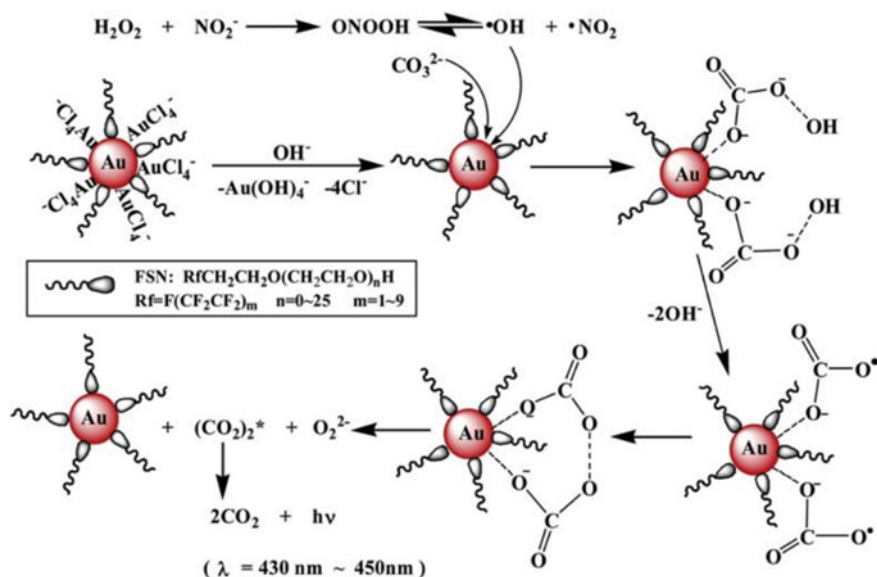
Fig. 8.9 CL mechanism for the FSN-capped AuNP–ONOOH–carbonate system. Reprinted with permission from Ref. [70]. Copyright 2011 Royal Society of Chemistry

CL intensity of Ce(IV)– Na_2SO_3 due to facilitating effect of AuNPs for the radical generations [72]. In addition to being a catalyst, AuNPs can also act as reducing agents in CL reaction. In acidic conditions, small-sized AuNPs (<6 nm) was able to rapidly react with $KMnO_4$ to form excited $Mn(II)^*$, while larger AuNPs had no such effect, indicating that the chemical reactivities of AuNPs were closely dependent on their sizes [73]. Accordingly, the acid $KMnO_4$ CL system could be used to detect AuNPs with size less than 6 nm, which had great application prospect in bioanalysis.

8.3 Platinum Nanoparticles-Involved CL System

As a common nano-catalyst, platinum nanoparticles (PtNPs) have been widely used in petroleum, fuel cells, analytical sensing and other fields. The catalytic activity of PtNPs depends largely on their size and morphology, which is similar to that of AuNPs. Therefore, a great deal of research has been devoted to the development of new PtNPs with unique morphology to improve their performance and explore their application potential in more fields [73–75]. Compared with the application of AuNPs in CL enhancing, the use of PtNP-involved CL systems has been less reported [76–79].

Following the report that AuNPs can be used to enhance the CL of luminol– H_2O_2, PtNPs have also been successfully applied to catalyze the luminol− H_2O_2 CL
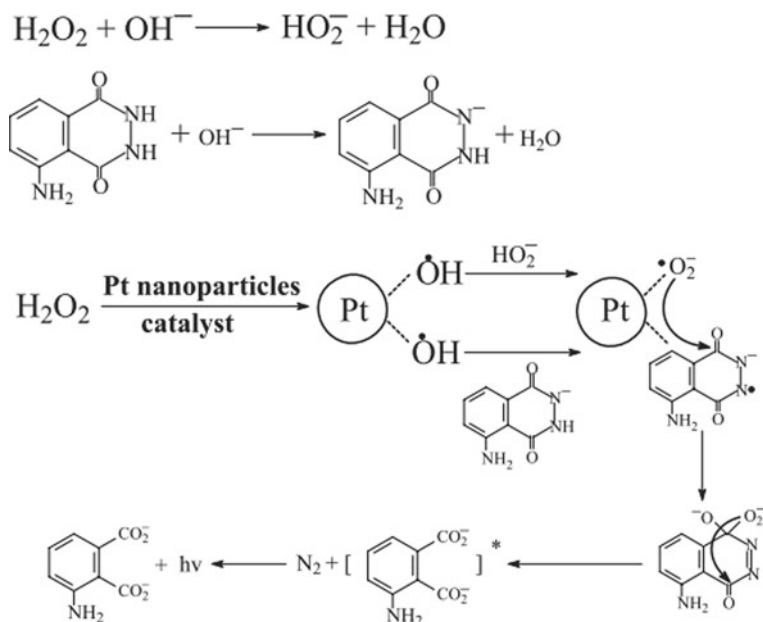
Fig. 8.10 Possible CL mechanism for the PtNP-enhanced luminol–H_2O_2 system. Reprinted with permission from Ref. [76]. Copyright 2006 John Wiley & Sons, Ltd.

in 2007 [76]. The mechanism of the PtNP-catalyzed luminol–H_2O_2 CL system was summarized in Fig. 8.10 [76]. Briefly, PtNPs-catalyzed the decomposition of H_2O_2 to generate •OH on the PtNP surface, which further reacted with HO_2^- and luminol anion to form $O_2^{\bullet -}$ and luminol radical, finally generating excited 3-aminophthalate anion, resulting in a strong CL. A photostimulated ON–OFF CL was achieved by coupling negatively charged PtNPs with a photoisomerized monolayer [77]. This strategy of combining photoelectrochemistry with CL technique provides a new idea to construct controllable CL analysis platforms.

A size-dependent catalytic activity of PtNPs on the CL reaction was observed in similar to that of AuNPs. The size-dependent catalysis of PtNPs has been investigated using PtNPs-encapsulated inside dendrimers, i.e. Pt dendrimer-encapsulated nanoparticles (DENs), whose size can be tailored with subnanometer accuracy over the range of 1–3 nm [78]. This size-sensitive catalysis was attributed to that of the chemical states that were different on the Pt DENs surface. Various oxidase substrates, including cholesterol, glucose, and choline, could be detected using the Pt DEN-catalyzed luminol CL. Owing to the peroxidase-like activity, PtNPs was able to catalyze the CL reaction of luminol in the absence of H_2O_2 [79]. The effects of PtNPs on the luminol CL were dependent on their capped agents and morphologies of PtNPs. The most intensive CL emission could be achieved by utilizing polyvinyl pyrrolidone (PVP)-capped PtNPs due to their better stability and resistance to alkaline environments.

PtNPs were commonly used as catalyst in the preparation of acetaldehyde from ethanol. Therefore, the addition of ethanol in some CL systems (e.g., lucigenin–NaOH) as a catalytic initiator could greatly improve the intensity of CL [80]. This ethanol-initiated CL system was characterized by an "induction" period, which could be controlled by altering PtNP concentration. The produced strong CL emission has great application potentials in cold light source and bioanalysis. In alkaline media, PtNPs had the ability of catalyzing the CL reaction of lucigenin–hydrazine [81]. Under the catalysis of PtNPs, hydrazine reacted with dissolved O_2 to form intermediate •OH and $O_2^{•-}$, which could oxidize lucigenin to yield strong CL ($\lambda_{max} =$ 480 nm). The CL intensity was found to be further increased by thiol-containing compounds. Thus, it is hopeful to achieve simultaneous determination of sulfur compound mixtures by the combination of highly sensitive CL detection and HPLC technique.

With the development of microfluidic chip, researchers are also exploring the combination of CL technology and microfluidic chip devices to improve reaction efficiency, response time, analysis performance and so on. By combination of PtNP-catalyzed CL (luminol–$AgNO_3$) with microfluidic chip, a CL system on the chip has been established to detect vitamin B1 (VB1) [82]. Under the catalysis of PtNPs, luminol radical was formed by the reaction of luminol and $AgNO_3$. At the same time, dissolved oxygen reacted with Vitamin C to generate $O_2^{•-}$. Reaction of the luminol radical with the $O_2^{•-}$ could form the excited 3-aminophthalate anion, thus emitting a strong CL light. The CL intensity of the luminol–$AgNO_3$–PtNPs would be improved by addition of VB1. This on-chip CL method for the VB1 detection showed a wide linear range (0.1–40 μM) and a relatively low LOD (4.8 nM).

8.4 Silver Nanoparticles-Involved CL System

In comparison with gold and platinum, silver has a lower redox potential, indicating its higher chemical activity [75, 83]. It was reported that the CL emission of the luminol–H_2O_2 would be improved by Ag nanoparticles (AgNPs) [84–87]. The CL mechanism has been proposed in Fig. 8.11 [84], electrons were transferred to H_2O_2 by the catalysis of AgNPs to generate •OH radicals, which were stabilized on the AgNP surface. HO_2^- and luminol anion were oxidized by •OH to produce $O_2^{•-}$ and luminol radicals. Luminol intermediate was generated from the reaction of $O_2^{•-}$ and luminol radicals, and finally a strong CL took place [84]. Halide ions and amino acids were able to absorb on the AgNP surface and consume reactive intermediates, thus inhibiting the CL of the AgNP-catalyzed luminol–H_2O_2. Among a variety of amino acids, cysteine displayed strongest inhibition on the CL. Based on this phenomenon, a sensitive CL method has been developed to determine cysteine [85]. Gao et al. investigated the CL intensity of Ag-$HSCH_2COOH$ or Ag-bovine serum albumin (BSA) in the presence/absence of AgNPs, and concluded that the AgNP nano-surface might be the site for the catalytic reactions [84]. The application of the proposed CL
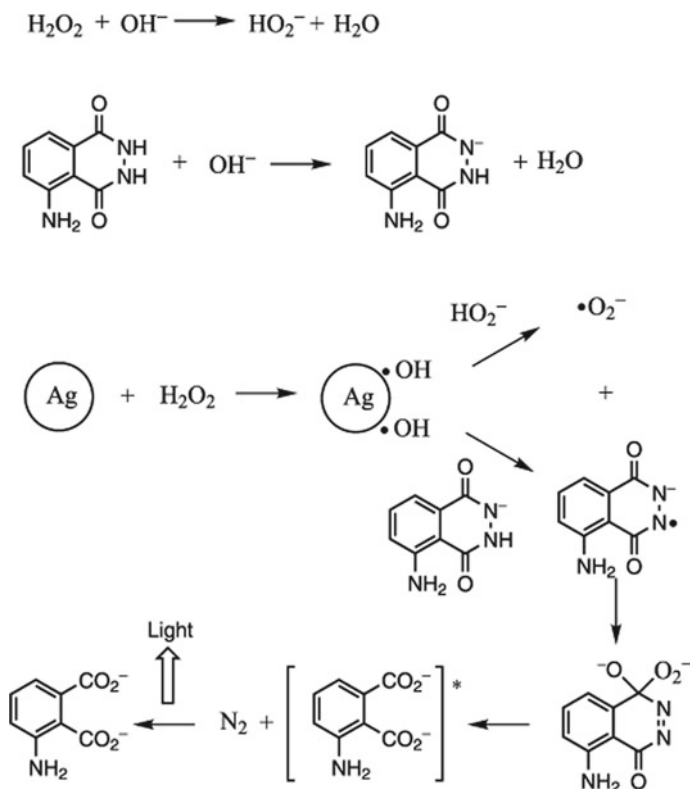
Fig. 8.11 Possible mechanism of silver nanoparticles-involved luminol CL reaction. Reprinted with permission from Ref. [84]. Copyright 2007 Elsevier Inc.

system has been expanded for the detection of isoniazid in pharmaceutical samples and nitrofurans in food safety field, as well as for pesticide discrimination [86–88].

Luminol-functionalized AgNPs could react with H_2O_2 to yield strong CL. The CL intensity and the time to appear CL or reach CL peak value could be tunable via a single experiment operation by changing reaction conditions including pH value, the H_2O_2 concentration, and addition of proteins [89]. Accordingly, a tri-channel analytical platform for protein sensing arrays has been constructed, which showed significant potential in biomedical application. Similarly, due to the catalytical action of AgNPs toward the H_2O_2 decomposition to •OH radical, AgNPs were used for some other H_2O_2-related CL systems, such as TCPO–H_2O_2 system [90, 91]. As illustrated in Fig. 8.12 [90]. •OH radical was rapidly produced by the catalysis of AgNPs, which could react with H_2O_2 to yield HO_2•. The produced HO_2• promoted the generation of an intermediate (1,2-dioxetanedione) that can transfer its high energy to nearby fluorescent dyes, such as dipyridamole (DIP) and safranin O (SO) to produce strong CL. The AgNP-catalyzed TCPO–H_2O_2 system has been utilized for pharmaceutical

$$AgNPs + H_2O_2 \longrightarrow AgNPs^+ + OH^- + \cdot OH \quad (1)$$

$$H_2O_2 + \cdot OH \longrightarrow HO_2^\bullet + H_2O \quad (2)$$

$$HO_2^\bullet + OH^- \longrightarrow O_2^{\bullet -} + H_2O \quad (3)$$

(4)

$$AgNPs^+ + O_2^{\bullet -} \longrightarrow AgNPs + H_2O \quad (5)$$

(6)

$$\text{[dioxetanedione]} + \text{dipyridamole (DIP)} \longrightarrow \text{[dioxetanedione]} \cdot DIP^{\bullet +} \quad (7)$$

(8)

$$\cdot DIP^{\bullet +} \longrightarrow CO_2 + DIP^* \quad (9)$$

$$DIP^* \longrightarrow DIP + h\nu \quad (10)$$
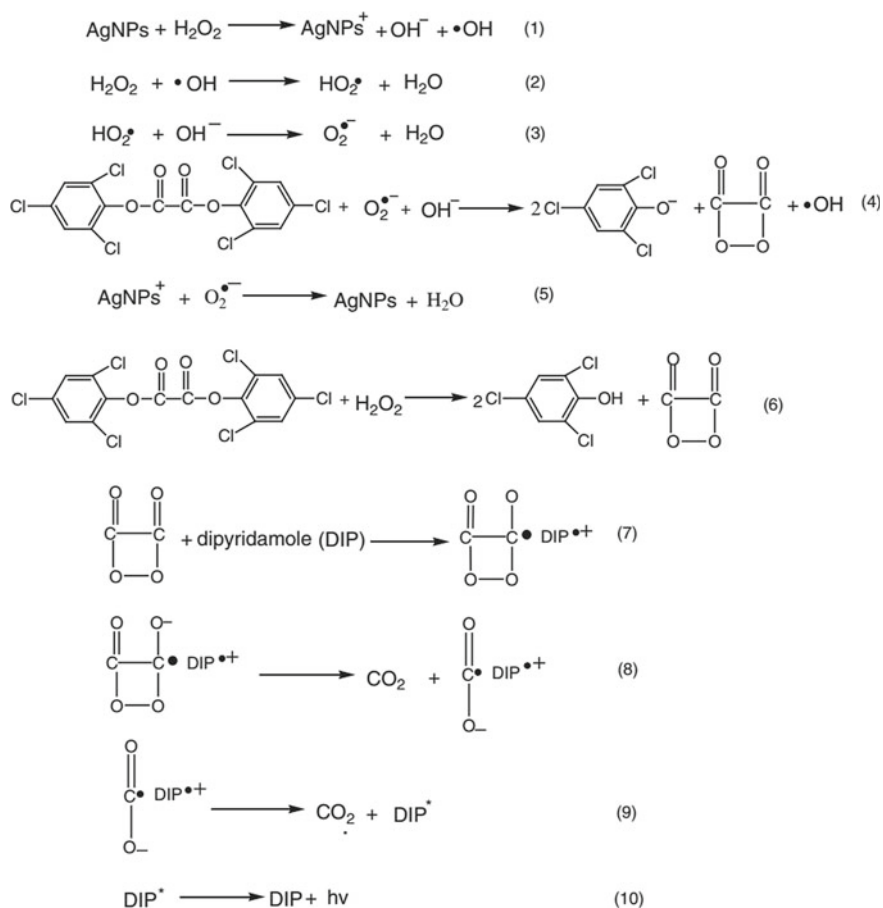
Fig. 8.12 The CL mechanism of AgNP-catalyzed TCPO–H_2O_2–dipyridamole system. Reprinted with permission from Ref. [90]. Copyright 2011 John Wiley & Sons, Ltd.

analysis, including the determination of dipyridamole and 6-mercaptopurine (6-MP) in pharmaceuticals.

AgNPs could also catalyze the CL of luminol–$AgNO_3$, following a similar principle with AuNP-catalyzed luminol–$AgNO_3$ CL system [92]. AgNPs catalyzed the oxidation of luminol by Ag^+. Excited 3-aminophthalate would be finally generated from the reaction of dissolved oxygen and the intermediate luminol radical, thus producing CL emission. In comparison with the AuNPs–luminol–$AgNO_3$ CL system, the reduction of Ag^+ on the AgNP surface was easier than that on the AuNP surface because easier deposition of Ag^0 on the AgNP surface. In addition, AgNPs showed strong enhance effect on the luminol–KIO_4 CL by addition of Co^{2+}[93]. Based on influences of organic compounds and amino acids on the CL of AgNP-catalyzed luminol system, effective CL methods were developed to measure these

compounds [93–95]. Chen et al. found that AgNPs could be oxidized to Ag^+ by $KMnO_4$. The produced Ag^+ enhanced the CL of luminol [96]. By incorporation of BPA into the luminol–$KMnO_4$–AgNPs system, the CL would be decreased, which may be attributed to the consumption of $KMnO_4$ by the oxidation of hydroxyl groups of BPA.

In the presence of Cu^{2+} and NaBr, the CL of luminol could be induced without H_2O_2 [97]. With the assistance of NaBr, the AgNPs could act as reductant to reduce $CuSO_4$. As a result, Cu(I) complex could be formed in the system, which reacted with dissolved O_2 to form $O_2^{\bullet-}$. A strong CL could be induced by the reaction between luminol and $O_2^{\bullet-}$. In this system, the Cu(I) complex was the key intermediate. It was found that AgNPs coud also catalyze the CL of luminol when other nucleophiles (e.g., hiosulfate, Cl^-, and I^-) were added into the system.

When adsorbates that can reduce the oxidation potential of the AgNPs were existed, lucigenin was able to be reduced by AgNPs and produce CL [98]. For instance, the reducing ability of AgNPs could be enhanced by iodide ion (I^-), thus inducing a stronger CL of the lucigenin–AgNPs system. In the presence of I^-, a monocation radical was generated from the reduction of lucigenin by AgNPs, which was able to react with oxygen to form $O_2^{\bullet-}$. When the monocation radical reacted with $O_2^{\bullet-}$, a strong CL occurred. Similarly, the addition of these adsorbents can also promote the reduction of AuNPs and PtNPs. However, the activity of AuNPs and PtNPs is very lower than that of AgNPs. Therefore, the CL intensity of lucigenin–AgNPs–KI system was very stronger than that of the lucigenin–AuNPs–KI system and the lucigenin–PtNPs–KI system.

It was reported that AgNPs had strong enhancement effect on the weak CL of Ce(IV)–Na_2SO_3 system [99]. Intermediate SO_2^* could be produced in the reaction of Ce(IV)–Na_2SO_3. In the presence of Tb^{3+} and norfloxacin (NFLX), the energy of SO_2^* could be transferred to Tb^{3+} via NFLX, significantly enhancing the signals of CL. When AgNPs were introduced, the CL process could be accelerated due to the electric activity of AgNPs. Consequently, CL emission of the Tb^{3+}–NFLX–Ce(IV)–Na_2SO_3 system was greatly improved. The method has been utilized to determine the NFLX in eyedrop samples with a very low detection limit (2.0 nmol·L^{-1}).

8.5 Bimetallic Nanoparticles-Involved CL System

Like the single metal nanoparticles, bimetallic nanoparticles possess interesting properties including size-dependent chemical, optical, and electrical properties. Compared with the monometallic counterparts, bimetallic nanoparticles may reveal a better catalytic effect [100, 101]. In the absence of H_2O_2, luminol could emit light by the reaction with acidic colloid of Pd/Ag bimetallic nanoparticle. Under acidic conditions, a Pd hydroperoxide species could be generated from the reaction between the Pd on the AuNP surface with dissolved oxygen [102]. Luminol could be oxidized by the formed Pd hydroperoxide species and emit light (Fig. 8.13). Switchable on–off CL emission could be achieved by simply adjusting the Pd/Ag colloid pH. The
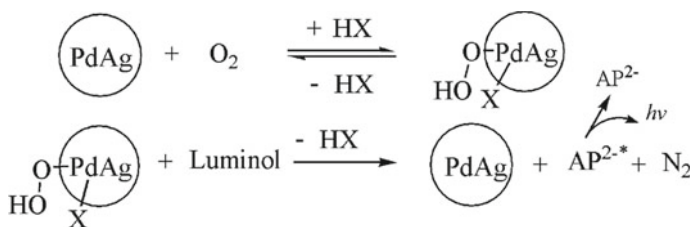
Fig. 8.13 Mechanism of the Au/Ag alloy nanoparticle-induced CL of luminol. Reprinted with permission from Ref. [102]. Copyright 2010 Royal Society of Chemistry

catalytic performance of Pd/Ag bimetal nanoparticles in the CL reaction could be regulated simply by adjusting the pH value without the assistance of functional shell on the surface. It provided a new sight for designing smart nanocatalysts.

In the presence of oxidizing agents such as H_2O_2 and $K_3Fe(CN)_6$, the luminol-based CL reactions could also be catalyzed by the bimetallic nanoparticles (e.g., silver/gold nanoalloy, Au/Pd core–shell nanoparticles and Co/Au bimetallic nanoclusters) [103–110]. Figure 8.14 showed the possible mechanism for the Au/Ag nanoalloy-catalyzed luminol–H_2O_2 CL reaction [104]. Under the catalysis of Au/Pd core-shell nanoparticles, H_2O_2 adsorbed on the nanoparticle surface decomposed to generate •OH radicals through the electron transfer process. Both luminol and HO_2^- generated from H_2O_2 were able to react with •OH and produce luminol radicals and $O_2^{•-}$, respectively. The reaction of luminol radicals and $O_2^{•-}$ would induce strong CL in the system. The proposed Au/Ag alloy nanoparticle-catalyzed luminol–H_2O_2 CL system has been successfully utilized for sensitive determination of some amino, thiol, or hydroxy group containing organic compounds and glucose [103–107].

In acid medium, Au/Ag alloy nanoparticles were capable of enhancing the CL of cerium (IV)–Rhodamine 6G(Ce(IV)–Rho6G) system [111]. Figure 8.15 showed the possible CL mechanism. Cerium (IV) could oxidize the Au/Ag alloy nanoparticles and Rhodamine 6G. During the reduction of cerium (IV), excited cerium (III)* was generated, whose energy could be accepted by Rhodamine 6G, thus leading to an intense CL. The influences of 22 organics and 17 amino acids on the CL signals of Au/Ag alloy nanoparticle–Ce (IV)–rhodamine 6G system were studied. The molecular structure (e.g., the type, number, and location of functional groups) has been found to change their effect on the Au/Ag alloy nanoparticle–Ce (IV)–rhodamine 6G system. On this basis, a CL detection method for the organics (phenols, polyphenols and amino acids) has been established.

Chaichi et al. reported that the Au/Ag alloy nanoparticles showed high enhancement effect on the TCPO–H_2O_2–Amplex red (AR) CL system [112]. The Au/Ag alloy nanoparticles could not only catalyze the decomposition of H_2O_2 but also adsorb molecules with reducing groups. Figure 8.16 showed the proposed CL reaction mechanism for this proposed system. Under the catalysis of the Au/Ag alloy nanoparticles, •OH radicals were generated and reacted with HO_2^- to form $O_2^{•-}$, which could oxidize TCPO to generate 1,2-dioxetanedione. On the other hand, the rigidity of AR

$$H_2O_2 + OH^- \longrightarrow HO_2^- + H_2O$$
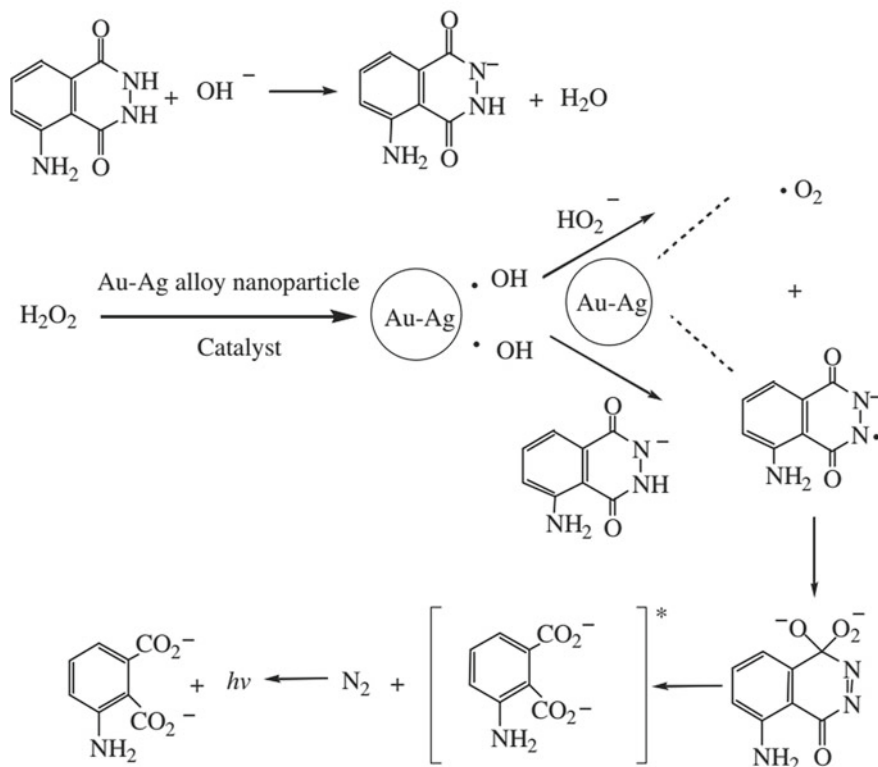
Fig. 8.14 The CL mechanism for the luminol–H_2O_2 system catalyzed by the Au/Ag alloy nanoparticles. Reprinted with permission from Ref. [104]. Copyright 2013 Elsevier B.V

molecules increased on the surface of nanoparticles, which could increase its fluorescence power, thus improving the CRET efficiency between 1,2-dioxetanedione and AR.

In addition, bimetallic nanoparticles could be used as excellent sensitizers for the ultra-weak CL system of $NaHCO_3$–H_2O_2 [113]. Lin's group proposed a simple reduction method for the preparation of BSA-capped Zn/Cu bimetal nanoclusters (Zn/Cu@BSA NCs), which were then used as catalysts for the HCO_4^--based CL reaction. The Zn/Cu@BSA NCs facilitated the generation of •OH and •CO_3^- radicals from the decomposition of HCO_4^-. Emitter intermediate $^1O_2$ ($\lambda_{max} = 634$ nm) was then produced through the reaction of H_2O_2 with the produced •OH and •CO_3^- radicals. Simultaneously, emitter intermediate $(CO_2)_2^*$ would be formed by the reaction between •OH and excess HCO_3^-, emitting light at 430–460 nm (Fig. 8.17) [113]. The optimized CL system with Zn/Cu bimetal NCs could be utilized as a highly sensitive sensor for H_2O_2 determination (LOD $= 30$ nM).

$$Ce(IV) \quad + \quad Rho\ 6G \xrightarrow[H_2SO_4]{Slow} Ce(III)^* \quad + \quad Rho\ 6G_{ox}$$

$$Ce(IV) \quad + \quad Au\text{-}Ag \xrightarrow[H_2SO_4]{Fast} Ce(III)^* \quad + \quad Ag(I) \quad + \quad Au(III)$$

$$Ce(III)^* \quad + \quad Rho\ 6G \longrightarrow Ce(III) \quad + \quad Rho\ 6G^*$$

$$Rho\ 6G^* \longrightarrow Rho\ 6G \quad + \quad hv\ (555\ nm)$$

$$Ce(III)^* \quad + \quad Rho\ 6G_{ox} \xrightarrow[Au\text{-}Ag\ Fast]{Electron\text{-}transfer} Ce(III) \quad + \quad [Rho\ 6G]^*_{ox}$$

$$[Rho\ 6G]^*_{ox} \longrightarrow [Rho\ 6G]_{ox} \quad + \quad hv\ (446\ nm)$$
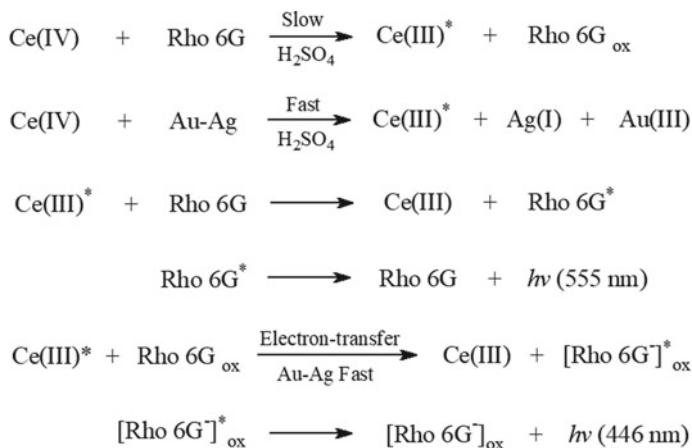
Fig. 8.15 Mechanism of the Au/Ag alloy nanoparticle–rhodamine 6G–cerium (IV) CL system. Reprinted with permission from Ref. [111]. Copyright 2009 American Chemical Society

8.6 Conclusions

In summary, we present a comprehensive overview on NMNs-involved CL systems over the last few years. It is apparent that a series of CL systems including luminol, TCPO, and ROS-induced CL, can be enhanced by NMNs. Since the catalytic effect of nanoparticles is usually dependent on their size and morphology, the mechanism for the enhancement of NMNs on CL is not unique and sometimes even contradictory results are obtained. Therefore, studying the effects of NMNs on different CL systems would improve our understanding or corroborate some possible enhancement mechanisms.

Thanks to the significantly enhanced CL signals, NMNs-involved CL methods can improve the detection sensitivity. However, there are few examples of real applications, especially in the field of bioanalysis. Although CL technology has been widely used in immunoassay, whose process is usually complex and time-consuming. The promotion and application of NMNs-involved CL systems still face great challenges. For example, in the complex systems, the application of NMNs-involved CL systems needs to simultaneously consider the sensitivity and specificity of analysis as well as the anti-interference toward complex environments. At the same time, simplifying the process of analysis and combining separation technology with CL detection to realize automatic and intelligent analysis is the current development trend.
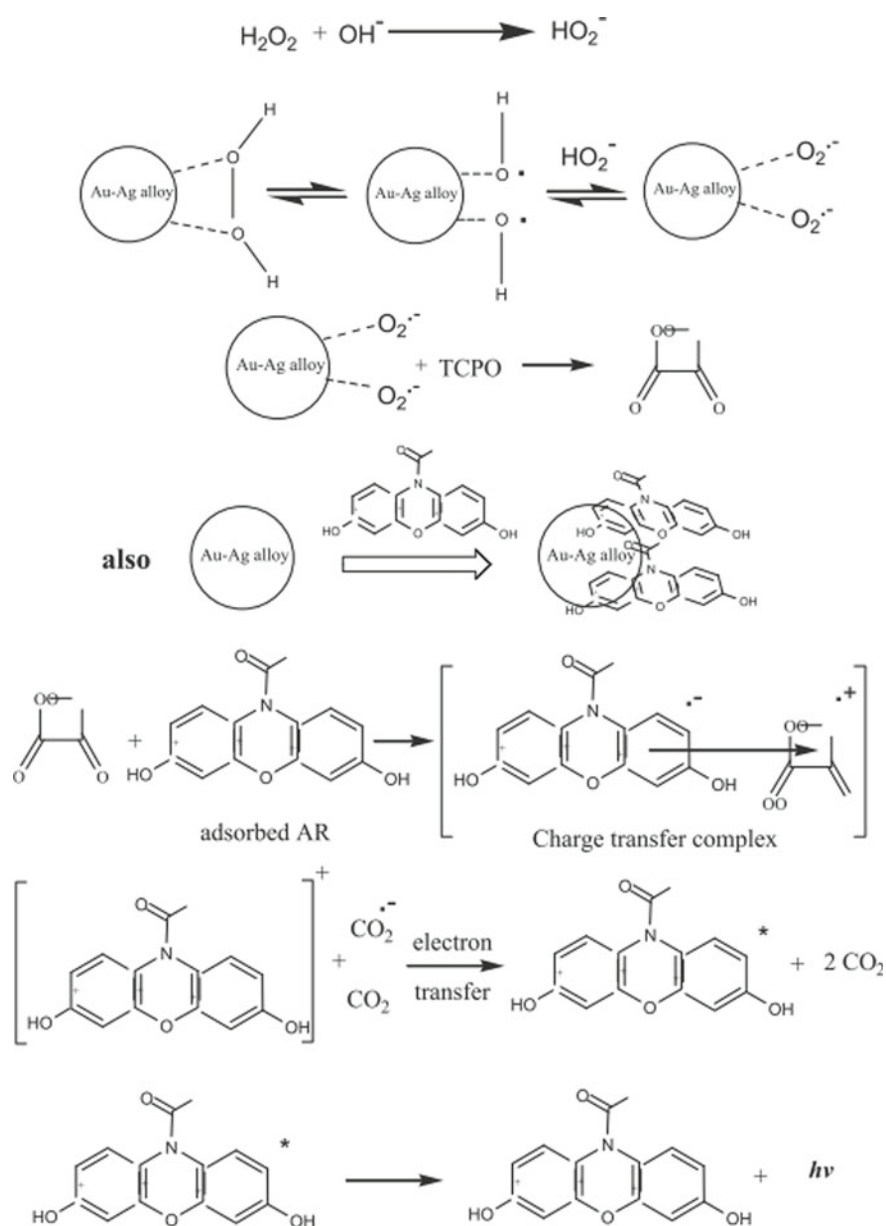
Fig. 8.16 The CL mechanism for the TCPO–H_2O_2–AR system. Reprinted with permission from Ref. [112]. Copyright 2012 Elsevier B.V
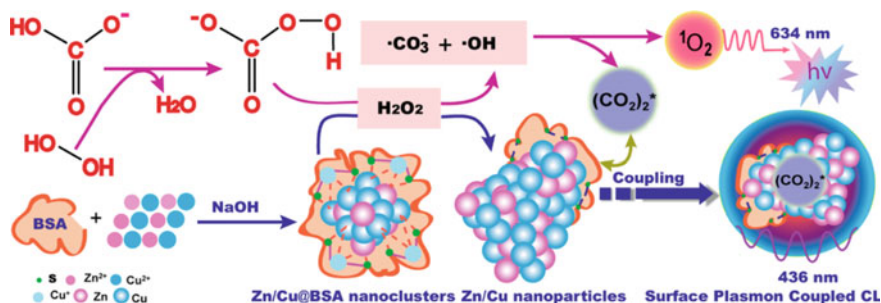
Fig. 8.17 Possible mechanism for the Zn/Cu@BSA NC-catalyzed NaHCO$_3$–H$_2$O$_2$ system. Reprinted with permission from Ref. [113]. Copyright 2015 American Chemical Society

References

1. Daniel M-C, Astruc D (2004) Gold nanoparticles: assembly, supramolecular chemistry, quantum-size-related properties, and applications toward biology, catalysis, and nanotechnology. Chem Rev 104:293–346
2. Cobley CM, Chen J, Cho EU et al (2011) Gold nanostructures: a class of multifunctional materials for biomedical applications. Chem Soc Rev 40:44–56
3. Sau TK, Rogach A (2010) Nonspherical noble metal nanoparticles: Colloid-chemical synthesis and morphology control. Adv Mater 22:1781–1804
4. Murray RW (2008) Nanoelectrochemistry: Metal nanoparticles, nanoelectrodes, and nanopores. Chem Rev 108:2688–2720
5. Peng Z, Yang H (2009) Designer platinum nanoparticles: Control of shape, composition in alloy, nanostructure and electrocatalytic property. Nano Today 4:143–164
6. Chen J, Lim B, Lee EP et al (2009) Shape-controlled synthesis of platinum nanocrystals for catalytic and electrocatalytic applications. Nano Today 4:81–95
7. Guo S, Wang E (2011) Noble metal nanomaterials: controllable synthesis and application in fuel cells and analytical sensors. Nano Today 6:240–264
8. Dreaden EC, Alkilany AM, Huang X et al (2012) The golden age: gold nanoparticles for biomedicine. Chem Soc Rev 41:2740–2779
9. Shi J, Zhu Y, Zhang X et al (2004) Recent developments in nanomaterial optical sensors. Trends Anal Chem 23(5):351–360
10. Ding S, Wang L, He Z et al (2021) Identifying exogenous DNA in liquid foods by gold nanoparticles: potential applications in traceability. ACS Food Sci Technol 1:605–613
11. Lin J-M, Yamada M (2000) Chemiluminescent reaction of fluorescent organic compounds with KHSO$_5$ using cobalt(II) as catalyst and its first application to molecular imprinting. Anal Chem 72:1148–1155
12. Lu C, Song GQ, Lin J-M (2006) Reactive oxygen species and their chemiluminescence-detection methods. Trends Anal Chem 25:985–995
13. Lin J-M, Yamada M (2003) Microheterogeneous systems of micelles and microemulsions as reaction media in chemiluminescent analysis. Trends Anal Chem 22:99–107
14. Chen J, Qiu H, Zhao S (2020) Fabrication of chemiluminescence resonance energy transfer platform based on nanomaterial and its application in optical sensing, biological imaging and photodynamic therapy. Trends Anal Chem 122:11574
15. Li QQ, Zhang LJ, Li JG et al (2011) Nanomaterial-amplified chemiluminescence systems and their applications in bioassays. Trends Anal Chem 30:401–413
16. Zhang ZF, Cui H, Lai CZ et al (2005) Gold nanoparticle-catalyzed luminol Chemiluminescence and its analytical applications. Anal Chem 77:3324–3329

17. Wang L, Yang P, Li YX et al (2007) A flow injection chemiluminescence method for the determination of fluoroquinolone derivative using the reaction of luminol and hydrogen peroxide catalyzed by gold nanoparticles. Talanta 72:1066–1072
18. Li F, Wu YY, Liu JC et al (2018) Catalyst metal ions and luminol bifunctionalized gold nanoparticles: unique chemiluminescence property for Cu(II) monitoring. J Photochem Photobiol A Chem 352:19–24
19. Qi YY, Li BX, Zhang ZJ (2009) Label-free and homogeneous DNA hybridization detection using gold nanoparticles-based chemiluiminescence system. Biosens Bioelectron 24:3581–3586
20. Islam MS, Kang SH (2011) Chemiluminescence detection of label-free C-reactive protein based on catalytic activity of gold nanoparticles. Talanta 84:752–758
21. Qi YY, Li BX (2013) Enhanced effect of aggregated gold nanoparticles on luminol chemiluminescence system and its analytical application. Spectrochim Acta A 111:1–6
22. Liu W, Luo J, Zhao M et al (2016) Effect of amino compounds on luminol-H_2O_2-gold nanoparticle chemiluminescence system. Anal Bioanal Chem 408:8821–8830
23. Li YX, Yang P, Wang P et al (2007) Development of a novel luminol chemiluminescent method catalyzed by gold nanoparticles for determination of estrogens. Anal Bioanal Chem 387:585–592
24. Liu W, Luo J, Guo YM et al (2014) Nanoparticle coated paper-based chemiluminescence device for the determination of L-cysteine. Talanta 120:336–341
25. Khajvand T, Chaichi MJ, Colagar AH (2015) Sensitive assay of hexythiazox residue in citrus fruits using gold nanoparticles-catalysed luminol-H_2O_2 chemiluminescence. Food Chem 173:514–520
26. Qi YY, Xiu FR (2016) Sensitive and rapid chemiluminescence detection of propranolol based on effect of surface charge of gold nanoparticles. J Lumin 171:238–245
27. Qi YY, He JH, Xiu FR et al (2019) A facile chemiluminescence sensing for ultrasensitive detection of heparin using charge effect of positively-charged AuNPs. Spectrochim Acta A 216:310–318
28. Lan D, Li BX, Zhang ZJ (2008) Chemiluminescence flow biosensor for glucose based on gold nanoparticle-enhanced activities of glucose oxidase and horseradish peroxidase. Biosens Bioelectron 24:934–938
29. Chaichi MJ, Ehsani MA (2016) Novel glucose sensor based on immobilization of glucose oxidase on the chitosan-coated Fe_3O_4 nanoparticles and the luminol-H_2O_2-gold nanoparticle chemiluminescence detection system. Sens Actuators B Chem 223:713–722
30. Syed LU, Swisher LZ, Huff H et al (2013) Luminol-labeled gold nanoparticles for ultrasensitive chemiluminescence-based chemical analyses. Analyst 138:5600–5609
31. Wu YC, Nie F (2015) Caspase-1 assay based on peptide and luminol labeled gold nanoparticle as chemiluminescence probe coupling magnetic separation technology. Sens Actuators B Chem 220:481–484
32. He L, Jiang ZW, Li W et al (2018) In situ synthesis of gold nanoparticles/metal-organic gels hybrids with excellent peroxidase-like activity for sensitive chemiluminescence detection of organophosphorus pesticides. ACS Appl Mater Interfaces 10:28868–28876
33. Lu C, Li QQ, Chen S et al (2011) Gold nanorod-catalyzed luminol chemiluminescence and its selective determination of glutathione in the cell extracts of saccharomyces cerevisiae. Talanta 85:476–481
34. Li QQ, Liu F, Lu C et al (2011) Aminothiols sensing based on fluorosurfactant-mediated triangular gold nanoparticle-catalyzed luminol chemiluminescence. J Phys Chem C 115:10964–10970
35. Chen QS, Bai SL, Lu C (2012) The new approach for captopril detection employing triangular gold nanoparticles-catalyzed luminol chemiluminescence. Talanta 89:142–148
36. Li QQ, Shang F, Lu C et al (2011) Fluorosurfactant-prepared triangular gold nanoparticles as postcolumn chemiluminescence reagents for high-performance liquid chromatography assay of low molecular weight aminothiols in biological fluids. J Chromatogr A 1218:9064–9070

37. Bai SL, Chen QS, Lu C et al (2013) Automated high performance liquid chromatography with on-line reduction of disulfides and chemiluminescence detection for determination of thiols and disulfides in biological fluids. Anal Chim Acta 768:96–101

38. Zhang LJ, Lu BQ, Lu C et al (2014) Determination of cysteine, homocysteine, cystine, and homocystine in biological fluids by HPLC using fluorosurfactant-capped gold nanoparticles as postcolumn colorimetric reagents. J Sep Sci 37:30–36

39. Zhang QL, Wu L, Lv C et al (2012) A novel on-line gold nanoparticle-catalyzed luminol chemiluminescence detector for high-performance liquid chromatography. J Chromatogr A 1242:84–91

40. Mu CL, Zhang Q, Wu D et al (2015) Simultaneous quantification of catecholamines in rat brain by high-performance liquid chromatography with on-line gold nanoparticle-catalyzed luminol chemiluminescence detection. Biomed Chromatogr 29:148–155

41. Mu C-L, Wu D, Lu H-F et al (2017) Simultaneous and sensitive determination of levodopa and carbidopa in pharmaceutical formulation and human serum by high performance liquid chromatography with on-line gold nanoparticles catalyzed luminol chemiluminescence detection. Chin J Anal Chem 45:e1726–e1733

42. Zhao SL, Niu TX, Song YR et al (2009) Gold nanoparticle-enhanced chemiluminescence detection for CE. Electrophoresis 30:1059–1065

43. Zhao SL, Lan XH, Liu YM (2008) Gold nanoparticles-enhanced capillary electrophoresis-chemiluminescence assay of trace uric acid. Electrophoresis 23:1–7

44. Cui H, Guo JZ, Li N et al (2008) Gold nanoparticle triggered chemiluminescence between luminol and $AgNO_3$. J Phys Chem C 112:11319–11323

45. Li N, Guo JZ, Liu B et al (2009) Determination of monoamine neurotransmitters and their metabolites in a mouse brain microdialysate by coupling high-performance liquid chromatography with gold nanoparticle-initiated chemiluminescence. Anal Chim Acta 645:48–55

46. Qi YY, He JH, Xiu FR et al (2019) A convenient chemiluminescence detection for bisphenol A in E-waste dismantling site based on surface charge change of cationic gold nanoparticles. Microchem J 147:789–796

47. Cai S, Lao KM, Lau C et al (2011) "Turn-on" chemiluminescence sensor for the highly selective and ultrasensitive detection of Hg^{2+} ions based on interstrand cooperative coordination and catalytic formation of gold nanoparticles. Anal Chem 83:9702–9708

48. Li Q, Wang JH, He Y (2016) Selective chemiluminescent sensor for detection of mercury(II) ions using non-aggregated luminol-capped gold nanoparticles. Sens Actuators B Chem 231:64–69

49. Wang ML, Kong YF, Li Y et al (2019) A chemiluminescence method for the determination of mercury(II) ions by tuning the catalytic activity of gold nanoparticles with ethylenediamine. Anal Methods 11:1317–1323

50. Kamruzzaman M, Alam AM, Kim KM et al (2013) Chemiluminescence microfluidic system of gold nanoparticles enhanced luminol-silver nitrate for the determination of vitamin B12. Biomed Microdevices 15:195–202

51. Li Q, He Y (2017) An Ultrasensitive chemiluminescence sensor for sub-nanomolar detection of manganese(II) ions in mineral water using modified gold nanoparticles. Sens Actuators B Chem 243:454–459

52. Duan CF, Cui H, Zhang ZF (2007) Size-dependent inhibition and enhancement by gold nanoparticles of luminol-ferricyanide chemiluminescence. J Phys Chem C 111:4561–4566

53. Dong YP, Gao TT, Chu XF et al (2014) Flow injection-chemiluminescence determination of ascorbic acid based on luminol-ferricyanide-gold nanoparticles system. J Lumin 154:350–355

54. Li SF, Li XZ, Xu J et al (2008) Flow-injection chemiluminescence determination of polyphenols using luminol-$NaIO_4$-gold nanoparticles system. Talanta 75:32–37

55. Zisimopoulos EG, Tsogas GZ, Giokas DL et al (2009) Indirect chemiluminescence-based detection of mefenamic acid in pharmaceutical formulations by flow injection analysis and effect of gold nanocatalysts. Talanta 79:893–899

56. Koutsoulis NP, Giokas DL, Vlessidis AG et al (2010) Alkaline earth metal effect on the size and color transition of citrate-capped gold nanoparticles and analytical implications in periodate-luminol chemiluminescence. Anal Chim Acta 669:45–52

57. Safavi A, Absalan G, Bamdad F (2008) Effect of gold nanoparticle as a novel nanocatalyst on luminol-hydrazine chemiluminescence system and its analytical application. Anal Chim Acta 610:243–248

58. Du JX, Quan JQ, Wang YD (2012) Chemiluminescence determination of timolol maleate by gold nanoparticles-catalyzed luminol-N-bromosuccinimide system. Talanta 90:117–122

59. Zhang LJ, Lu BQ, Lu C (2013) Chemiluminescence sensing of aminothiols in biological fluids using peroxymonocarbonate-prepared networked gold nanoparticles. Analyst 138:850–855

60. Halawa MI, Wu GX, Li BS (2021) Development of luminol-based chemiluminescence approach for ultrasensitive sensing of Hg(II) using povidone-I_2 protected gold nanoparticles as an efficient coreactant. Anal Bioanal Chem 413:649–659

61. Cui H, Zhang ZF, Shi MJ et al (2005) Light emission of gold nanoparticles induced by the reaction of bis(2,4,6-trichlorophenyl) oxalate and hydrogen peroxide. Anal Chem 77:6402–6406

62. Liang SX, Li HF, Lin JM (2008) Reaction mechanism of surfactant-sensitized chemiluminescence of bis(2,4,6-trichlorophyenyl) oxalate and hydrogen peroxide induced by gold nanoparticles. Luminescence 23:381–385

63. Zargoosh K, Chaichi MJ, Shamsipur M (2012) Highly sensitive glucose biosensor based on the effective immobilization of glucose oxidase/carbon-nanotube and gold nanoparticle in nafion film and peroxyoxalate chemiluminescence reaction of a new fluorophore. Talanta 93:37–43

64. Li LF, Lin D, Yang F et al (2021) Gold nanoparticle-based peroxyoxalate chemiluminescence system for highly sensitive and rapid detection of thiram pesticides. ACS Appl Nano Mater 4:3932–3939

65. Cui H, Zhang ZF, Shi MJ (2005) Chemiluminescent reactions induced by gold nanoparticles. J Phys Chem B 109:3099–3103

66. Lin JM, Liu ML (2008) Chemiluminescence from the decomposition of peroxymonocarbonate catalyzed by gold nanoparticles. J Phys Chem B 112:7850–7855

67. Lu C, Li JG, Yang Y et al (2010) Determination of bisphenol A based on chemiluminescence from gold(III)-peroxymonocarbonate. Talanta 82:1576–1580

68. Pan F, Liu L, Dong SC et al (2014) A new approach for bisphenol A detection employing fluorosurfactant-capped gold nanoparticle-amplified chemiluminescence from cobalt(II) and peroxymonocarbonate. Spectrochim Acta A 128:393–397

69. Li JG, Li QQ, Lu C et al (2011) Fluorosurfactant-capped gold nanoparticles-enhanced chemiluminescence from hydrogen peroxide-hydroxide and hydrogen peroxide-bicarbonate in presence of cobalt(II). Spectrochim Acta A 78:700–705

70. Li JG, Li QQ, Lu C et al (2011) Determination of nitrite in tap waters based on fluorosurfactant-capped gold nanoparticles-enhanced chemiluminescence from carbonate and peroxynitrous acid. Analyst 136:2379–2384

71. Zhang ZF, Cui H, Shi MJ (2006) Chemiluminescence accompanied by the reaction of gold nanoparticles with potassium permanganate. Phys Chem Chem Phys 8:1017–1021

72. Yu XJ, Bao JF (2009) Determination of norfloxacin using gold nanoparticles catalyzed cerium(IV)-sodium sulfite chemiluminescence. J Lumin 129:973–978

73. Puja P, Kumar P (2019) A perspective on biogenic synthesis of platinum nanoparticles and their biomedical applications. Spectrochim Acta A 211:94–99

74. Pedone D, Moglianetti M, De Luca E et al (2017) Platinum nanoparticles in nanobiomedicine. Chem Soc Rev 46:4951–4975

75. Mudd GM (2012) Key trends in the resource sustainability of platinum group elements. Ore Geol Rev 46:106–117

76. Xu SL, Cui H (2007) Luminol chemiluminescence catalysed by colloidal platinum nanoparticles. Luminescence 22:77–87

77. Niazov T, Shlyahovsky B, Willner I (2007) Photoswitchable electrocatalysis and catalyzed chemiluminescence using photoisomerizable monolayer-functionalized surfaces and Pt nanoparticles. J Am Chem Soc 129:6374–6375

78. Lim H, Ju Y, Kim J (2016) Tailoring catalytic activity of Pt nanoparticles encapsulated inside dendrimers by tuning nanoparticle sizes with subnanometer sccuracy for sensitive chemiluminescence-based analyses. Anal Chem 88:4751–4758

79. Zheng FJ, Ke W, Zhao Y et al (2019) Pt NPs catalyzed chemiluminescence method for Hg^{2+} detection based on a flow injection system. Electrophoresis 40:2218–2226

80. Duan CF, Cui H (2009) Time-tunable autocatalytic lucigenin chemiluminescence initiated by platinum nanoparticles and ethanol. Chem Commun 18:2574–2576

81. Liu B, He Y, Duan CF et al (2011) Platinum nanoparticle-catalyzed lucigenin-hydrazine chemiluminescence. J Photochem Photobiol A Chem 217:62–67

82. Kamruzzaman M, Alam AM, Lee SH et al (2013) Chemiluminescence microfluidic system on a chip to determine vitamin B1 using platinum nanoparticles triggered luminol-$AgNO_3$ reaction. Sens Actuators B Chem 185:301–308

83. Gorman BA, Francis PS, Dunstan DE et al (2007) Tris(2,2′-Bipyridyl)ruthenium(II) chemiluminescence enhanced by silver nanoparticles. Chem Commun 4:395–397

84. Chen H, Gao F, He R et al (2007) Chemiluminescence of luminol catalyzed by silver nanoparticles. J Colloid Interface Sci 315:158–163

85. Guo JZ, Cui H, Zhou W et al (2008) Ag nanoparticle-catalyzed chemiluminescent reaction between luminol and hydrogen peroxide. J Photochem Photobiol A Chem 193:89–96

86. Haghighi B, Bozorgzadeh S (2010) Flow injection chemiluminescence determination of isoniazid using luminol and silver nanoparticles. Microchem J 95:192–197

87. Liu W, Kou J, Jiang XL et al (2012) Determination of nitrofurans in feeds based on silver nanoparticle-catalyzed chemiluminescence. J Lumin 132:1048–1054

88. He Y, Xu B, Li WH et al (2015) Silver nanoparticle-based chemiluminescent sensor array for pesticide discrimination. J Agric Food Chem 63:2930–2934

89. He Y, He X, Liu X et al (2014) Dynamically tunable chemiluminescence of luminol-functionalized silver nanoparticles and its application to protein sensing arrays. Anal Chem 86:12166–12171

90. Wang L, Tang Y (2011) Determination of dipyridamole using TCPO-H_2O_2 chemiluminescence in the presence of silver nanoparticles. Luminescence 26:703–709

91. Biparva P, Abedirad SM, Kazemi SY (2015) Silver nanoparticles enhanced a novel TCPO-H_2O_2-safranin O chemiluminescence system for determination of 6-mercaptopurine. Spectrochim Acta A 145:454–460

92. Liu C, Li B (2011) Silver nanoparticle-initiated chemiluminescence reaction of luminol-$AgNO_3$ and its analytical application. Anal Bioanal Chem 401:229–235

93. Li SF, Wang HY, Min X et al (2014) Chemiluminescence behavior of luminol-KIO_4-Ag nanoparticles system and its analytical applications. J Biomed Sci Eng 7:307–315

94. Li S, Sun H, Wang D et al (2012) Enhanced chemiluminescence of the luminol-$AgNO_3$ system by Ag nanoparticles. Luminescence 27:211–216

95. Maddah B, Shamsi J, Barsang MJ et al (2015) The chemiluminescence determination of 2-chloroethyl ethyl sulfide using luminol-$AgNO_3$-silver nanoparticles system. Spectrochim Acta A 142:220–225

96. Chen X, Wang C, Tan X et al (2011) Determination of bisphenol A in water via inhibition of silver nanoparticles-enhanced chemiluminescence. Anal Chim Acta 689:92–96

97. Li N, Gu J, Cui H (2010) Luminol chemiluminescence induced by silver nanoparticles in the presence of nucleophiles and Cu^{2+}. J Photochem Photobiol A Chem 215:185–190

98. Guo JZ, Cui H (2007) Lucigenin chemiluminescence induced by noble metal nanoparticles in the presence of adsorbates. J Phys Chem C 111:12254–12259

99. Yu XJ, Jiang ZH, Wang QJ et al (2010) Silver nanoparticle-based chemiluminescence enhancement for the determination of norfloxacin. Microchim Acta 171:17–22

100. Lee I, Han SW, Kim K (2001) Production of Au–Ag alloy nanoparticles by laser ablation of bulk alloys. Chem Commun 1:1782–1783

101. Ibañez FJ, Zamborini FP (2008) Chemiresistive sensing of volatile organic compounds with films of surfactant-stabilized gold and gold-silver alloy nanoparticles. ACS Nano 2:1543–1552
102. Li N, Wang W, Tian DY et al (2010) PH-dependent catalytic properties of Pd-Ag nanoparticles in luminol chemiluminescence. Chem Commun 46:1520–1522
103. Li SF, Tao SJ, Wang FF et al (2010) Chemiluminescence reactions of luminol system catalyzed by nanoparticles of a gold/silver alloy. Microchim Acta 169:73–78
104. Chaichi MJ, Azizi SN, Heidarpour M (2013) A novel luminol chemiluminescent method catalyzed by silver/gold alloy nanoparticles for determination of anticancer drug flutamide. Spectrochim Acta A 116:594–598
105. Chaichi MJ, Alijanpour SO (2014) Chitosan-induced Au/Ag nanoalloy dispersed in IL and application in fabricating an ultrasensitive glucose biosensor based on luminol-H_2O_2-Cu^{2+}/IL chemiluminescence system. J Photochem Photobiol B Biol 140:41–48
106. Chaichi MJ, Alijanpour SO, Asghari S et al (2015) Evaluation of luminol chemilumines-cence based on simultaneous introducing of coumarin derivatives as green fluorophores and chitosan-induced Au/Ag alloy nanoparticle as catalyst for the sensitive determination of glucose. J Fluoresc 25:263–275
107. Yu HL, He Y (2015) Seed-assisted synthesis of dendritic Au-Ag bimetallic nanoparticles with chemiluminescence activity and their application in glucose detection. Sens Actuators B Chem 209:877–882
108. Zhang DK, Tang DL, Yamamoto T et al (2019) Improving biosynthesis of Au–Pd core-shell nanoparticles through escherichia coli with the assistance of phytochelatin for catalytic enhanced chemiluminescence and benzyl alcohol oxidation. J Inorg Biochem 199:110795
109. Gao BJ, Haghighatbin MA, Cui H (2020) Polymer-encapsulated cobalt/gold bimetallic nanoclusters as stimuli-responsive chemiluminescent nanoprobes for reactive oxygen species. Anal Chem 92:10677–10685
110. Zhang WS, Cao JT, Dong YX (2018) Enhanced chemiluminescence by Au-Ag core-shell nanoparticles: a general and practical biosensing platform for tumor marker detection. J Lumin 201:163–169
111. Li SF, Li XZ, Zhang YQ et al (2009) Enhanced chemiluminescence of the luminol-KIO_4 system by ZnS nanoparticles. Microchim Acta 167:103–108
112. Chaichi MJ, Alijanpour SO (2013) Determination of vitamin C in drugs using of an optimized novel TCPO-amplex red-gold/silver alloy nanoparticles-H_2O_2 chemiluminescence method by the box-behnken design. J Lumin 134:195–200
113. Chen H, Lin L, Li HF et al (2015) Aggregation-induced structure transition of protein-stabilized zinc/copper nanoclusters for amplified chemiluminescence. ACS Nano 9:2173–2183

Chapter 9
Semiconductor Nanoparticle-Amplified Chemiluminescence

Wenjuan Zhou and Chao Lu

Abstract Semiconductor quantum dots (QDs) is a class of extremely small nanoparticles with a diameter of $1-10$ nm. The optical and electronic properties of nanomaterials largely vary from that in the bulk. In this chapter, chemiluminescence (CL) analytical potential of QDs has been reviewed, focusing on the mechanism of the QD-based CL and prospects of their utilization in analytical chemistry. Some key QD-based nanomaterials and their CL properties developed in the fields of food analysis, pharmaceutical and clinical analysis, and environmental monitoring have been discussed. Simultaneously, we have summarized the recent advancements and applications of different kinds of QDs in the CL analysis and probed their various mechanisms. This may contribute to a deeper understanding of the role of QDs in CL and provide new strategies for the application of QDs in more fields.

Keywords Chemiluminescence · Peroxymonocarbonate · Semiconductor quantum dots · Nanomaterials · Energy transfer

9.1 Introduction

Semiconductor quantum dots (QDs) are one kind of quasi-zero-dimensional quantum structures consisted of a small number of atoms. The structure of QDs usually consists of a semiconductor metal core and a shell with a wider band gap [1–3]. They were usually constituted by atoms from groups II–VI, III–V, or IV–VI, such as CdTe [4–6], CdS [7–9], CdSe [10–12], ZnO [13, 14], PbS [15–17], CdSe/ZnS [18–20], GaAs, [21–23] and so on. Since the size of QDs directly affects the band gap level, the optical, electronic and catalytic properties of QDs can be controlled simply by adjusting their size, providing convenience for different applications. QDs display unique optical properties, including high quantum yield, wide excitation spectra

W. Zhou
Department of Chemistry, Capital Normal University, Beijing 100048, China

C. Lu (✉)
College of Chemistry, Beijing University of Chemical Technology, Beijing 100029, China
e-mail: luchao@mail.buct.edu.cn

and narrow emission spectra, accurately tuned emission wavelength, and negligible photobleaching, which make QDs widely used in photoluminescence (PL) and chemiluminescence (CL) analysis [24–27].

The QD-based CL production could be described by three possible mechanisms: direct CL from QDs, catalyzed CL by QD, and indirect CL from QDs as accepters of CL resonance energy transfer (CRET) [28]. In fact, it is difficult to figure out the CL emission in one system is originated whether from direct CL of QDs or from CRET process. In many QDs-involved CL systems, these two mechanisms may exist simultaneously. Therefore, it is a very challenging task to determine the role of QDs in CL reactions. In this chapter, we discussed the possible CL mechanisms of QDs and reviewed the recent advancements of QDs in various CL systems.

9.2 Direct Chemiluminescence

When the nanocrystals in solution are injected with both an electron and a hole simultaneously, a band edge CL from the nanocrystals can be induced [28, 29]. Semiconductor QDs can directly react with reactive oxygen species (ROS) to produce CL. The direct CL from QDs can be explained as follows: ROS produced during the redox process turn into strong oxidizing free radicals and reducing species, among them, the strong oxidizing free radicals inject holes into the HOMO of QDs, and the reducing species inject electrons into the LUMO of the QDs. As a result of the radiative recombination of electron–hole pairs, CL emission occurred (Fig. 9.1)[28].

9.2.1 QDs−H₂O₂ System

The first direct CL from QDs was observed by Talapin et al. [29] by addition of H_2O_2 to the colloid solution of CdSe/CdS (core/shell) QDs or the nanoparticulate layers. The film of CdSe/CdS nanocrystals on an F-doped SnO_2 or Pt substrate was placed into aqueous solution of KOH (0.1 mol·L^{-1}). CL emission was observed by injection

Fig. 9.1 Direct CL emission process of QDs with ROS. Reprinted with permission from Ref. [28]. Copyright 2012 Elsevier B.V.
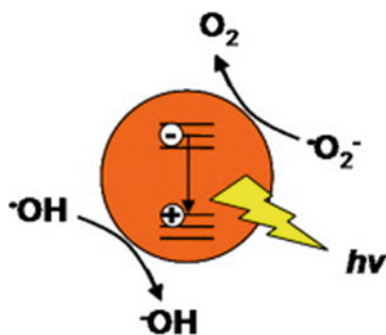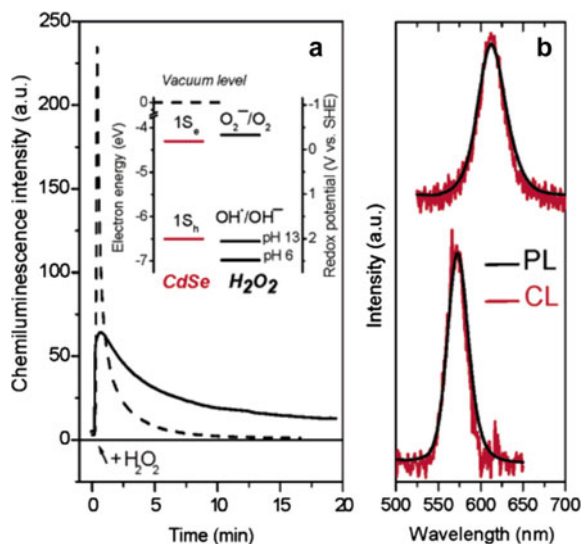
Fig. 9.2 **a** CL kinetics curve of H_2O_2-induced CL of CdSe/CdS nanocrystals in a film. **b** CL spectra of H_2O_2-induced CL of CdSe/CdS nanocrystals and PL spectra of CdSe/CdS nanocrystals in a film (black lines). Reprinted with permission from Ref. [29]. Copyright 2004 American Chemical Society

of H_2O_2 (1 M) under stirring. The H_2O_2-induced generation of CL was explained by the formation of the 1Se-1Sh exciton in CdSe/CdS QDs. Firstly, the F-doped SnO_2 or Pt substrate catalyzed the decomposition of H_2O_2 to form •OH. Subsequently, a hole injection occurred in the CdSe core and produce $CdSe(h^+_{1Sh})$/CdS. Alternatively, the H_2O_2 could react with •OH to yield $O_2^{\bullet-}$, which was able to inject an electron into the CdSe core to get $CdSe(e^-_{1Se})$/CdS (Fig. 9.2a). A band edge CL emission could be occurred through the recombination of $CdSe(h^+_{1Sh})$/CdS and $CdSe(e^-_{1Se})$/CdS (Fig. 9.2b).

The directly oxidized CL from QDs was also observed in thiol-capped QDs (e.g., thioglycolic acid-capped CdTe and CdS QDs) [30, 31]. The CL mechanism of thioglycolic acid (TGA)-capped CdTe–H_2O_2 system can be described in Fig. 9.3 [30]. Under alkaline conditions, thiols (RSH) were able to react with dissolved O_2 to generate $O_2^{\bullet-}$, which was able to convert into $^1O_2$ and •OH. The •OH and $O_2^{\bullet-}$ then injected a hole and an electron into CdTe QDs, respectively. As a result, $1S_h$ $CdTe(h^+_{1Sh})$ and $1S_e$ $CdTe(e^-_{1Se})$ exciton were produced, thus emitting light through the recombination of electron–hole pairs. Moreover, surfactants especially cationic surfactant, such as CTAB and β-CD, were found to promote CL emission of QDs. It was attributed to the formation of nanocrystal aggregates by the interaction between CTAB with TGA, which could decrease the distance between nanocrystals, thus reducing the non-radiative energy loss and promoting the generation of excited states [29]. Unlike CTAB, β-CD did not promote the aggregate formation, and its enhancement effect was mainly attributed to the inhibition of non-radiative processes by micellar nano-environment.

$$RSH \; + \; O_2 \; + \; OH^- \longrightarrow \; O_2^- \; + \; RS \; + \; H_2O$$
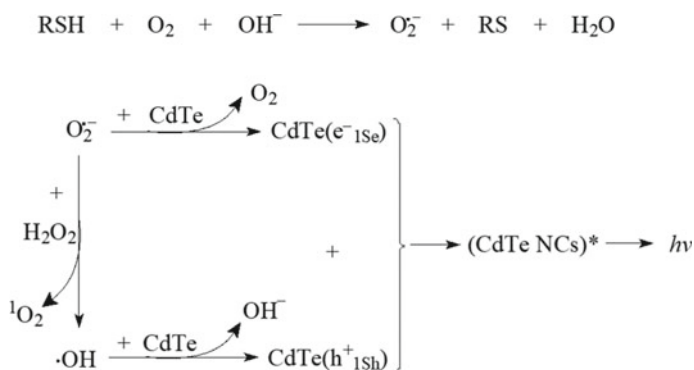
Fig. 9.3 The mechanism for the H_2O_2-induced direct CL of CdTe QDs

The CL of H_2O_2-QDs system can be further enhanced by some catalysts, such as lanthanide ions, amino acids, and horseradish peroxidase (HRP)-mimicking DNAzyme [32–35]. The addition of these substances may increase the pH value of the solution as well as promote the generation of •OH radicals, thus enhancing the CL signal. Based on these catalyzed CL reactions, the QDs-based CL system was utilized for the determination of Dy^{3+}, histidine, tryptophan, and biologic labels (HRP-mimicking DNAzyme) with high sensitivity.

On the contrary, some metal ions were found to decrease the H_2O_2-induced CL emission of the QDs because the electron transferred from QDs to metal ions [36, 37]. Thus, sensitive CL methods based on the inhibition of the H_2O_2-QDs reaction was established to detect metal ions (e.g., Hg^{2+}, Cu^{2+}, and Ag^+). Furthermore, a "turn off–on" CL method was constructed to determine glutathione (GSH) according to its recovery effect toward the Cu(II)-inhibited QDs–H_2O_2 CL system by the formation of Cu(II)–S bond, which could remove Cu(II) from the surface of QDs[38].

9.2.2 QDs−H₂O₂−NaHCO₃ System

In the H_2O_2–$NaHCO_3$ system, peroxymonocarbonate (HCO_4^-) could be generated from the H_2O_2–$NaHCO_3$ reaction. $O_2^{•-}$ and •OH radicals were then formed by the decomposition of HCO_4^-, thus inducing a band edge CL of QDs. Accordingly, mercaptoacetic acid-capped CdTe QDs were applied to improve the CL of the H_2O_2–$NaHCO_3$ system by Lin group [39]. The possible mechanism for CdTe QDs-sensitized CL reaction in the H_2O_2–$NaHCO_3$ system can be concluded in Fig. 9.4 [39]. In the H_2O_2–$NaHCO_3$–CdTe QDs system, four emitters ($CdTe^*$, $(CO_2)_2^*$, $^1O_2$, and $(O_2)_2^*$) have been detected, among which the $CdTe^*$ was generated by the hole and electron injection by the intermediate •OH and $O_2^{•-}$ radicals. The CL derived from the QDs exciton could be regulated by simple adjustment of the size of QDs,
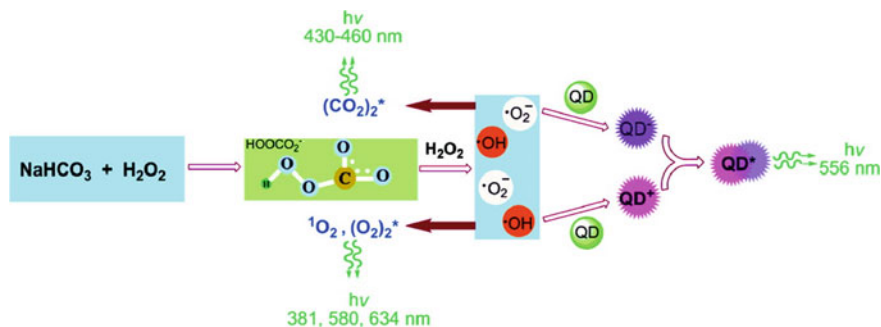
Fig. 9.4 Principle of CL in H_2O_2–$NaHCO_3$–CdTe QDs system. Reprinted with permission from Ref. [39]. Copyright 2010 American Chemical Society

which would provide promising for the further applications of QDs-based CL technique in the fields of medicine, biology, chemistry, etc. For instance, the H_2O_2–$NaHCO_3$–CdSe/CdS system has been utilized to measure ascorbic acid in human serum and epinephrine in pharmaceutical formulation with low interference and acceptable performance [40, 41].

9.2.3 QDs−KMnO$_4$ System

In the reported QDs–H_2O_2 CL systems, a high concentration of H_2O_2 were required (about 1 mol·L^{-1}), which would decompose fast in strong alkaline medium, leading an unstable CL signal. In order to improve the analytical performance, Khataee's group has developed CdS QDs-$KMnO_4$ CL system [42–46]. Recently, CL reaction of some other QDs, such as copper indium sulfide ($CuInS_2$) QDs, with $KMnO_4$ have also been demonstrated [47]. Take CdS QDs for example, $KMnO_4$ as a strong oxidizing agent had an ability to inject a hole into QDs (Reaction 9.1). At temperatures above absolute zero, electrons can be excited to high energy states (Reaction 9.2). Excitons would be generated through the electron–hole pair recombination (Reaction 9.3). When [CdS QDs]* returned to the ground state, strong light could be emitted (Reaction 9.4) [45]. In comparison with H_2O_2, $KMnO_4$ showed a stronger oxidizability, thus very intense CL signals can be obtained at a low concentration of $KMnO_4$ (0.04 mmol·Laccepts an electron from) [43, 45]. Furthermore, the energy of the formed excited QD* can transfer to some fluorescent acceptors (e.g., carminic acid and rhodamine B) [45, 46]. In the presence of meropenem, the distance between donor (QD*) and accepter (rhodamine B) increased, following a decrease in CL intensity. In the presence of meropenem, an inhibited CL was observed. Thus, a sensitive chemosensor was developed to determine meropenem in water samples [46].

$$5CdS\,QDs + 8H^+ \rightarrow 5[CdS\,QDs]^+ + Mn(II)^* + 4H_2O \qquad (9.1)$$

$$CdS\ QDs + e(\text{thermal excitation}) \rightarrow [CdS\ QDs]^- \tag{9.2}$$

$$[CdS\ QDs]^+ + [CdS\ QDs]^- \rightarrow [CdS\ QDs]^* \tag{9.3}$$

$$[CdS\ QDs]^* \rightarrow CdS\ QDs + h\upsilon \tag{9.4}$$
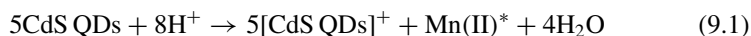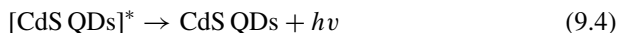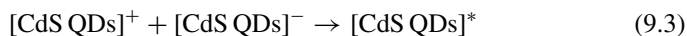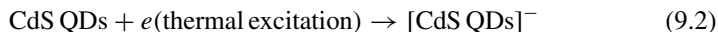
9.2.4 QDs−KIO4 System

In basic solution, periodate (KIO$_4$) is considered to be a weaker oxidizing agent than H$_2$O$_2$. Lin group investigated the CL of CdTe/CdS/ZnS QDs induced by KIO$_4$ [48]. During the injection of KIO$_4$ into the colloid solution of CdTe/CdS/ZnS QDs, a fast and strong CL was observed. The possible mechanism for KIO$_4$-induced CL of QDs could be illustrated in Fig. 9.5. In the KIO$_4$–QDs system, O$_2^{\bullet-}$ can be generated from two avenues: (1) the dissolved O$_2$ accepts an electron from QDs; (2) IO$_4^-$ reacts with the dissolved O$_2$ in an alkaline medium. The generated O$_2^{\bullet-}$ would be transformed into ^{1}O$_2$ and H$_2$O$_2$. Furthermore, •OH can be formed through the reaction of the evolved O$_2^{\bullet-}$ with H$_2$O$_2$. Then •OH injects a hole and O$_2^{\bullet-}$ injects an electron into the QDs, producing QD (h$^+_{1Sh}$) and QD (e$^-_{1Se}$) excitons. When QDs* returned to the ground state, CL occurred. If there were fluorescent acceptors (e.g., fluorescein) in the system, an efficient energy transfer would take place from the CL donor (QDs*) to the fluorescent acceptor. Some reductive substance (e.g., catechol) which could react with KIO$_4$ can be determined by using the QDs–KIO$_4$ CL system [49].
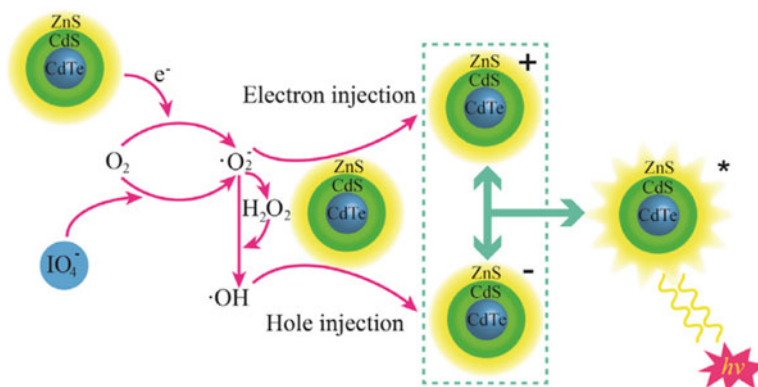
Fig. 9.5 CL mechanism for the KIO$_4$-induced CL of CdTe/CdS/ZnS QDs. Reprinted with permission from Ref. [48]. Copyright 2016 Chinese Chemical Society and Institute of Materia Medica, Chinese Academy of Medical Sciences. Published by Elsevier B.V.

9.2.5 Other QDs—ROS Systems

Among all kinds of ROS, a series of radicals could be generated from the decomposition of peroxynitrous acid/peroxynitrite (ONOOH/ONOO$^-$). ONOOH and ONOO$^-$ coexist under physiological conditions. In the ONOOH/ONOO$^-$ system, •OH and $O_2{}^{\bullet-}$ radicals would be simultaneously produced through the homolysis of ONOOH/ONOO−. Hole-injected QDs (QDs$^{\bullet+}$) were generated by the hole injections of •OH into QDs. Subsequently, CL emission occurred as a result of the electron-transfer annihilation between $O_2{}^{\bullet-}$ and QDs$^{\bullet+}$ (Fig. 9.6) [50]. Accordingly, a specific CL probe for ONOO$^-$ based on the unique character of the ONOO$^-$/ONOOH has been proposed by Lu's group and utilized in living cell systems.

When the ligands on the QD surface had the ability to donate electrons, holes would be injected into QDs by the strong oxidizing free radicals, at the same time the ligands inject electrons into the QDs, thus producing CL emission. Lu's group replaced the thioglycolic acid ligand on the CdTe QD surface with the citric acid ligand, which can be an electron donor on the surface of metal, and realized the selective determination of •OH radical in living cell systems [51]. Possible mechanism for the •OH-induced CL of citric acid-capped CdTe QDs was described in Fig. 9.7. As a result of the high redox potential of •OH among the ROS, it showed the unique property to inject holes into the CdTe core. In combination with the electron-injection ability of the citrate complex shell of the citric acid-capped CdTe QDs, excited QDs (QDs*) would be generated in the system, thus emitting light when QDs* returned to the ground state. This CL system has been used for not only the determination of exogenous •OH, but also the real-time monitoring of •OH in living cell systems.
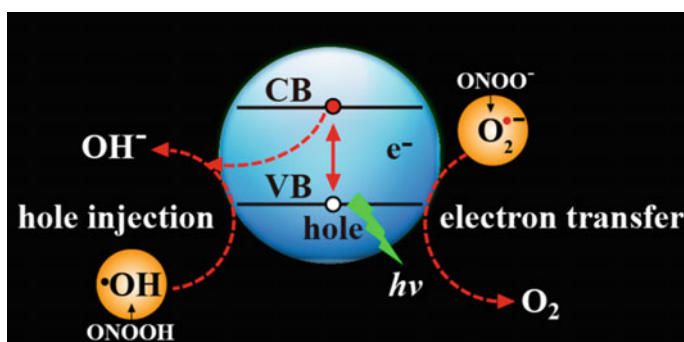
Fig. 9.6 CL mechanism for the ONOO$^-$/ONOOH-induced CL of CdTe QDs. Reprinted with permission from Ref. [50]. Copyright 2016 American Chemical Society
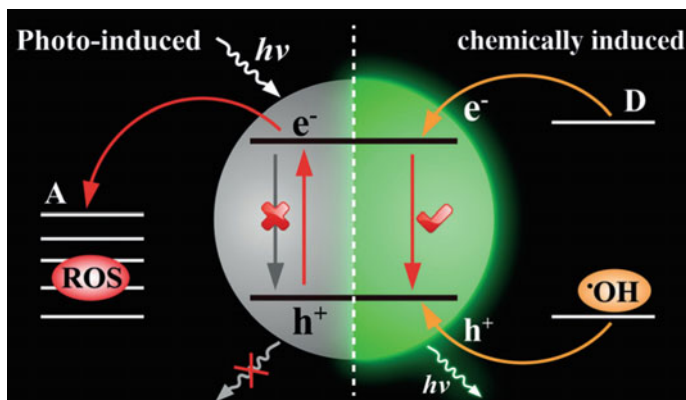
Fig. 9.7 The CL mechanism for the •OH-induced CL of citric acid-capped CdTe QDs. Reprinted with permission from Ref. [51]. Copyright © 2016 Wiley–VCH Verlag GmbH & Co. KGaA, Weinheim

9.3 Chemiluminescence Resonance Energy Transfer Acceptors

Chemiluminescence resonance energy transfer (CRET) is a process in which the CL donor delivers energy to the accepter in a non-radiative form if there is a suitable energy acceptor in the system. Efficient overlap between the emission spectra of the donor with the absorption spectra of the acceptor is necessary for the CRET process. The wide excitation spectra of QDs make them be excellent acceptors in CRET systems (Fig. 9.8)[28]. In CRET system, excited QDs (QDs*) are the emitters, which is the same as that in the direct oxidation of QDs. Therefore, it is difficult to study the CL mechanism of the QDs-involved system [28, 52]. As CRET acceptors, QDs were first used in luminol-based CL system, and then gradually extended to ROS-related CL system. It can not only regulate the emission band of the CL reaction, but also effectively enhance the weak CL signal.

Fig. 9.8 CL emission procedure with QDs as CRET acceptors. Reprinted with permission from Ref. [28]. Copyright © 2012 Elsevier B.V
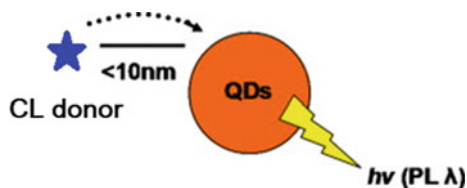
9.3.1 QDs−Luminol−H₂O₂ System

In the QDs-involved CRET systems, the efficiency of CRET is affected by the following factors: spectrum overlaps, donor–acceptor distance, the efficiency of CL reaction and the quantum yield of the QDs [28, 53]. Among them, the donor–acceptor distance was relatively easy to regulate and has been researched the most [54–57]. Ren's group first constructed an efficient CRET system using QDs as energy acceptors in 2006 [54], in which horseradish peroxidase (HRP)-catalyzed luminol–H_2O_2 CL reaction was used as energy donors. HRP could greatly catalyze the luminol–H_2O_2 CL. Since HRP was labeled on the QDs surface, the distance between the CL donor (luminol) and the energy acceptor (QDs) was decreased, resulting in an increase in CRET efficiency (Fig. 9.9a). On the other hand, bovine serum albumin (BSA) could be utilized as a linker to decrease the distance between luminol and QDs. At first, BSA was linked to CdTe QDs and the BSA antibody (anti-BSA) was conjugated
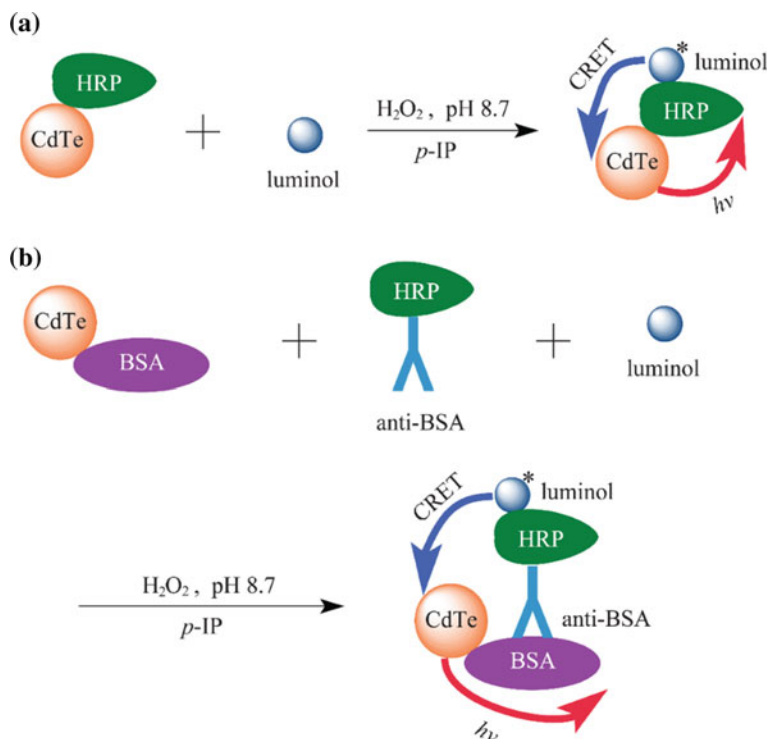
Fig. 9.9 **a** Schematic illustration of HRP-labeled CdTe QDs for the construction of luminol-based CRET system, **b** schematic illustration of BSA-linked CdTe QDs and HRP-labeled anti-BSA for the construction of luminol-based CRET system. Reprinted with permission from Ref. [54]. Copyright 2006 Wiley–VCH Verlag GmbH & Co. KGaA, Weinheim

with HRP. When the BSA-linked QDs (BSA-QDs) and HRP-labeled anti-BSA (anti-BSA-HRP) were mixed, the anti-BSA-HRP would bind to the BSA-QDs, leading to an efficient CRET (Fig. 9.9b). Through CRET, the emission band of luminol CL system can be transferred to that of the QDs, resulting a longer-wavelength emission, which provided practical strategies for the application of luminol-based CL systems in biological imaging.

Bright CL emission can be brought by tuning the conditions of CL reaction, which might be expected to be used for physical light sources. The luminol–H_2O_2 CL catalyzed by AuNPs, HRP, and p-iodophenol (PIP) has been utilized as luminescence donor to construct a photoelectrochemical analytical protocol [55]. In the system, AuNPs acted as both a carrier for luminol and a catalyst for the CL reaction. Nanocomposites of reduced graphene oxide (RGO) and CdS QDs were used to improve the photocurrent transfer efficiency. Double antibody sandwich method was used to shorten the donor–acceptor distance, thus improving CRET efficiency. Overlap of the absorption of CdS QDs with the CL emission of luminol–H_2O_2 system allowed the energy transfer between luminol–H_2O_2 and CdS QDs, achieving the photoinduced electron transfer. Electrons in the conduction band of QDs could be injected into the RGO that was modified on the FTO electrode surface to form a photocurrent. H_2O_2 in the system acted as an electron donor to inject electrons into the formed CdS QDs (h^+) to complete a cycle of photocurrent generation (Fig. 9.10) [55]. The design used CL emission instead of physical light sources for the construction of photoelectrochemical platforms, greatly simplifying the analytical instruments.

Besides the immune reaction-based strategy, aptamer has also been used to shorten the distance between HRP with QDs because it was able to specifically bind to certain
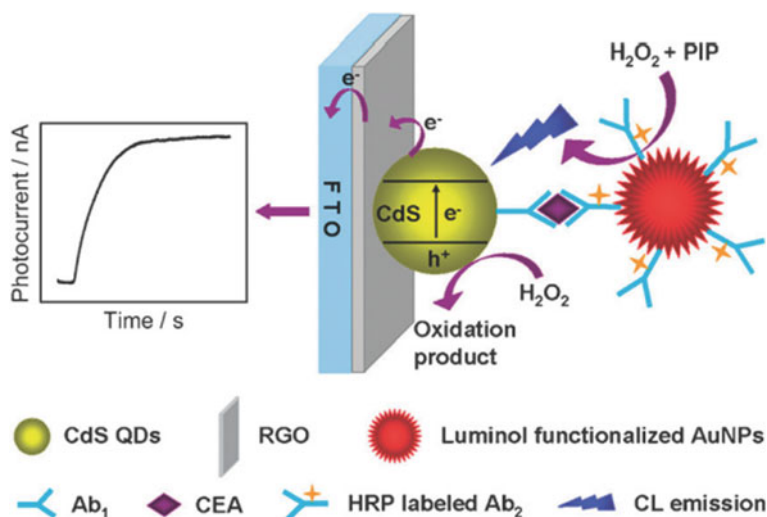
Fig. 9.10 Schematic illustration of CL source for the construction of photoelectrochemical platforms. Reprinted with permission from Ref. [55]. Copyright 2012 Royal Society of Chemistry
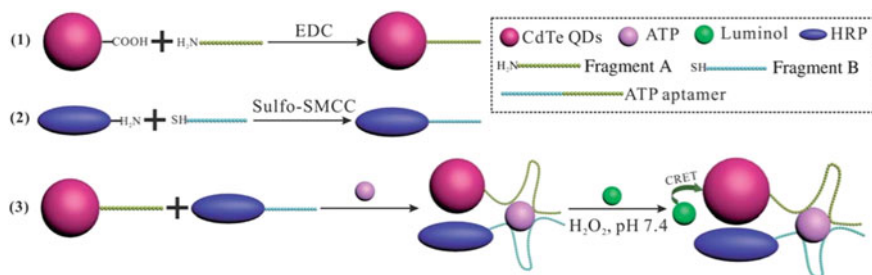
Fig. 9.11 Aptamer-based CRET system for the selective ATP detection. Reprinted with permission from Ref. [56]. Copyright 2012 Royal Society of Chemistry

targets and fold into special structures [56, 57]. As illustrated in Fig. 9.11, HRP and QDs were linked to two pieces of ssDNA cut from an adenosine aptamer, respectively [56]. These two pieces of ssDNA could be reassembled by addition of ATP to shorten the distance between HRP and QDs, promoting the occurrence of CRET. It could be utilized to selectively determine ATP in micromolar range.

To improve the efficiency of CL reaction, high concentrations of H_2O_2 were usually used, which could cause the oxidation of QDs. As a result, the luminescence of QDs was quenched, thereby inhibiting CRET performance. Bienzyme−QDs bioconjugate which could cause strong CL of luminol without addition of high concentrations of H_2O_2 has been developed as an energy acceptor for efficient CRET [58]. Oxidase and HRP were comodified onto the QDs surface for the H_2O_2 generation and luminol oxidation, respectively (Fig. 9.12). This strategy could effectively alleviate the fluorescence quenching of QDs and confine the CL reaction of luminol on the QDs surface, achieving a very high CRET efficiency (30−38%). This CRET system based on the bienzyme−QDs bioconjugate showed excellent performance for the

Fig. 9.12 Schematic illustration of CRET system based on bienzyme−QDs biconjugate. Reprinted with permission from Ref. [58]. Copyright 2016 American Chemical Society
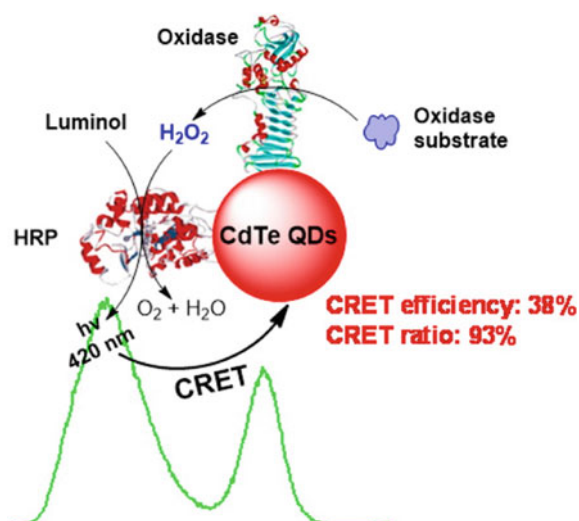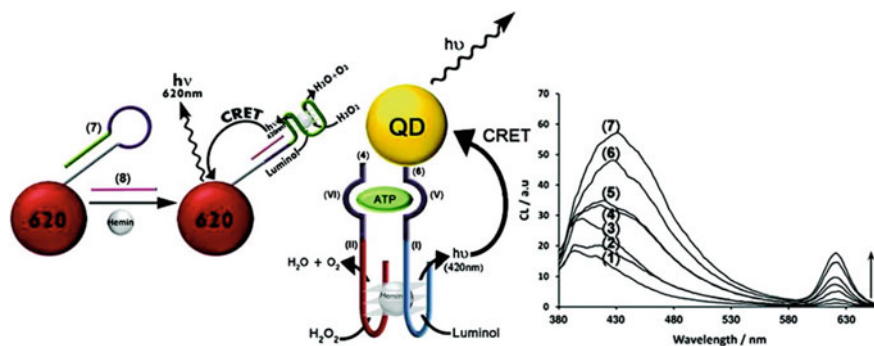
Fig. 9.13 CRET process in the QDs−luminol−H$_2$O$_2$−hemin/G-quadruplexes system. Reprinted with permission from Ref. [59]. Copyright 2011 American Chemical Society

ultrasensitive detection of various oxidase substrates such as glucose, cholesterol and benzylamine.

The hemin/G-quadruplex HRP mimicking DNAzyme has also been reported to enhance the CRET in the luminol−H$_2$O$_2$−QDs system. Willner group developed the QDs−luminol−H$_2$O$_2$ CRET systems using hemin/G-quadruplexes [59–63]. The self-assembled hemin/G-quadruplex nanostructures can be applied to detect aptamer-substrate complexes, metal ions, and DNA via CRET process between the luminol CL donor with CdSe/ZnS QDs (Fig. 9.13) [59]. The technique was able to achieve recognition of different DNA fragments by applying different sized QDs which was modified with different nucleic acids. Similarly, hemin could be bonded by different G-quadruplex aptamers to catalyze the CL reaction of luminol−H$_2$O$_2$. CRET-based biosensors for ATP and thrombin have been developed by conjugating CdSe/ZnS QDs to the nanostructures [60, 61].

In addition, they have also verified the utilization of the hemin/G-quadruplex DNAzymes in DNA machines [62]. When the molecular DNA devices were immobilized on the QDs, the DNA walker could be activated through the Hemin/G-quadruplex-catalyzed generation of photocurrents. The ON–OFF CL of QDs could be achieved by incorporating hemin into the G-quadruplex stabilized by K$^+$-ion (Fig. 9.14) [63]. The aggregation of CdSe/ZnS QDs could be induced by K$^+$-ion, which could be eliminated from the G-quadruplex by 18-crown-6-ether. Thus, the reversible ON–OFF CL of QDs could be realized through cyclic treatment by 18-crown-6-ether. By mixing two-sized QDs that were appropriately modified, the dual-wavelength ON–OFF CL of the QDs can be achieved.

9.3.2 QDs−TCPO−H$_2$O$_2$ System

Peroxyoxalate CL, as one of the nonenzyme-catalyzed CL reactions, has much higher quantum yield than the luminol-based CL system. CdTe QDs as energy acceptors
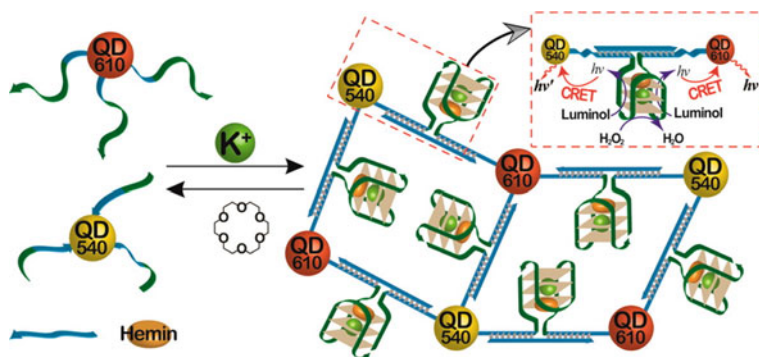
Fig. 9.14 CRET process in the QDs−luminol−H_2O_2−hemin/G-quadruplexes system. Reprinted with permission from Ref. [63]. Copyright 2014 American Chemical Society

in TCPO−H_2O_2 CL system was demonstrated in recent years [64, 65]. The mechanism for the CL emission of the CdTe QDs-involved TCPO–H_2O_2 system could be concluded in Fig. 9.15 [64]. The emitter in the CL system was demonstrated to be the excited CdTe QDs (CdTe QDs)*, which could be generated by the following two path: (1) the CRET from $C_2O_4^*$ to CdTe QDs; (2) the electron–hole annihilation of CdTe$^{•+}$ and CdTe$^{•−}$. Furthermore, CdTe QDs also acted as a catalyst for the formation of the reactive intermediates including •OH and $C_2O_4^*$, promoting the CRET and electron–hole annihilation. A significant quenching of CL intensity could be caused by phloroglucinol, thus a CL method based upon the QDs−TCPO−H_2O_2 system

Fig. 9.15 The mechanism for the CL from the CdTe QDs-involved TCPO–H_2O_2 system. Reprinted with permission from Ref. [64]. Copyright 2018 Royal Society of Chemistry
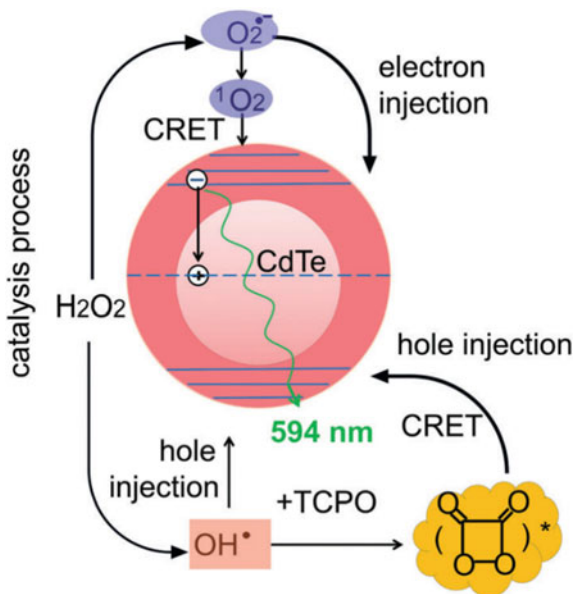
was proposed to determine phloroglucinol simply and rapidly [65]. However, the application of this peroxyoxalate CL system was limited by the low solubility and instability of peroxyoxalate in aqueous media.

9.3.3 QDs−K₃Fe(CN)₆ System

Potassium ferricyanide ($K_3Fe(CN)_6$) is a strong oxidant in alkaline solutions. It was reported that $K_3Fe(CN)_6$ was able to oxidize CdTe QDs to yield strong and stable CL [66]. The capping ligand of QDs would affect the efficiency of the QDs−$K_3Fe(CN)_6$ system. Reactions (9.5, 9.6 and 9.7) showed the possible reaction mechanism for the CL of CdTe QDs−$K_3Fe(CN)_6$ system. Under the alkaline conditions, the ligand (e.g., glutathione) of the CdTe QDs could be oxidized by $K_3Fe(CN)_6$ to form the excited intermediate (M^*), whose energy was able to transfer to the CdTe QDs to generate excited CdTe QDs (CdTe QDs)* and emit light when it returned to the ground state. Several metal ions including Hg^{2+}, Cu^{2+}, Mg^{2+}, Mn^{2+}, Ca^{2+}, Co^{2+}, Ni^{2+}, Cr^{3+} and Fe^{3+} showed remarkable inhibition effect on the CL. Simultaneous measurement of these metal ions could be realized by combining separation techniques (e.g., capillary electrophoresis) and the QDs−$K_3Fe(CN)_6$ CL system.

$$\text{ligand} + K_3Fe(CN)_6 \rightarrow M^* + K_4Fe(CN)_6 \tag{9.5}$$

$$\text{CdTe QDs} + M^* \rightarrow (\text{CdTe QDs})^* + M \tag{9.6}$$

$$(\text{CdTe QDs})^* \rightarrow \text{CdTe QDs} + h\upsilon \tag{9.7}$$
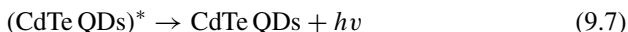
When a fluorescent dye whose absorption spectrum overlapped with the emission spectrum of the QDs existed, the energy of (CdTe QDs)* would further transfer to the fluorescent dye. An efficient energy transfer was obtained between the CL energy donor (CdTe QDs)* and the fluorescent acceptor calcein, which was further used to determine polyphenols in plant seeds [67].

9.3.4 QDs−SO₂* System

Excited sulfur dioxide molecules (SO_2^*) could be the CL emitter in some SO_3^{2-}, $S_2O_3^{2-}$, or HSO_3^- containing CL systems. The weak CL can be improved using CRET strategy by addition of fluorescent compounds which could accept the energy of SO_2^*. Usually used CL systems that can produce SO_2^* emitter include Ce (IV)−SO_3^{2-}, $KMnO_4$−$Na_2S_2O_3$, and $NaHSO_3$−H_2O_2 systems.

In acidic media, the oxidation of SO_3^{2-} by Ce (IV) would produce a weak CL, which could be increased by fluorophore compounds [68]. Li et al. firstly applied

TGA-capped CdTe QDs to improve the CL of Ce(IV)−SO$_3^{2-}$ system [69]. HSO$_3^\bullet$ radicals were formed through the oxidization of HSO$_3^-$ by Ce(IV) in the acid medium (Reaction 9.8). Two HSO$_3^\bullet$ combined to form S$_2$O$_6^{2-}$ (Reaction 9.9), which decomposed to produce excited intermediate SO$_2^*$ (Reaction 9.10). A CRET between SO$_2^*$ (donor) and QDs (acceptor) occurred (Reaction 9.11), and gave a strong CL emission when the excited (CdTe QDs)* returned to the ground state (Reaction 9.12). The QD-enhanced Ce(IV)−SO$_3^{2-}$ system has been used to determine analytes that could interact with QDs and cause an inhibition of the CL signal, such as electron transfer proteins (myoglobin, hemoglobin, and cytochrome c), gliclazide, glipizide, and cetirizine in pharmaceutical formulations [69–71]. By contrast, if there were some compounds (e.g., atropine) that could facilitate the generation of SO$_2^*$, the intensity of the QDs−Ce(IV)−SO$_3^{2-}$ CL would be enhanced [72]. Acorddingly, ultrasensitive CL detection of atropine has been realized (LOD $= 2.54 \times 10^{-10}$ mol·L^{-1}).

$$HSO_3^- + Ce(IV) \rightarrow HSO_3^\cdot + Ce(III) \tag{9.8}$$

$$2HSO_3^\cdot \rightarrow 2H^+ + S_2O_6^{2-} \tag{9.9}$$

$$S_2O_6^{2-} \rightarrow SO_2^* + SO_4^{2-} \tag{9.10}$$

$$CdTe\,QDs + SO_2^* \rightarrow (CdTe\,QDs)^* + SO_2 \tag{9.11}$$

$$(CdTe\,QDs)^* \rightarrow CdTe\,QDs + h\nu \tag{9.12}$$
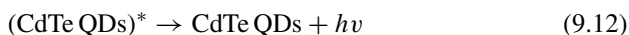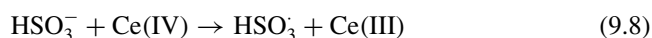
In acidic medium, Na$_2$S$_2$O$_3$ can react with KMnO$_4$ to produce weak CL due to the formation of SO$_2^*$, which can emit light at around 500 nm. If QDs whose absorption overlaps with this emission band, CRET from SO$_2^*$ to the QDs occurs. Joo group developed an enhanced CL system using L-cysteine capped CdS QDs to enhance the CL of the KMnO$_4$−Na$_2$S$_2$O$_3$ sytem [73]. The (CdS QDs)* could be generated in two path (Reaction 9.13–9.21): (1) CRET between SO$_2^*$ with CdS QDs; (2) radiative electron–hole annihilation of (CdS QDs)$^{\bullet+}$ and (CdS QDs)$^{\bullet-}$. In the presence of some compounds that can react or scavenge the generated reactive intermediates, the CL would be inhibited. Base on this, sensitive CL method was established to determine baclofen and selegiline in pharmaceutical formulation and water samples [73, 74].

$$MnO_4^- + HSO_3^- \rightarrow HSO_3^\cdot + MnO_4^{2-} \tag{9.13}$$

$$2HSO_3^\cdot \rightarrow H_2S_2O_6 \tag{9.14}$$

$$H_2S_2O_6 \rightarrow SO_2^* + H_2SO_4 \tag{9.15}$$

$$SO_2^* \rightarrow SO_2 + hv \tag{9.16}$$

$$CdS\ QDs + SO_2^* \rightarrow (CdTe\ QDs)^* + SO_2 \tag{9.17}$$

$$CdS\ QDs + MnO_4^- \rightarrow (CdS\ QDs)^{\cdot+} + MnO_4^{2-} \tag{9.18}$$

$$CdS\ QDs + HSO_3^- \rightarrow (CdTe\ QDs)^{\cdot-} + SO_3 + H^+ \tag{9.19}$$

$$(CdS\ QDs)^{\cdot+} + (CdS\ QDs)^{\cdot-} \rightarrow (CdS\ QDs)^* \tag{9.20}$$

$$(CdS\ QDs)^* \rightarrow CdS\ QDs + hv \tag{9.21}$$
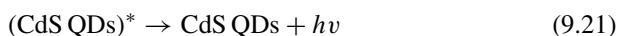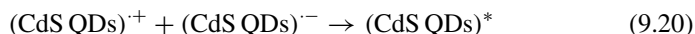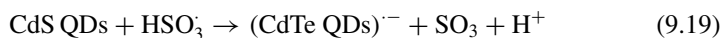
The CL system of $NaHSO_3-H_2O_2$ was also proved to generate SO_2^* during the CL reactions. Mercaptopropanoic acid-capped ZnS QDs were used to enhance the $NaHSO_3-H_2O_2$ CL under acid conditions [75]. Various ROS intermediates like $O_2^{\cdot-}$, $\cdot OH$, $SO_3^{\cdot-}$, and $SO_4^{\cdot-}$ could be formed during the CL reaction. The combination of $QDs^{\cdot+}$ and the $QDs^{\cdot-}$ could induce the CL emission of QDs. Moreover, the CL emission of the ZnS QDs would also be attributed to the CRET from SO_2^* and $^1O_2$ to the ZnS QDs (Fig. 9.16).
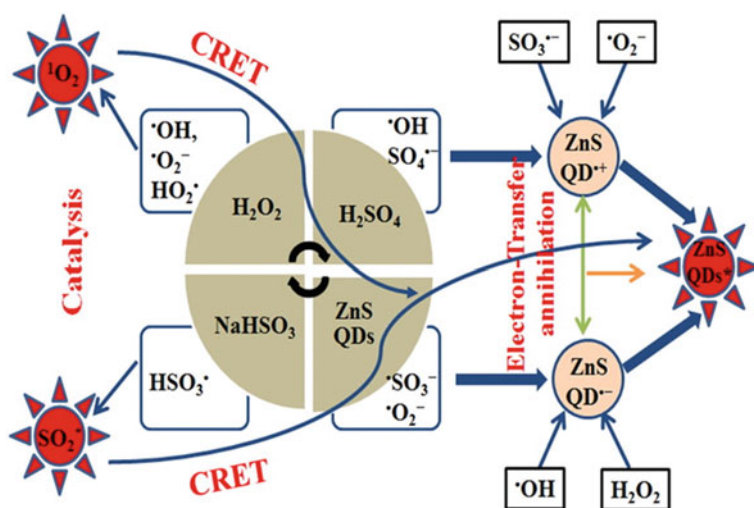
Fig. 9.16 The mechanism for the CL of the ZnS QDs−NaHSO$_3$−H$_2$O$_2$ system. Reprinted with permission from Ref. [75]. Copyright 2016 American Chemical Society

9.3.5 QDs−(CO₂)₂* System

Excited $(CO_2)_2^*$ can be generated in the $ONOOH/ONOO^- - Na_2CO_3$ or $HCO_3^- - H_2O_2$ CL system. It can rapidly decompose to CO_2 and produce ultra-weak CL ($\lambda_{max} = 400-460$ nm). In the presence of QDs that have overlapped absorption bands with the emission of the $(CO_2)_2^*$, CRET can be occured, thus significantly enhance the CL[76, 77]. The mechanism for the CdTe QDs−ONOOH−Na₂CO₃ CL could be concluded in Reactions (9.22)–(9.28) [76]. ONOOH could be prepared by the on-line reaction of nitrite and acidified H_2O_2, which could decompose into •OH and •NO₂. Then the formed •OH reacted with CO_3^{2-} to generated $CO_3^{\bullet-}$. Two $CO_3^{\bullet-}$ radicals combined to produce $(CO_2)_2^*$, which could transfer its energy to CdTe QDs. Similarly, CRET could occur in the CsSe QDs−HCO₃⁻−H₂O₂ CL system. Selective recognition of CN^- was achieved by the inhibition of gold nanoclusters and the leaching effect of CN^- on Au NCs[77].

$$HNO_2 + H_2O_2 \rightarrow ONOOH + H_2O \tag{9.22}$$

$$ONOOH \rightarrow \cdot NO_2 + \cdot OH \tag{9.23}$$

$$CO_3^{2-} + \cdot OH \rightarrow CO_3^{\cdot-} + OH^- \tag{9.24}$$

$$2CO_3^{\cdot-} \rightarrow O_2 + (CO_2)_2^* \tag{9.25}$$

$$(CO_2)_2^* \rightarrow 2CO_2 + h\nu \tag{9.26}$$

$$CdTe\ QDs + (CO_2)_2^* \rightarrow (CdTe\ QDs)^* + 2CO_2 \tag{9.27}$$

$$(CdTe\ QDs)^* \rightarrow CdTe\ QDs + h\nu \tag{9.28}$$
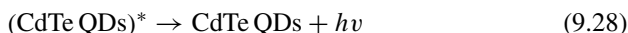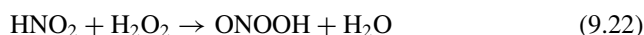
9.3.6 QDs−(O₂)₂* System

In the H_2O_2–$NaIO_4$ CL system, excited molecules $(O_2)_2^*$ are usually considered to be the CL emitter, which can also act as energy donor in CRET systems. Lin group constructed a QDs−KIO₄−H₂O₂ CRET system using Mn-doped ZnS QDs capped with molecularly imprinted polymer (MIP) as energy acceptor and H_2O_2−$NaIO_4$ as energy donor[78]. In brief, $O_2^{\bullet-}$ is produced through the reaction of H_2O_2 and $NaIO_4$. Two molecules of $O_2^{\bullet-}$ reacted to form $(O_2)_2^*$, which could transfer their energy to the QDs (Reactions 9.29, 9.30, 9.31 and 9.32). The CL performance of the

QDs was proved to be affected not only by the size of QDs, but also by their capping ligands and the silica film protection[79]. When 4-nitrophenol was added into the QDs$-$KIO$_4$$-H_2O_2$ system, 4-nitrophenol was absorbed on the QD surface, leading to fluorescence quching of the MIP-capped Mn-doped ZnS QDs. As a result, the CL intensity decreased with the addition of 4-nitrophenol. The utilization of MIPs as capping agents could endow the QDs with high selectivity, achieving specific determination of analytes.

$$H_2O_2 + IO_4^- \rightarrow O_2^{\cdot -} + IO_3 + H_2O \tag{9.29}$$

$$2O_2^{\cdot -} \rightarrow (O_2)_{2*} \tag{9.30}$$

$$QD + (O_2)_2^* \rightarrow (QD)^* + 2O_2 \tag{9.31}$$

$$(QD)^* \rightarrow QD + h\nu \tag{9.32}$$

Based on the reaction between NaClO and H$_2$O$_2$, singlet oxygen (^{1}O$_2$) was produced. The ^{1}O$_2$ was also active, which could transform to excited (^{1}O$_2$)$_2$* and act as an energy donor in CRET systems. It was found that water-soluble Mn-doped ZnS@Si QDs capped with L-cysteine were able to improve the NaClO$-$H$_2$O$_2$ CL in basic medium [80]. Figure 9.17 showed the possible mechanism for the enhancement effect of Mn-doped ZnS@Si QDs on the CL of NaClO$-$H$_2$O$_2$ system. In alkaline medium, ClO$^-$ interacted with H$_2$O$_2$ to produce ClO• and •OH radicals. The decomposition of H$_2$O$_2$ was catalyzed by Mn-doped ZnS@Si QDs to form O$_2$$^{\bullet -}$ and •OH. Then the formed O$_2$$^{\bullet -}$ interacted with the •OH and ^{1}O$_2$ was generated. Furthermore, the coupling of ClO• and •OH might produce HO$_2$Cl, which decomposed to obtain ^{1}O$_2$ and further produce the emitter intermediate (^{1}O$_2$)$_2$*. The Mn-doped ZnS@Si QDs were able to accept the energy of (^{1}O$_2$)$_2$*, thus generating excited QDs and emitting light.

9.4 Chemiluminescence Catalysts

QDs exhibit the electrical conductivity and the ability to capture electrons, thus QDs can be utilized as catalyst during the CL reactions. The valence band of the QDs can be injected a hole by a strong oxidizer and the conduction band of the QDs received an electron from a reducer (Fig. 9.18) [28]. In this manner, QDs can not only promote the radical generation to oxidize CL reagents (e.g., luminol) [52–57], but also act themselves individually as radicals[28].

$$ClO^- + H_2O_2 \longrightarrow ClO^{\cdot} + {}^{\cdot}OH + {}^-OH$$

$$^-OH + H_2O_2 \longrightarrow HO_2^- + H_2O$$
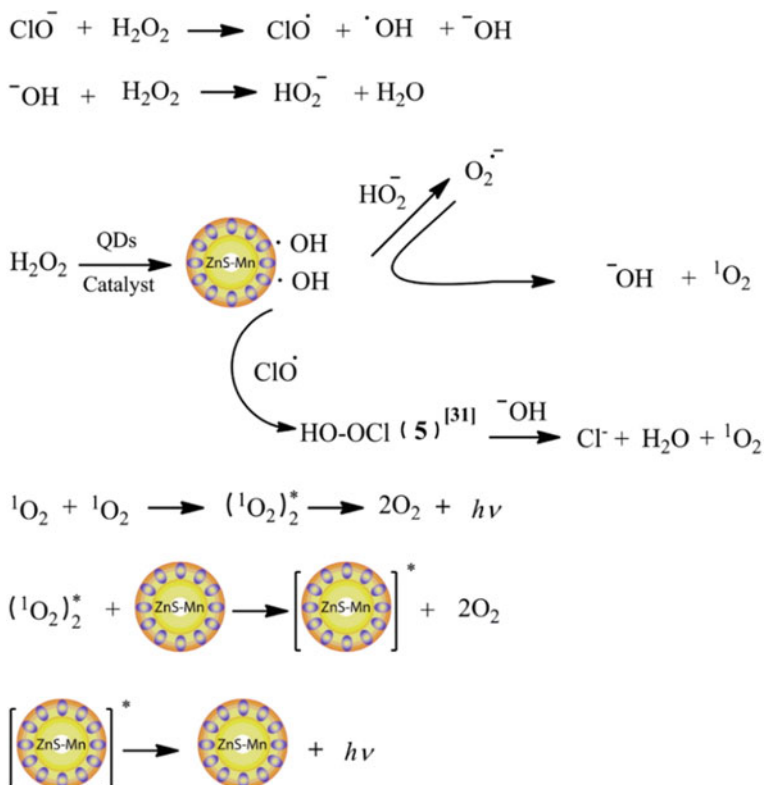
Fig. 9.17 The mechanism for the CL of NaClO−H₂O₂ system enhanced by L-cysteine capped Mn-doped ZnS@Si QDs. Reprinted with permission from Ref. [80]. Copyright 2011 Elsevier B.V.
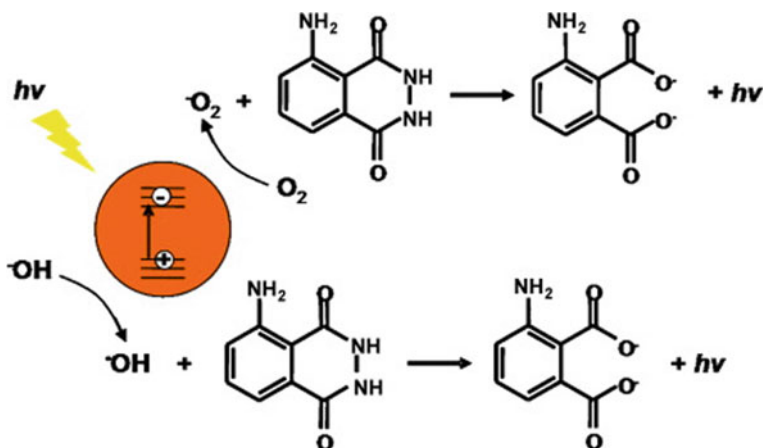
Fig. 9.18 CL emission with QDs as catalyst. Reprinted with permission from Ref. [28]. Copyright 2012 Elsevier B.V.

9.4.1 QDs−Luminol−H₂O₂ System

Semiconductor nanoparticles were proved to be able to catalyze the formation of some reactive intermediates (e.g., •OH and $O_2^{•-}$) from the decomposition of H_2O_2, enhancing CL emission of luminol−H_2O_2 system [81–83]. ZnO QDs with a diameter of 6−21 nm showed enhancement effect on the luminol−H_2O_2 CL, which might be attributed to the catalysis of ZnO QDs toward the decomposition of H_2O_2 to generate •OH and $O_2^{•-}$. Luminol could be oxidized by these radicals to generate luminol radicals, further reacting with $O_2^{•-}$ to form excited 3-aminophthalate anion, and then emitting light (Fig. 9.19) [81]. Moreover, some organic compounds containing −SH, −NH₂, and −OH groups, such as amino acid and carvedilol, were able to decrease the CL of the ZnO QDs-catalyzed luminol−H_2O_2 system [81, 82], indicating application potentials of the CL system to detect such compounds. Furthermore, the QDs-catalyzed luminol−H_2O_2 CL can be combined with separation techniques such as capillary electrophoresis to realize simultaneous determination of multiple substances[83].
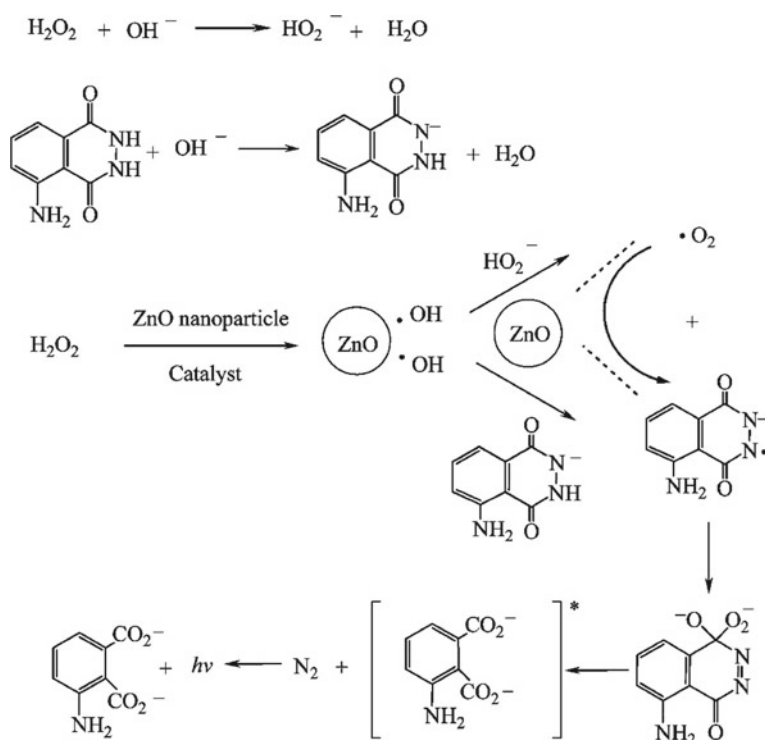
Fig. 9.19 Possible CL mechanism for the enhancement effect of the ZnO QDs on the luminol−H_2O_2 system. Reprinted with permission from Ref. [81]. Copyright 2009 American Chemical Society
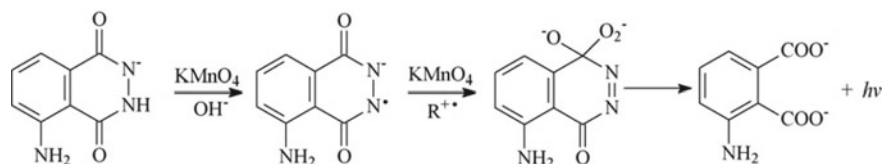
Fig. 9.20 Possible luminol CL mechanisn in the presence of CdTe QDs and $KMnO_4$. Reprinted with permission from Ref. [84]. Copyright 2008 Elsevier B.V.

9.4.2 QDs−Luminol−KMnO₄ System

It was supposed that $KMnO_4$ has the ability to oxidize QDs to form $QDs^{•+}$, or some ROS intermediates (e.g., $O_2^{•−}$ and $•OH$), which could be a sensitizer or co-oxidant in the luminol−$KMnO_4$ CL reaction [84, 85]. Li's group introduced TGA-capped CdTe QDs into the CL system of luminol−$KMnO_4$ [84]. The oxidized species of CdTe ($R^{+•}$) could accelerate the CL reaction of luminol and $KMnO_4$. Figure 9.20 showed a simple form of possible mechanism for the enhancement effect of CdTe QDs on the luminol−$KMnO_4$ system. Among several oxidants, $KMnO_4$ showed the stronger enhancement CL signals, which might be ascribed to the differences in the energy-matching degree or the oxidation ability. The application of the QDs−luminol−$KMnO_4$ system has been demonstrated to detect ascorbic acid and human IgG by a 3-channel FIA CL sandwich-type immunoassay. The phenol compounds were also detected according to the CL quenching caused by these compounds.

9.4.3 QDs−Luminol−KIO₄ System

In the absence of catalysts, KIO_4 was able to oxidize luminol to produce weak CL. The catalyst semiconductor nanoparticles (e.g., CdTe, ZnS, ZnSe) may interact with the intermediates or the reactants in luminol−KIO_4 system to produce more active oxygen-containing reactant intermediates, enhancing the CL emission [86–89]. Li's group demostrated that MA-capped ZnS QDs could increase the luminol−KIO_4 CL[86]. It was assumed that ZnS QDs could promote the radical ($•OH$ and $O_2^{•−}$) formation and the electron transfer. Moreover, the ZnS QD surface could stabilize the produced $•OH$ radicals, and thus more amount of excite 3-aminophthalate anion might be generated on the ZnS QD surface, reducing the energy loss by the collision between the solvent molecules and the excite 3-aminophthalate. Moreover, the addition of fluoroquinolones (FQs) could further dramatically increase the CL of the ZnS QDs−luminol−KIO_4 system, which might interact with ZnS QDs and participate in the reaction (Fig. 9.21) [86]. Therefore, a sensitive CL method was established to determine several fluoroquinolones with very low detection limit (10^{-10} $g·mL^{-1}$).
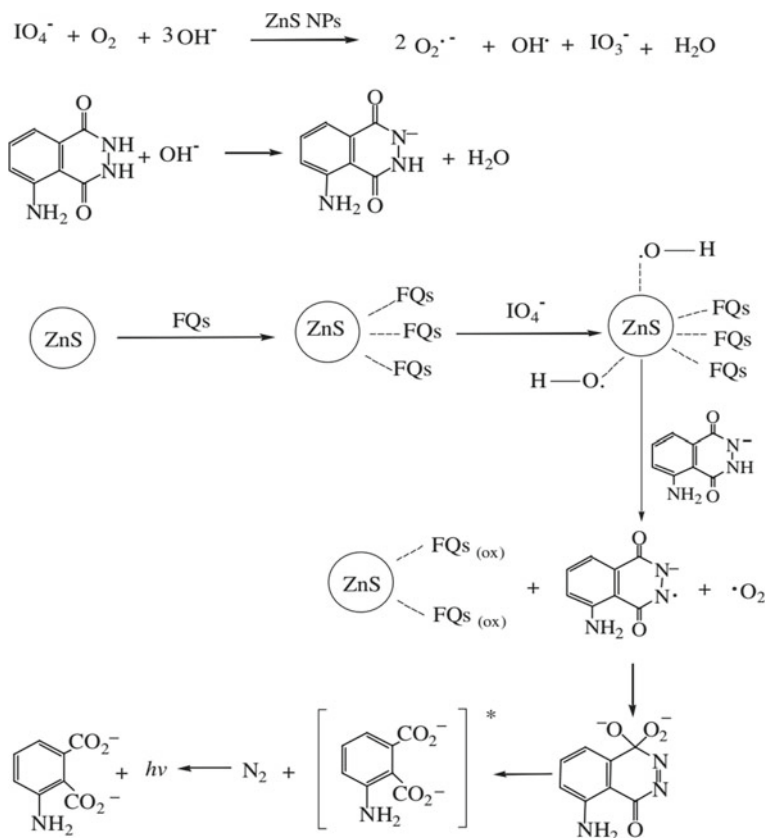
Fig. 9.21 Possible CL mechanism for the ZnS QDs$-$luminol$-$KIO$_4$ system in the presence of FQs. Reprinted with permission from Ref. [86]. Copyright 2009 Springer-Verlag

Similarlly, CdTe QDs-catalyzed luminol$-$KIO$_4$ CL was succesfully utilized to detect methionine and theophylline in pharmaceutical formulations [88, 89].

9.4.4 QDs$-$Luminol$-$K$_3$Fe(CN)$_6$ System

In the same way with the QDs$-$luminol$-$KIO$_4$ system, the catalyst ZnSe QDs was used to enhance the luminol$-$K$_3$Fe(CN)$_6$ CL [90]. The formation of O$_2^{\bullet-}$ played the key role in the ZnSe QDs$-$luminol$-$K$_3$Fe(CN)$_6$ CL system, which could promote the oxidation of luminol, thus the CL emission enhanced (Fig. 9.22). What's more, the presence of phenols could strongly inhibit the CL from ZnSe QDs$-$luminol$-$K$_3$Fe(CN)$_6$ system. Based on this inhibition, the proposed
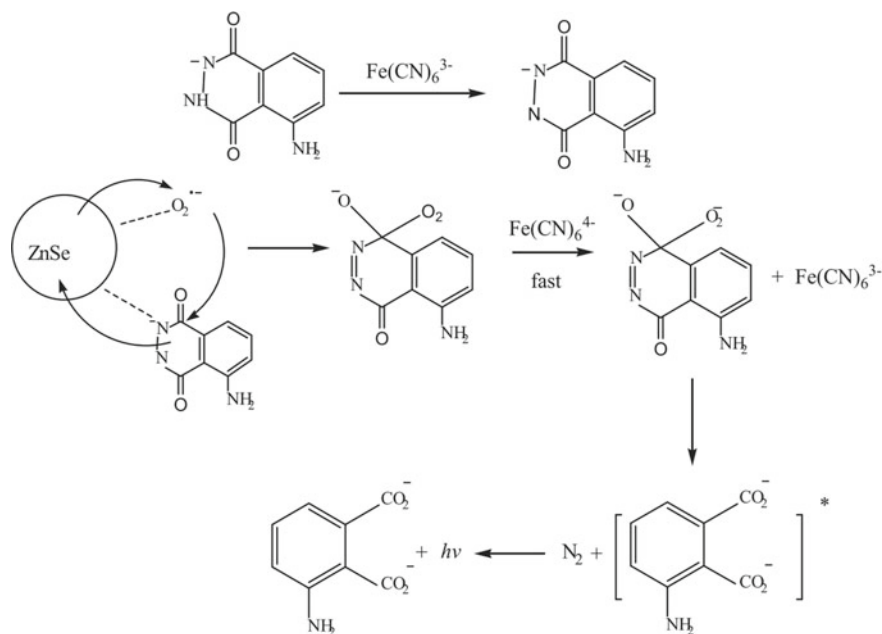
Fig. 9.22 Possible mechanism for enhancement effect of the ZnSe QDs to the luminol−$K_3Fe(CN)_6$ CL system. Reprinted with permission from Ref. [90]. Copyright 2012 Elsevier B.V

QDs−luminol−$K_3Fe(CN)_6$ system was utilized to detect three kinds of phenols in the aquatic environment.

9.5 Conclusions

In this section, we described three possible mechanisms that could explain the roles of QDs in CL reactions. According to the unique CL properties, QDs have been success-fully utilized for the development of novel optical sensors and establishment of highly selective and sensitive analytical methods. We believe that the QDs-involved CL has great potential in analytical chemistry due to its easy modification and operation. Combining the QD-sensitized CL and other techniques such as HPLC, electrochem-ical analysis to construct convenient, automatic and intelligent analysis and sensing platform is undoubtedly the future development trend.

References

1. Dios AS, Díaz-García ME (2010) Multifunctional nanoparticles: analytical prospects. Anal Chim Acta 666:1–22
2. Nehilla BJ, Allen PG, Desai TA (2008) Surfactant-free, drug-quantum-dot coloaded poly(lactide-co-glycolide) nanoparticles: towards multifunctional nanoparticles. ACS Nano 2:538–544
3. Morales-Narváez E, Montón H, Fomicheva A et al (2012) Signal enhancement in antibody microarrays using quantum dots nanocrystals: application to potential Alzheimer's disease biomarker screening. Anal Chem 84:6821–6827
4. Amelia M, Lincheneau C, Silvi S et al (2012) (2012) Electrochemical properties of CdSe and CdTe quantum dots. Chem Soc Rev 41:5728–5743
5. Wang T, Jiang X (2013) Size-dependent stability of water-solubilized CdTe quantum dots and their uptake mechanism by live HeLa cells. CS Appl Mater Interfaces 5:1190–1196
6. Jaiswal J, Sanger A, Tiwari P et al (2020) MoS_2 hybrid heterostructure thin film decorated with CdTe quantum dots for room temperature NO_2 gas sensor. Sens Actuators B Chem 305:127437
7. Wu X, Xie S, Liu C et al (2019) Ligand-controlled photocatalysis of CdS quantum dots for lignin valorization under visible light. ACS Catal 9:8443–8451
8. Shivaji K, Mani S, Ponmurugan P et al (2018) Green synthesis derived CdS quantum dots using tea leaf extract: antimicrobial, bioimaging and therapeutic applications in lung cancer cell. ACS Appl. Nano Mater 1:1683–1693
9. Wang S, Yu J, Zhao P, Guo S et al (2021) One-step synthesis of water-soluble CdS quantum dots for silver-ion detection. ACS Omega 6:7139–7146
10. Zillner E, Fengler S, Niyamakom P et al (2012) Role of ligand exchange at CdSe quantum dot layers for charge separation. J Phys Chem C 116:16747–16754
11. Washington LA, Foley ME, Cheong S et al (2012) Ostwald's rule of stages and its role in CdSe quantum dot crystallization. J Am Chem Soc 134:17046–17052
12. Fan XB, Yu S, Wang X et al (2018) Susceptible surface sulfide regulates catalytic activity of CdSe quantum dots for hydrogen photogeneration. Adv Mater 31:1804872
13. Zhang L, Yin L, Wang C et al (2010) Origin of visible photoluminescence of ZnO quantum dots: defect-dependent and size-dependent. J Phys Chem C 114:9651–9658
14. Park Y, Yoo R, Park S et al (2019) Highly sensitive and selective isoprene sensing performance of ZnO quantum dots for a breath analyzer. Sens Actuators B Chem 290:258–266
15. Nelson CA, Zhu X-Y (2012) Reversible surface electronic traps in PbS quantum dot solids induced by an order−disorder phase transition in capping molecules. J Am Chem Soc 134:7592–7595
16. Jaiswal A, Ghsoh SS, Chattopadhyay A (2012) Quantum dot impregnated-chitosan film for heavy metal ion sensing and removal. Langmuir 28:15687–15696
17. Kennehan ER, Munson KT, Doucette GS et al (2020) Dynamic ligand surface chemistry of excited PbS quantum dots. J Phys Chem C 11:2291–2297
18. Jackson BP, Bugge D, Ranville JF et al (2012) Bioavailability, toxicity, and bioaccumulation of quantum dot nanoparticles to the amphipod leptocheirus plumulosus. Environ Sci Technol 46:5550–5556
19. Barea EM, Shalom M, Gimenez S et al (2010) Design of injection and recombination in quantum dot sensitized solar cells. J Am Chem Soc 132:6834–6839
20. Zhang H, Jin Q, Song X et al (2020) Oxazine-functionalized CdSe/ZnS quantum dots for photochemical pH sensing. ACS Appl Nano Mater 3:10996–11006
21. Yakes MK, Cress CD, Tischler JG et al (2010) Three-dimensional control of self-assembled quantum dot conurations. ACS Nano 4(7):3877–3882
22. Uccelli E, Arbiol J, Morante JR et al (2010) InAs quantum dot arrays decorating the facets of GaAs nanowires. ACS Nano 4(10):5985–5993
23. Tamada A, Ota Y, Kuruma K et al (2019) Single plasmon generation in an InAs/GaAs quantum dot in a transfer-printed plasmonic microring resonator. ACS Photonics 6:1106–1110

24. Gill R, Zayats M, Willner I (2008) Semiconductor quantum dots for bioanalysis. Angew Chem Int Ed 47:7602–7625
25. Bae Y, Myung N, Bard AJ (2004) Electrochemistry and electrogenerated chemiluminescence of CdTe nanoparticles. Nano Lett 4(6):1153–1161
26. Yao J, Li L, Li P et al (2017) Quantum dots: from fluorescence to chemiluminescence, bioluminescence, electrochemiluminescence, and electrochemistry. Nanoscale 9:13364–13383
27. Song H, Su Y, Zhang L et al (2019) Quantum dots-based chemiluminescence probes: an overview. Luminescence 34:530–543
28. Frigerio C, Ribeiro DSM, Rodrigues SSM et al (2012) Application of quantum dots as analytical tools in automated chemical analysis: a review. Anal Chim Acta 735:9–22
29. Poznyak SK, Talapin DV, Shevchenko EV et al (2004) Quantum dot chemiluminescence. Nano Lett 4:693–698
30. Wang ZP, Li J, Liu B et al (2005) Chemiluminescence of CdTe nanocrystals induced by direct chemical oxidation and its size-dependent and surfactant-sensitized effect. J Phys Chem B 109:23304–23311
31. Li YX, Yang P, Wang P et al (2007) CdS nanocrystal induced chemiluminescence: reaction mechanism and applications. Nanotechnology 18:225602
32. Hosseini M, Ganjali MR, Vaezi Z et al (2014) Selective recognition of dysprosium(III) ions by enhanced chemiluminescence CdSe quantum dots. Spectrochim Acta A 121:116–120
33. Hosseini M, Ganjali MR, Jarrahi A et al (2014) Enhanced chemiluminescence CdSe quantum dots by histidine and tryptophan. Spectrochim Acta A 132:629–633
34. Hosseini M, Ganjali MR, Vaezi Z et al (2015) Selective recognition histidine and tryptophan by enhanced chemiluminescence ZnSe quantum dots. Sens Actuators B Chem 210:349–354
35. Zhang JL, Li BX (2014) Enhanced chemiluminescence of CdTe quantum dots-H_2O_2 by horseradish peroxidase-mimicking DNAzyme. Spectrochim Acta A 125:228–233
36. Li XZ, Li J, Tang JL et al (2008) Study of influence of metal ions on CdTe/H_2O_2 chemiluminescence. J Lumin 128:1229–1234
37. Sheng ZH, Han HY, Liang JG (2009) The behaviors of metal ions in the CdTe quantum dots-H_2O_2 chemiluminescence reaction and its sensing application. Luminescence 24:271–275
38. Liu LL, Ma Q, Li Y et al (2013) Detection of biothiols in human serum by QDs based flow injection "turn off-on" chemiluminescence analysis system. Talanta 114:243–247
39. Chen H, Lin L, Lin Z et al (2010) Chemiluminescence arising from the decomposition of peroxymonocarbonate and enhanced by CdTe quantum dots. J Phys Chem A 114:10049–10058
40. Chen H, Li RB, Lin L et al (2010) Determination of L-ascorbic acid in human serum by chemiluminescence based on hydrogen peroxide-sodium hydrogen carbonate-CdSe/CdS quantum dots system. Talanta 81:1688–1696
41. Azizi SN, Chaichi MJ, Shakeri P et al (2013) Determination of epinephrine in pharmaceutical formulation by an optimized novel luminescence method using CdS quantum dots as sensitizer. J Fluoresc 23:227–235
42. Khataee A, Hasanzadeh A, Lotfi R et al (2015) Determination of dexamethasone by flow-injection chemiluminescence method using capped CdS quantum dots. Spectrochim Acta A 150:63–71
43. Khataee A, Lotfi R, Hasanzadeh A et al (2016) Flow-injection chemiluminescence analysis for sensitive determination of atenolol using cadmium sulfide quantum dots. Spectrochim Acta A 157:88–95
44. Khataee A, Lotfi R, Hasanzadeh A et al (2016) A flow injection chemiluminescence method for determination of nalidixic acid based on KMnO$_4$-morin sensitized with CdS quantum dots. Spectrochim Acta A 154:243–251
45. Khataee A, Hasanzadeh A, Lotfi R et al (2016) Enhanced chemiluminescence of carminic acid-permanganate by CdS quantum dots and its application for sensitive quenchometric flow injection assays of cloxacillin. Talanta 152:171–178
46. Khataee A, Lotfi R, Hasanzadeh A (2017) A novel and sensitive chemosensor based on a KMnO$_4$-rhodamine B-CdS quantum dot chemiluminescence system for meropenem detection. Photochem Photobiol Sci 16:170–177

47. Rasoulzadeh F, Amjadi M, Ghorbani M (2020) A highly sensitive chemiluminescence assay for diniconazole by using $CuInS_2$ quantum dots. Microchem J 159: 105323.
48. Li Y, Zheng YZ, Zhang DK et al (2017) Enhanced chemiluminescence from reactions between CdTe/CdS/ZnS quantum dots and periodate. Chinese Chem Lett 28:184–188
49. Cai N, Yang DQ, He YY et al (2018) Enhanced chemiluminescence of the fluorescein–KIO_4 system by CdTe quantum dots for determination of catechol. Luminescence 33:871–876
50. Zhou WJ, Cao YQ, Sui DD et al (2016) Radical pair-driven luminescence of quantum dots for specific detection of peroxynitrite in living cells. Anal Chem 88:2659–2665
51. Zhou WJ, Cao YQ, Sui DD et al (2016) Turn-on luminescent probes for the real-time monitoring of endogenous hydroxyl radicals in living cells. Angew Chemie Int Ed 55:4236–4241
52. Sklenářová H, Voráčová I, Chocholouš P et al (2017) Quantum dots as chemiluminescence enhancers tested by sequential injection technique: Comparison of flow and flow-batch conditions. J Lumin 184:235–241
53. Wang HQ, Li YQ, Wang JH et al (2008) Influence of quantum dot's quantum yield to chemiluminescent resonance energy transfer. Anal Chim Acta 610:68–73
54. Huang XY, Li LQ, Qian HF et al (2006) A resonance energy transfer between chemiluminescent donors and luminescent quantum-dots as acceptors (CRET). Angew Chemie Int Ed 45:5140–5143
55. Tu WW, Wang WJ, Lei JP et al (2012) Chemiluminescence excited photoelectrochemistry using graphene-quantum dots nanocomposite for biosensing. Chem Commun 48:6535–6537
56. Zhou ZM, Yu Y, Zhao YD (2012) A new strategy for the detection of adenosine triphosphate by aptamer/quantum dot biosensor based on chemiluminescence resonance energy transfer. Analyst 137:4262–4266
57. Zhou ZM, Feng Z, Zhou J et al (2015) Quantum dot-modified aptamer probe for chemiluminescence detection of carcino-embryonic antigen using capillary electrophoresis. Sens Actuators B Chem 210:158–164
58. Xu SX, Li XM, Li CB et al (2016) In situ generation and consumption of H_2O_2 by bienzyme-quantum dots bioconjugates for improved chemiluminescence resonance energy transfer. Anal Chem 88:6418–6424
59. Freeman R, Liu XQ, Willner I (2011) Chemiluminescent and chemiluminescence resonance energy transfer (CRET) detection of DNA, metal ions, and aptamer-substrate complexes using hemin/G-quadruplexes and CdSe/ZnS quantum dots. J Am Chem Soc 133:11597–11604
60. Liu XQ, Freeman R, Golub E et al (2011) Chemiluminescence and chemiluminescence resonance energy transfer (CRET) aptamer sensors using catalytic hemin/G-quadruplexes. ACS Nano 5:7648–7655
61. Golub E, Niazov A, Freeman R et al (2012) Photoelectrochemical biosensors without external irradiation: Probing enzyme activities and DNA sensing using hemin/G-quadruplex-stimulated chemiluminescence resonance energy transfer (CRET) generation of photocurrents. J Phys Chem C 116:13827–13834
62. Liu XQ, Niazov-Elkan A, Wang F et al (2013) Switching photonic and electrochemical functions of a DNAzyme by DNA machines. Nano Lett 13:219–225
63. Hu LZ, Liu XQ, Cecconello A et al (2014) Dual switchable CRET-induced luminescence of CdSe/ZnS quantum dots (QDs) by the hemin/G-quadruplex-bridged aggregation and deaggregation of two-sized QDs. Nano Lett 14:6030–6035
64. Zong C, Wu J, Zang Y et al (2018) Resonance energy transfer and electron-hole annihilation induced chemiluminescence of quantum dots for amplified immunoassay. Chem Commun 54:11861–11864
65. Cai N, Yang DQ, Chen FN (2019) A novel chemiluminescence system based on bis(2,4,6-trichlorophyenyl) oxalate and hydrogen peroxide induced by CdTe QDs for determination of phloroglucinol. Microchem J 144:345–350
66. Zhang LJ, Xu CL, Li BX (2010) Chemiluminescence of CdTe quantum dots using $K_3Fe(CN)_6$ as oxidant and its capping ligand-dependent effect. Microchem J 95:186–191
67. Kang J, Li XW, Geng JY et al (2012) Determination of hyperin in seed of cuscuta chinensis lam. by enhanced chemiluminescence of CdTe quantum dots on calcein/$K_3Fe(CN)_6$ system. Food Chem 134:2383–2388

68. Li LQ, Sun HW, Chen XY (2008) Flow-injection chemiluminescence analysis of lomefloxacin in drugs and biological fluids. Curr Anal Chem 4:152–156
69. Sun CY, Liu B, Li JH (2008) Sensitized chemiluminescence of CdTe quantum-dots on Ce(IV)-sulfite and its analytical applications. Talanta 75:447–454
70. Fortes PR, Frigerio C, Silvestre CI et al (2011) Cadmium telluride nanocrystals as luminescent sensitizers in flow analysis. Talanta 84:1314–1317
71. Kouhestany RH, Azizi SN, Shakeri P et al (2016) Sensitive determination of cetirizine using CdS quantum dots as oxidase mimic-mediated chemiluminescence of sulfite. Int Curr Pharm J 5:59–62
72. Azizi SN, Chaichi MJ, Shakeri P (2013) Determination of atropine using Mn-doped ZnS quantum dots as novel luminescent sensitizers. J Lumin 144:34–40
73. Khataee A, Hasanzadeh A, Iranifam M et al (2015) A novel flow-injection chemiluminescence method for determination of baclofen using L-cysteine capped CdS quantum dots. Sens Actuators B Chem 215:272–282
74. Khataee A, Lotfi R, Hasanzadeh A et al (2016) Comparison of two methods for selegiline determination: a flow-injection chemiluminescence method using cadmium sulfide quantum dots and corona discharge ion mobility spectrometry. Spectrochim Acta A 153:273–280
75. Shah SNA, Zheng YZ, Li HF et al (2016) Chemiluminescence character of ZnS quantum dots with bisulphite-hydrogen peroxide system in acidic medium. J Phys Chem C 120:9308–9316
76. Zhang HX, Zhang LJ, Lu C et al (2012) CdTe nanocrystals-enhanced chemiluminescence from peroxynitrous acid-carbonate and its application to the direct determination of nitrite. Spectrochim Acta A 85:217–222
77. Vahid B, Hassanzadeh J, Khodakarami B (2019) CdSe quantum dots-sensitized chemiluminescence system and quenching effect of gold nanoclusters for cyanide detection. Spectrochim Acta A 212:322–329
78. Liu JX, Chen H, Lin Z et al (2010) Preparation of surface imprinting polymer capped Mn-doped ZnS quantum dots and their application for chemiluminescence detection of 4-nitrophenol in tap water. Anal Chem 82:7380–7386
79. Liu JX, Chen H, Lin L et al (2010) Sensitized chemiluminescence reaction between hydrogen peroxide and periodate of different types of Mn-doped ZnS quantum dots. Chinese Sci Bull 55:3479–3484
80. Zhou Y, Chen H, Ogawa N et al (2011) Chemiluminescence from NaClO–H$_2$O$_2$ and enhanced by L-cysteine capped Mn-doped ZnS quantum-dots. J Lumin 131:1991–1997
81. Li SF, Tao SJ, Wang FF et al (2010) Chemiluminescence reactions of luminol system catalyzed by nanoparticles of a gold/silver alloy. Microchim Acta 169:73–78
82. Biparva P, Abedirad SM, Kazemi SY (2014) ZnO nanoparticles as an oxidase mimic-mediated flow-injection chemiluminescence system for sensitive determination of carvedilol. Talanta 130:116–121
83. Zhao YS, Zhao SL, Huang JM et al (2011) Quantum dot-enhanced chemiluminescence detection for simultaneous determination of dopamine and epinephrine by capillary electrophoresis. Talanta 85:2650–2654
84. Wang ZP, Li J, Liu B et al (2009) CdTe nanocrystals sensitized chemiluminescence and the analytical application. Talanta 77:1050–1056
85. Du B, Wang T, Han S et al (2015) Determination of 2-methoxyestradiol by chemiluminescence based on luminol–KMnO$_4$–CdTe quantum dots system. Spectrochim Acta A 136:149–154
86. Li SF, Li XZ, Zhang YQ et al (2009) Enhanced chemiluminescence of the luminol-KIO$_4$ system by ZnS nanoparticles. Microchim Acta 167:103–108
87. Li SF, Zhang L, Chen L et al (2016) Determination of rutin by chemiluminescence based on a luminol-potassium periodate-ZnSe system. Anal Methods 8:4056–4063

88. Zhou M, Wang AL, Li C et al (2017) Flow-based determination of methionine in pharmaceutical formulations exploiting TGA-capped CdTe quantum dots for enhancing the luminol-KIO$_4$ chemiluminescence. J Lumin 183:206–211
89. Zhou M, Chen QQ, Wang AL et al (2019) Flow-injection chemiluminescence of the luminol–potassium periodate system enhanced by TGA–capped CdTe quantum dots for the determination of theophylline. Luminescence 34:673–679
90. Guo C, Zeng HJ, Ding XJ et al (2013) Enhanced chemiluminescence of the luminol-K$_3$Fe(CN)$_6$ system by ZnSe quantum dots and its application. J Lumin 134:888–892

Chapter 10
Layered Double Hydroxide-Amplified Chemiluminescence

Xu Teng and Chao Lu

Abstract Layered double hydroxide (LDH) materials are a kind of typical two-dimensional products, which have attracted substantial interest from academia and industry. LDHs provide a clear layered structure with high porosity, large surface area, and high interlayer anion mobility and layer charge density. In this chapter, we discuss the enhancement effect of interlayer anions or surface in LDHs on various chemiluminescence (CL) systems, including luminol-H_2O_2 system, singlet oxygen system, fenton-like system, peroxynitrous acid/peroxynitrite ($ONOOH/ONOO^-$) system and CL resonance energy transfer (CRET) system. Simultaneously, we summarize the recent advancements and applications of different kinds of LDHs in the CL analysis. The study may offer a novel strategy for more researchers to utilize LDHs for more extensive application in CL field.

Keywords Chemiluminescence · Layered double hydroxide · Luminol · Singlet oxygen · Fenton-like system · Peroxynitrous acid·peroxynitrite · Energy transfer

10.1 Introduction

Layered double hydroxides (LDHs) are well-known as hydrotalcites [1]. They are widely used in both academia and industry [2, 3]. The general preparation of LDHs is also relatively simple and economical. LDHs could be revealed as the general formula: $M_{1-x}^{II}M_x^{III}(OH)_2\left[A_{x/n}^{n-}\right] \cdot mH_2O$, where A^{n-}, M^{II} and M^{III} are the n-valent anions, di- and trivalent metal cations, respectively [4]. The structure of LDHs has been displayed as shown in Fig. 10.1. The typical and common LDH material was the Mg–Al–CO_3 LDHs, which could be swiftly synthesized with cheap raw materials. On the other hand, LDHs display outstanding capacity to catch all kinds of anions due

X. Teng
Qingyuan People's Hospital, The Sixth Affiliated Hospital of Guangzhou Medical University, Qingyuan 511518, China

C. Lu (✉)
College of Chemistry, Beijing University of Chemical Technology, Beijing 100029, China
e-mail: luchao@mail.buct.edu.cn

201

Fig. 10.1 Schematic representation of the LDH structure. Reprinted with permission from Ref. [4]. Copyright 2008 Elsevier B.V
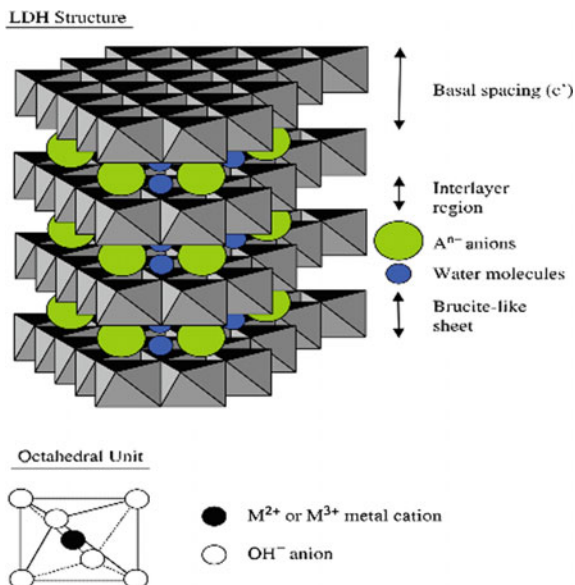
to their relatively weak interlayer bonding [5]. Moreover, the compelling properties of LDHs include good thermal stability, high anion exchange ability, high porosity, huge surface area, and interlayer anion mobility. Accordingly, LDHs have been extensively utilized in variety important areas including electrochemistry, environmental, catalysis, magnetization and biomedical application [6]. For example, LDHs have been used in catalyzing the redox processes, catalyzing the results of chemicals, and catalyzing acid–base processes with the enhanced activity and recovery of immobilized catalyst [7, 8]; The interlayer anions with the functions of photodimerization and photoisomerization in the LDHs could yield some valuable photoresponsive materials [9, 10]; LDHs have also been applied as electrodes for nanocomposite polymer electrolytes and alkaline secondary cells [11, 12]; LDHs have been potentially used in growth of novel delivery systems and pharmaceutical formulations in biomedical scientific research [13, 14]; LDHs have been utilized as stabilizing agents, heat retention additives in flame retardants, plastic films for precursors to magnetic materials, and polymers [15–17].

In this chapter, we focus on a review of the development in LDH-involved CL and their applications in analytical fields. We highlight the different CL systems, including CO_3–LDHs, NO_3–LDHs, organo-modified LDHs, and organo-modified LDH-quantum dot/organic chromophore nanocomposites. Finally, we also offer some perspectives on the potential roles of LDHs in more extensively analytical fields.

10.2 LDH-Catalyzed Luminol-H_2O_2 CL Reaction

Considering that the discovery of the luminol CL system by Albrecht, luminol system has become one of the useful and attractive method in analytical application [18, 19]. However, the increasing need for higher sensitivity in analytical methods is demanding higher CL efficiency of luminol–H_2O_2 system. Therefore, all efforts have been made to improve the CL efficiency of luminol–H_2O_2 system [20]. In this section, we present the luminol–H_2O_2–LDH CL system, including luminol–H_2O_2–CO_3–LDH CL, structurally ordered catalyst-amplified CL signals, CL flow biosensor for glucose using CO_3–LDHs as catalysts and buffer solutions, and an effect carmine acid quenching CL sensor.

10.2.1 CO_3–LDH–Catalyzed Luminol–H_2O_2 CL Reaction

It has been demonstrated that carbonate solution could improve the CL signals from luminol system [21, 22]. In luminol CL system, the carbonate molecules are also served as the buffer [23]. Unfortunately, in the absence of catalyst, the improvement effect of carbonate molecules on the luminol CL system was lowered [24, 25]. Until 2011, Lu and co-works reported that the interlayer carbonate in Mg–Al LDHs could dramatically improve the CL system of lumnol–H_2O_2 [26]. The CO_3–LDH-enhanced CL mechanism had been summarized as shown in Fig. 10.2. Firstly, LDHs surface with the positive charge could attract and concentrate both the peroxide ions and the luminol dianions. Subsequently, the interlayer carbonate could easily and effectively react with the concentrated peroxide ions and luminol dianions. Therefore, in the existence of LDHs, the emission of H_2O_2–luminol at 425 nm was greatly enhanced due to the improvement of the yield of the 3-aminophthalate anions. Furthermore, a novel CL assay of H_2O_2 was achieved using the CO_3–LDHs catalyzed the luminol reaction [27]. It is discovered that H_2O_2 could be assayed in the range of 0.05– 10 μM with a detection limit of 0.02 μM (S/N = 3). Finally, the luminol–H_2O_2– CO_3–LDH CL system was utilized for the detection of H_2O_2 in rainwater. The proposed CL detection method exhibited high tolerance toward a good deal of matrix interference ions in rainwater. In conclusion, this strategy shows remarkable potential in biological/chemical sensing for H_2O_2 in real samples or monitor the generation of H_2O_2 in numerous other oxidase-based reactions.

10.2.2 Structurally Ordered Catalyst-Amplified CL Signals

The catalysts with highly ordered structure has sprung up a large number of unique properties [28–30]. Recently, the structurally ordered ionic liquid has been successfully fabricated by using the LDH matrix [31]. It is found that the hydrogen bond
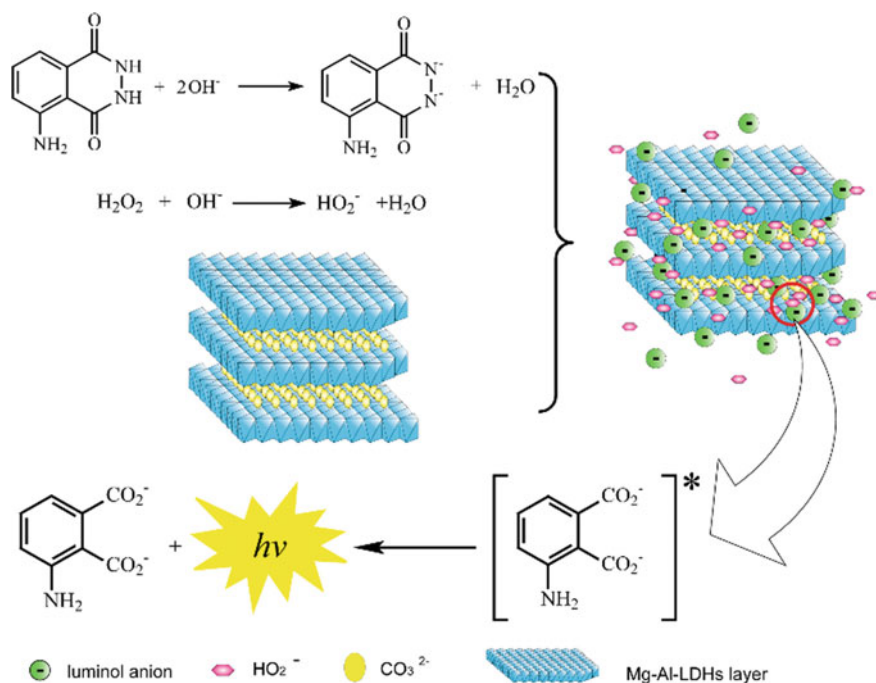
Fig. 10.2 Possible mechanism for CO_3–LDH–catalyzed luminol–H_2O_2 CL reaction. Reprinted with permission from Ref. [26]. Copyright 2011 The Royal Society of Chemistry

played a critical role in interactions between the ionic liquid and the LDH matrix. In comparison with the disordered ionic liquid, the structurally ordered ionic liquid could significantly improve the CL emission from H_2O_2–luminol system. The mechanism of the phenomenon has been summarized as shown in Fig. 10.3. Firstly, the mass transport from the mixture to the LDH-ionic liquid assembly was accelerated by the structurally ordered arrangement. Secondly, the amounts of $^{\bullet}OH$ and $O_2^{\bullet-}$ radicals were increased in presence of the ordered structure. In addition, the emissions of the luminol oxidation products were greatly enhanced using ionic liquids with the highly orderly arrangement because of the facilitation of the electron transfer. The study could provide a novel strategy for the enhancement of CL method and extends the scope of the relationship between the catalytic properties and the geometrical configuration.
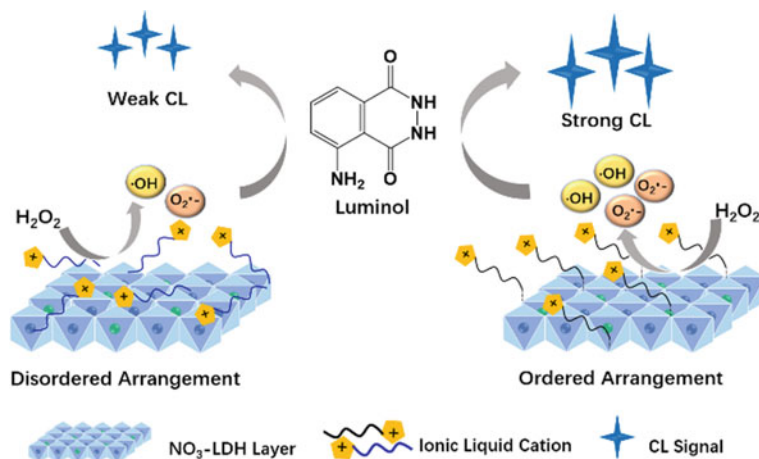
Fig. 10.3 Schematic diagram of structurally ordered catalyst-amplified the signals from luminol–H_2O_2 CL system. Reprinted with permission from Ref. [31]. Copyright 2020 American Chemical Society

10.2.3 CL Flow Biosensor for Glucose Using CO₃–LDHs as Catalysts and Buffer Solutions

The CL flow biosensors have received great attention due to the instrumental simplification, operational convenience, low cost, environmental friendliness, increased accuracy, and resource savings [32, 33]. However, in order to fabricate the micro device, the immobilization of both enzyme and luminol in one column have been a great challenge. It is because of the pH incompatibility issues. Briefly, in order to retain the maximum activity of glucose oxidase, the pH of the solution should be 5.5; while it is necessary to produce a strongly basic solution (*i.e.*, pH 10–11) for the reaction of luminol CL system. Accordingly, the CL flow biosensors were generally developed by immobilizing the glucose oxidase, which could produce H_2O_2. The luminol was addition by a mobile mode [34–36].

Recently, a CL flow cell has been constructed by Lu and co-works [37]. In the CL flow cell, the silica sol–gel with the horseradish peroxidase and glucose oxidase had been packed in the first half of the inside surface of the quartz tube. At the same time, the mixture of CO₃–LDHs and luminol was immobilized in the second half (Fig. 10.4). The CO₃–LDHs was applied as catalysts of luminol system, the supports for the immobilization of luminol reagent, and the buffer for the luminol reaction. Therefore, a strong light could emit in neutral medium/weak acid by using the simple micro-fabricated device, avoiding the issues of the pH incompatibility. The new CL flow biosensor was utilized for the determination of the glucose in plasma with shorter response time, simple procedures, wide pH compatibility and high selectivity. The CL flow biosensor could be refabricated for the detection of other analytes by changing the enzyme species.
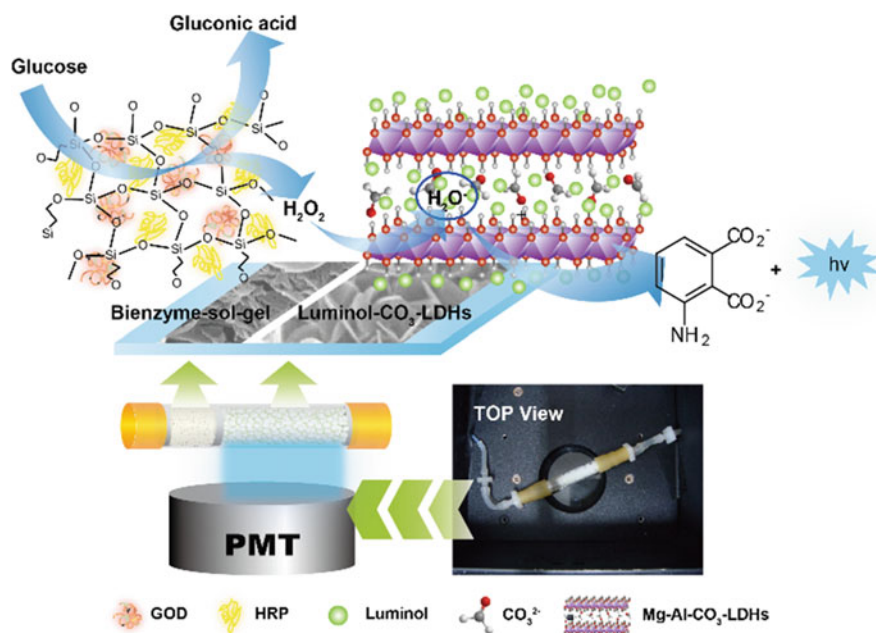
Fig. 10.4 Schematic illustration of CL flow biosensor for glucose using CO_3–LDHs as catalysts and buffer solutions. Reprinted with permission from Ref. [37]. Copyright 2012 Elsevier B.V

10.2.4 *An Effect Carmine Acid Quenching CL Sensor*

A rapid, facile, accurate and sensitive detection method for carmine acid (CA) has been fabricated by the H_2O_2–luminol–LDH CL system [38]. It is discovered that the detection mechanism was assigned to occupation of positively charged centers, ROS reduction, and synergistic effect of CRET (Fig. 10.5). On the other hand, the technique showed high sensitivity and selectivity toward CA with a linear range from 0.5 to 10 μM and a detection limit of 0.03 μM. The radical scavenging methods and the CL spectrum demonstrated that the CA-induced quenching of CL emission was due to both the various CL quenching mechanisms and the electrostatic attraction. The study provides novel opportunities for the development of the luminol CL nano-sensors.

10.3 Organo-Modified LDH-Enhanced CL from Singlet Oxygen System

Since micellar microenvironment has great potential as the reaction medium for the enhancement of the signals from various CL systems, it has received much attention
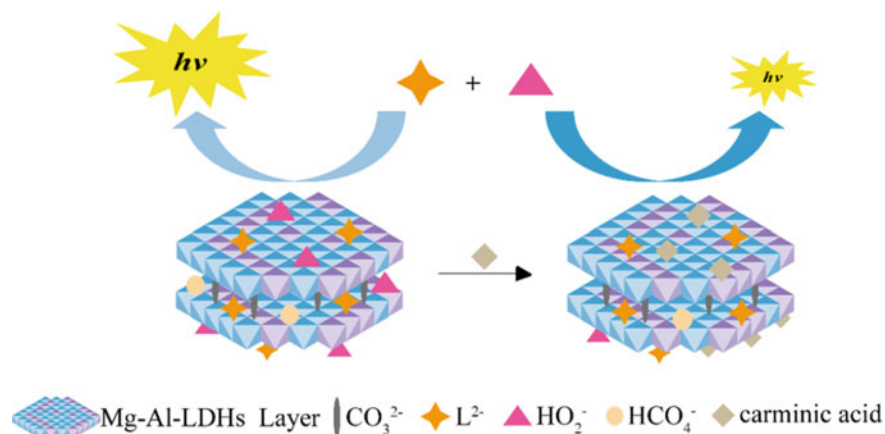
Fig. 10.5 Possible mechanism of CL sensor for carmine acid. Reprinted with permission from Ref. [38]. Copyright 2018 American Chemical Society

[39, 40]. Unfortunately, there are few reports about the enhancement effect of anionic surfactant on the CL signals. It is because that the electrostatic attraction between anionic reactants and cationic surfactants could help to concentrate the reactants on the surface of micellar, and most reactants are anionic in the CL reactions. Therefore, cationic surfactants are widely used in the CL reactions.

Sodium dodecylbenzenesulfonate (SDBS) is one of the widely used as anionic surfactant [41]. It has been reported that SDBS could improve the CL emission from IO_4^-–H_2O_2 [42]. In these studies, the solutions of SDBS micellar acted as a protective microenvironment for the energy acceptor or the reactive oxygen species. In addition, the long-chain organic guest species in LDHs could fabricate unique nanocomposite structure of alternating inorganic–organic assemblies. Many research showed that the long-chain surfactant anions could be intercalated via anion exchange method, which could expand the rendering the surface hydrophobicity and interlayer distance [43]. Therefore, the organo-modified LDHs have provided a unique environment for the exploration of the profound study on the physical and chemical properties of the guest molecules. On the other hand, the organo-modified LDHs have been extended to the applications as chemical sensors, as the adsorbents of organic contaminants for the treatment of waste water, and as artificial membranes [44].

In alkaline solution, IO_4^- could oxidize H_2O_2 to produce a slight CL signal from the excited singlet oxygen dimol species [42]. The signals of IO_4^-–H_2O_2 CL system could be improved using the anionic surfactant, a suitable fluorescent, non-polar organic solvents, and carbonate [45]. Lu and co-workers found that the CL signals from the reaction between IO_4^- and H_2O_2 could be significantly enhanced using the DBS-modified LDHs [46]. When SDBS-modified LDHs involved in the IO_4^-–H_2O_2 system, the maximum CL emission wavelength was about 510 nm. Since the excited singlet oxygen dimol species were decomposed, the CL emission dramatically decreased in the existence of 50 mM 1,4-diazabicyclo[2.2.2]octane

[47]. The studies implied that the singlet oxygen dimol species were luminophor for the IO_4^-–H_2O_2–DBS-modified LDHs system (Fig. 10.6). This study offers more options for the utilization of anionic surfactants and explores a novel strategy for the enhancement of CL emission using micelle.

Subsequently, the interactions of SDBS and poly (ethylene glycol) (PEG) at the surface of LDHs have been monitored via the H_2O_2–IO_4^- CL system [48]. The results implied that PEG concentration, SDBS concentration, and PEG molecular weight had an effect on the configuration of SDBS@PEG at the surface of LDHs, accompanying with the different CL intensity. Briefly, at low concentrations of SDBS, the CL intensity was extremely low (Fig. 10.7). Since SDBS hydrophobic tails pointed to the aqueous solution, the LDHs in the solution could become aggregates. Then the CL signals were increased with the increasing of SDBS concentration. It is because that in the LDH microenvironment, electrostatic repulsion between CL reactants/intermediates and SDBS head groups had partially disappeared. The study would open novel ways to use the CL technique for the investigation of the surfactant-polymer interactions.
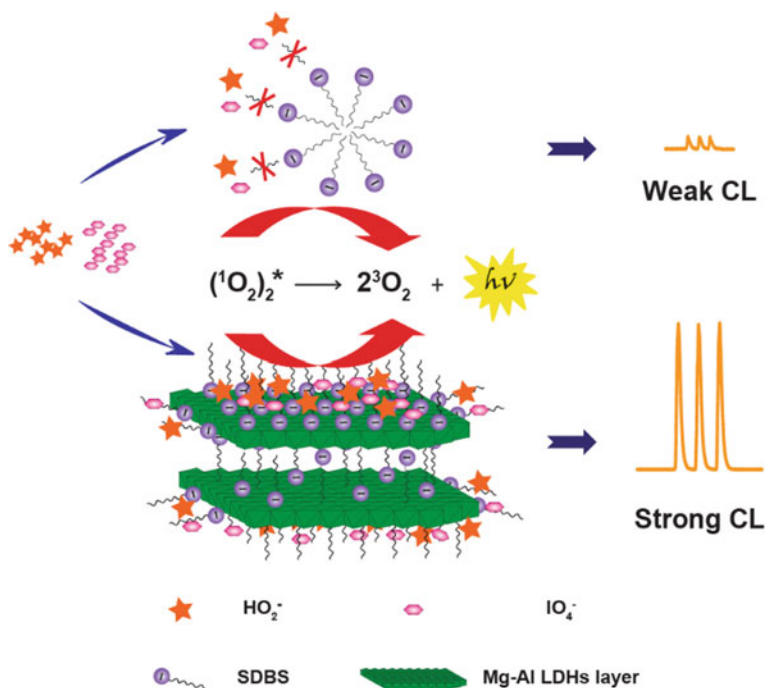
Fig. 10.6 Schematic illustration of DBS-modified LDH–IO_4^-–H_2O_2 CL system. Reprinted with permission from Ref. [46]. Copyright 2012 American Chemical Society
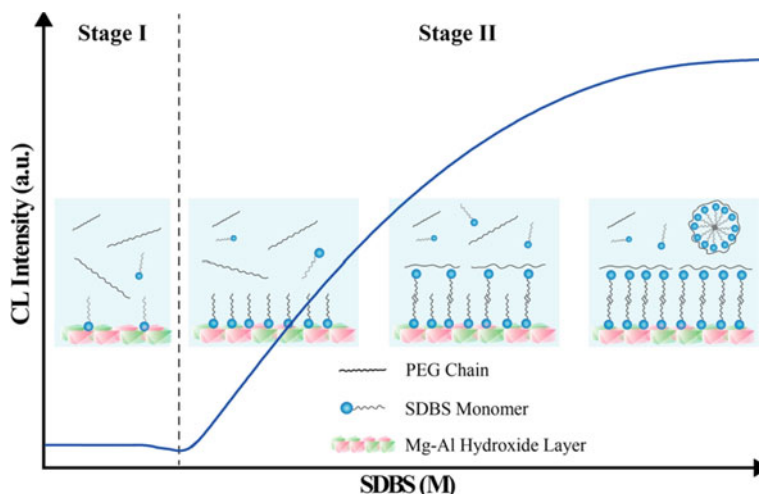
Fig. 10.7 CL features of SDBS@PEG-IO$_4^-$–H$_2$O$_2$ CL system. Reprinted with permission from Ref. [48]. Copyright 2014 American Chemical Society

10.4 Organo-Modified LDH-Enhanced CL from Fenton-Like System

It is reported that when the light-amplifying substance (*i.e.*, amino acid, gold nanoparticles, DNA and luminol) is added into the homogeneous Fenton-like system, a strong CL signal could be observed [49–51]. In addition, the microheterogeneous systems have been applied to improve the intensity or quantum yield for different CL systems because they could organize, concentrate and solubilize reactants [40]. Lu's group has demonstrated that the DBS-LDHs could greatly improve the ultra-weak signals of the Co(II)–OH–H$_2$O$_2$ CL system; while the weak CL signals could not be amplified by the DBS micelles [52]. The mechanism of the proposed CL reaction was summarized in Fig. 10.8. Firstly, H$_2$O$_2$ could concentrate on the surface of DBS-LDHs, and dissociate to provide hydroperoxylanion in an alkaline environment (Reaction 10.1) [53]. Secondly, the output of •OH radical could be easily facilitated by the hydrophobic microenvironment of the DBS-LDHs (Reaction 10.2) [54]. Subsequently, the •SO$_3^-$ radical was generated from the reaction between the intercalated DBS in LDHs and the abundant •OH radical (Reaction 10.3) [55]. Then, the intermediate SO$_2$* was generated from the recombination of •SO$_3^-$ radical. Finally, the CL signal at 430 nm was observed as the intermediate SO$_2$* returned to its ground state (Reactions 10.4–10.6) [56–58]. The study exhibited the potential use for detecting of radical production, and opened up the effective application of surfactant-LDHs in CL field.

$$H_2O_2 + HO^- \rightleftharpoons HO_2^- + H_2O \tag{10.1}$$
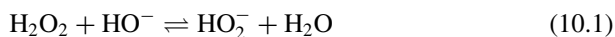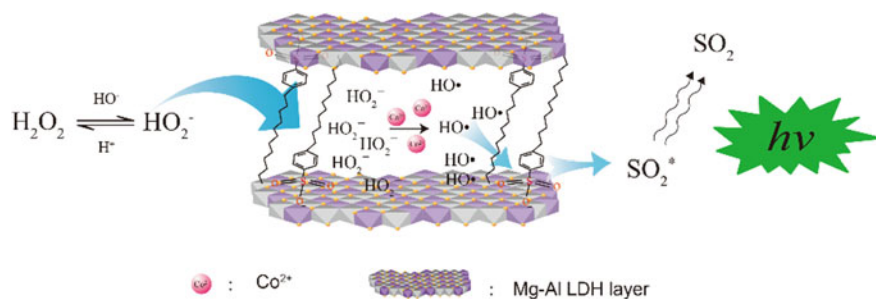
Fig. 10.8 Possible mechanism for the enhancement of H_2O_2–Co(II) CL reaction using DBS-LDHs. Reprinted with permission from Ref. [52]. Copyright 2012 American Chemical Society

$$H_2O_2 + Co(II) \rightarrow HO \cdot + Co(III) + OH^- \qquad (10.2)$$

$$HO \cdot + DBS \rightarrow H_2O + \cdot SO_3^- + byproduct \qquad (10.3)$$

$$\cdot SO_3^- + \cdot SO_3^- \rightarrow S_2O_6^{2-} + H_2O \qquad (10.4)$$

$$S_2O_6^{2-} \rightarrow SO_4^{2-} + SO_2^* \qquad (10.5)$$

$$SO_2^* \rightarrow SO_2 + h\upsilon(\lambda = 430\,nm) \qquad (10.6)$$
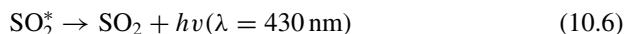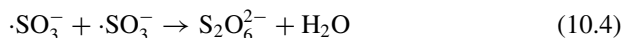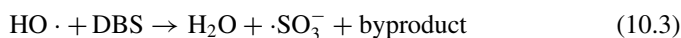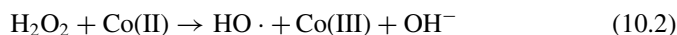
10.5 CO₃-LDH-Enhanced ONOOH/ONOO⁻ CL

The spontaneous CL decomposition of ONOO⁻ or ONOOH has attracted considerable attention as an ultra-weak CL system [59]. It is reported that the generated CL emissions could be considerably amplified using energy acceptors (*e.g.*, gold nanoparticles, CdTe quantum dots, fluoroquinolones and uranine) [60–62]. On the other hand, ONOO⁻ or ONOOH could oxidize bilirubin, chloroquine and pholasin to generate strong CL emission [63–65]. In addition, it is found that the interaction between CO_3^{2-} anions and ONOO⁻ could produce a slight CL signal because of the formation of bicarbonate radical [66]. It is observed that in comparison with the aqueous carbonate solutions, the interlayer carbonate anions displayed extremely greater catalytic activity for the ONOOH CL reaction [67]. Moreover, the logarithm of concentration of ascorbic acid was proportional to the logarithm of CL intensity. The CL spectrum of ONOOH–CO₃–LDH system showed that the excited-state bicarbonate radical was the luminophor for the proposed CL system, and the maximum emission wavelength was about 430 nm [66]. The outcomes showed that
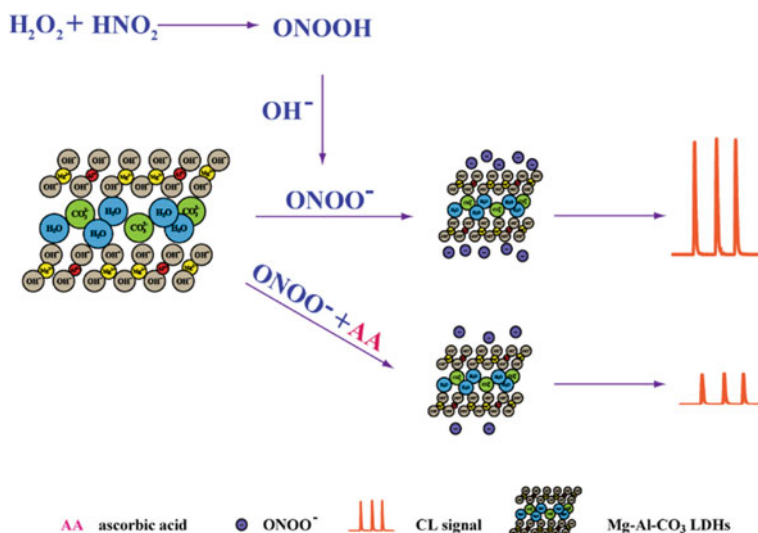
Fig. 10.9 Possible mechanism for ONOOH–CO₃–LDH CL reaction. Reprinted with permission from Ref. [67]. Copyright 2012 The Royal Society of Chemistry

there was no new luminophors in the reaction between ONOOH and the CO_3-LDHs. The CL mechanism of the ONOOH-CO_3-LDH system was summarized as shown in Fig. 10.9. Firstly, the LDHs surface could concentrate the $ONOO^-$ via the electrostatic attraction. Subsequently, the intercalated carbonate could quickly interact with the concentrated $ONOO^-$. Accordingly, the ONOOH CL intensity could be enhanced by CO_3-LDHs. Since both $ONOO^-$ and its decomposition products (*i.e.*, $\cdot NO_2$ and $\cdot OH$) could react with ascorbic acid, oxygen-related radicals in the ONOOH–CO_3–LDH system decreased by the addition of ascorbic acid. As a result, ascorbic acid could significantly inhibit the signals from the ONOOH–CO_3–LDH CL system. The strategy could be utilized for the determination of ascorbic acid in real samples.

10.6 CRET System Based on Organo-Modified LDH-Quantum Dot/Organic Chromophore Nanocomposites

CRET includes dipole-dipole nonradiative energy transfer between a CL donor and an appropriate acceptor [68–70]. CRET happens by means of the certain oxidation of a luminophor throughout the CL reaction without intense background light, an external excitation source, bleaching triggered by external light excitation and minimizing nonspecific signals in comparison with fluorescence resonance energy transfer. Since the photoactive organic molecules have the advantages of high fluorescent quantum yields, photostability and strong fluorescence intensity, they have been utilized as

the energy acceptors [71–73]. On the other hand, the photoactive organic molecules could not consume themselves during the CRET process. Therefore, CRET strategy provides a good incentive to develop a new CL system.

10.6.1 CL Flow Device Based on Directed Self-Assembly of Chromophores on LDH Materials

During CRET, the use of high concentrations of the chromophores is necessary. As a result, the chromophores may occur the nonradiative deactivation process and the light self-absorption [73]. Therefore, it is important to produce unique fluorescence materials to solve the above problem, focusing on the enhancement of CRET performance between the chromophores and the CL donors.

LDHs, as a inorganic matrices for chromophores, own the powerful capability to capture the chromophores from the aqueous solutions [74]. It is found that in contrast with the aqueous organic molecules, the optical stability and the fluorescence efficiency of chromophores could be enhanced. In addition, the fluorescence quenching and the molecular thermal agitation of the chromophores could be reduced after the organic chromophores incorporated into LDH galleries. The reason for the phenomenon is that the organic chromophores could be oriented between the LDH sheets [75]. On the other hand, chromophores could orderly assemble on LDHs and serve as the CL acceptors. The proposed LDH-chromophore composite materials could enhance the emissions from various donors (*e.g.*, Na_2SO_3-N-bromosuccinimide system and ONOOH system) [76]. Both the improvement of molecular orientation and the suppression of intermolecular $\pi - \pi$ stacking interactions among aromatic rings could make high CRET efficiency (Fig. 10.10). On the other hand, a CL flow-through column based on CRET strategy was produced by constructing chromophores on LDHs. In comparison with the flow device in the lack of chromophores, the sensitivity for ONOOH/nitrite detection could be greatly enhanced by utilizing the new LDH-chromophore column. This work not only shows their potential application in CL flow device, but also supplies an approach for the establishment of CRET process with orientated materials.

10.6.2 Novel CRET Probe Based on the Organo-Modified Hydrotalcite-Quantum Dot Nanomaterials

In 2004, Talapin first observed the CL phenomenon of CdS/CdSe QDs [77]. Since then, QDs have been utilized as the signal enhancers. The signal enhancement mechanism was based on the electron-transfer annihilation of hole-injected and electron-injected QDs during direct oxidation process of the QDs by using the strong oxidants (*e.g.*, H_2O_2 and $KMnO_4$) [78]. It is first demonstrated that QDs could be used as

Fig. 10.10 Schematic illustration of universal CL flow device. Reprinted with permission from Ref. [76]. Copyright 2013 American Chemical Society

the acceptors to obtain an efficient CRET in the H_2O_2–luminol-HRP reaction [68]. The main reasons for the QD-amplified CL signal of H_2O_2–luminol CL system were credited to the fact that the H_2O_2–luminol CL reaction could be catalyzed by the HRP-QDs materials. In addition, the close distance between QDs and the light source could bring about high CRET efficiency. Subsequently, the QDs acceptors and the luminol donors-involved CRET process has been carried out to establish the sensors for the measurement of thrombin, RNA or DNA [69, 70]. Nevertheless, since the QDs could be oxidized by using high concentration of H_2O_2, resulting in the fluorescence quenching of QDs, the use of H_2O_2–luminol–QDs CL system has been significantly limited [68]. On the other hand, non-radiative deactivation process and light self-absorption of QDs would happen when the concentration of QDs was high [45]. Recently, Lu and co-workers fabricated a novel CRET probe based on the QD-LDH materials (Fig. 10.11) [79]. The CL property- structure relationship of the QD-LDH materials was studied by using the H_2O_2–luminol system. Fluorescence microscopy images, zeta potentials, fluorescence spectra, steady-state fluorescence polarization measurements, and transmission electron microscopy images demonstrated that during the CRET process, the non-radiative relaxation and oxidation of QDs had been inhibited, and the radiative decay rate of QDs was increased. Finally, the novel CRET material was applied to fabricate the CL flow column for the detection of H_2O_2. The study showed high sensitivity toward H_2O_2 with a linear range from 0.5 to 60 μmol L^{-1} and a detection limit of 0.3 μmol L^{-1}. The present method had been successfully used for the detection of H_2O_2 in the snow samples. The outcomes implied that the study not only shows the potential application of QD-LDHs during CRET process, but also offers a facile approach for the CRET acceptors preparation.
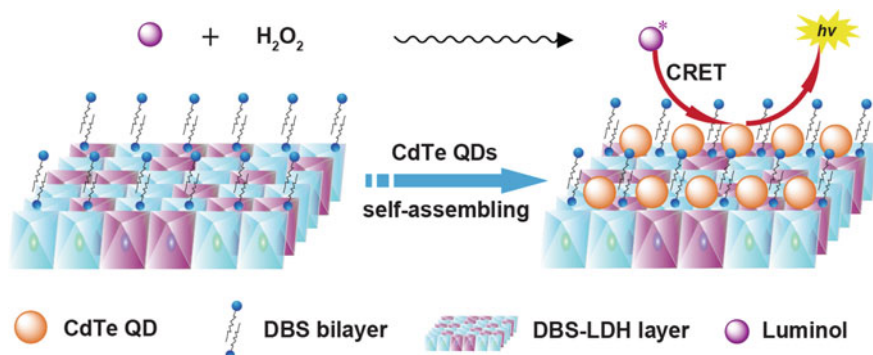
Fig. 10.11 Schematic illustration of CdTe QDs and DBS on exterior surfaces of the organo-modified LDH. Reprinted with permission from Ref. [79]. Copyright 2013 American Chemical Society

10.6.3 Orderly Arranged Dyes as the Efficient CRET Probe for ONOO⁻

The orderly arranged sodium dodecyl sulfate (SDS)-calcein particles were fabricated when the LDH structure was broken down in an acidic medium (Fig. 10.12) [80]. The orderly arranged SDS-calcein molecules could enhance the CRET efficiency between calcein acceptor and ONOOH* donor. Based on the energy-matching rules, the orderly arranged calcein-SDS molecules exhibited remarkable selectivity toward ONOO⁻. Therefore, the orderly arranged calcein-SDS molecules were used as the CL probe for the measurement of ONOO⁻. On the other hand, the validation of
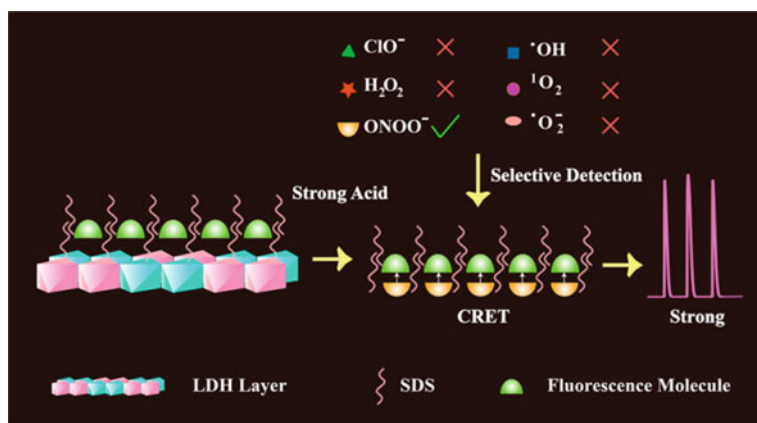
Fig. 10.12 Possible mechanism for the detection of ONOO⁻ using the highly efficient CRET probe. Reprinted with permission from Ref. [80]. Copyright 2015 American Chemical Society

the CL probe had been examined by monitoring the production of $ONOO^-$ from 3-morpholinosydnonimine and identifying $ONOO^-$ in plasma samples. This success not only expands the application range of LDH in the improvement of fluorescence emissions, but also provides new opportunities for highly sensitive and selective measurement of $ONOO^-$.

10.7 Conclusions

As green materials, LDHs have been exploited for enhancing a series of CL systems. They provide new insights into the well-known enhancers of different CL reactions, and exhibit greater flexibility and potential applications for various CL devices. These studies have successfully constructed a bridge between the CL spectroscopy and the LDH inorganic materials, which would certainly prompt interdisciplinary scientists to further explore the impact of a range of anions-LDHs on the CL properties. We believe that LDH-involved CL has huge potential in biological and chemical sensing.

References

1. Lee S, Bai L, Hu X (2020) Deciphering iron-dependent activity in oxygen evolution catalyzed by nickel-iron layered double hydroxide. Angew Chem Int Ed 59:8072–8077
2. Dionigi F, Zeng Z, Sinev I, Merzdorf T, Deshpande S, Lopez MB, Kunze S, Zegkinoglou I, Sarodnik H, Fan D, Bergmann A, Drnec J, Araujo JF, Gliech M, Teschner D, Zhu J, Li WX, Greeley J, Cuenya BR, Strasser P (2020) In-situ structure and catalytic mechanism of NiFe and CoFe layered double hydroxides during oxygen evolution. Nat Commun 11:2522
3. Yu L, Wu L, McElhenny B, Song S, Luo D, Zhang F, Yu Y, Chen S, Ren Z (2020) Ultrafast room-temperature synthesis of porous S-doped Ni/Fe (oxy)hydroxide electrodes for oxygen evolution catalysis in seawater splitting. Energy Environ Sci 13:3439–3446
4. Goh KH, Lim TT, Dong ZL (2008) Application of layered double hydroxides for removal of oxyanions: a review. Water Res 42:1343–1368
5. Tran HN, Nguyen DT, Le GT, Tomul F, Lima EC, Woo SH, Sarmah AK, Nguyen HQ, Nguyen PT, Nguyen DD, Nguyen TV, Vigneswaran S, Vo DN, Chao HP (2019) Adsorption mechanism of hexavalent chromium onto layered double hydroxides-based adsorbents: a systematic in-depth review. J Hazard Mater 373:258–270
6. Laipan M, Yu J, Zhu R, Zhu J, Smith AT, He H, O'Hare D, Sun L (2020) Functionalized layered double hydroxides for innovative applications. Mater Horiz 7:715–745
7. Wen Y, Wei Z, Liu J, Li R, Wang P, Zhou B, Zhang X, Li J, Li Z (2021) Synergistic cerium doping and MXene coupling in layered double hydroxides as efficient electrocatalysts for oxygen evolution. J Energy Chem 52:412–420
8. Xie ZH, Zhou HY, He CS, Pan ZC, Yao G, Lai B (2021) Synthesis, application and catalytic performance of layered double hydroxide based catalysts in advanced oxidation processes for wastewater decontamination: a review. Chem Eng J 414:128713.
9. Khayyami A, Karppinen M (2018) Reversible photoswitching function in atomic/molecular-layer-deposited ZnO: azobenzene superlattice thin films. Chem Mater 30:5904–5911
10. Gao R, Yan D (2019) Recent development of Ni/Fe-based micro/nanostructures toward photo/electrochemical water oxidation. Adv Energy Mater 10:1900954

11. Abdelkareem MA, Sayed ET, Mohamed HO, Obaid M, Rezk H, Chae KJ (2020) Nonprecious anodic catalysts for low-molecular-hydrocarbon fuel cells: theoretical consideration and current progress. Prog Energy Combust Sci 77:100805

12. Gao X, Zhao Y, Dai K, Wang J, Zhang B, Shen X (2020) NiCoP nanowire@NiCo-layered double hydroxides nanosheet heterostructure for flexible asymmetric supercapacitors. Chem Eng J 384:123373

13. Dong W, Lu Y, Wang W, Zhang M, Jing Y, Wang A (2020) A sustainable approach to fabricate new 1D and 2D nanomaterials from natural abundant palygorskite clay for antibacterial and adsorption. Chem Eng J 382:122984

14. Zhang LX, Hu J, Jia YB, Liu RT, Cai T, Xu ZP (2021) Two-dimensional layered double hydroxide nanoadjuvant: recent progress and future direction. Nanoscale 13:7533–7549

15. Chen J, Wu L, Ding X, Liu Q, Dai X, Song J, Jiang B, Atrens A, Pan F (2021) Effects of deformation processes on morphology, microstructure and corrosion resistance of LDHs films on magnesium alloy AZ31. J Mater Sci Technol 64:10–20

16. Feng C, Faheem MB, Fu J, Xiao Y, Li C, Li Y (2020) Fe-based electrocatalysts for oxygen evolution reaction: progress and perspectives. ACS Catal 10:4019–4047

17. Fan H, Peng M, Strauss I, Mundstock A, Meng H, Caro J (2020) High-flux vertically aligned 2D covalent organic framework membrane with enhanced hydrogen separation. J Am Chem Soc 142:6872–6877

18. Irkham RRR, Ivandini TA, Fiorani A, Einaga Y (2021) Electrogenerated chemiluminescence of luminol mediated by carbonate electrochemical oxidation at a boron-doped diamond. Anal Chem 93:2336–2341

19. Zhang L, Ouyang H, Zhang D, Fu Z (2021) Novel cobalt-based metal-organic frameworks with superior catalytic performance on N-(4-aminobutyl)-N- ethylisoluminol chemiluminescent reaction. Anal Chim Acta 1148:238174

20. Roda A, Cavalera S, Di Nardo F, Calabria D, Rosati S, Simoni P, Colitti B, Baggiani C, Roda M, Anfossi L (2021) Dual lateral flow optical/chemiluminescence immunosensors for the rapid detection of salivary and serum IgA in patients with COVID-19 disease. Biosens Bioelectron 172:112765

21. Lin J-M, Yamada M (1999) Oxidation reaction between periodate and polyhydroxyl compounds and its application to chemiluminescence. Anal Chem 71:1760–1766

22. Xiao CB, Palmer DA, Wesolowski DJ, Lovitz SB, King DW (2002) Carbon dioxide effects on luminol and 1,10-phenanthroline chemiluminescence. Anal Chem 74:2210–2216

23. Feng N, Lu JR, He YH, Du J (2005) Post-chemiluminescence behaviour of Ni^{2+}, Mg^{2+}, Cd^{2+} and Zn^{2+} in the potassium ferricyanide–luminol reaction. Luminescence 20:266–270

24. Lin J-M, Liu M (2008) Chemiluminescence from the decomposition of peroxymonocarbonate catalyzed by gold nanoparticles. J Phys Chem B 112(26):7850–7855

25. Xiao CB, King DW, Palmer DA, Wesolowski DJ (2000) Study of enhancement effects in the chemiluminescence method for Cr(III) in the ng·L^{-1} range. Anal Chim Acta 415:209–219

26. Wang ZH, Liu F, Lu C (2011) Mg-Al-carbonate layered double hydroxides as a novel catalyst of luminol chemiluminescence. Chem Commun 47(19):5479–5481

27. Wang ZH, Liu F, Teng X, Zhao C, Lu C (2011) Detection of hydrogen peroxide in rainwater based on Mg-Al-carbonate layered double hydroxides-catalyzed luminol chemiluminescence. Analyst 136:4986–4990

28. Kim D, Xie C, Becknell N, Yu Y, Karamad M, Chan K, Crumlin EJ, Norskov JK, Yang P (2017) Electrochemical activation of CO_2 through atomic ordering transformations of AuCu nanoparticles. J Am Chem Soc 139:8329–8336

29. Liu Z, Fu G, Li J, Liu Z, Xu L, Sun D, Tang Y (2018) Facile synthesis based on novel carbon-supported cyanogel of structurally ordered Pd_3Fe/C as electrocatalyst for formic acid oxidation. Nano Res 11:4686–4696

30. Chattot R, Le Bacq O, Beermann V, Kuhl S, Herranz J, Henning S, Kuhn L, Asset T, Guetaz L, Renou G, Drnec J, Bordet P, Pasturel A, Eychmuller A, Schmidt TJ, Strasser P, Dubau L, Maillard F (2018) Surface distortion as a unifying concept and descriptor in oxygen reduction reaction electrocatalysis. Nat Mater 17:827–833

31. Cheng W, Teng X, Lu C (2020) Structurally ordered catalyst-amplified chemiluminescence signals. Anal Chem 92:5456–5463
32. Li BX, Zhang ZJ, Jin Y (2001) Plant tissue-based chemiluminescence flow biosensor for glycolic acid. Anal Chem 73:1203–1206
33. Yu J, Lei G, Ping D, Ge S, Liu S (2010) A novel enzyme biosensor for glucose based on rhodanine derivative chemiluminescence system and mesoporous hollow silica microspheres receptor. Biosens Bioelectron 25:2065–2070
34. Lan D, Li BX, Zhang ZJ (2008) Chemiluminescence flow biosensor for glucose based on gold nanoparticle-enhanced activities of glucose oxidase and horseradish peroxidase. Biosens Bioelectron 24:940–944
35. Li BX, Lan D, Zhang ZJ (2008) Chemiluminescence flow-through biosensor for glucose with eggshell membrane as enzyme immobilization platform. Anal Biochem 374:64–70
36. Lin J-M, Shan XQ, Hanaoka S, Yamada M (2001) Luminol chemiluminescence in unbuffered solutions with a Cobalt(II)-ethanolamine complex immobilized on resin as catalyst and its application to analysis. Anal Chem 73:5043–5051
37. Wang ZH, Liu F, Lu C (2012) Chemiluminescence flow biosensor for glucose using Mg-Al carbonate layered double hydroxides as catalysts and buffer solutions. Biosens Bioelectron 38:284–288
38. Pan F, Zhang Y, Yuan Z, Lu C (2018) Sensitive and selective carmine acid detection based on chemiluminescence quenching of layer doubled hydroxide-luminol-H_2O_2 system. ACS Omega 3:18836–18842
39. Hu D, Yang L, Deng S, Hao Y, Zhang K, Wang X, Liu Y, Liu H, Chen Y, Xie M (2021) Development of nanosensor by bioorthogonal reaction for multi-detection of the biomarkers of hepatocellular carcinoma. Sens Actuators B 334:129653
40. Lin J-M, Yamada M (2003) Microheterogeneous systems of micelles and microemulsions as reaction media in chemiluminescent analysis. Trends Anal Chem 22:99–107
41. Pintossi D, Saakes M, Borneman Z, Nijmeijer K (2021) Tailoring the surface chemistry of anion exchange membranes with zwitterions: toward antifouling RED membranes. ACS Appl Mater Interfaces 13:18348–18357
42. Zhang GF, Chen HY (2000) Studies of micelle and trace non-polar organic solvent on a new chemiluminescence system and its application to flow injection analysis. Anal Chim Acta 409:75–81
43. Schrijvers DL, Leroux F, Verney V, Patel MK (2014) Ex-ante life cycle assessment of polymer nanocomposites using organo-modified layered double hydroxides for potential application in agricultural films. Green Chem 16:4969–4984
44. Gao Z, Du B, Zhang G, Gao Y, Duan X (2011) Adsorption of pentachlorophenol from aqueous solution on dodecylbenzenesulfonate modified nickel-titanium layered double hydroxide nanocomposites. Ind Eng Chem Res 50:5334–5345
45. Liu JX, Chen H, Lin Z, Lin J-M (2010) Preparation of surface imprinting polymer capped Mn-doped ZnS quantum dots and their application for chemiluminescence detection of 4-nitrophenol in tap water. Anal Chem 82:7380–7386
46. Zhang MC, Han DM, Lu C, Lin J-M (2012) Organo-modified layered double hydroxides switch-on chemiluminescence. J Phys Chem C 116:6371–6375
47. Li JG, Li QQ, Lu C, Zhao L, Lin J-M (2011) Fluorosurfactant-capped gold nanoparticles-enhanced chemiluminescence from hydrogen peroxide-hydroxide and hydrogen peroxide-bicarbonate in presence of cobalt(II). Spectrochim Acta A 78:700–705
48. Guan W, Zhou W, Huang Q, Lu C (2014) Chemiluminescence as a novel indicator for interactions of surfactant–polymer mixtures at the surface of layered double hydroxides. J Phys Chem C 118:2792–2798
49. Liu ML, Li BX, Zhang ZJ, Lin J-M (2005) Enhancing effect of DNA on chemiluminescence from the decomposition of hydrogen peroxide catalyzed by copper(II). Anal Bioanal Chem 381:828–832
50. Kładna A, Aboul-Enein HY, Kruk I (2003) Enhancing effect of melatonin on chemiluminescence accompanying decomposition of hydrogen peroxide in the presence of copper. Free Radic Biol Med 34:1544–1554

51. Soichi H, Lin J-M, Yamada M (2000) Chemiluminescence behavior of the decomposition of hydrogen peroxide catalyzed by copper (II)-amino acid complexes and its application to the determination of tryptophan and phenylalanine. Anal Chim Acta 409:65–73

52. Zhang LJ, Zhang ZM, Lu C, Lin J-M (2012) Improved chemiluminescence in fenton-like reaction via dodecylbenzene-sulfonate-intercalated layered double hydroxides. J Phys Chem C 116:14711–14716

53. McMurray HN, Wilson BP (1999) Mechanistic and spatial study of ultrasonically induced luminol chemiluminescence. J Phys Chem A 103:3955–3962

54. Krylova G, Dimitrijevic NM, Talapin DV, Guest JR, Borchert H, Lobo A, Rajh T, Shevchenko EV (2010) Probing the surface of transition-metal nanocrystals by chemiluminescence. J Am Chem Soc 132:9102–9110

55. Mendez-Diaz J, Sanchez-Polo M, Rivera-Utrilla J, Canonica S, Gunten UV (2010) Advanced oxidation of the surfactant SDBS by means of hydroxyl and sulphate radicals. Chem Eng J 163:300–306

56. Xue W, Lin Z, Chen H, Lu C, Lin J-M (2011) Enhancement of ultraweak chemiluminescence from reaction of hydrogen peroxide and bisulfite by water-soluble carbon nanodots. J Phys Chem C 115:21707–21714

57. Li RB, Chen H, Li Y, Lu C, Lin J-M (2012) Enhancing effect of alcoholic solvent on hydrosulfite-hydrogen peroxide chemiluminescence system. J Phys Chem A 116:2192–2197

58. Li RB, Kameda T, Toriba A, Hayakawa K, Lin J-M (2012) Determination of benzo[a]pyrene-7,10-quinone in airborne particulates by using a chemiluminescence reaction of hydrogen peroxide and hydrosulfite. Anal Chem 84:3215–3221

59. Lu C, Song GQ, Lin J-M (2006) Reactive oxygen species and their chemiluminescence-detection methods. Trac Trend in Anal Chem 25:985–995

60. Li JG, Li QQ, Lu C, Zhao L (2011) Determination of nitrite in tap waters based on fluorosurfactant-capped gold nanoparticles-enhanced chemiluminescence from carbonate and peroxynitrous acid. Analyst 136:2379–2384

61. Lu C, Qu F, Lin J-M, Yamada M (2002) Flow-injection chemiluminescent determination of nitrite in water based on the formation of peroxynitrite from the reaction of nitrite and hydrogen peroxide. Anal Chim Acta 474:107–114

62. Zhang HX, Zhang LJ, Lu C, Zhao L, Zheng Z (2012) CdTe nanocrystals-enhanced chemiluminescence from peroxynitrous acid-carbonate and its application to the direct determination of nitrite. Spectrochim Acta A 85:217–222

63. Glebska J, Koppenol WH (2005) Chemiluminescence of pholasin caused by peroxynitrite. Free Radic Biol Med 38:1014–10122

64. Lu C, Lin J-M, Huie CW (2004) Determination of total bilirubin in human serum by chemiluminescence from the reaction of bilirubin and peroxynitrite. Talanta 63:333–337

65. Liang YD, Song J-F (2004) Flow-injection chemiluminescence determination of chloroquine using peroxynitrous acid as oxidant. Talanta 62:757–763

66. Lu C, Lin J-M, Huie CW, Yamada M (2004) Chemiluminescence study of carbonate and peroxynitrous acid and its application to the direct determination of nitrite based on solid surface enhancement. Anal Chim Acta 510:29–34

67. Wang ZH, Teng X, Lu C (2012) Carbonate interlayered hydrotalcites-enhanced peroxynitrous acid chemiluminescence for high selectivity sensing of ascorbic acid. Analyst 137:1876–1881

68. Huang XY, Li L, Qian HF, Dong C, Ren J (2006) A resonance energy transfer between chemiluminescent donors and luminescent quantum-dots as acceptors (CRET). Angew Chem 118:5264–5267

69. Liu XQ, Freeman R, Golub E, Willner I (2011) Chemiluminescence and chemiluminescence resonance energy transfer (CRET) aptamer sensors using catalytic hemin/g-quadruplexes. ACS Nano 5:7648–7655

70. Freeman R, Liu XQ, Willner I (2011) Chemiluminescent and chemiluminescence resonance energy transfer (CRET) detection of DNA, metal ions, and aptamer-substrate complexes using hemin/G-quadruplexes and CdSe/ZnS quantum dots. J Am Chem Soc 133:11597–11604

71. Bi S, Zhang JL, Hao SY, Ding C, Zhang S (2011) Exponential amplification for chemiluminescence resonance energy transfer detection of microrna in real samples based on a cross-catalyst strand-displacement network. Anal Chem 83:3696–3702
72. Zhao SL, Liu JW, Huang Y, Liu YM (2012) Introducing chemiluminescence resonance energy transfer into immunoassay in a microfluidic format for an improved assay sensitivity. Chem Commun 48:699–701
73. Bi S, Zhao TT, Luo BY (2012) A graphene oxide platform for the assay of biomolecules based on chemiluminescence resonance energy transfer. Chem Commun 48:106–108
74. Costa AL, Gomes AC, Pillinger M, Goncalves IS, Seixas de Melo JS (2015) Controlling the fluorescence behavior of 1-pyrenesulfonate by cointercalation with a surfactant in a layered double hydroxide. Langmuir 31:4769–4778
75. Shi WY, He S, Wei M, Evans DG, Xue D (2010) Optical pH sensor with rapid response rased on a fluorescein-intercalated layered double hydroxide. Adv Funct Mater 20:3856–3863
76. Wang ZH, Teng X, Lu C (2013) Universal chemiluminescence flow-through device based on directed self-assembly of solid-state organic chromophores on layered double hydroxide matrix. Anal Chem 85:2436–2442
77. Poznyak SK, Talapin DV, Shevchenko EV, Weller H (2004) Quantum dot chemiluminescence. Nano Lett 4:693–698
78. Chen H, Lin L, Lin Z, Guo G, Lin J-M (2010) Chemiluminescence arising from the decomposition of peroxymonocarbonate and enhanced by CdTe quantum dots. J Phys Chem A 114:10049–10058
79. Dong S, Liu F, Lu C (2013) Organo-modified hydrotalcite-quantum dot nanocomposites as a novel chemiluminescence resonance energy transfer probe. Anal Chem 85:3363–3368
80. Wang Z, Teng X, Lu C (2015) Orderly arranged fluorescence dyes as a highly efficient chemiluminescence resonance energy transfer probe for peroxynitrite. Anal Chem 87:3412–3418

Chapter 11
Aggregation-Induced Emission-Amplified Chemiluminescence

Xu Teng and Chao Lu

Abstract The development of aggregation-induced emission (AIE) has brought the unique opportunity for scientists. AIE materials with advantages of strong photostability, large Stokes' shift, and low background noise have found wide use in various fields. In this chapter, we provide insights into the applications of AIE molecules on various chemiluminescence (CL) systems, including bis-(2,4,6-trichlorophenyl) oxalate (TCPO)/bis(3,5,6-trichloro-2-carbopentyloxy) oxalate (CPPO)–H_2O_2 system, singlet oxygen system, superoxide anion system, and other AIE material-involved CL system. Furthermore, we discuss the enhancement mechanism of AIE materials in the CL analysis. These may offer a unique system for the CL-enhanced detection based on AIE materials.

Keywords Chemiluminescence · Aggregation-induced emission · TCPO · Singlet oxygen · Superoxide anion · 1,2-Dioxetane

11.1 Introduction

Aggregation-induced emission (AIE) is the photophysical phenomenon related to the aggregation of chromophore [1–3]. In 2001, the principle of AIE was created by Tang's group [4–7]. The development of AIE can sweep away the shortcomings of aggregation-caused quenching (ACQ) [8–13]. The AIE phenomenon could be interpreted by various hypotheses, such as the restriction of intramolecular motion (RIM), *J*-aggregates, excimer formation, inhibition of twisted intramolecular charge transfer (TICT) process [14–18].

Benefiting from the enthusiastic efforts of researchers, lots of AIE materials have been established, such as tetraphenylethene (TPE), silole, tetraphenylprazine (TPP),

X. Teng
Qingyuan People's Hospital, The Sixth Affiliated Hospital of Guangzhou Medical University, Qingyuan 511518, China

C. Lu (✉)
College of Chemistry, Beijing University of Chemical Technology, Beijing 100029, China
e-mail: luchao@mail.buct.edu.cn

quioline-malonontrile (QM), etc. [19–23]. For AIE materials, in diluted solution, there was no or weak light signal, while in high concentration solution, the signal of the solution was high [24, 25]. On the other hand, the AIE materials are featured with strong photostability and large Stokes' shift [26]. Based on the special properties of AIE materials, several chemical sensors, biological imaging, and optoelectronic devices have been developed by using the AIE materials [27–31].

In this chapter, we focus on a review of the development in AIE material-involved CL and their applications in analytical fields published in recent years. We summarized the latest advances of the AIE material-involved CL field with representative examples for the different AIE-CL systems, such as bis-(2,4,6-trichlorophenyl) oxalate (TCPO)/bis(3,5,6-trichloro-2-carbopentyloxy) oxalate (CPPO)–H_2O_2 system, singlet oxygen system, superoxide anion system, and other AIE material-involved CL system.

11.2 AIE-Amplified CL Signals from TCPO/CPPO-H_2O_2 System

TCPO and CPPO could be oxidized by H_2O_2 and produce an intermediate, namely 1,2-dioxetanedione [32, 33]. Based on the chemically started electron-exchange luminescence procedure, the intermediates could excite the nearby fluorescent molecules to emit light [34]. In 2015, the Lu group first investigates the influences of AIE on the CL emissions [35]. Briefly, three AIE materials (*i.e.*, the gold nanocluster aggregates, Au(I)-thiolate complexes and 9,10-bis[4-(3-sulfonatopropoxyl)-styryl] anthracene (BSPSA)) have been applied for the study of their influences on the CL reaction of TCPO–H_2O_2, respectively (Fig. 11.1). The AIE materials exhibited significantly improved efficiencies toward the CL emission due to the CRET between AIE acceptors and TCPO donors. The results indicated that the AIE materials could be applied as novel type of CRET acceptors. The work expands the prospective applications of AIE in analytical chemistry. Subsequently, Li and co-works used H_2O_2–TCPO–Au(I)-thiolate complex CL reaction to detect Hg^{2+} contents in water samples [36]. It is found that the addition of Hg^{2+} could quench the CL signals. The reason for the phenomenon is that the structure of Au(I)-thiolate complexes could be interrupted by the strong interaction between Hg^{2+} and –SH groups in the proposed complexes. This strategy has successfully detected Hg^{2+} in real sample. The study provides the appealing viewpoints for creating the CL methods for the detection of heavy metals based on AIE materials.

Subsequently, Liu's group has established a unique theranostic system by using the AIE dots [37]. The results showed that the AIE dots could react with H_2O_2 to produce the singlet oxygen, accompanying with the emission of long-wavelength light. The AIE dots were fabricated in the solution of soybean oil by co-encapsulating an AIE material (*i.e.*, TPE-BT-DC) with far-red/near-infrared (FR/NIR) emissions and CPPO into amphipathic pluronic (Fig. 11.2). This work could overcome the
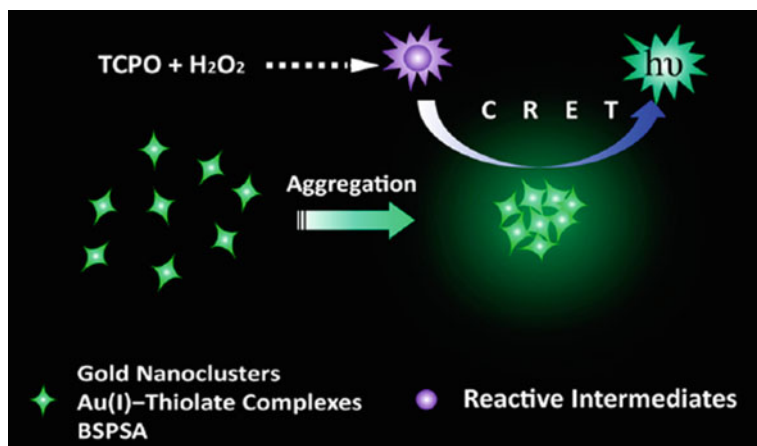
Fig. 11.1 Schematic illustration of AIE material enhanced H_2O_2-TCPO CL. Reprinted with permission from Ref. [35]. Copyright 2015 American Chemical Society
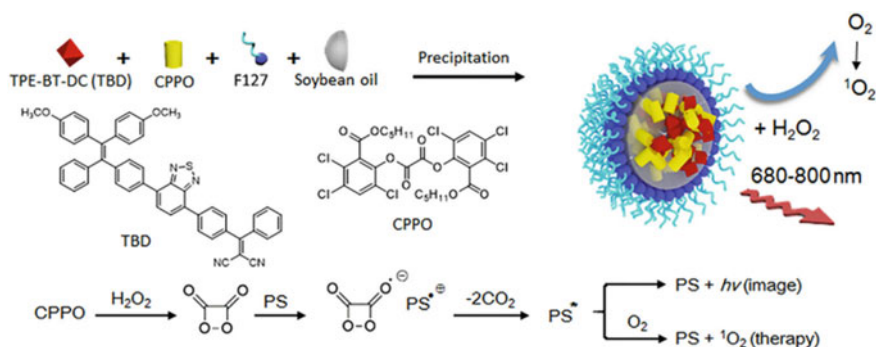
Fig. 11.2 Design of AIE dots for H_2O_2 detection and $^1O_2$ production. Reprinted with permission from Ref. [37]. Copyright 2017 Elsevier B.V

obstacles of deep penetrations, and offered a novel approach for the light-source-free image-guided therapeutic systems using the CL technique in clinical practice. Subsequently, Kim and coworkers have designed an easy nanophotonic method of near-infrared CL [38]. A low-band gap conjugated AIE polymer was utilized as the novel non-conventional bright emitter. This approach was based on the intraparticle energy transfer for the detection of inflammatory H_2O_2. This method presents a high tissue penetration depth and a detection limit of H_2O_2 with 10^{-9} mol L^{-1}, which could be useful for diagnostic biomedical uses.

11.3 AIE-Amplified CL Signals from Singlet Oxygen System

Singlet oxygen ($^1O_2$) plays a substantial function in pathological procedures and innate immune reaction [39–42]. Many researches focus on the study of efficient $^1O_2$ generation, and the quantitative and qualitative detection of $^1O_2$ [43–47]. In 2016, Lu and coworkers developed a novel platform for the detection of $^1O_2$, which was produced in the photodynamic therapy process. (Fig. 11.3) [48]. The platform was made up of a tetraphenylethenesodium dodecyl sulfonate anionic surfactant (TPE-SDS), which was used as the energy acceptor to enhance the $^1O_2$ emission. This investigation could provide useful support for optimization of the irradiation time throughout photodynamic therapy, and deepen the understanding of the behaviors of photosensitizers.

In addition, Zhang and coworkers have established a unique afterglow luminogen based upon the poly[(9,9-di(2-ethylhexyl)-9H-fluorene-2,7-vinylene)-co-(1-methoxy-4-(2-ethylhexyloxy)-2,5-phenylenevinylene)] (PFPV) and the AIE material (i.e., 2-((5-(4- (diphenylamino) phenyl) thiophen-2-yl) methylene) malononitrile (TTMN)) for in vivo tumor imaging [49]. To perform a reliable process of energy transfer for afterglow emission, an amphiphilic triblock copolymer had been used to confine the above two useful materials in a uniform nanostructure. The process of $^1O_2$ generation and imaging is that the TTMN could be excited by afterglow emission of the dioxetane-PFPV intermediates which could be constantly to produce $^1O_2$ and the afterglow wavelength had red-shifted. Subsequently, PFPV could be constantly oxidized by the delayed $^1O_2$ to form the intermediates of dioxetane-PFPV for self-circulating afterglow. The work could motivate the growth of other reliable afterglow materials based on AIE for tumor imaging. Subsequently, Lu and coworkers have developed a distinct CL sensor *via* intramolecular energy transfer mechanism and ultra-high aggregated CL systems in one particle [50]. This
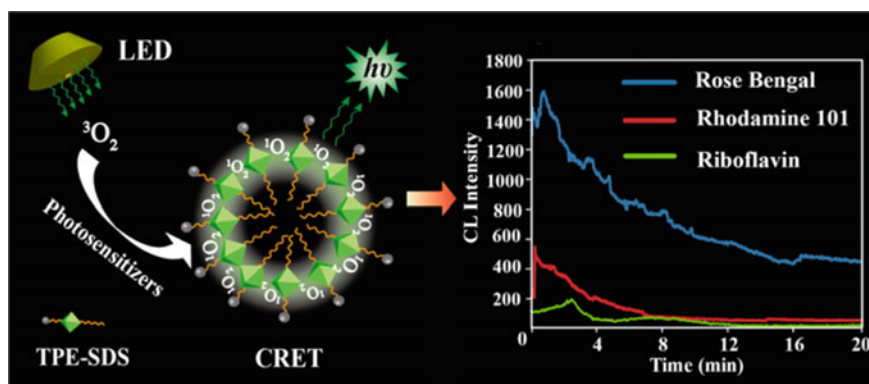
Fig. 11.3 Schematic Illustration of the luminescence platform by using AIE materials. Reprinted with permission from Ref. [48]. Copyright 2016 American Chemical Society

strategy showed that phthalhydrazid (PH)-tetraphenylethylene (TPE) with AIE characteristic could be utilized to amplify CL signals (Fig. 11.4). The mechanism was that the PH moiety in the PH-NTPE could react with $^1O_2$ to produce an intermediate radical (*i.e.*, an unstable peroxide). Subsequently, the PH-NTPE could be activated by the reaction energy. After that, the CL emission would release by means of the intramolecular energy transfer channel. This experiment demonstrated that the as-prepared sensor could yield a selective CL action toward $^1O_2$ among usual reactive oxygen species, and was sensitive to an nM level $^1O_2$.

On the other hand, Tang and coworkers have developed a novel AIE-active NIR CL emitter, which was consisted of chemically conjugating luminol with triphenylamine and benzothiadiazole [51]. The CL emission of emitter could last a long time (*i.e.*, 60 min). The proposed method had been used for in vivo qualitative and in vitro quantitative measurement of $^1O_2$. In this study, the tissues with the thickness of 3 cm could be penetrated through by the CL emission. Since the concentration of ROS in tumor tissues was relatively high, the proposed method has successfully distinguished tumor tissues from normal ones. The study shows considerable capacity of AIE-containing CL process for imaging-guided disease diagnosis.

In 2021, Lu's group found that an AIE-active fluorophore (*i.e.*, Na$_4$TCBPE) could exhibit high-efficiency luminescence after it was externally adsorbed onto layered double hydroxides (LDHs) (Fig. 11.5)[52]. During the CL reaction, negatively charged Na$_4$TCBPE was used as the CRET acceptor, and $^1O_2$ was utilized as the CRET donor. On the other hand, the LDHs with positively charge could be utilized as the support material for concentrating Na$_4$TCBPE. Therefore, the strategy has been used to detect NaNO$_2$, which could be assayed in the range from 1.0 to 100 μM with a detection limit of 0.5 μM. The analytical applications of the approach
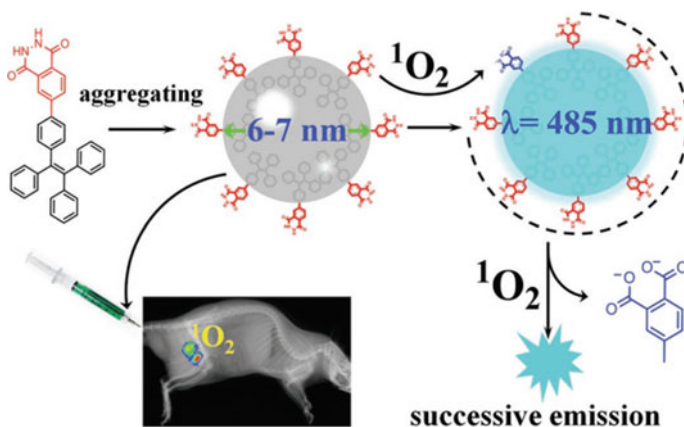
Fig. 11.4 Schematic representation of real-time imaging of ultra-trace $^1O_2$ in mouse via a CL nanosensor based on the AIE material. Reprinted with permission from Ref. [50]. Copyright 2019 John Wiley & Sons, Ltd.
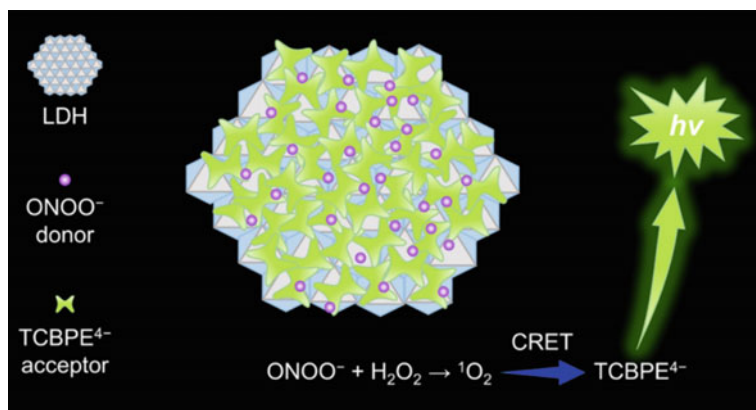
Fig. 11.5 Schematic representation of the assembly of the AIE-LDH materials in the efficient CRET process. Reprinted with permission from Ref. [52]. Copyright 2021 American Chemical Society

were analyzed by detecting $NaNO_2$ in sausage samples. This success of the study could motivate more highly sensitive and convenient CRET-based detection methods.

11.4 AIE-Amplified CL Signals from Superoxide Anion System

Superoxide anion ($O_2^{\bullet-}$) is one of the main forms of reactive oxygen species [53–56]. It plays an important role in a variety of diseases, senescence, apoptosis and cell differentiation [57–60]. Tang and coworkers developed a unique organic system with turn-on CL and fluorescence emissions especially regulated by $O_2^{\bullet-}$ (Fig. 11.6) [61]. In this platform, imidazopyrazinone (CLA) was used as the responsive part, as well as tetraphenylethene was used as CL/fluorescence improving part through CRET principle. The detection limit of $O_2^{\bullet-}$ was 0.21 nm for fluorescence and 0.38 nm for CL, respectively. Finally, the developed platform was used to image $O_2^{\bullet-}$ in Raw 264.7 cells and boosted $O_2^{\bullet-}$ in inflamed cells, and monitor the endogenous $O_2^{\bullet-}$ in acetaminophen overdosed cells. The results indicated that it is feasible to use AIE materials to achieve both the CL and the fluorescence determination.

11.5 AIE-Amplified CL Signals from 1,2-Dioxetane System

CL emitters are all based on the in situ production of short-lived and high-energy emitting species by oxidation reactions or analytes, respectively [62–64]. The emitting species could make spontaneously uncontrollable photons release [65–67]. It is
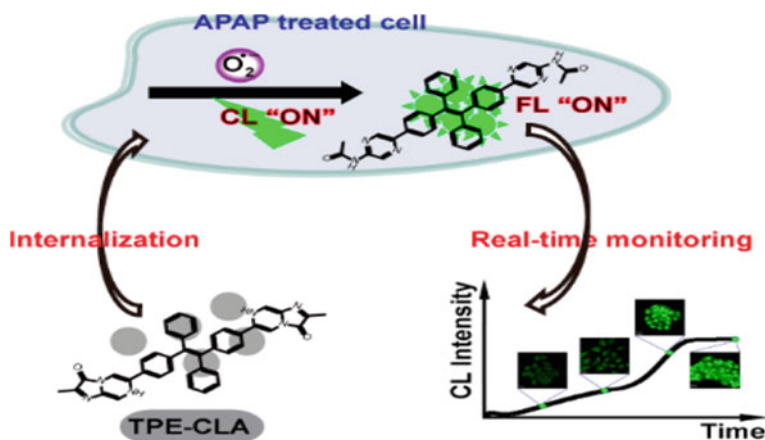
Fig. 11.6 Schematic representation of simultaneous FL and CL turned on by AIE for monitoring of endogenous $O_2^{\bullet-}$. Reprinted with permission from Ref. [61]. Copyright 2017 American Chemical Society

difficult to meet the measuring apparatus in a dynamic biological milieu and highly heterogeneous. Therefore, how to achieve the precise activate enriched, bright and controlled CL emission in bio-imaging continues to be the significant challenge. In order to solve the above problems, Guo and coworkers proposed a dual-lock strategy for optical imaging with sensitive CL emissions and fluorescent emissions using the sequence-dependent triggers [68]. As shown in Fig. 11.7, the dual-lock strategy is as follows. Firstly, the concealing part was activated and removed by the analyte. Where after stable pre-chemiluminophores generated and accumulated. Secondly, the LED light irradiation could activate the above pre-chemiluminophores to produce the 1,2-dioxetane with high energy. Finally, the decomposition of 1,2-dioxetane occurred and accompanied the improvement of CL emissions. The dual-lock strategy could motivate the development of a novel production of metabolic assays in a physiological environment, and broaden the bioanalytical toolbox for clinical applications and basic life science research.
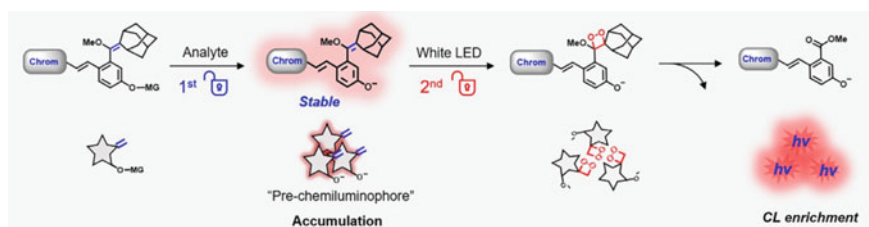
Fig. 11.7 Schematic representation of dual-lock strategy for bright and long-emission CL probe. Reprinted with permission from Ref. [68]. Copyright 2020 John Wiley & Sons, Ltd.

11.6   Conclusions

AIE materials have great advantages as the new CRET acceptors in different CL system. Due to the unique aggregation property, AIE materials could display significantly improved performances toward the CL emissions. On the other hand, the AIE effect could tackle the problem of aggregation-caused quenching. Therefore, the utilization of AIE materials achieves the substantial innovation for the enhancement of CRET efficiency, and offers prospects for various highly sensitive and discriminative sensing. In conclusion, the AIE material-involved CL systems are expected to act as the practical and powerful platform for comprehensive sensing applications.

References

1. Wang D, Tang BZ (2019) Aggregation-induced emission luminogens for activity-based sensing. Acc Chem Res 52:2559–2570
2. Mei J, Leung NL, Kwok RT, Lam JW, Tang BZ (2015) Aggregation-induced emission: together we shine, united we soar! Chem Rev 115:11718–11940
3. Cai XM, Lin Y, Li Y, Chen X, Wang Z, Zhao X, Huang S, Zhao Z, Tang BZ (2021) BioAIEgens derived from rosin: how does molecular motion affect their photophysical processes in solid state? Nat Commun 12:1773
4. Feng Z, Bai S, Qi J, Sun C, Zhang Y, Yu X, Ni H, Wu D, Fan X, Xue D, Liu S, Chen M, Gong J, Wei P, He M, Lam JWY, Li X, Tang BZ, Gao L, Qian J (2021) Biologically excretable aggregation-induced emission dots for visualizing through the marmosets intravitally: horizons in future clinical nanomedicine. Adv Mater 33:2008123
5. Gao M, Tang BZ (2017) Fluorescent sensors based on aggregation-induced emission: recent advances and perspectives. ACS Sens 2:1382–1399
6. Wu D, Liu S, Zhou J, Chen R, Wang Y, Feng Z, Lin H, Qian J, Tang BZ, Cai X (2021) Organic dots with large pi-conjugated planar for cholangiography beyond 1500 nm in rabbits: a non-radioactive strategy. ACS Nano 15:5011–5022
7. Wang Y, Nie J, Fang W, Yang L, Hu Q, Wang Z, Sun JZ, Tang BZ (2020) Sugar-based aggregation-induced emission luminogens: design, structures, and applications. Chem Rev 120:4534–4577
8. Guo X, Yuan P, Fan J, Qiao X, Yang D, Dai Y, Sun Q, Qin A, Tang BZ, Ma D (2021) Unraveling the important role of high-lying triplet-lowest excited singlet transitions in achieving highly efficient deep-blue AIE-based OLEDs. Adv Mater 33:2006953
9. Liu Z, Zou H, Zhao Z, Zhang P, Shan GG, Kwok RTK, Lam JWY, Zheng L, Tang BZ (2019) Tuning organelle specificity and photodynamic therapy efficiency by molecular function design. ACS Nano 13:11283–11293
10. Hu X, Zhang P, Wang D, Jiang J, Chen X, Liu Y, Zhang Z, Tang BZ, Li P (2021) AIEgens enabled ultrasensitive point-of-care test for multiple targets of food safety: aflatoxin B1 and cyclopiazonic acid as an example. Biosens Bioelectron 182:113188
11. Xia Q, Meng L, He T, Huang G, Li BS, Tang BZ (2021) Direct visualization of chiral amplification of chiral aggregation induced emission molecules in nematic liquid crystals. ACS Nano 15:4956–4966
12. Niu G, Zhang R, Gu Y, Wang J, Ma C, Kwok RTK, Lam JWY, Sung HH, Williams ID, Wong KS, Yu X, Tang BZ (2019) Highly photostable two-photon NIR AIEgens with tunable organelle specificity and deep tissue penetration. Biomaterials 208:72–82

13. Siddharth K, Alam P, Hossain MD, Xie N, Nambafu GS, Rehman F, Lam JWY, Chen G, Cheng J, Luo Z, Chen G, Tang BZ, Shao M (2021) Hydrazine detection during ammonia electro-oxidation using an aggregation-induced emission dye. J Am Chem Soc 143:2433–2440

14. Yang Z, Zhang Z, Lei Z, Wang D, Ma H, Tang BZ (2021) Precise molecular engineering of small organic phototheranostic agents toward multimodal imaging-guided synergistic therapy. ACS Nano 15:7328–7339

15. Liu C, Bai H, He B, He X, Zhang J, Chen C, Qiu Y, Hu R, Zhao F, Zhang Y, He W, Chau JHC, Chen S, Lam JWY, Tang BZ (2021) Functionalization of silk by aiegens through facile bioconjugation: full-color fluorescence and long-term bioimaging. Angew Chem Int Ed 60:12424–12430

16. Liu S, Li Y, Kwok RTK, Lam JWY, Tang BZ (2021) Structural and process controls of AIEgens for NIR-II theranostics Chem Sci 12:3427–3436

17. Chen K, Zhang R, Wang Z, Zhang W, Tang BZ (2019) Structural modification orientated multifunctional aie fluorescence probes: organelles imaging and effective photosensitizer for photodynamic therapy. Adv Opt Mater 8:1901433

18. Zheng Z, Li D, Liu Z, Peng HQ, Sung HHY, Kwok RTK, Williams ID, Lam JWY, Qian J, Tang BZ (2019) Aggregation-induced nonlinear optical effects of aiegen nanocrystals for ultradeep in vivo bioimaging. Adv Mater 31:1904799

19. Bai H, He W, Chau JHC, Zheng Z, Kwok RTK, Lam JWY, Tang BZ (2021) AIEgens for microbial detection and antimicrobial therapy. Biomaterials 268:120598

20. Liu S, Feng G, Tang BZ, Liu B (2021) Recent advances of AIE light-up probes for photodynamic therapy. Chem Sci 12:6488–6506

21. Chen K, He P, Wang Z, Tang BZ (2021) A feasible strategy of fabricating type I photosensitizer for photodynamic therapy in cancer cells and pathogens. ACS Nano 15:7735–7743

22. Feng HT, Li Y, Duan X, Wang X, Qi C, Lam JWY, Ding D, Tang BZ (2020) Substitution activated precise phototheranostics through supramolecular assembly of AIEgen and calixarene. J Am Chem Soc 142:15966–15974

23. Huang D, Liu Y, Qin A, Tang BZ (2019) Structure–property relationship of regioregular polytriazoles produced by ligand-controlled regiodivergent ru(ii)-catalyzed azide–alkyne click polymerization. Macromolecules 52:1985–1992

24. Guo J, Fan J, Lin L, Zeng J, Liu H, Wang CK, Zhao Z, Tang BZ (2019) Mechanical insights into aggregation-induced delayed fluorescence materials with anti-kasha behavior. Adv Sci 6:1801629

25. Zhang L, Li Y, Che W, Zhu D, Li G, Xie Z, Song N, Liu S, Tang BZ, Liu X, Su Z, Bryce MR (2019) AIE multinuclear ir(III) complexes for biocompatible organic nanoparticles with highly enhanced photodynamic performance. Adv Sci 6:1802050

26. Duo Y, Zhu D, Sun X, Suo M, Zheng Z, Jiang W, Tang B Z (2021) Patient-derived microvesicles/AIE luminogen hybrid system for personalized sonodynamic cancer therapy in patient-derived xenograft models. Biomaterials 272: 120755.

27. Li Y, Liu F, Zhang J, Liu X, Xiao P, Bai H, Chen S, Wang D, Sung SHP, Kwok RTK, Shen J, Zhu K, Tang BZ (2021) Efficient killing of multidrug-resistant internalized bacteria by aiegens in vivo. Adv Sci 8:2001750

28. Ni X, Zhang X, Duan X, Zheng HL, Xue XS, Ding D (2019) Near-infrared afterglow luminescent aggregation-induced emission dots with ultrahigh tumor-to-liver signal ratio for promoted image-guided cancer surgery. Nano Lett 19:318–330

29. Li J, Peng K, Li Y, Wang J, Huang J, Yan Y, Wang D, Tang BZ (2020) Exosome-mimetic supramolecular vesicles with reversible and controllable fusion and fission. Angew Chem Int Ed 59:21510–21514

30. Wei P, He X, Zheng Z, He D, Li Q, Gong J, Zhang J, Sung HHY, Williams ID, Lam JWY, Liu M, Tang BZ (2021) Robust supramolecular nano-tunnels built from molecular bricks. Angew Chem Int Ed 60:7148–7154

31. Yi X, Hu JJ, Dai J, Lou X, Zhao Z, Xia F, Tang BZ (2021) Self-guiding polymeric prodrug micelles with two aggregation-induced emission photosensitizers for enhanced chemo-photodynamic therapy. ACS Nano 15:3026–3037

32. Wang Z, Liu F, Lu C (2014) Evolution of biogenic amine concentrations in foods through their induced chemiluminescence inactivation of layered double hydroxide nanosheet colloids. Biosens Bioelectron 60:237–243
33. Biparva P, Abedirad SM, Kazemi SY, Shanehsaz M (2016) Chemiluminescence recognition of berberine triggered by biomimetically synthesized silver nanoparticles. Sens Actuators B 234:278–285
34. Li L, Lin D, Yang F, Xiao Y, Yang L, Yu S, Jiang C (2021) Gold nanoparticle-based peroxyoxalate chemiluminescence system for highly sensitive and rapid detection of thiram pesticides. ACS Appl Nano Mater 4:3932–3939
35. Zhang L, He N, Lu C (2015) Aggregation-induced emission: a simple strategy to improve chemiluminescence resonance energy transfer. Anal Chem 87:1351–1357
36. Hou Y, Chen Y, Guo X, Liu W, Zhang L, Lv C, Xu Y, Jin Y, Li B (2021) Aggregation-induced chemiluminescence system for sensitive detection of mercury ions. Anal Bioanal Chem 413:625–633
37. Gu X, Tang BZ (2017) No UV irradiation needed! chemiexcited aie dots for cancer theranostics. Chem 3:922–924
38. Seo YH, Singh A, Cho HJ, Kim Y, Heo J, Lim CK, Park SY, Jang WD, Kim S (2016) Rational design for enhancing inflammation-responsive in vivo chemiluminescence via nanophotonic energy relay to near-infrared AIE-active conjugated polymer. Biomaterials 84:111–118
39. Mangalath S, Saneesh Babu PS, Nair RR, Manu PM, Krishna S, Nair SA, Joseph J (2021) Graphene quantum dots decorated with boron dipyrromethene dye derivatives for photodynamic therapy. ACS Appl Nano Mater 4:4162–4171
40. Dai J, Li Y, Long Z, Jiang R, Zhuang Z, Wang Z, Zhao Z, Lou X, Xia F, Tang BZ (2020) Efficient near-infrared photosensitizer with aggregation-induced emission for imaging-guided photodynamic therapy in multiple xenograft tumor models. ACS Nano 14:854–866
41. Zheng Q, Liu X, Zheng Y, Yeung KWK, Cui Z, Liang Y, Li Z, Zhu S, Wang X, Wu S (2021) The recent progress on metal-organic frameworks for phototherapy. Chem Soc Rev 50:5086–5125
42. Shih CY, Huang WL, Chiang IT, Su WC, Teng H (2021) Biocompatible hole scavenger-assisted graphene oxide dots for photodynamic cancer therapy. Nanoscale 13:8431–8441
43. Chen B, Yang Y, Wang Y, Yan Y, Wang Z, Yin Q, Zhang Q, Wang Y (2021) Precise monitoring of singlet oxygen in specific endocytic organelles by super-ph-resolved nanosensors. ACS Appl Mater Interfaces 13:18533–18544
44. Xie BR, Yu Y, Liu XH, Zeng JY, Zou MZ, Li CX, Zeng X, Zhang XZ (2021) A near infrared ratiometric platform based pi-extended porphyrin metal-organic framework for O_2 imaging and cancer therapy. Biomaterials 272:120782
45. Zhao S, Zang G, Zhang Y, Liu H, Wang N, Cai S, Durkan C, Xie G, Wang G (2021) Recent advances of electrochemical sensors for detecting and monitoring ROS/RNS. Biosens Bioelectron 179:113052
46. Shafikov MZ, Suleymanova AF, Kutta RJ, Brandl F, Gorski A, Czerwieniec R (2021) Dual emissive dinuclear Pt(II) complexes and application to singlet oxygen generation. J Mater Chem C 9:5808–5818
47. Yu W, Zhao L (2021) Chemiluminescence detection of reactive oxygen species generation and potential environmental applications. Trac Trend in Anal Chem 136:116197
48. Zou F, Zhou W, Guan W, Lu C, Tang BZ (2016) Screening of photosensitizers by chemiluminescence monitoring of formation dynamics of singlet oxygen during photodynamic therapy. Anal Chem 88:9707–9713
49. Xu Y, Yang W, Yao D, Bian K, Zeng W, Liu K, Wang D, Zhang B (2020) An aggregation-induced emission dye-powered afterglow luminogen for tumor imaging. Chem Sci 11:419–428
50. Zhang S, Cui H, Gu M, Zhao N, Cheng M, Lv J (2019) Real-time mapping of ultratrace singlet oxygen in rat during acute and chronic inflammations via a chemiluminescent nanosensor. Small 15:1804662
51. Liu C, Wang X, Liu J, Yue Q, Chen S, Lam JWY, Luo L, Tang BZ (2020) Near-infrared AIE dots with chemiluminescence for deep-tissue imaging. Adv Mater 32:2004685

52. Zhang L, Shi M, Zhou W, Guan W, Lu C (2021) Disordered assembly of donors and acceptors on layered double hydroxides for high-efficiency chemiluminescence resonance energy transfer. Anal Chem 93:7724–7731
53. Wang Y, Han J, Xu Y, Gao Y, Wen H, Cui H (2020) Taking advantage of the aromatisation of 7-diethylamino-4-methyl-3,4-dihydrocoumarin in the fluorescence sensing of superoxide anion. Chem Commun 56:9827–9829
54. Ji K, Shan J, Wang X, Tan X, Hou J, Liu Y, Song Y (2021) Rational design of near-infrared fluorescent probes for superoxide anion radical: Enhancement of self-stability and sensitivity by self-immolative linker. Free Radic Biol Med 167:36–44
55. Gao Q, Zhao H, Wang Z, Cai X, Zhou L, Lan M (2021) Fabrication of hierarchically porous carbon networks for the electrochemical determination of superoxide anion released from living cells. Sens Actuators B 330:129309
56. Ding Q, Tian Y, Wang X, Li P, Su D, Wu C, Zhang W, Tang B (2020) Oxidative damage of tryptophan hydroxylase-2 mediated by peroxisomal superoxide anion radical in brains of mouse with depression. J Am Chem Soc 142:20735–20743
57. Wang Z, Zhao H, Gao Q, Chen K, Lan M (2021) Facile synthesis of ultrathin two-dimensional graphene-like CeO_2-TiO_2 mesoporous nanosheet loaded with Ag nanoparticles for non-enzymatic electrochemical detection of superoxide anions in HepG2 cells. Biosens Bioelectron 184:113236
58. Zhong GC, Zhao ZB, Cheng Y, Wang YB, Qiu C, Mao LH, Hu JJ, Cai D, Liu Y, Gong JP, Li SW (2021) Epigenetic silencing of GCH1 promotes hepatocellular carcinoma growth by activating superoxide anion-mediated ASK1/p38 signaling via inhibiting tetrahydrobiopterin de novo biosynthesis. Free Radic Biol Med 168:81–94
59. Li JX, Zhang LM, Liu CC, Wu QN, Li SP, Lei XP, Huang YG, Feng GN, Yu XY, Sun XQ, Guo ZM, Fu JJ (2021) Doxorubicin-loaded hydrogen peroxide self-providing copper nanodots for combination of chemotherapy and acid-induced chemodynamic therapy against breast cancer. J Colloid Interface Sci 593:323–334
60. Ma S, Ma Y, Liu Q, Lin W. (2021) A two-photon fluorescent probe with lysosome targetability for imaging endogenous superoxide anion in living cells, zebrafish and pneumonia tissue. Sens Actuators B 332:129523
61. Niu J, Fan J, Wang X, Xiao Y, Xie X, Jiao X, Sun C, Tang B (2017) Simultaneous fluorescence and chemiluminescence turned on by aggregation-induced emission for real-time monitoring of endogenous superoxide anion in live cells. Anal Chem 89:7210–7215
62. Huang J, Huang J, Cheng P, Jiang Y, Pu K (2020) Near-infrared chemiluminescent reporters for in vivo imaging of reactive oxygen and nitrogen species in kidneys. Adv Funct Mater 30:2003628
63. Brown K, Jacquet C, Biscay J, Allan P, Dennany L (2020) Tale of two alkaloids: ph-controlled electrochemiluminescence for differentiation of structurally similar compounds. Anal Chem 92:2216–2223
64. Gnaim S, Green O, Shabat D (2018) The emergence of aqueous chemiluminescence: new promising class of phenoxy 1,2-dioxetane luminophores. Chem Commun 54:2073–2085
65. Lu C, Zhang C, Wang P, Zhao Y, Yang Y, Wang Y, Yuan H, Qu S, Zhang X, Song G, Pu K (2020) Light-free generation of singlet oxygen through manganese-thiophene nanosystems for pH-responsive chemiluminescence imaging and tumor therapy. Chem 6:2314–2334
66. Wang Y, Shi L, Ye Z, Guan K, Teng L, Wu J, Yin X, Song G, Zhang XB (2020) Reactive oxygen correlated chemiluminescent imaging of a semiconducting polymer nanoplatform for monitoring chemodynamic therapy. Nano Lett 20:176–183
67. Shen C-L, Lou Q, Liu K-K, Dong L, Shan C-X (2020) Chemiluminescent carbon dots: synthesis, properties, and applications. Nano Today 35:100954
68. Zhang Y, Yan C, Wang C, Guo Z, Liu X, Zhu WH (2020) A sequential dual-lock strategy for photoactivatable chemiluminescent probes enabling bright duplex optical imaging. Angew Chem Int Ed 59:9059–9066

Index